CORA Cork Open Research Archive
Cartlann Taighde Oscailte Chorcaí

Title	Monitoring the vegetation start of season (SOS) across the island of Ireland using the MERIS global vegetation index
Authors	O'Connor, Brian
Publication date	2011-08
Original Citation	O'CONNOR, B. 2011. Monitoring the vegetation Start of Season (SOS) across the island of Ireland using the MERIS Global Vegetation Index. PhD, University College Cork.
Type of publication	Doctoral thesis
Link to publisher's version	http://library.ucc.ie/record=b2027888~S0
Rights	© 2011, Brian O'Connor - http://creativecommons.org/licenses/by-nc-nd/3.0/
Download date	2024-04-20 01:24:48
Item downloaded from	https://hdl.handle.net/10468/501

UCC
University College Cork, Ireland
Coláiste na hOllscoile Corcaigh

Monitoring the vegetation Start of Season (SOS) across the island of Ireland using the MERIS Global Vegetation Index

Brian O'Connor B.Sc.

Thesis submitted to the National University of Ireland, Cork, in fulfillment of the requirements for the Degree of Doctor of Philosophy

Department of Geography,
School of Geography and Archaeology: The Human Environment,
College of Arts, Celtic Studies and Social Sciences,
University College Cork,
Ireland
and
Coastal and Marine Research Centre (CMRC),
Environmental Research Institute,
University College Cork

Head of Department: Dr. Barry Brunt
Research Supervisors: Dr. Ned Dwyer and Dr. Fiona Cawkwell

August, 2011

Table of Contents

Abstract i

Dedication and Acknowledgements iv

List of Figures.....v

List of Tables.....x

Acronyms xii

Chapter 1. Introduction to vegetation phenology 1

1.1 Background……...1

1.1.1 Phenology as an indicator of climate change and ecosystem health.... 2

1.1.2 Monitoring vegetation phenology 3

1.1.3 Phenology and climate..... 7

1.1.4 Phenology and non-climatic factors 10

1.2 Study aim……12

1.3 Research objectives……13

Chapter 2. Satellite remote sensing of vegetation 16

2.1 The Physical Principles of Remote Sensing…… 16

2.1.1 Overview of Optical Remote Sensing 19

2.1.2 Further Concepts in Optical Remote Sensing 21

2.2. Monitoring Vegetation Using Optical Sensors……..22

2.2.1 Broad scale monitoring sensors..... 25

2.2.1.1 National Oceanic and Atmospheric Administration (NOAA) Advanced Very High Resolution Radiometer (AVHRR), NOAA-AVHRR.....25

2.2.1.2 SPOT VEGETATION…….. 26

2.2.1.3 National Aeronautics and Space Administration (NASA) Sea-viewing Wide Field-of-view Sensor (SeaWiFs)…… 27

2.2.2 Regional scale monitoring sensors 27

2.2.2.1 Terra/Aqua (MODIS) Moderate-Resolution Imaging Spectroradiometer…….28

2.2.2.2. Envisat (MERIS) Medium Resolution Imaging Spectrometer……28

2.2.3 Local Scale Monitoring 30

2.2.3.1 Landsat Multi Spectral Scanner (MSS) and Thematic Mapper (TM/ETM+)……..31

2.2.3.2 GeoEye-1, IKONOS, Quickbird, WorldView-1 and WorldView-2.32

2.3 Vegetation Indices and their application to vegetation monitoring…… 33

2.3.1 Simple vegetation Indices 33

2.3.1.1 Simple Ratio (SR) Index……...33

2.3.1.2 Normalised Difference Vegetation Index (NDVI)……34

2.3.2 Intermediate Vegetation Indices..... 36

2.3.2.1 Global Environmental Monitoring Index (GEMI)…… 36

2.3.2.2 Soil Adjusted Vegetation Index (SAVI)…… 37

2.3.2.3 Tasselled Cap……38

2.3.3Optimised Vegetation Indices 39

2.3.3.1 MERIS Global Vegetation Index (MGVI)……40

2.3.3.2 MODIS Enhanced Vegetation Index (EVI)……..45

2.3.3.3 Advantages of optimised indices for vegetation monitoring……45

2.4 Remote Sensing of Land Surface Phenology (LSP)……...46

2.4.1 Background to LSP studies 47

2.4.2 Monitoring LSP by phenological metrics 49

2.4.3 Global to continental scale trends in land surface phenology..... 51

2.4.4 Monitoring phenology in an agricultural context..... 53

2.4.5 Monitoring the vegetation Start of Season (SOS)..... 55

2.5 Conclusion…….56

Chapter 3. The implications of cloud cover for vegetation seasonality monitoring 59

3.1 Time compositing high temporal frequency satellite data…….60

3.1.1 The aims of time-compositing satellite data 60

3.1.2 The factors influencing composite period selection..... 62

3.2 Primary data…….63

3.2.1 The Joint Research Centre (JRC) FAPAR products 63

3.2.2 The advantages of the Medium Resolution Imaging Spectrometer (MERIS) for vegetation monitoring..... 64

3.2.3 Acquiring a time series of MERIS FAPAR over Ireland 65

3.2.3.1 The ESA-ESRIN G-POD……. 65

3.2.3.2. The FAPAR time-composite algorithm……...67

3.3 Methods and data for composite period selection…….....68

3.3.1 In-situ phenological data..... 69

3.3.1.1 Description of Site……69

3.3.1.2 The recording of phenological data……...70

3.3.1.3 The rate of change in mixed woodland vegetation……...73

3.3.1.4 The inter-species variation in the timing of leafout……..74

3.3.1.5 The photographic documentation of leaf unfolding in a tree canopy……...75

3.3.1.6 Fieldwork findings……76

3.3.2 Armagh Observatory cloud data 77

3.3.2.1 Temporal patterns in cloud cover at Armagh Observatory……..78

3.3.2.2 Temporal analysis of cloud-flagged pixels in 10-day and 7-day MERIS image composites…….82

3.3.2.3 Spatio-temporal analysis of cloud-flagged pixels in 10-day and 7-day MERIS image composites…….83

3.3.2.4 Generating annual cloud composite images from MERIS data……86

3.3.3 Summary of composite period selection..... 89

3.4 Verification of MGVI clear sky values with the METEOSAT cloud mask90

3.4.1 Cloud detection in the MGVI product..... 91

3.4.2 The selection of the METEOSAT Cloud Mask (CLM) 93

3.4.3The analysis of MGVI clear-sky values using the CLM 94

3.4.3.1 The five comparison tests…….....95

3.4.3.2 The verification of MGVI by the METEOSAT CLM for the total sample……98

3.4.4. The influence of cloud-flagged values on MGVI time series data...100

3.4.5 Summary of validation results…….....103

3.4.6 Other contributing factors to MGVI time series noise……..104

3.4.6.1 MERIS top of atmosphere radiance……....106

3.5 Discussion……111

3.6 Conclusion……114

Chapter 4. Optimising time series analysis software to estimate the Start of Season (SOS) ……116

4.1 Time series analysis methods for land surface phenology monitoring…116

4.2 Overview of the time series analysis software- TIMESAT……121

4.3 TIMESAT processing of VI time series……..122

4.3.1 The Savitzky-Golay filter 123

4.3.2 Least-squares fit to a basis function 124

4.3.3 Curve-fitting per pixel using the TIMESAT GUI.....126

4.4 Justification of a fitting method……128

4.5 Setting sensitivity analysis……133

4.5.1 Data Range.....134

4.5.2 Spike method.....134

4.5.3 Seasonality parameter.....135

4.5.4 Upper envelope iterations and adaptation strength 135

4.5.5 Force to minimum value 138

4.5.6 Threshold determination 139

4.6 The SOS imagery estimated from the fitted functions……140

4.7 Discussion……143

4.8 Conclusion……146

Chapter 5. The spatio-temporal patterns in SOS across the island of Ireland based on time series analysis 148

5.1 Spatio-temporal variability in the SOS……149

5.2 Spatial analysis of SOS……154

5.2.1 Latitudinal SOS analysis.....154

5.2.2 Longitudinal SOS analysis.....158

5.3 The SOS anomalies from 2003 to 2009……161

5.4 The SOS and landcover……165

5.4.1 CORINE Land Cover (CLC) 165

5.4.2 Seperability analysis of the landcover classes by SOS dates in 2006 169

5.4.3 The Cumulative Start of Season (SOS) in 2006.....171

5.5 The SOS and Elevation……175

5.6 The SOS and grassland management……...177

5.7 The SOS and air temperature……179

5.8 Discussion……183

5.9 Conclusion……189

Chapter 6. Air temperature as a determinant of SOS.....192

6.1 Background……192

6.2 The SOS and air temperature……193

6.3 Climate data……...197

6.4 Statistical techniques……..200

6.4.1 Correlation methods……200

6.4.1.1 Pearson product-moment correlation……...200

6.4.1.2 Spearman rank-order correlation……..201

6.4.1.3 Statistical significance of correlation……201

6.4.2 Regression models……202

6.4.3 Preparation and use of the climate data……...205

6.4.4 Initial correlation results 206

6.5 The North Atlantic Oscillation (NAO) Index……..213

6.6 The SOS and Accumulated Growing Degree Days (AGDD)…….215

6.6.1 Calculating growing degree days……217

6.6.2 Statistical treatment of growing degree days per landcover type…220

6.6.3 Variation in growing degree days per landcover type……...221

6.6.4 Varying the base temperature for pastures 226

6.7 Discussion…… 228

6.8 Conclusions……..234

Chapter 7. Conclusions and Perspectives 237

7.1 Conclusions.....237

7.2 Perspectives.....240

7.3 The future of land surface phenology studies 245

References 249

Appendix A: Fieldwork observations and field journal 264

Appendix B: METEOSAT/MERIS overpass times 283

Appendix C: The coordinates and offset of the MERIS Level 1 (L1) radiance and MGVI pixels 285

Appendix D: MERIS Level 3 data format (hdf 4.2) 286

Appendix E: Composite period, day of year and calendar dates 287

Declaration

I certify that this thesis has not been previously submitted for a degree in this or any other university. This thesis is the result of my own investigations and all secondary sources of information have been acknowledged and references to all literature used have been provided.

_____

Brian O' Connor

Abstract

The aim of this study was to develop a methodology, based on satellite remote sensing, to estimate the vegetation Start of Season (SOS) across the whole island of Ireland on an annual basis. This growing body of research is known as Land Surface Phenology (LSP) monitoring.

The SOS was estimated for each year from a 7-year time series of 10-day composited, 1.2 km reduced resolution MERIS Global Vegetation Index (MGVI) data from 2003 to 2009, using the time series analysis software, TIMESAT. The selection of a 10-day composite period was guided by *in-situ* observations of leaf unfolding and cloud cover at representative point locations on the island. The MGVI time series was smoothed and the SOS metric extracted at a point corresponding to 20% of the seasonal MGVI amplitude. The SOS metric was extracted on a per pixel basis and gridded for national scale coverage. There were consistent spatial patterns in the SOS grids which were replicated on an annual basis and were qualitatively linked to variation in landcover. Analysis revealed that three statistically separable groups of CORINE Land Cover (CLC) classes could be derived from differences in the SOS, namely agricultural and forest land cover types, peat bogs, and natural and semi-natural vegetation types. These groups demonstrated that managed vegetation, e.g. pastures has a significantly earlier SOS than in unmanaged vegetation e.g. natural grasslands. There was also interannual spatio-temporal variability in the SOS. Such variability was highlighted in a series of anomaly grids showing variation from the 7-year mean SOS. An initial climate analysis indicated that an anomalously cold winter and spring in 2005/2006, linked to a negative North Atlantic Oscillation index value,

delayed the 2006 SOS countrywide, while in other years the SOS anomalies showed more complex variation. A correlation study using air temperature as a climate variable revealed the spatial complexity of the air temperature-SOS relationship across the Republic of Ireland as the timing of maximum correlation varied from November to April depending on location. The SOS was found to occur earlier due to warmer winters in the Southeast while it was later with warmer winters in the Northwest. The inverse pattern emerged in the spatial patterns of the spring correlates. This contrasting pattern would appear to be linked to vegetation management as arable cropping is typically practiced in the southeast while there is mixed agriculture and mostly pastures to the west. Therefore, land use as well as air temperature appears to be an important determinant of national scale patterns in the SOS.

The TIMESAT tool formed a crucial component of the estimation of SOS across the country in all seven years as it minimised the negative impact of noise and data dropouts in the MGVI time series by applying a smoothing algorithm. The extracted SOS metric was sensitive to temporal and spatial variation in land surface vegetation seasonality while the spatial patterns in the gridded SOS estimates aligned with those in landcover type. The methodology can be extended for a longer time series of FAPAR as MERIS will be replaced by the ESA Sentinel mission in 2013, while the availability of full resolution (300m) MERIS FAPAR and equivalent sensor products holds the possibility of monitoring finer scale seasonality variation.

This study has shown the utility of the SOS metric as an indicator of spatio-temporal variability in vegetation phenology, as well as a correlate of other environmental variables such as air temperature. However, the satellite-based method is not seen as a replacement of ground-based observations, but rather as a complementary approach to studying vegetation phenology at the national scale. In future, the method can be extended to extract other metrics of the seasonal cycle in order to gain a more comprehensive view of seasonal vegetation development.

Dedication

To my parents, Terence and Anna O' Connor

Acknowledgments

I am indebted to my two supervisors, Dr. Ned Dwyer and Dr. Fiona Cawkwell, for their dedicated, attentive and careful supervision throughout the course of this PhD thesis, especially Dr. Dwyer without whom this study would never have been possible. I am equally grateful to the EPA who initially provided M.Sc funding under the STRIVE initiative and then facilitated the extension of the project to PhD. The European Space Agency provided the MERIS data free of charge. My colleagues at the CMRC have all helped out in way or another over the years so thank you all. There have been a few individuals beyond UCC who have kindly provided technical and financial support to the project. These include Alison Donnelly of the Climate Change Impacts on Phenology project at TCD, Stuart Green at Teagasc, Seamus Walsh at Met Éireann and Lars Eklundh at Lund University, Sweden. Finally, I am very grateful to those beyond the academic realm, who encouraged and supported me when I needed it most, especially my family and friends for putting up with me for so long! The completion of a PhD thesis is a challenge on many levels and without the support of all these people I would never have succeeded. Mile Maith agaibh!

List of Figures

Figure 1.1: The locations of the phenological gardens in Ireland (Garden names listed in table 1.1) 5

Figure 1.2: Measurements in Hawaii since 1958 and Mace Head since 1992 show the seasonality of the carbon cycle as well as steadily increasing concentrations of atmospheric CO2 11

Figure 2.1: The Electromagnetic Spectrum (John Hopkins University, 2011) ... 16

Figure 2.2: Solar Radiation is subject to varying atmospheric processes in the Earth's Atmosphere (Ackerman and Whittaker, 2011) 17

Figure 2.3: Reflectance from Earth surface features in the remote sensing Process (CRISP, 2001) 18

Figure 2.4: Multispectral remote sensing. The spectral response of water and vegetation are clearly distinguishable with increasing wavelength in the near infrared (>700 nm) (CRISP, 2001) 20

Figure 3.1: Stages in the Reduced Resolution (RR) MGVI product generation using the ESA-ESRIN G-POD 66

Figure 3.2: Location of in-situ field observations, Currabinny Wood, Co. Cork with a satellite image of the area acquired on the 8th of June, 2008 from Google Earth 70

Figure 3.3: the Currabinny GPS points show the perimeter of the field site in relation to the coastline and the corresponding MGVI pixels. Currabinny Wood crosses two pixels in which surrounding water and other vegetation types contribute to the FAPAR response. 73

Figure 3.4: The average rate of leafout in the Beech and Birch trees in 2008 and 2009. The % leaf cover was estimated weekly and the values are plotted cumulatively until the canopies had 100% leaf cover (Day 50 represents the 20th February, 2008 and 2009 while day 150 represents May 30th in 2008 and May 29th in 2009) 74

Figure 3.5: Various phases in onset of the beginning of leaf unfolding (BO) in Birch (Betula pubescens). (A) Birch in dormancy, (B) Budburst, (C) 20% BO, (D) 40% BO, (E) 50% BO, (F) 70% BO, (G) 90% BO, (H) 100% BO..... 76

Figure 3.6: Location of Armagh Observatory, site of daily cloud estimates 78

Figure 3.7: The 7-day average cloud cover amounts (Okta) observed at Armagh Observatory for the growing season of 2005 to 2007 79

Figure 3.8: Same as in figure 3.7 but using a 10-day averaging period 80

Figure 3.9: A comparison of cloud estimates at Armagh with the percentage of cloud-flagged pixels per MGVI 10-day composite for the growing season, beginning 1st of February and ending, 31st of October, 2007. 81

Figure 3.10: A comparison of the percentage of MERIS pixels over the island of Ireland that are cloud-covered per 7-day and 10-day composite period during spring 2006 (Day 1 represents March 1st and day 121, June 29th)..... 83

Figure 3.11: The number of cloud-covered composite periods per pixel over the island of Ireland in the period, March 1st to June 29th, 2006 (a) using 7-day composites and (b) using 10-day composites. 84

Figure 3.12: A frequency distribution of the number of cloud flags per pixel in a time series of eighteen 7-day and thirteen 10-day composite images in the period, March 1st to June 29th, 2006 85

Figure 3.13: Annual 10-day cloud composites generated over the island of Ireland using both cloud flags derived from the MERIS cloud mask and the MGVI cloud-detection algorithm (A) 2003, (B) 2004, (C) 2005, (D) 2006 (E) 2007, (F) 2008, (G) 2009. The colour bar indicates the number of cloud-covered 10-day periods from a total of 36 87

Figure 3.14: The percentage of cloud-covered 10-day periods per pixel from 2003 to 2009. The pixels were selected from each region of the country to show variability in cloud cover per year 88

Figure 3.15: (a): The blue line represents the raw MGVI time series. (b) The thick black line shows the fitted smoothing function. 91

Figure 3.16: (a): The dMGVI grid on the 21st January, 2006. The representative MGVI pixels selected on that day to represent the composite period are shown in white, (b): The 21st January, 2006, result grid from the comparison of MGVI and METEOSAT CLM 11 a.m. grid: The grid pixel values correspond to the appropriate test number: 0 is un-compared value, 1 is valid MGVI and land, 2 is invalid MGVI and cloud, 3 is valid MGVI and cloud, 4 is invalid MGVI and land, 5 is invalid MGVI and ocean. 97

Figure 3.17: The composite value at period 156 is anomalous with respect to the left and right neighbour indicated by an upward spike. The mean line is calculated from the left and right neighbouring value and the +20% value is also shown. 101

Figure 3.18: A column chart showing the percentage of cloud-covered and cloud-free MGVI values that produced spikes in the MGVI time series values.....103

Figure 3.19: An example of atmospheric correction by the 6S model (Vermote et al., 1997). Note the absorption features at 760 nm and 865 nm in the top of atmosphere reflectance which are related to the presence of oxygen and water vapour. These are almost smoothed out in the corrected reflectance. 105

Figure 3.20: (a)-(h): The 2008 MGVI time series are displayed on the left (a,c,e,g), in black lines, with temporal deviation over the composite period represented as error bars. The 2008 MERIS radiance time series are located in their respective bands on the right (b,d,f,h), in multicoloured lines, with each pair corresponding to a single pixel and all four pixels identified as pastures.....109

Figure 4.1: Key seasonality metrics extracted from TIMESAT: Points (a) and (b) correspond to the start and end of the season, (c) and (d) mark the mid-season levels , (e) is the season maximum, (f) is the seasonal amplitude, (g) is the season length, (h) is the small seasonal integral and (i), the large seasonal integral, both of which describe seasonal productivity (Eklundh and Jönsson, 2010). 122

Figure 4.2: (a) The Savitsky-Golay (SG) filtering with a window size of 3 and (b) with a window size of 6. 124

Figure 4.3: The double logistic basis function in which the parameters x_1 and x_3 determine the position of the left and right inflection points respectively (Eklundh and Jönsson, 2010) 125

Figure 4.4: Asymmetric Gaussian local functions. In (a) the local parameter function which determines the width of the right function half has been decreased (solid line) and increased (dashed line) compared to the right function half. In (b) the parameter which determines the flatness of the right function half has been decreased (solid line) and increased (dashed line) compared to the value of the left half (Eklundh and Jönsson, 2010). 125

Figure 4.5: The TIMESAT Graphical User Interface (GUI) showing a time series of MERIS FAPAR data, 2003-2009, the first and last years are replicate years inserted to fit local model functions before they are merged for the global fit ..127

Figure 4.6: Four steps in applying TIMESAT curve fits to a pixel of mixed forest (51.810558N, 8.3172W). (A) Raw MGVI time series (B) Spike removal (C) Number of seasons calculated (D) Gaussian fit 128

Figure 4.7: Inter-comparisons of four sample fits to pixels of pasture land with the Savitzky-Golay filter (a)-(d) and asymmetric Gaussian functions (e)-(h) ...129

Figure 4.8: A comparison of the SOS image produced from the SG-filtered time series with a window size of 14 with that produced from fits to asymmetric Gaussian functions. The difference in range of SOS estimates produced by both methods can be seen in the histograms 130

Figure 4.9: A single time series modelled with both asymmetric Gaussian and double logistic fits.....131

Figure 4.10: Scaled relative frequency histograms for comparing the distribution of differences from (a) Logistic and (b) Gaussian model fits averaged over 100 pixels 132

Figure 4.11: The approach to RMSE analysis from which the asymmetric Gaussian fitting function was selected.....133

Figure 4.12: (a): The thin blue line represents raw MGVI time series. The thick black line shows the fitted Gaussian function from the first step without upper envelope setting applied, (b): Same as (a) except that the fitted Gaussian functions have been twice fitted to the upper envelope of the MGVI time series 137

Figure 4.13: The Gaussian model was fit to the valid MGVI range (1-255) with spikes removed and no upper envelope iteration applied. The base of the curve fit is shown by a red line.....138

Figure 4.14: The 2003 SOS estimated from an asymmetric Gaussian fit with minimum values forced to 100 with data gaps appearing in areas of vegetation below the FAPAR cut-off value for that season.....139

Figure 4.15 (a)-(h): Start of Season estimated from the asymmetric Gaussian fitted functions; (a) 2003, (b) 2004, (c) 2005, (d) 2006, (e) 2007, (f) 2008, (g) 2009, (h) 7-year mean. Time is in 10-day periods from 1 (Jan 1-10) to 20 (Jul 10-19) where 0 is no data. 142

Figure 5.1: The 2003-2009 mean SOS image calculated from an average of the annual input images from 2003 to 2009. A line transect has been drawn from West to East to show spatial variation in the SOS while the histogram, derived from the image, is indicative of the temporal trend in SOS. 150

Figure 5.2: The location of place names referred to in the text, and meteorological stations in section 5.7.....151

Figure 5.3:The variations in SOS dates over the marked transect (A-B) in figure 5.1. 151

Figure 5.4: The GTOPO 30 Digital Elevation Model (DEM) of Ireland with an elevation profile derived from the GTOP30 DEM at the same latitude as the SOS profile in figure 5.1. 153

Figure 5.5: The 2003 to 2009 mean number of SOS pixels per row (latitude) counted per 10-day period and normalised by the number of land pixels per row. 154

Figure 5.6: A relative density measure of SOS pixels per row (latitude) per 10-day period from 2003 to 2009. The number of SOS pixels has been normalised by the number of land pixels in each row. The scale shows the relative amount of SOS pixels per 10-day period. The same method was applied to CORINE landcover pixels to show the geographical distribution of landcover classes per degree latitude.....157

Figure 5.7: The 2003 to 2009 mean number of SOS pixels per column (longitude) counted per 10-day period and normalised by the number of land pixels per column. 158

Figure 5.8: The number of SOS pixels per column (longitude) per 10-day period from 2003 to 2009. The number of SOS pixels has been normalised by the number of land pixels in each column. The scale shows the relative amount of SOS pixels per 10-day period. The same method was applied to CORINE landcover pixels to show the geographical distribution of landcover classes per degree longitude 160

Figure 5.9: Annual SOS anomalies from the 7-year mean SOS in 10-day periods displayed as images (left) and histograms (right) showing the temporal patterns in anomaly values within each year 162

Figure 5.10: The annual percentage of pixels per anomaly bin. Changes in the magnitude and direction of the anomaly indicate shifts towards early or later SOS. 164

Figure 5.11: The merged CORINE 2000 (NI) and 2006 (ROI) landcover map with vegetation classes used in the analysis of SOS estimates 168

Figure 5.12 (a)-(d): Cumulative SOS in 2006 for three groups of landcover classes whose membership was derived from the K-W test. (a)Group A1, (b) Group A2 (c) Group B and (d) Group C 172

Figure 5.13: (a)-(d): Interannual variability in the median SOS for four groups of landcover classes whose membership was derived from the K-W test. (a)Group A1 , (b) Group A2, (c) Group B and (d) Group C . The first and third quartile values have been plotted as error bars. 174

Figure 5.14: The frequency distribution of elevation values in the resampled DEM grid and the cumulative percentage of the values per 50m interval. 176

Figure 5.15: The median start dates for grass growth in Ireland derived from Connaughton (1973) are shown with the 7-year mean (2003-2009) SOS estimated for pastures 178

Figure 5.16: Winter (a) and spring (b) mean air temperature at Valentia Observatory, Mullingar and Dublin airport with errors bars of 1 standard deviation 181

Figure 6.1: The scatter plot of SOS in 2009 and mean December temperature (2008). The marginal histograms show the distribution of values in the sample. The mixture of ordinal and continuous data creates a striped pattern in the scatter plot. 208

Figure 6.2: (a) Maximum rank correlation between SOS and mean monthly air temperature. (b) Timing of the maximum rank correlation (month), (c) Timing of

the maximum rank correlation (season), (d) p-value of the maximum rank correlation.....210

Figure 6.3 (a)-(d): The spatial distribution of the (a) extremely significant (b) highly significant (c) significant and (d) insignificant maximum rank correlations 211

Figure 6.4: (a) The significant winter maximum rank correlates (b) significant spring maximum rank correlates 212

Figure 6.5: Monthly mean NAO index from 2003 to 2011 214

Figure 6.6: The 2003-2009 annual grids of accumulated degree days from January 1st until day of year prior to SOS, calculated from daily minimum and maximum temperature data.....219

Figure 6.7: Frequency distributions and summary statistics for AGGDs in 2009 for the five most abundant landcover classes.....221

Figure 6.8: Box plots for the five landcover types illustrating the dispersion of the AGDDs on an interannual basis and the extent of outliers 225

Figure 6.9: AGDDs for the five landcover types using a base temperature of 0°C 227

List of Tables

Table 1.1: The current phenological garden network in Ireland, NPN=National Phenology Network, IPG=International Phenological Garden 6

Table 2.1: Current optical sensors used for vegetation monitoring (FR=Full Resolution, RR=Reduced Resolution, VIS=Visible, NIR=Near Infrared, TIR=Thermal Infrared, LWIR=Long Wave Infrared, PAN=Panchromatic) 24

Table 2.2: MERIS spectral band characteristics (ESA, 2005) 30

Table 3.1: The earliest and latest BO of the sampled tree species in 2008 and 2009..... 74

Table 3.2: The acquisition times of MERIS sensor per pixel during the composite period from 21st to the 30th January, 2006..... 95

Table 3.3: New pixel values assigned based on the comparison of coincident METEOSAT and MGVI pixels (note that an ocean mask prevents MGVI being calculated over open water) and the five test results from 21st January, 2006... 96

Table 3.4: The sample percentage values for test 1 and 3 were calculated from the number of pixels identified by each test as a percentage of valid MGVI values on that day. The mean test results per composite period are also included. 99-100

Table 3.5: The criteria for the six tests used to cross-check spiked and non-spiked values with the corresponding cloud flags are shown. 102

Table 4.1: A summary of the extracted seasonality metrics in TIMESAT 3.0 ..121

Table 4.2: Summary of the chosen TIMESAT settings for processing the entire MGVI dataset 134

Table 5.1: CORINE Landcover classes and their codes used in spatial analysis of the SOS.....156

Table 5.2: The proportions of the CORINE dataset that were included and excluded for the analysis of SOS including the thirteen vegetation classes and their percentage coverage.....167

Table 5.3: The landcover groups selected for SOS analysis by landcover type 171

Table 5.4: Coefficient of determination, slope and intercept of the linear regression of elevation and SOS.....177

Table 5.5: Mean and deviation from the 7-year mean winter temperatures (2003-2009) at the three meteorological stations used in the analysis of the SOS anomalies.....182

Table 5.6: Mean and deviation from the 7-year mean spring temperatures (2003-2009) at the three meteorological stations used in the analysis of the SOS anomalies.....182

Table 6.1: Error statistics for Tmax and Tmin, calculated on a daily basis and averaged over the year 204

Table 6.2: Spearman's rho (ρ) for the SOS and monthly and seasonal mean air temperature correlations, all correlations in bold are significant ($p<0.05$).....207

Table 6.3: The median AGDD per landcover type form 2003 to 2009, the 7-year median is included as a summary measure and the inter quartile range (IQR) is included to indicate the extent of variance within the seven year record 222

Table 6.4: The ranked landcover classes in terms of the number of AGDDs per year..... 22

Acronyms

1. AGDD Accumulated Growing Degree Day
2. API Application Programming Interface
3. ASCII American Standard Code for Information Interchange
4. AVHRR Advanced Very High Resolution Radiometer
5. BGS Beginning of the Growing Season
6. BIL Band Interleaved by line
7. BO Beginning of Leaf unfolding
8. BRDF Bidirectional Reflectance Distribution Function
9. BRF Bidirectional Reflectance Factor
10. CAP Common Agricultural Policy
11. CCRS Canada Centre for Remote Sensing
12. CEH Centre for Ecology and Hydrology
13. CEOS Committee on Earth Observation Satellites
14. CLM Cloud Mask product
15. CCI Climate Change Initiative (ESA)
16. CMRC Coastal ad Marine Research Centre
17. CORINE (Co-ORdination of INformation on the Environment)
18. CLC CORINE Land Cover
19. CSR Clear Sky Radiance Product
20. CYCLOPES Satellite products for change detection and carbon cycle assessment at the regional and global scales
21. DEM Digital Elevation Model
22. ECMWF European Centre for Medium Range Weather Forecasting
23. ECV Essential Climate Variable
24. EEA European Environment Agency
25. EGS End of growing season
26. EM ElectroMagnetic
27. EMR Electromagnetic Radiation
28. ENVISAT ENVIronmental SATellite
29. EPA Environmental Protection Agency
30. EROS Earth Resources Observation and Science
31. ESA European Space Agency
32. ESRI Environmental Systems Research Institute
33. ESRIN European Space Research Institute
34. ETM Enhanced Thematic Mapper
35. EUMETSAT European Organisation for the Exploitation of Meteorological Satellites
36. EVI Enhanced Vegetation Index
37. FAPAR Fraction of Absorbed Photosynthetically Active Radiation
38. FORTRAN The IBM Mathematical FORmula TRANslating System
39. FR Full Resolution
40. FTP File Transfer Protocol
41. GAC Global Area Coverage
42. GCOS Global Climate Observing System
43. GDD Growing Degree Day
44. GIMMS Global Inventory Mapping and Monitoring Studies
45. GIS Geographic Information System
46. GLOBCARBON Global Land Products for Carbon Model Assimilation
47. GMES Global Monitoring for Environment and Security
48. G-POD Grid Processing on Demand
49. GPS Global Positioning System
50. GPA Gradient Pattern Analysis
51. GUI Graphical User Interface
52. GVI Global Vegetation Index
53. HDF Hierarchal data format

54. IDL Interactive Data Language
55. IDW Inverse Distance Weighting
56. IFOV Instantaneous Field Of View
57. IPG International Phenological Gardens
58. IPCC Intergovernmental Panel on Climate Change
59. IQR Inter Quartile Range
60. IRS Indian Remote Sensing Satellite
61. ITC University of Twente's Faculty of Geo-Information Science and Earth Observation
62. JRC Joint Research Centre
63. K-W Kruskal-Wallis test
64. LAC Local Area Coverage
65. LAI Leaf Area Index
66. LOOCV Leave One Out Cross Validation
67. LF Leaf Fall
68. LGS Length of Growing Season
69. Lidar Light Detection and Ranging
70. LPV Land Product Validation subgroup of CEOS
71. LSP Land Surface Phenology
72. LST Land Surface Temperature
73. LUCAS Land Use/Cover Area frame Statistical survey
74. MARF Meteorological Archive and Retrieval Facility
75. MERIS Medium Resolution Imaging Spectrometer
76. MGVI MERIS Global Vegetation Index
77. MISR Multiangle Imaging Spectroradiometer
78. MLAP MERIS Land Surface Aggregated Product
79. MODIS Moderate Resolution Imaging Spectroradiometer
80. MSG Meteosat Second Generation
81. MSS Multi Spectral Scanner
82. MTCI MERIS Terrestrial Chlorophyll Index
83. MTCP MERIS level 3 Time-Composited Products
84. MVC Maximum Value Composite
85. NAO North Atlantic Oscillation
86. NASA National Aeronautics and Space Administration
87. NDVI Normalised Difference Vegetation Index
88. NetCDF Network Common Data Frame
89. NI Northern Ireland
90. NIR Near Infrared
91. NN Nearest Neighbour
92. NOAA National Oceanic and Atmospheric Administration
93. PAR Photosynthetically Active Radiation
94. REP Red Edge Position
95. ROI Republic of Ireland
96. RR Reduced Resolution
97. SAVI Soil Adjusted Vegetation Index
98. SeaWiFS Sea-viewing Wide Field-of-view Sensor
99. SEDAC Socioeconomic Data and Applications Centre
100. SEVIRI Spinning Enhanced Visible and Infrared Imager
101. SOS Start of Season
102. SPOT Système Probatoire d'Observation de la Terre
103. SR Simple Ratio
104. SWIR Short Wave Infrared
105. TIR Thermal Infrared
106. TM Thematic Mapper
107. TOA Top of Atmosphere
108. UAV Unmanned Airborne Vehicle
109. UKMO UK Meteorological Office
110. UNFCCC United Nations Framework Convention on Climate Change
111. USGS United States Geological Survey
112. UTC Coordinated Universal Time

113. VGT VEGETATION
114. VI Vegetation Index
115. VIS Visible
116. WV Water Vapour

Chapter 1. Introduction to vegetation phenology

1.1 Background

Phenology is chiefly concerned with studying the temporal patterns of biological events (de Beurs and Henebry, 2008a). Another similar term is seasonality which can describe the timing of events in both biotic and abiotic components of the Earth system (Leith, 1974). Therefore, seasonality can influence phenology and vice versa, for example, the annual spring thaw in snow-covered regions initiates budburst and leaf development in underlying vegetation. The terms, vegetation seasonality and phenology are closely related; however their use varies according to the discipline of study. Several definitions of phenology exist, the earliest by the Greek botanist, Theophrastus (372-288 B.C.): *'…Instead every plant must possess a certain adjustment to the season, since the season turns out to be more responsible [for sprouting] than anything else…'* The Swedish botanist Linnaeus, who is regarded as the father of phenology, stated in his Philosophia Botanica (1751) '*that observations of first flowering, leafing, fruiting and leaf-fall should be made all over Sweden, along with local weather'*. The more recent and widely accepted definition is by Leith in 1974: "*Phenology is generally described as the art of observing life cycle phases or activities of plants and animals in their temporal occurrence throughout the year*" (Leith, 1974). However, he defines seasonality as "*the occurrence of certain obvious biotic and abiotic events or groups of events within a definite limited period or periods of the astronomic (solar, calendar) year*". These definitions imply that while

seasonal events are expected to occur on an annual basis, phenology is not restricted to annual phenomena.

1.1.1 Phenology as an indicator of climate change and ecosystem health

Phenology is a ready indicator of the impact of climate change on the biosphere (Sweeney et al., 2002). Indeed, an extension of the growing season in trees and shrubs by 10.8 days since the early 1960s has been identified across Europe as a result of changes in air temperature over the same time period (Menzel and Fabian, 1999). Phenology is also an important economic indicator in sectors such as agriculture and forestry. Observing the phenology of fruit trees, crops and forests can potentially be used in forecasting yield and monitoring the health of plants and trees. However, phenology is also an essential component of ecosystem functioning. For example, the timing of onset or duration of a phenological phase, or "phenophase", can trigger other components of the ecosystem such as the availability of water, the onset of pests and disease, nutrient and carbon uptake and storage in plant biomass ((van Vliet, Overeem et al. 2002), Butterfield and Malström, 2009). Furthermore, the lifecycles of groups of organisms in an ecosystem are reliant on one another in a process known as synchrony (Thackeray et al., 2010). In terrestrial communities, the ecosystem structure is delicately balanced with development of the vegetation canopy (Fitter and Fitter, 2002) and the synchrony of life cycles can therefore be easily disrupted if phenophases in trees and plants are altered under changing climate conditions.

1.1.2 Monitoring vegetation phenologyObservations of the following phenological phases are made in the International Phenological Gardens (IPG, 2005):

- Leaf unfolding: The first regular surfaces of leaves become visible in three or four places on the same plant. The leaf must have emerged from the bud up to the leaf stalk.
- Mayshoot: First sign of the spring sprout in conifers. However the needles are not yet expanded
- St. John's sprout: The first sprouts of oaks and mountain ashes are followed by a second sprout which can be identified by its fresher colour
- Beginning of flowering: The first flowers emerge in several places on the observed plant resulting in the release of pollen by the anthers
- General flowering: More than half of the flowers on the observed plant have blossomed
- First ripe fruits: The fruits have ripened in several places on the observed plant and can be characterised by a definite colour
- Autumn colouring: More than half the leaves of the observed plant have changed their colour due to the drop in air temperature as opposed to decolouration accompanying withering in summer due to drought
- Leaf fall: More than half the leaves of the observed plant have fallen

The leaf unfolding stage, which marks the beginning of the growing season, has garnered the most interest as it has exhibited strong responses to temperature changes over the last few decades. For example, the onset of spring and summer phases such as leaf unfolding and flowering has advanced by 2.5 to 6.7 days per

ºC warmer spring on the basis of long term (1951-2000) observations of 20 plant species across Germany (Menzel, 2003). In a study of four tree species observed at the IPG network (*Betula pubescens*, *Prunus avium*, *Sorbus aucuparia* and *Ribes alpinum*) from 1969 to 1998, spring warming (February to April) across Europe has been linked to an advance in leafing dates by 8 days (Chmielewski and Rotzer, 2001). A later study found that 78% of all leafing, flowering and fruiting records had advanced (30% significantly) across Europe from 1971-2000 (Menzel et al., 2006). Other studies have analysed phenophases in an ensemble of taxonomic groups, such as migratory dates in birds and butterfly emergence, as well as budburst and leaf unfolding dates in tree species, and have shown an advance of spring phenophases in recent decades in the Northern Hemisphere by 2.8 days per decade (Parmesan, 2007) and across Europe by 2.5 days per decade from 1971 to 2000 (Menzel et al., 2006).

In contrast to the systematic observations of phenophases in certain tree species conducted at the IPG gardens, other vegetation types such as grasslands do not exhibit such readily observable phenophases. Therefore, historical records of phenological timing in these vegetation types are less common and evidence to support their responses to climate change difficult to find. Much of the data on tree phenology across Europe has been from the International Phenological Garden (IPG) network which was established in Europe in 1957 to gather phenological data from tree species of identical genetic stock (Chmielewski and Rotzer, 2001). There are currently 50 IPGs across Europe in which 23 tree species are observed (Chmielewski and Rotzer, 2001); six of these sites were established in Ireland between 1966 and 1967 (Donnelly et al., 2006), although

two of the sites, at Glenveagh National Park and the Armagh Observatory do not actively contribute data to the IPG network. The active Irish IPG gardens are located at Valentia Observatory in Co. Kerry, John F. Kennedy Arboretum and Johnstown Castle in Co. Wexford and the National Botanic Gardens in Co. Dublin. The data are gathered by Met Éireann staff and archived at the IPG centre at Humboldt Universität in Berlin (Sweeney et al., 2002). The phenological garden network has since been regenerated and expanded (Proctor and Donnelly, 2009). The location of the new and expanded network of gardens is shown in figure 1.1, while the garden names and the network to which they belong is listed in table 1.1

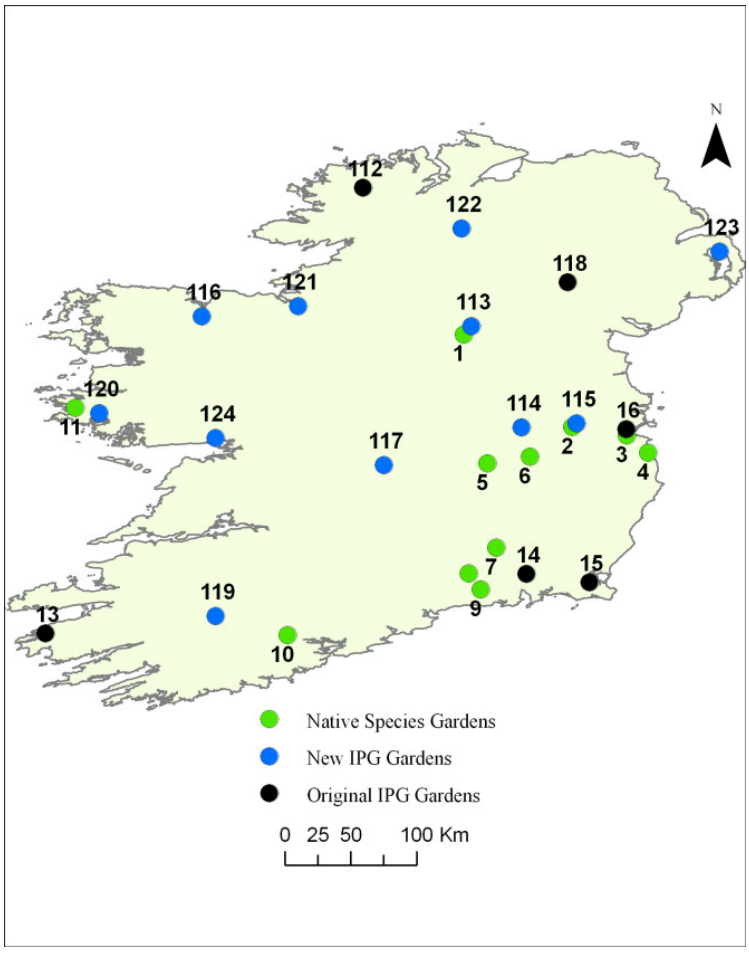

Figure 1.1: The locations of the phenological gardens in Ireland (Garden names listed in table 1.1)

Table 1.1: The current phenological garden network in Ireland, NPN=National Phenology Network, IPG=International Phenological Garden

Garden No.	Network	Name
1	NPN-IE	Farnham Estate, Co. Cavan
2	NPN-IE	Lodge Park Walled Garden, Co. Kildare
3	NPN-IE	Airfield Trust, Co. Dublin
4	NPN-IE	Killruddery House, Co. Wicklow
5	NPN-IE	Emo Court, Co. Laois
6	NPN-IE	Irish National Stud Co Ltd, Co. Kildare
7	NPN-IE	Mount Juliet, Co. Kilkenny
8	NPN-IE	Kildalton Horticultural College, Co Kilkenny
9	NPN-IE	Mount Congreve, Co Waterford
10	NPN-IE	Blarney Castle, Co. Cork
11	NPN-IE	Errislannan Manor Gardens, Co. Galway
13	IPG	Valentia Observatory, Co. Kerry
14	IPG	JFK Arboretum, New Ross, Co. Wexford
15	IPG	Johnstown Castle, Co. Wexford
16	IPG	National Botanic Gardens, Co. Dublin
112	IPG	Glenveagh National Park, Co. Donegal
113	IPG	Ballyhaise College, Co. Cavan
114	IPG	Williamstown House, Co. Kildare
115	IPG	Carton Estate , Co. Kildare
116	IPG	Enniscoe House, Co. Mayo
117	IPG	Birr Castle, Co. Offaly
118	IPG	Armagh Observatory, Co. Armagh, Northern Ireland
119	IPG	Millstreet Country Park, Co. Cork
120	IPG	Ballynahinch Castle, Connemara, Co. Galway
121	IPG	Markree Castle, Co. Sligo
122	IPG	Baronscourt ,Tyrone, Northern Ireland
123	IPG	Mount Stewart, Down, Northern Ireland

However professional observer networks such as the IPG network are not the only source of ground-based phenology data. For example, the recording of phenological phases in plants has been a continual practice for amateur observers as far back as the 1730s in the U.K. (Sparks et al., 2000) and a single observer has recorded first flowering times of 557 plant species over 47 years in one location in south-central England (Fitter and Fitter, 2002). In western Canada, historical databases of flowering data for many native plant species date back to the late 1800s (Beaubien and Freeland, 2000). Such datasets are valuable in terms of offering historical records on particular plant or tree species but lack the spatial coverage offered by more widespread coordinated observer networks or

remote sensing for example. In Ireland, Nature Watch has been established by the National Biodiversity Data Centre as an online repository for public sightings of phenological events (National Biodiversity Data Centre, 2009). A similar initiative, Nature's Calendar, has been operated by the Woodland Trust and Centre for Ecology and Hydrology (CEH) in the U.K since 2000 and now has 40,000 registered observers (Amano et al., 2010). There is a spectrum of expertise in ground-based observing methods from untrained citizen networks of observers in scattered locations to skilled professionals forming a dedicated network. However, while they provide extensive spatial coverage and historical records on phenology, the citizen networks do not systematically record the same plant species over common time periods and tend to be less objective than observations from professional networks.

1.1.3 Phenology and climate

The observational data from the four active IPG gardens in Ireland were subjected to a preliminary analysis on three of the nine tree species observed at the four gardens from 1970 to 2000; *Betula pubescens* (White or Downy birch), *Fagus sylvatica 'Har'* (common beech) and *Tilia cordata* (Small-leaved lime) (Sweeney et al., 2002). A refinement of the study was later carried out which included all nine tree species and applied more rigorous statistical techniques to demonstrate relationships between climate and phenology (Sweeney et al., 2008). Preliminary results showed that the beginning of the growing season (BGS), determined from the date of leaf unfolding, showed the strongest response to climate differences. The refined results confirmed that the BGS at all sites has become significantly earlier since 1970 for some but not all tree species. At Valentia, all species/cultivars, except *Betula pubescens* are now leafing earlier

than in the 1970s (Sweeney et al., 2008) and by 2000 the BGS for *Fagus sylvatica* was occurring at Valentia up to ten days per decade earlier than 30 years previously. This is one of the most marked increases in any of the European IPG sites and, with a later leaf fall date, has caused a lengthening of the growing season at Valentia, for that species, by as much as 90 days (Donnelly et al., 2006). However, there was little evidence to suggest that the end of the growing season (the date of leaf fall) occurred later in any of the other observed species (Sweeney et al., 2002).

The length of growing season (LGS) increased significantly across the whole European IPG network period from 1959 to 1993. The extension of the season by 10.8 days has been caused by an advancement of the BGS by 6 days and a delay in leaf fall by 4.8 days, linked to increases in air temperature over the same time period (Menzel and Fabian, 1999). Similar results have been shown in the flowering time of 385 British flowering species, as the average first flowering date had advanced by 4.5 days during the 1990s compared to the previous four decades (Fitter and Fitter, 2002). It was also shown that for species flowering in the spring months, increases in the previous month's spring temperature were correlated with earlier flowering times. More recent evaluations of the phenology of 726 UK terrestrial, freshwater and marine spring and summer events have proven their advancement at a rate more rapidly than previously thought (Thackeray et al., 2010). Of the taxonomic groups examined which included plants, invertebrates and vertebrates, leafing, flowering and fruiting dates of terrestrial plants showed the most rapid mean rate of change (0.58 days per year) and the highest percentage of advancing trends (92.5%). Such changes have

been consistent with warming trends. Of a 250-year community level index of first flowering dates for 405 plant species across Britain, the most recent 25 years was 2.2–12.7 days earlier than any other consecutive 25-year period since 1760. The mean Central England Temperature (CET) record from February to April showed the strongest correlation with the index indicating that a rate of advance with temperature of five days per 1°C rise (Amano et al., 2010).

In a study of the phenology of natural vegetation as well as fruit trees and field crops from 1961-2000 in Germany, it was found that an increase in average air temperature in early spring of 1°C leads to an advanced beginning of growing season in annual crops such as maize and sugar beet and in the blossoming of fruit trees by about 5 days (Chmielewski et al., 2004). It was concluded that climatic changes influenced annual crops and fruit trees in much the same way as natural vegetation, demonstrating that a similar physiological response occurs in all plants in response to changing air temperatures.

The results of Chmielewski and Rotzer for Europe (2001) are similar to those for the same time period in North America (Schwartz and Reiter, 2000). However, there has not been a continent-wide network of phenological gardens in the United States comparable to that of the European IPG network. The USA National Phenology Network (NPN) originated in 1956 from a network of lilac observers in 12 states on the west coast which amounted to 2,500 observers by 1972 and spread to the east coast in 1961, which had 300 observers in 1970 (USA NPN, 2011). Therefore, due to the limited amount of phenological garden data, budburst and leaf fall dates across North America have been simulated

using phenological models, stating an average advancement of 5-6 days in spring growth (Schwartz and Reiter, 2000). These results show broad agreement over two continents with respect to the onset of early spring growth, however Schwartz and Reiter (2000) could not make a similar comparison with autumn leaf fall dates due to a paucity of phenology data for that time of year. Therefore no reliable estimates have been derived from *in-situ* observations for the length of the growing season in North America.

1.1.4 Phenology and non-climatic factors

Temperature may not be the only variable influencing the observed trends in phenology. Previous research has recognised the problematic issue of multiple, non-climatic factors in driving phenological change (de Beurs and Henebry, 2004, White et al., 2005, Xiao and Moody, 2005). Other than climate change, improved fertilisation and the availability of greater amounts of atmospheric CO_2 have also been argued as contributory factors to the observed greening trend. It has also been suggested that changing agricultural practices are equal to, if not more influential than, climate on global greening patterns (Xiao and Moody, 2005). For example, the extent to which the phenology of vegetation can be altered on a national-scale due to institutional change as was shown in Kazakhstan following the collapse of communism and the resulting change in land management practices (de Beurs and Henebry, 2004).

Generally, carbon uptake by growing plants at the beginning of the growing season is coincident with a decline in atmospheric carbon dioxide (CO_2) which can be observed in the global carbon cycle. The interdependence of the vegetation growing season and the carbon cycle can be seen in the seasonal

variation in CO_2 measured at the Mauna Loa Observatory, Hawaii since the 1960s (Keeling et al., 1996). Figure 1.2 shows this seasonal variation measured at Mauna Loa and Mace Head Observatory, Ireland, as well as the general trend of increasing CO_2 concentration in the atmosphere.

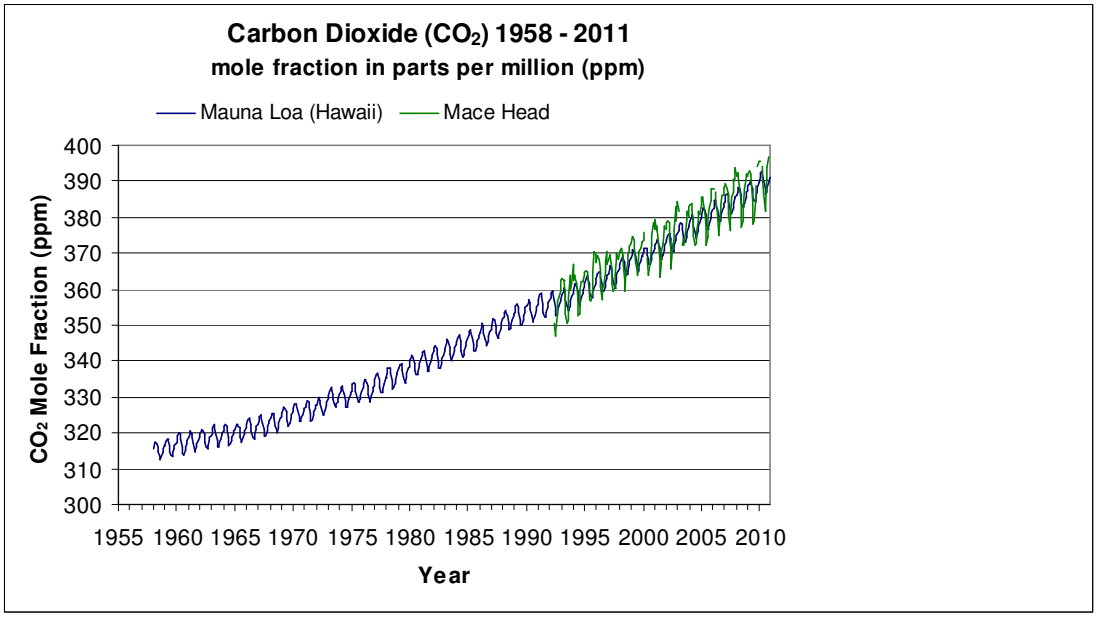

Figure 1.2: Measurements in Hawaii since 1958 and Mace Head since 1992 show the seasonality of the carbon cycle as well as steadily increasing concentrations of atmospheric CO_2

A later seven-day phase shift in the declining part of the cycle was observed and attributed to a lengthening of the growing season in Northern Hemisphere vegetation. This greening trend, coupled with an increase in the seasonal amplitude of atmospheric CO_2, indicate increasing CO_2 assimilation by terrestrial vegetation due to climate warming. Future increases in atmospheric CO_2 as a result of continued fossil fuel burning and other anthropogenic activities may therefore further alter the spatial distribution of vegetation biomes. For example, were CO_2 to double in the next 100 years in Russia, new biomes such as scrubland, would appear for the first time in European Russia while others, e.g. grassland could expand (Belotelov et al., 1996).

The urban/rural fabric of an area can also determine phenological timing. For urban vegetation, greenup onset occurs earlier and dormancy onset later, relative to rural surrounds, driven by an elevated land surface temperature (LST) in urban areas (Zhang et al., 2004b). Elevated LST causes mean annual temperatures and average spring temperatures to be about 1-3ºC higher than rural surrounds. The length of the growing season in urban areas of the U.S.A. has been found to be up to 15 days longer than in rural areas. The impact of the urban heat island on vegetation phenology was more pronounced in the U.S.A. than in Europe or Asia as the differences in LST between urban and rural areas was greater in the U.S.A. (Zhang et al., 2004b).

1.2 Study aim

The temporal trends observed in tree phenology in Ireland have been based on observations from four phenological gardens located in the southern half of the country where tree species have been selected based on the IPG criteria. While these studies have been invaluable in demonstrating the changes in phenology of trees due to climate change at point locations in Ireland, the results do not reflect broad-scale patterns in vegetation phenology across the whole island or in a variety of vegetation types. Therefore, the aim of this study was to investigate the feasibility of using satellite remote sensing as a tool to characterise these broad-scale patterns by monitoring vegetation seasonality on a national-scale. This study has developed a methodology for monitoring national-scale vegetation phenology across the island of Ireland based on low resolution satellite imagery acquired on a near daily basis from 2003-2009. A seven year time series of satellite imagery permits interannual variation in seasonality patterns to be

tracked, with the potential for linking them to trends in climate factors over the same time period. The findings of this study are intended to complement existing ground-based observations of vegetation phenology and highlight the utility of remote sensing as a broad-scale monitoring tool.

1.3 Research objectives

Within the overall aim of this research, it was necessary to choose an appropriate time series analysis method and adapt it to a multi-annual image set at an appropriate temporal and spatial resolution in order to characterise and investigate spatio-temporal patterns in the vegetation Start of Season (SOS) across the island of Ireland. It was necessary to gather MGVI data, acquired at an appropriate temporal and spatial resolution, to achieve the national-scale aims of the study. The link between interannual variability in SOS and climate was also explored using air temperature as a climate variable. In order to achieve the study aim, a number of sub-objectives were established which guided the research in a stepwise approach:

1. To identify a sensor with near daily medium spatial resolution image acquisition over Ireland, which would permit the use of a vegetation index (VI) with maximal sensitivity to changes in the seasonality of land surface vegetation.
2. To select an appropriate composite period for the daily VI data that would minimise the data loss due to cloud while retaining sensitivity to vegetation seasonality changes. Criteria used to guide the selection of a composite period were based on ground-based observations of tree greening and cloud cover at representative point locations on the island.

3. To establish the most appropriate methodology for the systematic extraction of a SOS measure from the time series of VI data.
4. To describe both qualitatively and quantitatively the spatio-temporal patterns in the vegetation SOS across the island of Ireland. In order to achieve this objective, SOS spatial patterns were first characterised descriptively and then explanatory factors such as landcover were used to statistically analyse the degree of similarity in SOS between different landcover types.
5. To explore the consistency in the estimated SOS between managed and natural landcover types. As vegetation seasonality is closely linked to landcover and land use, there would be differences expected in SOS between natural and managed vegetation.
6. To determine if statistically significant relationships exist between climate variables based on air temperature and the SOS given the proven dependence between growing season timing in Northern high latitudes and air temperature variation.

The thesis is composed of seven chapters. The first chapter is a background introduction to the science of phenology which describes *in-situ* phenology monitoring and the outcomes from the last few decades of research, both in Ireland and further afield. The second chapter introduces the physical principles underlying optical satellite remote sensing of vegetation and the methods that have evolved to monitor vegetation phenology at a variety of spatial and temporal scales. Chapter three identifies the implications of cloud cover over Ireland for vegetation seasonality monitoring and how techniques such as time compositing were used to generate sufficient cloud-free imagery of the whole

island to allow the national-scale aims of the study to be achieved. Chapter four describes a methodology to extract seasonality metrics from the time series of satellite-derived data. Chapter five examines the spatio-temporal patterns in vegetation seasonality in the data generated from the time series analysis and demonstrates the link between landcover and climate with the spatio-temporal patterns observed. Chapter six is an analysis of gridded air temperature measurements provided by Met Éireann linking them to variability in SOS over the 7-year period of the study. Raw air temperatures as well as growing degree days were used to explore the SOS-climate interactions. The final chapter highlights the major findings of the thesis and assesses the significance of the work in the wider context of land surface phenology studies. The future of the research discipline is discussed in terms of upcoming vegetation monitoring satellite sensors. The task of validating satellite-derived phenology products with ground-based sensors is also described as is Ireland's potential contribution to this growing field of international research.

Chapter 2. Satellite remote sensing of vegetation

2.1 The Physical Principles of Remote Sensing

Electromagnetic radiation (EMR) is energy propagated through space via electric and magnetic fields. The electromagnetic spectrum (figure 2.1) is the expanse of that energy encompassing cosmic rays, gamma rays, X-rays and ultraviolet to visible and infrared radiation including microwave energy (EROS, 2011). However, the visible, infrared and microwave wavelengths of the spectrum are most useful for space-based remote sensing as gamma, x-rays and ultraviolet rays are attenuated by the Earth's atmosphere and are poorly transmitted through space. Therefore remote sensing systems such as satellite sensors have been designed to measure radiation in very narrow parts of the visible to microwave spectrum which allows them to record information about distant objects.

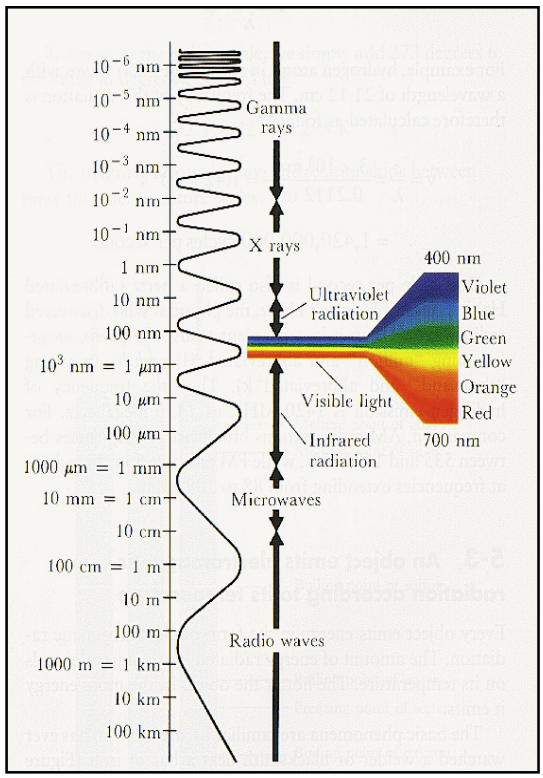

Figure 2.1: The Electromagnetic Spectrum (John Hopkins University, 2011)

The wavelike characteristics of electromagnetic radiation form the basis of the electromagnetic spectrum (Mather, 1999). The characteristics and behaviour of EMR depends on its wavelength, therefore, data about a target object recorded in one part of the spectrum, differs from that in other wavelengths of the spectrum (SEDAC, 2011). Unlike other wave types which require a medium to travel through, e.g. water waves, electromagnetic waves can travel through a vacuum. It is this key concept that allows space-borne sensors to record EMR reflected or emitted from an Earth-based target located a considerable distance from the sensor. The Sun is the main source of EMR. As incident solar radiation encounters the Earth's surface, it is transmitted, absorbed or reflected. Some of the absorbed component heats the surface and is reradiated as infrared radiation (figure 2.2). However, not all the reflected solar or reradiated thermal radiation escapes the Earth's atmosphere. The processes of absorption, transmission and reflectance modify incoming solar radiation as it propagates through the atmosphere, for instance, gas molecules scatter and absorb some EMR.

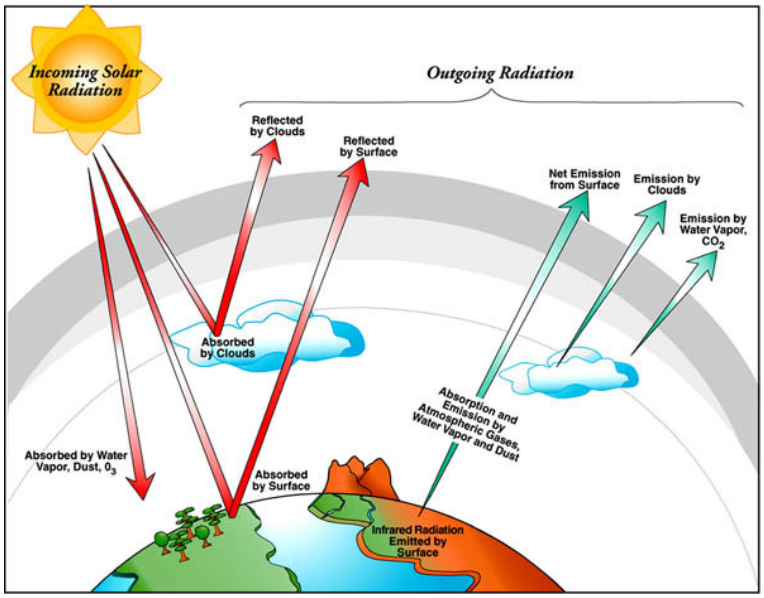

Figure 2.2: Solar Radiation is subject to varying atmospheric processes in the Earth's Atmosphere (Ackerman and Whittaker, 2011)

The energy incident on the Earth's surface follows the principle of conservation of energy:

Incident Energy = Reflected energy + Absorbed energy + Transmitted energy

As reflected energy propagates away from the surface of the Earth, it is attenuated (weakened) to some degree by the Earth's atmosphere however; the exact magnitude of this is usually unknown. Therefore, the principle of conservation of energy is used as a basis to construct radiative transfer equations to deduce the unknown quantitative of reflected, absorbed or transmitted solar energy when the incident energy is known. Inversely, incident radiation can also be derived from satellite reflectance data when the values of the other three parameters are known. In analysing the reflectance properties of an object, the remote sensing analyst can infer its spectral characteristics. Some of the various physical surfaces encountered by a space-borne satellite sensor are illustrated in figure 2.3.

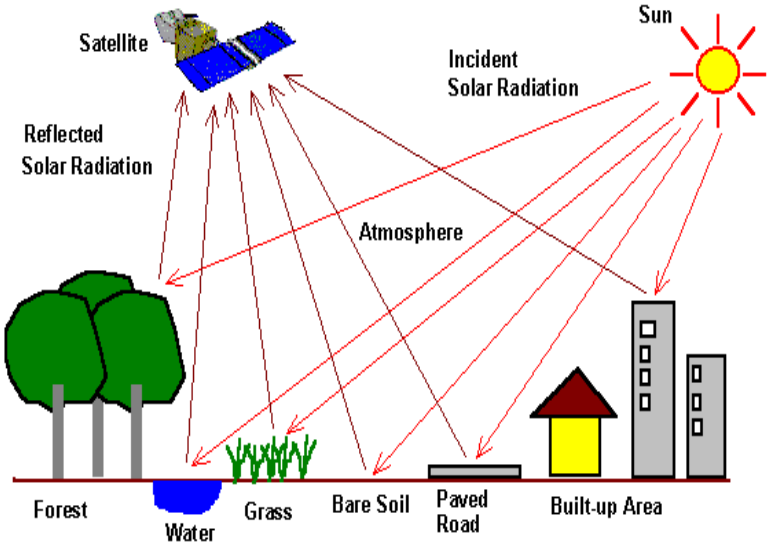

Figure 2.3: **Reflectance from Earth surface features in the remote sensing process (CRISP, 2001)**

These surfaces exhibit different physical properties which will determine the nature of interaction with incident energy, and as a result, the proportion of

energy reflected. When a surface is smooth, such as a paved road, it reflects radiation in one direction behaving much like a mirror. This type of reflectance, directed equally in one direction, is known as isotropic reflectance and reflectors of this nature can appear as bright surfaces in satellite imagery if energy is reflected in the direction of the satellite sensor; otherwise they appear dark. However, in the case of a rough surface, such as a tree canopy, the reflected radiation will be diffused unequally in many directions, causing surface reflectance to vary with the angle of observation; this is known as anisotropic reflectance. In order to account for anisotropy, a correction factor known as the bidirectional reflectance distribution function (BRDF) is applied to satellite-measured reflectance data.

2.1.1 Overview of Optical Remote Sensing

The optical spectrum spans the visible (blue, green and red) and near-infrared wavelengths of the electromagnetic spectrum from 400 to 900 nm. As there is a continuum of EMR in the spectrum, a spectral signature for a surface can be defined by regular measurements of reflectance at closely–spaced intervals within defined wavelength intervals, or bandwidths. This segmentation of the spectrum into discrete parts is exploited by multispectral remote sensing, providing a tool for readily identifying different surfaces in the same image scene by inspection of their spectral signatures. Depending on the sensor's spectral resolution, i.e. the wavelength of electromagnetic waves measured by a sensor, how close together the measurement intervals are and the bandwidth of the intervals, the spectral signature of an object can be refined to varying levels of detail. Therefore, the use of multispectral images for distinguishing surface materials increases with the sensor's spectral range and spectral resolution.

Greater spectral resolution results in a clearer separation among the surface objects. Hyperspectral sensors measure radiation in very finely-spaced intervals and are used to identify subtle differences between surface materials, e.g. identification of different rock types. Coarser differences in surface features, e.g., grass, soil, snow or bare rock, are easily defined by wider spectral bands carefully positioned in the spectrum to exploit the different spectral properties of these features. This principle of multispectral remote sensing is illustrated in the spectral signatures of figure 2.4 as the percentage reflectance varies according to the type of surface material; healthy vegetation is clearly distinguishable from clear water in the red and infrared portion of the spectrum (between 0.7 and 1.0 µm) but is barely distinguishable from turbid water in the green spectrum (0.6-0.7 µm). Multispectral analysis permits the characterisation of different surfaces in satellite imagery, for example urban from rural areas, distinguishing forests from fields as well as many other natural and artificial surface categorisations.

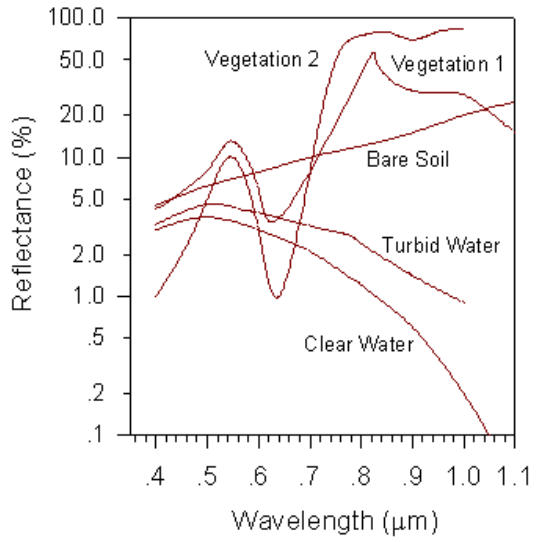

Figure 2.4: Multispectral remote sensing. The spectral response of clear water and vegetation are clearly distinguishable with increasing wavelength in the near infrared (>.7 µm) (CRISP 2001).

2.1.2 Further Concepts in Optical Remote Sensing

The Instantaneous Field Of View (IFOV) of a satellite sensor is a measure of the ground area covered by the sensor as it scans across the swath width. Therefore, the IFOV is smaller in the centre of the image swath and larger at its edges. The IFOV is an important determinant of the sensor's spatial resolution, which indicates the minimum size of the objects that can be identified and thus the detail depicted in a satellite image. The spatial resolution is maximised at the sensor's nadir while it degrades towards the edges due to the high angle of observation of the instrument and the resultant increase in the IFOV, however pixels are later resampled to the same spatial resolution across the image scene. The spatial resolution is measured in metres and determines the dimensions of the basic image unit, the pixel, which is an averaged percentage energy value per unit area.

The orbit of a remote sensing satellite describes its movement along a fixed path in navigating around the globe. Low Earth observation satellites are normally near-polar orbiting so that they scan the Earth in strips as they descend in a North- South and ascend in a South-North direction across the Equator. The rotation of the Earth in an easterly direction below the sensor ensures that the entire Earth surface is imaged over a period of time. As the satellite always follows the same orbit, imagery is acquired on a regular and repeatable basis although differences in solar illumination conditions at the time of image acquisition can be mistakenly interpreted as changing surface conditions. To minimise this effect, Earth observation satellites are sun-synchronous in orbit. A sun-synchronous orbit will ensure that imagery is acquired at the same mean local solar time for any point on the Earth's surface at the same time each year.

However, seasonal variations in the angle of solar illumination means that illumination conditions are different even for imagery acquired at the same time of day, especially at higher latitudes. The reliance of optical sensors on the Sun as a source of illumination prevents them from functioning at night. Clouds pose a further challenge as water vapour absorbs near infrared radiation and reflects visible light; therefore, acquiring clear imagery of the Earth's surface is impossible in the optical domain where cloud cover is present.

2.2. Monitoring Vegetation Using Optical Sensors

Healthy, living, green vegetation synthesises food through a series of complex chemical reactions, harnessing carbon dioxide in the atmosphere and releasing oxygen in a process called photosynthesis. Chemical reactions driving the process take place in the presence of the chlorophyll in the leaf and are activated by incident solar radiation (Campbell, 2002). Photosynthesising plants strongly absorb light in the red portion of the visible spectrum and strongly scatter it in the near infrared portion, as can be seen from the spectral signature of vegetation in figure 2.4. This differential reflectance of light is due to the internal leaf structure of plants (Campbell, 2002). The inverse relationship in reflectance between the red and infrared spectrum is captured in the location of the Red Edge Position (REP) which marks the transition from red absorption to near infrared reflection. The accurate detection of red and near infrared reflectance and the determination of the REP forms the basis for the construction of vegetation indices (see section 2.3). The scattering of light in a vegetation canopy can be more complex than that from an individual leaf. However, as internal reflection occurs between the soil and various canopy layers, and reflection shadows are

created between them. Indeed, it has been shown that the strength of the satellite-measured NIR reflectance from coniferous trees is determined by the canopy volume due to this internal scattering effect (Danson and Curran, 1993).

Optical satellite sensors employed for the monitoring of vegetation are designed to measure reflectance using spectral bands in the visible (400 nm – 700 nm) and near (700-1100 nm) to mid (1100 – 3000 nm) infrared portion of the electromagnetic spectrum. Satellite sensors that are commonly employed for vegetation monitoring are briefly described below and their characteristics summarised in table 2.1. The sensors can be broadly categorised into three groups determined by their spatial resolution. Coarse spatial resolution sensors (> 1km) offer daily global coverage of large areas but in low spatial detail. Medium spatial resolution sensors (250m-1km) image the globe in one to three days but generally offer better spectral range and resolution and finer image detail than broad coverage sensors. High spatial resolution sensors (1- 250m) can take approximately two weeks to acquire global image data but provide a higher level of spatial detail with a moderate spectral range and resolution. Very high spatial resolution sensors (≤ 1m) allow extremely precise spatial details to be resolved in narrow-swath imagery, however this is typically in a limited range of spectral bands and they are therefore rarely used in vegetation monitoring applications.

Table 2.1: Current optical sensors used for vegetation monitoring (FR=Full Resolution, RR=Reduced Resolution, VIS=Visible, NIR=Near Infrared,

Platform	*Sensor*	*Launch date*	*Orbit Altitude (km)*	*Swath Width (km)*	*Revisit Time (days)*	*Spatial & Spectral Resolution*			*Band Arrangement*	*Status*	
						No. of bands	*Spatial resolution (Metres)*	*Spectral Range (nm)*		**Access**	**Cost**
Envisat	MERIS	2002	800	1150 (FR)/ 575 (RR)	3	15	300 (FR)/ 1200 (RR)	VIS (412-775) NIR (865-900)	1-12 (VIS) 13-15 (NIR	G-POD No charge	
Terra	MODIS	1999	705	2330	1-2	36	250 (bands 1-2) 500 (bands 3-7) 1000 (bands 8-36)	VIS (405-753) NIR (841-1250)	1,3,4,8-15 (VIS) 2,5,16-19 (NIR)	Different online archive depending on desired product No charge	
Aqua		2002									
NOAA10,11,12 ,14, METOP	AVHRR 2	1986-2006	817-870	3000	0.5	5	1100 (FR)/ 4000 (RR)	VIS (580-680) NIR (725-1100, 1580-1640)	1(VIS), 2 (NIR), 3 (SWIR), 4-5 (TIR)	Global datasets freely available	
	AVHRR 3					6			1 (VIS) 2, 3A (NIR) 3B, 4,5 (TIR)		
SPOT 4	VEGETATION	1998	832	2250	1	4	1000	VIS (430-470, 610-680),NIR (780-890)	1-2 (VIS) 3 (NIR)	On request from SPOT with costing	
SPOT 5		2002									
Orbview-2	SeaWiFS	1997	705	2801(FR)/ 1502(RR)	1	8	1100 (FR)/4500 (RR)	VIS (402-785) NIR (845-885)	1-7 (VIS) 8 (NIR)	Freely available for research	
Landsat 5	Thematic Mapper (TM)	1984	705	185	16	7	30 (bands 1-5,7) 120 (band 6)	VIS (450-900) NIR (1550-1750) TIR (10,400-12,500)	1-4 (VIS),5(NIR), 6 (TIR), 7 (FIR)	Freely available for research: USGS Earth Explorer tool	
Landsat 7	Enhanced Thematic Mapper (ETM)	1999	705	183	16	8	30 (bands 1-5,7) 60 (band 6) 15 (band 8)	Same as Landsat 5 with: LWIR (2,090-2,350) Pan (520-900)	1-4 (VIS), 5 (SWIR), 6 (TIR), 7 (LWIR), 8 (PAN)		

TIR=Thermal Infrared, LWIR=Long Wave Infrared, PAN=Panchromatic)

2.2.1 Broad scale monitoring sensors

Broad scale coverage satellite sensors are designed to gather large quantities of data at coarse spatial resolutions in order to examine global-scale Earth surface processes (Reed et al., 1994). These sensors tend to have fewer spectral bands operating over a narrower spectral range. As these sensors image large areas of the Earth in one pass, they have a high revisit frequency of once or twice daily. Broad scale satellite sensors discussed here are the Advanced Very High Resolution Radiometer (AVHRR), Système Probatoire d'Observation de la Terre (SPOT) VEGETATION and the Sea-viewing Wide Field-of-view Sensor (SeaWiFS).

2.2.1.1 National Oceanic and Atmospheric Administration (NOAA) Advanced Very High Resolution Radiometer (AVHRR), NOAA-AVHRR.

The NOAA -AVHRR sensors are mounted on near-polar orbiting, sun-synchronous weather satellites and have been in operation since 1982. Advantages for monitoring vegetation dynamics are the high temporal frequency of NOAA satellites and their broad scale coverage afforded by a swath width of 1.1 km, which resulted in AVHRR images being the only data suitable for global-scale remote sensing of vegetation in the 1980s and 1990s (Townshend et al., 1985). Numerous studies on global scale vegetation dynamics have resulted (Chen et al., 2005, Xiao and Moody, 2005, Maignan et al., 2008, Reed et al., 1994). Some issues with atmospheric interference have arisen in the use of AVHRR data. Early studies noted the error in AVHRR 2 data due to interference from cloud cover (Justice et al., 1985). In attempting to rectify this problem a thermal infrared band was included in AVHRR

3 for the improved detection of cloud. Nevertheless, it is still suggested that the broad width of the red and near infrared spectral bands (580–680 nm; 720 –1100 nm), which include the spectral region of water absorption, remain sensitive to fluctuations in seasonal water vapour in the atmosphere (Kawamura et al., 2004). More recent AVHRR datasets, such as the Global Inventory Mapping and Monitoring Studies (GIMMS), have been enhanced through the implementation of atmospheric adjustments and more precise angular measurements (Julien and Sobrino, 2009).

2.2.1.2 SPOT VEGETATION

The VEGETATION 1 sensor was launched in 1998 followed by VEGETATION 2 in 2002, carried on board SPOT satellites 4 and 5 respectively. The sensors are uniquely designed for the purpose of global vegetation monitoring. The orbit is near-polar and sun-synchronous, descending across the Equator at 10:30 a.m. local solar time. Data applications include the study of atmosphere-biosphere exchanges, for example the exchanges of heat between the land and atmosphere which are influenced by vegetation dynamics, as well as land cover mapping, ecosystem production estimates and the modelling of nutrient cycling through the biosphere. The SPOT VEGETATION instruments have four spectral bands: blue for atmospheric correction, red and near infrared for photosynthetic monitoring and shortwave infrared for vegetation moisture content. This band arrangement is identical to that of the SPOT HRVIR (High-Resolution Visible & Infrared) and HRV (High-Resolution Visible) instruments; however these replace the blue band

with green. Mid to high latitudes (above and below 35° North and South) are imaged at least once a day at a spatial resolution of one kilometre. The SPOT VEGETATION bandwidth is quite large for red (70 nm) and near infrared (110 nm) compared to the narrower bandwidth offered by other sensors such as Envisat MERIS (10 nm) or Terra/Aqua MODIS (3.75-15 nm).

2.2.1.3 National Aeronautics and Space Administration (NASA) Sea-viewing Wide Field-of-view Sensor (SeaWiFs)

The SeaWiFS sensor is mounted onboard the OrbView-2 spacecraft which has been in operation since 1997, in a sun-synchronous, near- polar orbit, passing the Equator at 12 noon local solar time. Reflectance is measured in eight spectral bands ranging from the blue to the near infrared (Feldman, 2011). As it is designed to monitor oceanic processes such as rate of photosynthesis in microscopic ocean plants, terrestrial chlorophyll amounts can also be readily measured (Hooker et al., 1992). The data are recorded at two levels of resolution, 1.1 km local area coverage (LAC) and 4.5 km global area coverage (GAC), and global coverage is complete in two days. The terrestrial vegetation information gathered by the sensor has been implemented in the study of large scale vegetation dynamics at a spatial resolution of two kilometres (Gobron et al., 2006a).

2.2.2 Regional scale monitoring sensors

The medium spatial resolution satellite sensors were developed to compensate for the lack of spatial and spectral resolution offered by coarser spatial resolution, broad-scale coverage sensors. Technological advancements in the design of medium

spatial resolution satellite sensors also allowed more onboard data storage and lighter payloads. The regional scale sensor has a typical spatial resolution of somewhere between 200 and 500 metres and has a large array of finely-tuned spectral bands. In covering smaller areas of the Earth in greater detail, medium resolution satellites have a more infrequent revisit time, between 1 and 3 days, than broad scale satellites. Here the MERIS and MODIS medium spatial resolution satellite sensors are discussed.

2.2.2.1 Terra/Aqua (MODIS) Moderate-Resolution Imaging Spectroradiometer

The Moderate-Resolution Imaging Spectroradiometer (MODIS), aboard NASA satellites, Terra launched in 1999 and Aqua launched in 2002, acquires data in 36 spectral bands, covering a spectral range from the visible to the near, mid and shortwave infrared as well as thermal infrared. As the sensor platforms, Terra and Aqua, cross the Equator in opposite directions a few hours apart, the same area can be viewed by both sensors in the morning and afternoon; the whole Earth's surface being imaged in 1 to 2 days (Maccherone, 2011). This capability allows the satellites to monitor events twice daily over the Equator with increasing regularity towards the Poles. MODIS has ground spatial resolutions of 250m, 500m and 1km, depending on the spectral band (see table 2.1).

2.2.2.2. Envisat (MERIS) Medium Resolution Imaging Spectrometer

The Medium Resolution Imaging Spectrometer (MERIS), launched in 2002, is an oceanic and terrestrial monitoring sensor aboard the Envisat platform which is in a

sun-synchronous, near-polar orbit with an acquisition time of 10 a.m. mean local solar time (ESA, 2006a). The MERIS sensor can be classed as a coarse or medium spatial resolution sensor as data are acquired at full spatial resolution (300m) and reduced spatial resolution of (1.2 km) at the sub satellite point (ESA, 2006b). Global coverage is achieved in 3 days, data are acquired in 15 spectral bands, and the bands are programmable in order to alter the bandwidth for different applications (see table 2.2). Although the sensor was primarily designed as an ocean-colour monitoring sensor, terrestrial parameters such as the amount of photosynthetically active radiation are also derived (Rast and Bezy, 1999). Surface reflectance values in bands 5, 8 and 13 detect chlorophyll content in plant tissues, while band 2 is sensitive to atmosphere. A combination of these bands is used to produce measures of vegetation growth (ESA, 2006a).

Table 2.2: MERIS spectral band characteristics (ESA, 2005)

Band Number	Spectral region (nm)	Band Width (nm)	Application
1	412.5	10	Yellow substance and detrital pigments
2	442.5	10	Chlorophyll absorption maximum
3	490	10	Chlorophyll and other pigments
4	510	10	Suspended sediment, red tides
5	560	10	Chlorophyll absorption minimum
6	620	10	Suspended sediment
7	665	10	Chlorophyll absorption & fluorescence reference
8	681.25	7.5	Chlorophyll fluorescence peak
9	708.75	10	Fluorescence reference, atmosphere corrections
10	753.75	7.5	Vegetation, cloud
11	760.63	3.75	O2 R- branch absorption band
12	778.75	15	Atmosphere corrections
13	865	20	Vegetation, water vapour reference
14	885	10	Atmosphere corrections
15	900	10	Water vapour, land

2.2.3 Local Scale Monitoring

Local-scale monitoring sensors are capable of high detail imagery of small areas. The concept of smaller, special purpose sensors addressed the need for precision applications of remotely-sensed data for specific users, e.g. linking fieldwork findings to satellite observations and vice versa, as well as applications in disaster relief and emergency responses. Here, the Landsat satellite systems are discussed because of their significance as predecessors to the more recently developed,

privately-operated very high spatial resolution IKONOS, Quickbird and WorldView-1 sensors.

2.2.3.1 Landsat Multi Spectral Scanner (MSS) and Thematic Mapper (TM/ETM+)

Landsat satellites provide a long time series of remotely sensed imagery from Landsat 1 in 1972 to the present Landsat 7 since 1999. The first five Landsat missions carried a MSS with four spectral bands covering the green, red and near infrared portions of the spectrum, however Landsat 3 also carried a fifth thermal band (Campbell, 2002). The MSS IFOV is 68 by 83 metres producing a pixel of 79m spatial resolution at nadir which was later improved to 30m in the Thematic Mapper (TM) from Landsat 5 onwards. This spatial resolution is of particular advantage in small areas of heterogeneous vegetation, but the 16-day revisit time is insufficient to detect rapid surface change especially under consistently cloudy areas (Justice et al., 1985). Two near infrared bands are used to cover a broad width of the spectrum (400nm), in comparison to MERIS which also has two near infrared bands but a much narrower region (135nm) or MODIS which has six bands in an equally broad spectrum (409 nm). Therefore, the temporal resolution and spectral range of the Landsat sensors is not appropriate for monitoring vegetation seasonality at fine temporal resolution over large areas. However, the Landsat spatial resolution is advantageous for comparison to ground-based measures of vegetation growth especially on a local scale e.g. deciduous forest stands in southern New England, United States (Fisher et al., 2006).

2.2.3.2 GeoEye-1, IKONOS, Quickbird, WorldView-1 and WorldView-2

The very high spatial resolution satellite sensors such as GeoEye-1, IKONOS, Quickbird and WorldView are commercial Earth-imaging satellites which have evolved from military technology designed to acquire very high detailed imagery of small areas for surveillance purposes (Campbell, 2002). The IKONOS system was launched in 1999, Quickbird in 2001, WorldView-1 in 2007, GeoEye-1 in 2008 and WorldView-2 in 2009. The sensors acquire data in panchromatic and/or multispectral mode. In panchromatic mode, IKONOS acquires data at 0.82m spatial resolution and Quickbird at 0.61m resolution, while in multispectral mode, IKONOS imagery is at 4m spatial resolution and Quickbird is 2.44 m. WorldView-1 operates in panchromatic mode only (400-900 nm) and gathers imagery at 0.5m spatial resolution. However, WorldView-2 is an 8-band multi-spectral sensor which provides 0.46m panchromatic resolution and 1.85m multispectral resolution. GeoEye-1 has the finest spatial resolution of these sensors in panchromatic mode (0.41m, resampled to 0.5m for all users except the US government) while it acquires 1.65m multispectral imagery. In order to provide fine detail coverage of small areas, the image swath of these sensors is narrow compared to lower spatial resolution sensors. For example, the swath is only 11 km wide for IKONOS, 15.2 km for GeoEye-1, 16.4 km for WorldView-2, 16.5 km for Quickbird and 17.7 km for WorldView-1. The IKONOS and GeoEye-1 systems are marketed under the brand name GeoEye (GeoEye, 2011) and the Quickbird, WorldView-1 and WorldView-2 sensors form a constellation of sensors operated by DigitalGlobe (DigitalGlobe,

2011). Applications of such high spatial resolution imagery include disaster relief, emergency planning, risk assessment, monitoring emergency response, damage assessment and recovery, change detection and in-depth image analysis.

2.3 Vegetation Indices and their application to vegetation monitoring

Meaningful data about the biophysical properties, state and health of living green vegetation can be derived from a mathematical combination of red and near infrared reflectance values to produce a vegetation index (VI). Though the VI is mathematically derived to produce a single value, its interpretation is based on the actual physical characteristics of the vegetation surface. Generally, the VI is designed to indicate the presence of green vegetation in an image, the higher the value, the higher the vegetative content. The VI data can act as a proxy for other vegetation parameters such as plant biomass and growth vigour (Butterfield and Malmstrom, 2009). The methods used to derive VIs vary in complexity as much as the input satellite data used to generate them. A selection of these indices is briefly described below in order of complexity and represents an evolution in the techniques used to derive VI data.

2.3.1 Simple vegetation Indices

2.3.1.1 Simple Ratio (SR) Index

The SR index represents the inverse relationship between spectral reflectance from growing vegetation in the red and near infrared spectrum (equation 1). The band

ratio method is effective because it produces a single value which is a function of the contrast between the two bands' reflectance. The SR is limited to the range $0 \leq SR < \infty$.

Equation 1: the Simple Ratio (SR) index is the basic ratio of red to near infrared reflectance

$$SR = NIR/R$$

Where,

NIR is near-infrared reflectance

R is visible-red reflectance

The most vegetated surfaces have a SR value of approximately 10 and non-vegetated surfaces, e.g. bare soil a SR value closer to 1.25 (Pinty and Verstraete, 1992). The varying magnitude of this ratio is useful in qualitatively assessing the abundance and vigour of vegetation over an area, as well as in the discrimination of vegetated from non-vegetated surfaces. The weakness of this simple, linear combination is that any error in the red and near infrared sensor measurements due to atmospheric or angular interference is included in the measurement.

2.3.1.2 Normalised Difference Vegetation Index (NDVI)

The NDVI captures the contrast between the visible-red and near-infrared reflectance of vegetation canopies (equation 2), much like the SR index, except that its range is limited between -1 and +1.

Equation 2: The NDVI ratio is based on the normalised differences in red and near infrared reflectance

$$NDVI = (NIR-RED)/(NIR+RED)$$

NDVI values in the range 0.1 to 1.0 represent increasing amounts of vegetation; however Huete *et al.* (2002) found the upper limits of the MODIS NDVI to be

clearly defined at 0.90. The effectiveness of this index is in its simplicity in that it uses the principle of band ratios to exploit the inverse red/near infrared relationship, and it is normalised to allow direct comparison of images from different locations. The resulting ratio is sensitive to the physiological state of the plant and its growth stage. However, the weakness of the NDVI, like the SR index, is its sensitivity to factors other than the plants growth such as atmospheric turbidity and soil brightness. The fact that NDVI values derived from different sensors are not easily comparable (due to different bandwidths of red and NIR sensors) and nonlinear in that values saturate in densely vegetated areas (Huete et al., 2002), leads to problems with its use. Furthermore, it has been suggested that the inherent complexity of the vegetation spectral response is lost in the NDVI ratio method and too simply summarised in a single number (Pinty and Verstraete, 1998). Nevertheless, NDVI remains one of the most widely used indices to discriminate green vegetation. Comparisons of NDVI from different sensors is difficult because bandwidths and viewing angle vary according to the sensor, and hence provide non-comparable information about the vegetative state. The same is true in comparing values of NDVI over a period of time when external factors are constantly changing. In a comparison study of MODIS derived NDVI and the NDVI derived from the AVHRR, the MODIS index was proved to be more robust to changes in biome type, particularly in a humid atmosphere where the AVHRR-NIR band is distorted by atmospheric water vapour (Huete et al., 2002). This result was verified in comparing NDVI derived from AVHRR GIMMS (Global Inventory Modelling and

Mapping Studies) with MODIS NDVI and SPOT VEGETATION (VGT) NDVI for a time series of overlapping years from 2000 to 2007 for both semi-arid and humid zones of the African Sahel (Fensholt et al., 2009). The slope values resulting from a linear least squares regression trend analysis of the average annual NDVI profiles differed considerably, especially in zones of different precipitation amounts. The SPOT VGT NDVI had positive slope values while the MODIS NDVI had negative slope values in areas of medium density vegetation (>1000 mm rainfall), but inconsistencies arising from the VGT 1 to the VGT 2 switch in 2003 may have influenced results. The AVHRR GIMMS NDVI and MODIS NDVI regression slope values were closer in the semi-arid areas than in zones of higher humidity. This suggests that comparing NDVI trends from different sensors becomes less reliable with increasing humidity.

2.3.2 Intermediate Vegetation Indices

2.3.2.1 Global Environmental Monitoring Index (GEMI)

Initial research on minimising the influence of atmospheric processes like scattering and absorption, focused on the NDVI and Simple Ratio (SR) index values, and incorporated mathematical parameters in the index calculation to simulate the atmosphere (Pinty and Verstraete, 1992). The goal of the Global Environmental Monitoring Index (GEMI) was to maximise the transmission of spectral information through the atmosphere so that the ratio of the top of atmosphere (TOA) reflectance to surface reflectance would be as close to 1 as possible. The mathematical formula

to derive the GEMI from red and near infrared reflectance data is shown in equation 3.

Equation 3: The non-linear index GEMI which contains the same spectral input information as SR or NDVI but with atmospheric interference accounted for

$$GEMI = \eta(1-0.25_{\eta}) - \frac{\rho_1 - 0.125}{1-\rho_1}$$

Where

ρ_1 = measured reflectance in the visible region

ρ_2 = measured reflectance in the near infrared region

$$\eta = \frac{2(\rho_2^2 - \rho_1^2) + 1.5\rho_2 + 0.5\rho_1}{\rho_2 + \rho_1 + 0.5}$$

The values of the GEMI index vary between 0 and + 1 over continental areas, equivalent to the SR range between 1 and infinity, or NDVI between 0 and + 1. However, although there is no loss of vegetation information in the GEMI calculation, it is less sensitive to atmospheric interference than NDVI because the relative influence of atmospheric processes such as scattering and absorption have been removed. Additionally, for the first time in vegetation index design, GEMI accounted for soil optical properties, as well as atmospheric effects for a globally-averaged standard atmosphere. This resulted in high sensitivity of the index to bright surfaces such as desert soils, snow and clouds (Verstraete and Pinty, 1996).

2.3.2.2 Soil Adjusted Vegetation Index (SAVI)

The goal of the SAVI was to minimise the influence of soil brightness in spectral vegetation indices using red and near-infrared wavelengths (Huete, 1988). This

advancement minimised some of the uncertainty in simple VIs since it reduces interference from the background reflectance of the soil surface underlying the vegetation which, in the case of non-soil adjusted indices, contributes to a mixed soil-vegetation spectral response. The SAVI combination of red and near infrared reflectance values and a soil parameter can be seen in equation 4.

Equation 4: the SAVI accounts for soil optical properties and so is useful in arid or sparsely-vegetated areas

SAVI= [NIR-R/NIR+R+L] [1+L]

Where L is an empirically-determined soil-adjustment parameter.

SAVI is used in partially vegetated areas such as arid ecosystems as it is more sensitive than the NDVI to variation in vegetative cover (Huete, 1988).

2.3.2.3 Tasselled Cap

The aim of the Tasselled Cap technique is to separate out soil reflectance data from vegetation reflectance data in two-dimensional data space so that the major components of an agricultural scene in one dimension are clearly separable from the background, redundant information. It was pioneered by Kauth and Thomas (1976) working on combinations of four bands from the Multispectral Scanner Subsystem (MSS) onboard Landsat 1, 2, 3, 4 and 5. The four output bands conceived by Kauth and Thomas (1976) are termed 'brightness, 'greenness', 'yellowness' and 'non such'. The advantages of the Tasselled Cap transformation is that the first two bands, brightness and greenness, contain most of the useful information on an agricultural scene. In plotting data for an entire growing season in two-dimensions, the distribution of these values takes a consistent form, that of a cap-like shape. The

information contained in the 'yellowness' band is of little use, describing unhealthy and withering vegetation, the 'non such' band represents atmospheric noise.

2.3.3Optimised Vegetation Indices

The SR index, NDVI, GEMI, SAVI and Tasselled Cap indices have been widely used to date. However, the idea of an optimal spectral index was conceived in order to integrate physical modelling with remotely-sensed reflectance measurements which could be targeted for specific end user applications, satellite instruments and vegetation parameters (Verstraete and Pinty, 1996). The advantage of an optimal spectral index is in the ability to set fixed values for the parameters which artificially change the measurement from that which would be expected from a pure vegetation spectral response. For instance, parameter values for soil brightness and atmospheric scattering can be set in a radiative transfer equation for which the solution is provided by the sensor-derived reflectance measurements. The remaining unknown value is the vegetation parameter itself, which is easily solved by inverse modelling. In this way, the vegetation index is the component of the equation whose value represents the vegetation photosynthetic activity alone. Therefore it is very sensitive to the presence and state of the vegetation cover but insensitive to external factors. However, the parameters must be tuned for sensor-specific characteristics, which therefore require prior knowledge of a sensor for optimisation (Verstraete and Pinty, 1996). An example of an optimal index is the MERIS Global Vegetation Index (MGVI) which has been optimised to estimate a biophysical variable of vegetation

growth known as the Fraction of Absorbed Photosynthetically Active Radiation (FAPAR) (Gobron et al., 1999, Govaerts et al., 1999).

2.3.3.1 MERIS Global Vegetation Index (MGVI)

The MGVI algorithm has been designed to exhibit maximum sensitivity to the presence of green vegetation, and minimal sensitivity to atmospheric interference, soil brightness and angles of illumination and observation. The MGVI acts as an integrated indicator of the vegetation cover in terms of photosynthetic activity and vegetation health (Gobron et al., 1999). The index has evolved from theoretical work on optimal spectral indices such as the GEMI, which showed the benefits of optimising indices for specific applications and sensors rather than applying the generic NDVI (Verstraete and Pinty, 1996, Pinty and Verstraete, 1992). The theory was put into practice with the advent of sensors like MERIS and MODIS which provided the required technical specification for designing optimal indices, e.g. the presence of a blue spectral band. Feasibility studies were carried out on MERIS data to optimise an index for the Fraction of Absorbed Photosynthetically Active Radiation (FAPAR) (Govaerts et al., 1999). Subsequent work focused on the physical and mathematical basis for an index optimised for the MERIS sensor and to estimate FAPAR which became known as the MERIS Global Vegetation Index (MGVI) (Gobron et al., 1999). The design of the generic FAPAR algorithm is described from equations 5-6 (Joint Research Centre (JRC), 2011). The calculation of FAPAR from red, near infrared and blue reflectance values follows a two step

procedure, the first of which normalises the top of atmosphere (toa) channel values by the anisotropy function to take into account the angular effects (Eq. 5).

Equation 5: The rectification of red and near infrared reflectance values

$$\tilde{\rho}(\lambda_i) = \frac{\rho^{toa}(\Omega_O, \Omega_V, \lambda_i)}{F\left(\Omega_O, \Omega_V, K_{\lambda_i}, \Omega^{HG}_{\lambda_i}, \rho_{\lambda_i c}\right)}$$

where λ_i stands for the wavelength (blue (442 nm), red (681 nm) or near-infrared (865 nm)) of spectral band i, and $\rho^{toa}(\Omega_0, \Omega_v, \lambda_i)$ denotes the Bidirectional Reflectance Factor (BRF) values measured by the sensor in the spectral band λ_i, as a function of the actual geometry of illumination (Ω_0) and observation (Ω_v). The spectral anisotropy reflectance function, $F(\Omega_0, \Omega_v, k_{\lambda i}, \Omega^{HG}{}_{\lambda i}, \rho_{\lambda ic})$, represents the shape of the radiance field. The triplet ($k_{\lambda i}$, $\Omega^{HG}{}_{\lambda i}$, $\rho_{\lambda ic}$) is the bidirectional reflectance model (called the RPV model). In the case of MERIS FAPAR, illumination conditions are simulated at solar zenith angles at 20° and 50°, and observation angles at a satellite zenith angle of 0° and 25° (Gobron et al., 1999). The rectification of the red and near infrared band is then carried out:

$$\rho_{R_{red}} = g_1[\tilde{\rho}(\lambda_{blu}), \tilde{\rho}(\lambda_{red})]$$

$$\rho_{R_{nir}} = g_1\left[\tilde{\rho}(\lambda_{blu}), \tilde{\rho}\left(\lambda_{nir}\right)\right]$$

The rectification process produces estimated values of red and near infrared spectral reflectance emerging at the top of the canopy (toc) corrected for atmospheric and angular radiative effects. The rectified red and near infrared bands are then combined together in the second step of the procedure using a mathematical formula to generate the FAPAR values (Eq. 6) (Gobron et al., 2006a).

Equation 6: The calculation of FAPAR from the rectified reflectance values

$$g_o\left(\rho_{R_{red}}, \rho_{R_{nir}}\right) = \frac{l_{0,1}\rho_{R_{nir}} - l_{0,2}\rho_{R_{red}} - l_{0,3}}{\left(l_{0,4} - \rho_{R_{red}}\right)^2 + \left(l_{0,5} - \rho_{R_{nir}}\right)^2 + l_{0,6}}$$

Where the coefficients $l_{0,m}$ of polynomial g_0 have been optimized *a priori* to force $g_0(\rho_{Rred}, \rho_{Rnir})$ to take on values as close as possible to the FAPAR simulated in various plant canopy scenarios used to train the algorithm. Once the coefficients are optimized for a specific sensor, the inputs of the algorithm are the BRF values in the blue, red and near-infrared bands and the observation and illumination angles values. The JRC MERIS FAPAR is determined from direct incoming radiation and is estimated for green leaves without the background absorption of woody materials such as tree bark (Gobron and Verstraete, 2008). In contrast the NASA MODIS FAPAR is a measure of both direct and diffuse radiation and would therefore be expected to produce slightly different estimates of absorbed PAR in the vegetation canopy.

The Fraction of Absorbed Photosynthetically Active Radiation (FAPAR) is a biogeophysical measure of vegetation growth but is a unitless value that estimates the fraction of the incoming solar radiation at the top of the vegetation canopy. Numerical values of FAPAR are scaled continuously in ever increasing amounts of vegetation from 0 (non-vegetated) to 1 (fully vegetated). The typical range of FAPAR for a beech forest (*Fagus Sylvatica*) measured from May to June from SeaWiFS data is from 0.2 to 0.9, while it is around 0.4 for much of the year in

evergreen-dominated vegetation (*Quercus ilex*) with higher peaks in April and November (Gobron et al., 2006b). The surface area receiving the Photosynthetically Active Radiation (PAR) is determined by the leaf area of the vegetation canopy estimated by the Leaf Area Index (LAI), therefore FAPAR is largely controlled by LAI (Arndt et al., 2010). The LAI has been found to be a better correlate of the REP than pure reflectance data or NDVI (Danson and Plummer, 1995). In this way, there is a quantifiable relationship linking VI data with other biogeophysical parameters such as LAI and FAPAR which require sensor-specific algorithms to model. In a comparison of the performance of the JRC, MODIS, CYCLOPES and GLOBCARBON FAPAR products over Northern Eurasia in the year 2000 (McCallum et al., 2010), the MODIS, CYCLOPES and JRC FAPAR values were consistent for croplands and deciduous broadleaf forests but in other cover types such as needle leaf and mixed forests, there tended to be noticeable differences. Overall, for Northern Eurasia in the year 2000, the JRC FAPAR was found to be the most conservative estimate of FAPAR which can be applied across all landcover types, in contrast to the other products which were inconsistent when compared between land cover types. It was also noted that MODIS and CYCLOPES FAPAR values were, on average, higher than FAPAR values from the other two methods due to the algorithm design or sensor-related differences. Similarly, in comparing MERIS and MODIS FAPAR over local sites and at the regional scale across the Iberian Peninsula, the MODIS values were consistently higher than MERIS FAPAR and they also showed higher regional spatial variability. Additionally, there was

seasonality in the correlation between the datasets with higher values in summer and lower values in winter (Seixas et al., 2009). In an assessment of the performance of two JRC-FAPAR products, SeaWiFs and MERIS, over a number of European sites in 2003 (Gobron et al., 2003), it was shown that the average difference between the products is within the stated accuracy range of the JRC FAPAR product (±0.1 FAPAR). These studies have confirmed that there appears to be a consistency to the MERIS FAPAR product when applied to a variety of vegetation types and spatial scales which was not present in the other sensor FAPAR products. The FAPAR has been recognised by the Global Climate Observing System (GCOS) as one of 16 terrestrial Essential Climate Variables. As an integrated indicator of the physical, physiological and biochemical status of the plant cover, satellite-derived FAPAR has been applied to the study of vegetation dynamics at a variety of spatial and temporal scales (Gobron et al., 2005a, 2005b, and 2007, Verstraete et al., 2008) and has been used as a proxy measure of gross primary productivity (Jung et al., 2008). For instance, the FAPAR has been used in drought detection (Gobron et al., 2005) and to highlight global and regional anomalies in vegetation productivity (Arndt et al., 2010). In the 2009 global FAPAR anomalies, areas of the southern hemisphere were shown to be suffering severe drought while areas of the Northern Hemisphere experienced favourable growing conditions. There were however, consistent negative anomalies between 30°S and 50 °S which were related to increased aridity associated with the Southern Oscillation Index (SOI). Globally-averaged FAPAR anomalies from 2000 to 2009 have revealed a decline in the FAPAR from 2000 to

2003 and since 2007 which may be indicative of a reduction in CO_2 assimilation by vegetation (Gobron et al., 2010).

2.3.3.2 MODIS Enhanced Vegetation Index (EVI)

The MODIS EVI and NDVI are both globally produced indices at 250m, 1km and 500m spatial resolutions which complement each other in terms of temporal and spatial coverage. The MODIS NDVI was designed to extend the AVHRR NDVI time series, and the EVI has optimised the vegetation signal to respond more effectively to high biomass regions where NDVI tended to saturate (Kawamura et al., 2005). Overall, the MODIS EVI has improved vegetation monitoring through careful removal of the canopy background signal and corrections for Raleigh scattering and ozone absorption (Huete et al., 2002). Whereas the NDVI is chlorophyll sensitive, the EVI is more sensitive to variation in the canopy structure, including leaf area index (LAI), canopy type, plant physiognomy, and canopy architecture (Huete et al., 2002, Boyd et al., 2011). The EVI atmospheric correction also utilises blue band data using the wavelength dependency concept of aerosol scattering (Huete et al., 2002).

2.3.3.3 Advantages of optimised indices for vegetation monitoring

The inclusion of the blue band in atmospheric correction for MODIS EVI and the MERIS GVI is a clear advantage over simpler VIs, such as the NDVI derived from the AVHRR which does not have an automated correction procedure in the absence of a blue channel. Techniques such as bidirectionally-adjusted reflectance values and radiative transfer modelling have minimised the influence of changing angles of

illumination and observation, atmospheric interference and soil background reflectance on the VI value. The MGVI has been shown to be a better indicator of the impact of the 2003 European-wide drought in the seasonality of vegetation in comparison to the NDVI. For a site of agricultural crops near Chartres, France, it was shown that there were greater noise levels in the NDVI time series which made it difficult to detect annual vegetation seasonality compared to the MGVI. In the drought year of 2003, any potential NDVI response to the drought was masked by such noise (Gobron et al., 2005). Huete et al. (2002) compared the difference of MODIS NDVI with that of MODIS EVI across different biomes, from humid tropical to arid. Though the NDVI and EVI contain similar information on several variables of vegetation growth such as Leaf Area Index (LAI), Photosynthetically Active Radiation (PAR) and chlorophyll activity, EVI was found to exhibit increased sensitivity in densely vegetated areas. Additionally, the EVI had been better designed than NDVI in separating out reflectance from the background canopy (underlying leaf litter and rock substrates) from the photosynthetically active leaf canopy.

2.4 Remote Sensing of Land Surface Phenology (LSP)

Repeatable and large-scale measures of vegetation growth from satellite sensors have provided a global view of landcover change and vegetation ecosystem dynamics (Justice et al., 1985, Townshend et al., 1985). The study of phenology, in particular, has benefited from the synthesis of satellite and ground-based measures

(Soudani et al., 2008, Studer et al., 2007). The term Land Surface Phenology (LSP) has been conceived to describe the study of the spatio-temporal development of the vegetated land surface as revealed by synoptic space borne sensors (White et al., 2009). This definition is distinct from traditional definitions of phenology which refer to specific life cycle events in individual plants or species (see section1.1). However, although the observed patterns in remotely sensed phenology are still related to biological phenomena, they are distinct from ground-based events owing to the aggregation of information at moderate (500m) to coarse (25km) spatial resolutions (Friedl et al., 2010). An important characteristic of LSP monitoring, which distinguishes it from ground-based phenology observations is that remotely-sensed phenological patterns are observed from multiple vegetation systems and not a single plant or tree species. These patterns can also be influenced by spatio-temporal changes in agricultural practices, and other human influences such as urbanisation (White et al., 2005). Therefore, the multiple factors driving land surface phenology are different from those that would be expected in an analysis of an individual tree or plant, e.g. local climate (White et al., 2005).

2.4.1 Background to LSP studies

The spatial coverage and the regularity of satellite imagery were cited as the major factors for using satellite remote sensing as a tool for global-scale phenological monitoring (Cleland et al., 2007). From the early 1980s, vegetation dynamics, in particular spatial and temporal changes in global vegetation phenology, were observable using coarse spatial resolution sensors (> 1km) such as the NOAA-

AVHRR (Justice et al., 1985). Coarse-spatial resolution data are still favoured for global-scale phenological monitoring, especially owing to the availability of long time series products and global coverage (Julien and Sobrino, 2009, Stöckli and Vidale, 2004). From the late 1990s onwards, the medium spatial resolution sensors have been used for studying regional and local scale phenological patterns. For example, 16-day composites of the 1 km MODIS EVI were used to show phenological variability with climate in northern mid and high latitudes across Europe, Asia and North America in 2001 (Zhang et al., 2004a). At coarser spatial resolutions, 10-day composites of SeaWiFS FAPAR (2 km spatial resolution) were used to characterise growing season cycles from 1998 to 2004 at local sites of various land cover types in Europe, South Africa and North America (Verstraete et al., 2008) and from 1998 to 2000 over forest vegetation in Europe (Gobron et al., 2006b). In some cases, where local-scale analysis for comparison to field measurements has been possible with the use of full spatial resolution MERIS and MODIS data (250-300m) (Wardlow et al., 2007, Soudani et al., 2008, Gobron et al., 2005). However optimal field-level monitoring requires Landsat-like spatial resolutions, e.g. fused MERIS full resolution (300m) and Landsat TM-5 imagery (25m) has shown promising results in studying heterogeneous landscapes in the Netherlands due to the combined spectral and spatial resolution of both sensors (Zurita-Milla et al., 2009).

2.4.2 Monitoring LSP by phenological metrics

Phenological metrics parameterise the seasonal cycle of vegetation growth so that discrete points in the seasonal cycle can be identified and quantified. These metrics can be interpreted as an event in the phenological cycle, but cannot necessarily be explicitly related to a ground-based phenological measure. For example, the beginning of measurable photosynthesis is frequently described by the vegetation Start of Season (SOS), but as of yet there is no quantifiable relationship between the SOS metric and a similar ground-based event. Among researchers, there is no general agreement about what defines the start of a growing season. The difficulty in establishing such a relationship is the species-specific nature of phenological events which do not occur at the same time, or in the same manner, across all species. One of the uncertainties surrounding the use of SOS from an optimised VI is that its relation to vegetation phenology has not been defined in contrast to the more widely used NDVI. For example, in deciduous vegetation and snow-free conditions the NDVI-derived SOS is generally responsive to the development of leaf foliage, and the NDVI would start increasing after bud-burst (L. Eklundh, 2011, pers. comm.). However, the MGVI, for example, would be expected to behave differently as it is an estimate of uptake of Photosynthetically Active Radiation (PAR) in the vegetation canopy as opposed to NDVI which has not been tuned for any specific vegetation parameter. Therefore, this creates uncertainty when attempting to relate the SOS to a specific ground-based phenological event. The general problem of comparing satellite-derived metrics with ground-based events is also a consequence

of the large number of external influencing factors inherent in satellite-derived data (White et al., 2005), compared to the strict standards set for *in-situ* phenological observations by the IPG network (IPG, 2005). Additionally, comparing field observations with pixel-derived metrics presents a spatial conflict since the former are relative to small areas, e.g. 1-100m, and the latter typically areas of a few hundred metres or square kilometers. Due to these shortcomings, it has been suggested that it is more appropriate to compare growing season events from different remote sensing products to achieve coherency between them, rather than direct comparison with ground observations (Verstraete et al., 2008). Nevertheless, efforts to establish a global network of ground validation sites for satellite-derived phenology products are underway with the establishment of the Committee on Earth Observation Satellites (CEOS) Working Group on Calibration and Validation (WGCV) Land Product Validation (LPV) subgroup, which should yield considerably more insight into satellite-derived phenology validation methods (Nickeson, 2011). However, discussions on accuracy and bias in remotely-sensed phenology products, and how to achieve consistency between the different sensors' products are ongoing, and as yet no consensus has been achieved between the various users of these products on accuracy issues. This debate is summarised in a recent web-based discussion hosted by the CEOS-LPV subgroup. The discussion centred on the nuances of LSP studies and the current challenges facing this field of study, in particular the difficulties experienced in relating satellite-based findings to

those from ground-based phenology studies (Vegetation Index and Phenology (VIP) Research Group, 2011).

Despite the difficulties in establishing a protocol for validation of LSP metrics with ground-based measures, phenology metrics have been shown to adequately demonstrate the expected phenological characteristics of different vegetation types from spring wheat to tropical rainforest. The level of interannual variation in these characteristics can then be discerned from multiannual time series (Reed et al., 1994). The variability in phenology metrics can also be related to changes in climatic factors such as land surface temperature (Zhang et al., 2004a). They can be used as correlates of climate variables (de Beurs and Henebry, 2008b, Xiao and Moody, 2005), or as inputs to global biosphere-climate models. Remotely-sensed interpretations of land surface phenology are particularly important to parameterise such models for the influence of vegetation phenology on the natural cycles of water, energy, carbon, and other trace gases (Friedl et al., 2010).

2.4.3 Global to continental scale trends in land surface phenology

As described in Chapter 1 (section 1.1.2) for ground-based measures, evidence for an earlier greening trend in some regions has been found from satellite-derived data. Most of the global-scale analysis on trends in phenology has been carried out using the NOAA-AVHRR sensor (Xiao and Moody, 2005, Justice et al., 1985, White et al., 2005). Justice et al. (1985) used NDVI derived from the AVHRR sensors to compare global phenological trends between April 1982 and November 1983. They used a global scale equivalent of the NDVI called the Global Vegetation Index

(GVI) but found anomalously high GVI values occurred over certain regions of the globe (northern high latitudes) due to low angles of solar illumination as well as depression of the vegetation index value due to atmospheric attenuation. Later work with the newer Pathfinder AVHRR-NDVI dataset by Xiao and Moody (2005) revealed significant greening trends in the northern mid to high latitudes for a 17 year period from 1982-1998 which globally exhibits a strong latitudinal and longitudinal variability. The Pathfinder dataset was an improvement on previous versions of the AVHRR NDVI as any residual noise associated with atmospheric effects, orbital drift effects, inter sensor variations, and stratospheric aerosol effects was minimised by a series of corrections, including temporal compositing, spatial compositing, orbital correction, and climate correction (Xiao and Moody, 2005). Continental scale studies over China, Africa, North America and Europe have employed MODIS (Zhang et al., 2004a, Wardlow et al., 2007), MERIS and SeaWiFS (Gobron et al., 2006a, Gobron et al., 2005) and NOAA-AVHRR data (Brown et al., 2010, Reed and Brown, 2005). These sensors generally provide a compromise between revisit time, spatial resolution, global coverage and free availability of the datasets. Combining datasets from two different sensors of similar spatial resolution is not uncommon, exploiting the spectral properties of both sensors and increasing the time period over which data can be gathered (Zurita-Milla et al., 2007). For example, the fusion of Landsat and MERIS full resolution imagery was successfully used to generate MERIS-based vegetation indices at Landsat-like spatial and MERIS-like spectral and temporal resolution (Zurita-Milla et al., 2009).

2.4.4 Monitoring phenology in an agricultural context

Phenology and agriculture are closely linked through knowledge of the crop calendar which varies according to the genetic characteristics of the crop, local climate, soil type and agricultural practices of a particular region (Campbell, 2002). However, crop cycles can be modified by changes in climate. Therefore, it is important to monitor phenology in an agricultural context as well as in natural tree species. Crop phenological parameters such as the start and end of growing season are important determinants of crop management plans in order to intensify or diversify agricultural practices (Brown et al., 2010). Monitoring these parameters in agricultural areas over long time periods can indicate changes in food productivity, and hence early warnings for crises in the developing world such as food shortages, or indicate mass shifts in cultivation systems following institutional change (Brown et al., 2010, de Beurs and Henebry, 2004). Crop growth models which integrate satellite data with meteorological and other environmental information are implemented in the Crop Growth Monitoring System (CGMS) of the Monitoring Agriculture with Remote Sensing (MARS) project of the European Commission (Genovese et al., 2001). This information is used to forecast crop yields on a national and regional scale. Crop growth is monitored using remote sensing on a systematic basis and findings published for the 27 EU member states in monthly bulletins (Monitoring Agriculture with Remote Sensing (MARS), 2011). Japanese rice paddy fields have been monitored using MODIS EVI data for the 2002 growing season (Sakamoto et al., 2005), as have rice and wheat fields across various sites in

Europe using Envisat MERIS and SeaWiFS from 1998 to 2004 (Gobron et al., 2005). These studies show that seasonal rice cycles are quite strong, exhibiting growth from April onward, reaching maturity in late August followed by a sharp decline in activity in September with crop cultivation. As they are heavily irrigated, annual cycles were reproducible and consistent so that climatic factors have less impact in determining cycle changes due to artificial water availability. This is in contrast to natural vegetation such as in beech forests (*Fagus sylvatica*) at Hesse, France (Gobron et al., 2006b). There, the seasonal cycle exhibits a surge in growth in early summer followed by two gradual dips in vegetation activity corresponding to late summer and early autumn. Although there is more variation in the growth cycle than for rice cultivation, the interannual variability is not large, provided no stress event such as drought occurs, and environmental conditions remain normal. These studies show the utility of using time series of vegetation indices such as the MODIS EVI and MERIS GVI for monitoring annual cycles of photosynthetic activity in cultivated and natural environments. The impact of climate anomalies such as drought, and human-induced change in the growth cycle by irrigation has been effectively monitored using optimised vegetation indices. Satellite remote sensing provides the means to monitor the phenology of the crop cycle at fine temporal and spatial resolutions which has practical benefits for agro meteorological forecasting, crop yield assessment and drought detection. Aside from practical uses to gather statistics and inform land use managers, monitoring vegetation phenology in agriculture also has implications for carbon accounting. As an Annex 1 signatory

to the UN Framework Convention on Climate Change (UNFCCC), Ireland is among many countries obliged to report an annual inventory of its greenhouse gas (GHG) emissions and removals. Moreover under the Kyoto protocol such reporting is also required for the first commitment period 2008-2012. For all countries committed to limiting their GHG emissions it is vital that carbon emission/sequestration estimates are accurate and calculated from routinely and systematically data collected such as that from space-based systems.

2.4.5 Monitoring the vegetation Start of Season (SOS)

White et al. (2009) proposed a conceptual definition for the SOS metric as the first sustained increase in values of satellite-derived VI time series after a prolonged period of reduced photosynthetic activity. Similarly, Reed et al. (1994) proposed an interpretation of the timing of onset of greenness metric as the beginning of measurable photosynthesis. The SOS has been widely studied as it provides both a convenient phenological marker for studying land cover dynamics and climate variation, and has generally been responsive to large-scale climate oscillations such as the Inter Tropical Convergence Zone (ITCZ) (Jönsson and Eklundh, 2002) and the North Atlantic Oscillation (NAO) index (Julien and Sobrino, 2009). In contrast, coherent spatial patterns in End of Season (EOS) have proven difficult to detect in satellite imagery and ground-based evidence shows that leaf fall and decolouration has demonstrated little variation with climate (Cleland et al., 2007, Menzel, 2003). The length of growing season (LGS) can be estimated from the SOS and EOS, although the difficulties in characterising EOS potentially create uncertainty in

interpreting the LGS. There have been many methods devised to estimate the SOS which have been adapted for different sensor products and in some cases tailored for specific ground-based events. In a relative comparison of the SOS across North America, derived using 10 different methodologies, the first observed leaf was most similar in timing to the ensemble of SOS estimates, although the SOS defined by some methods tended to be earlier, sometimes by several weeks (White et al., 2009). The methods for SOS estimation will be described in more detail in Chapter 4. Other aspects of the seasonal cycle can be described by different phenological metrics. For example, the integral of the area below a fitted time series curve is an indicator of vegetation productivity (Jönsson and Eklundh, 2004).

2.5 Conclusion

This chapter outlined the physical principles and technical bases for a satellite-based approach to vegetation seasonality monitoring. Owing to the variety of temporal, spatial and spectral resolutions offered by the suite of optical satellite sensors discussed, the selection of an appropriate sensor product for such a task is not trivial. The difficulty in selection is compounded by data access, and availability of appropriate geophysical products from the chosen sensor. The NDVI, although widely used, is subject to considerable uncertainty in terms of parameterisation for specific biophysical properties of the vegetation canopy and is sensitive to error in angles of illumination and observation and saturates at high values. In contrast the MGVI has been optimised to represent the FAPAR, a widely recognised

biogeophysical parameter which is directly linked to the state and productivity of the vegetation system.

A new direction for global vegetation phenology research has been established in the discipline of land surface phenology which gives an overview of spatial-temporal changes in vegetation phenology at multiple spatial scales. This is in contrast to finite, point measures of phenological stages in tree species on which historical records are based. Yet LSP has not been monitored on a national scale in Ireland, nor in many other countries, to date. Therefore, there is an opportunity to contribute to and benefit from this growing field of international research. Potential benefits of a space-based approach include broad-scale coverage of terrestrial vegetation, systematic measurements of vegetation canopy reflectance and multiannual time series data. However, there are specific challenges to LSP monitoring in Ireland. For instance, cloud cover is present on daily basis across some or the entire island, and the landcover is predominately grassland interspersed with small areas of agriculture, natural and semi-natural vegetation, and therefore heterogeneous and fragmented in nature. Together these limitations mean that vegetation seasonality cannot be monitored with daily frequency on a national scale by near-polar orbiting satellites nor can vegetation seasonality measures be representative of pure vegetation species.

Despite such challenges, LSP measures can potentially complement ground-based observations. As was described in the previous chapter, current methods of

phenological observation in Ireland are entirely ground-based, at the IPG sites, and although the network has been greatly expanded, national-scale phenological monitoring of multiple land cover types is only possible using remote sensing technology. A combination of land surface and ground-based measures has the potential for an integrated approach for future phenological monitoring. The extension of the growing season which has already been demonstrated for certain tree species at the IPG gardens could possibly increase the carbon storage capacity in terrestrial vegetation and reduce GHG emissions, with subsequent impacts on national carbon budgeting activities. This is particularly important for agricultural systems as Ireland is obliged to report its GHG emissions and removals as an Annex 1 signatory to the UNFCC.

Chapter 3. The implications of cloud cover for vegetation seasonality monitoring

Regional-scale studies of vegetation phenology have been facilitated by the availability of multi-annual time series of satellite imagery (Reed et al., 1994, Reed and Brown, 2005). Here, seven years of MERIS Global Vegetation Index (MGVI) data have been obtained over Ireland from the ESA-ESRIN G-POD service for a national-scale study of vegetation seasonality. The MGVI has been selected for this study to capitalise on advances in VI optimisation techniques which reduce error in empirically-based indices such as the NDVI and because it can be measured *in-situ* with ground-based sensors if necessary. The justification for selection of this MERIS product will be outlined in further detail in this chapter.

A time-compositing algorithm was applied to the daily MGVI data in the G-POD to overcome the presence of data gaps in the daily imagery. However, in order to define an appropriate time-compositing interval, an analysis of ancillary data was required. These included weekly *in-situ* phenological observations of a number of tree species in a forest stand, daily observations of cloud cover trends at a representative location on the island, as well as analysis of cloud in composited imagery themselves. The first section of this chapter (3.1-3.3) will describe how estimates of the beginning of growing season from *in-situ* observations of vegetation phenology, combined with observations of cloud cover, were used to refine the

composite period length. This was followed by an analysis of the satellite imagery themselves to determine the appropriate composite period length. The second section of this chapter (3.4) documents the validation of the remotely-sensed vegetation index data using an independent satellite-derived cloud mask. The need for validation has been driven by concerns about the quality of the MGVI time series data and the potential of undetected cloud cover to reduce their quality. A condensed version of this chapter has been submitted as a paper to a special issue of the Journal of Irish Geography, based on the proceedings of the joint Irish Earth Observation (IEOS)/Remote Sensing and Photogrammetry Society (RSPSoc) 2010 annual conference, University College Cork, Ireland.

3.1 Time compositing high temporal frequency satellite data

3.1.1 The aims of time-compositing satellite data

The aim of the compositing process is to combine consecutive satellite images over a period of time in order to generate as much cloud-free imagery as possible (O'Connor et al., 2008). Satellite imagery can be time-composited to fill in the gaps created by clouds or other effects such as cloud shadow and poor atmospheric corrections (Pinty et al., 2002). Therefore, the resulting composite image is more spatially-consistent and consists of cloud-free, or best quality, pixels from several scenes (Justice et al., 1985).

Some compositing schemes have been designed specifically for certain sensors, or to attain optimal pixel conditions for specific surface products. For example, the MODIS vegetation index compositing algorithm aims to standardise the variability in sensor view and solar illumination angle by favouring near-nadir value selection (van Leeuwen et al., 1999). Image pixels acquired under near-nadir viewing geometries are favoured because the atmospheric path is shortest and the spatial resolution of pixels degrades off-nadir (Cihlar et al., 1994). A generic time-compositing scheme has been designed by Pinty et al. (2002) for applications to a variety of daily satellite surface products, e.g. MGVI or surface albedo. The technique rejects poor-quality pixels using a series of pixel flags which indicate the pixel state, e.g. cloud, water and bright surface flags, in daily imagery (Gobron et al., 2007). Generally, a good compositing method ensures that the value selected over the compositing interval is the most representative of the surface state during that interval (Pinty et al., 2002). Therefore, composited values should be consistent enough from one period to the next to ensure that robust time-series analysis can be conducted (Huete et al., 2002).

Many studies typically advocate the use of days to estimate phenological events even when using composite data. For example, White et al. (2009) estimated Start of Season (SOS) by day of year across North America using 15-day NDVI composites, and daily trends in European growing seasons were also derived from 15-day composites (Julien and Sobrino, 2009). The use of a composite period, rather than

days, avoids bias towards any particular day within the composite (Zhang et al., 2004a), although it may introduce uncertainty in estimating phenological events by day of year (Thayn and Price, 2008). Furthermore, authors using a 10-day MERIS FAPAR products have also reported growing season events in decads (Verstraete et al., 2008).

3.1.2 The factors influencing composite period selection

There are two important factors which determine the number of days in the composite interval. Firstly, the interval must be within the time period during which significant surface change can occur. Secondly, there must a sufficient number of cloud-free days in the interval to provide enough valid data to fill the gaps created by missing data (Pinty et al., 2002). Therefore, an appropriate composite period is selected, not only with a good understanding of the rate of change of the surface cover, but also of the temporal trends in causes of missing data such as cloud. Moreover, the link between composite period and the size of study area is also an important consideration. For example, 4-day and 8-day composites of MODIS LAI/FAPAR were examined, for monitoring the transition of phenological phases in vegetation, over a selection of 1200×1200 km tiles in North America (Yang et al., 2006). While a 4 to 8 day interval is appropriate for such local-scale applications, global studies employ very long periods to attain cloud-free conditions worldwide, e.g. a 4-week period (Justice et al., 1985). Therefore, though shorter composite periods give fine-scale temporal measurements, an extended period is required to account for cloud cover over large areas. Compositing periods of 4, 8 and16 days in

the case of MODIS LAI, EVI and NDVI (Huete et al., 2002, Yang et al., 2006), 10 days and monthly for MERIS and SeaWiFS products (Gobron et al., 2006b) and 14 days for AVHRR NDVI (Reed et al., 1994) have been used in remote sensing phenology studies.

3.2 Primary data

3.2.1 The Joint Research Centre (JRC) FAPAR products

The Institute for Environment and Sustainability, within the JRC of the European Commission in Italy, has generated FAPAR products for Western Europe using a range of satellite sensors (SeaWiFS, MODIS, MERIS and MISR). The longest time series of the JRC FAPAR product has been generated from SeaWiFS data at 2.17 km spatial resolution from 1997, followed by the 1.1 km resolution MODIS product since 1999 and the 1.2 km MERIS FAPAR product since May 2002 (pers comm, Gobron, 2009). The JRC MERIS FAPAR was chosen as an appropriate satellite product for this study, as SeaWiFS FAPAR, though over a longer time series, is at a coarser spatial resolution (2.17 km), and the MODIS FAPAR, at a slightly higher spatial resolution (1.1 km), is not an operational JRC product but was only used in a feasibility study of the JRC algorithm. The NASA MODIS FAPAR is produced instead at Boston University, using a slightly different algorithm, which has proven to be comparable to JRC FAPAR for most landcover types but exhibits differences in mixed and needle leaf forests (McCallum et al., 2010), as described in section 2.3.3.1. The time-composited, full resolution (300m) MERIS FAPAR product was

still under development as an operational product for ESA data users at the time of writing. Therefore, the time-composited Reduced Resolution (RR) MERIS FAPAR product was selected for this study. There are three advantages of using the RR product. It is an easily accessible and fully processed MERIS level 3 product which can be time-composited over periods specified by the user. The RR MGVI is at an appropriate spatial resolution to address the national-scale aims of this feasibility study. Therefore, provided the methodology is successful with the RR product, higher spatial resolution products can be used in future studies. The disadvantage of the RR product arises from the heterogeneity of Irish landcover at this pixel scale. The estimated error of the MERIS FAPAR product is ±0.1 (unitless) (Gobron et al., 2003). This error is a combination of errors arising from radiometric calibration uncertainties, whose values depend on the year as the reprocessing of MERIS data is ongoing. However, current accuracy (25/5/2011) tends to be on average less than 0.03. There is also error coming from the optimization procedure itself which is approximately 0.05 (N.Gobron, 2011, pers comm).

3.2.2 The advantages of the Medium Resolution Imaging Spectrometer (MERIS) for vegetation monitoring

The MERIS sensor was briefly introduced in Chapter 2 (section 2.2.2.2). There are four key technical characteristics of the MERIS instrument which make it suitable for vegetation monitoring. Firstly, Envisat has global coverage every three days, with near-daily passes over Ireland. Secondly, MERIS has a wide image swath (1150 km) capable of capturing the full 280 km width of Ireland in one pass. The

RMS absolute MERIS geolocation error remains within the range of 212 ± 22 meters (Jackson et al., 2011), or approximately one sixth of a reduced resolution pixel. Thirdly, the range of narrow spectral bands in the visible to near infrared spectral region (412 to 900 nm) enables precise measurements to be made of red/near infrared absorption and reflectance by vegetation, and fourthly, the presence of a blue spectral band, sensitive to aerosol scattering, enables more robust atmospheric corrections (Rast and Bezy, 1999).

3.2.3 Acquiring a time series of MERIS FAPAR over Ireland

3.2.3.1 The ESA-ESRIN G-POD

The ESA / ESRIN G-POD facility is widely used for the dissemination of both ESA and third-party mission data products to the scientific community via an online web portal[1]. Computing resources are distributed to a number of processing nodes, enabling large volumes of data to be parallel-processed at high speeds (ESA G-POD Team, 2008). A number of ESA Earth Observation data products can be accessed via the G-POD services menu, access to these products being granted through registration and approval from the service. An ESA category 1 (ID: 5199) proposal for academic research, requesting access to the time series of reduced resolution MGVI products over Ireland since the beginning of the MERIS mission, was submitted to the G-POD administrator. Initially, requests for the data were submitted as tasks directly to the G-POD portal, where the results were published instantaneously. This was useful for generating the product for specific months and

[1] http://gpod.eo.esa.int/

years during the testing phase. However, once the data requirements had been determined, a scheduled service was arranged. A publishing server was set up locally to download the requested MGVI time series, via a secure ftp site, due to the large volume of data generated. The data were delivered approximately two weeks after acquisition. The process of MGVI production and provision to G-POD users is summarised in figure 3.1.

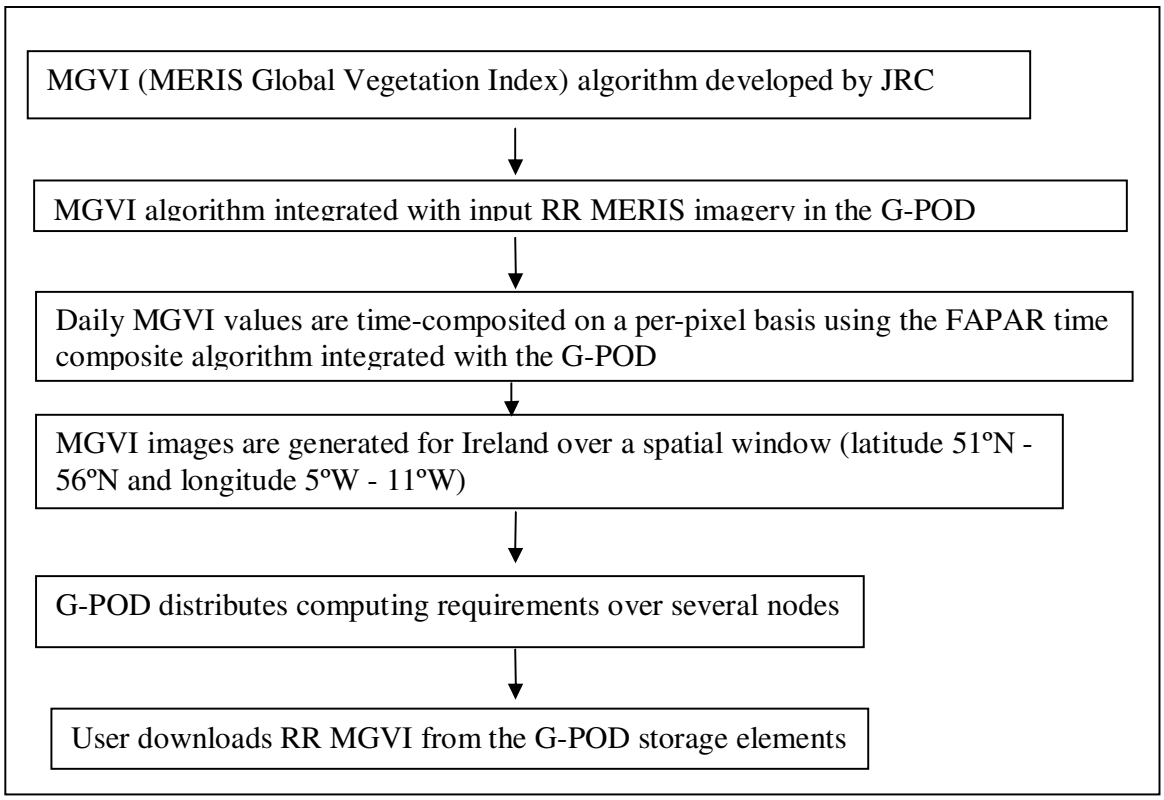

Figure 3.1: Stages in the Reduced Resolution (RR) MGVI product generation using the ESA-ESRIN G-POD

3.2.3.2. The FAPAR time-composite algorithm

The FAPAR time-composite algorithm was integrated with the processing capabilities of the ESA G-POD so that multi-annual time series of the composited product could be generated within the stated geographical window (Pinty et al., 2002). In equation 3.1 and 3.2, the time composite algorithm is described.

Equation 3.7: The calculation of the temporal average of the daily valid values in the composite period

$$\overline{S} = \frac{1}{T}\sum_{t=1}^{T} S(t)$$

Equation 3.8: The average deviation of the valid values in the composite period

$$\Delta_S^T = \frac{1}{T}\sum_{t=1}^{T} \left| S(t) - \overline{S} \right|$$

The term T represents the number of valid clear sky values during the compositing period of N days. The term, $S(t)$ is the daily product value at time (t), $\overline{S}$ is the temporal average index value, and Δ_S^T is the average deviation of the distribution.

The value selected as most representative for the N-day period, $\hat{S}$, is the one that minimises the quantity $\left|S(t) - \overline{S}\right|$, i.e. the daily value closest to the mean of valid values. This initial step is applied twice so that $S(t)$ values which exceed the range $\overline{S} \pm \Delta_S^T$ are excluded as outliers (Pinty et al., 2002). For a spatial window of daily images, the algorithm generates an array of values for each N-day period, where each pixel value is regarded as the most representative of the period. In the case

where a valid value does not exist for the N-day period, pixel flags state the reason why. The final time-composite product is composed of the composite values, along with arrays of pixel flags where no valid data are returned. Both arrays of valid data and pixel flags are provided with measures associated with conditions of value acquisition such as the geometry of illumination and observation, and the date of value acquisition (Pinty et al., 2002). In the case of only one valid value during the composite period, it is automatically selected by the algorithm and in the case of two valid values, the largest one is chosen. Temporal uncertainty increases with fewer valid values during the composite period because there are insufficient daily data to generate valid statistics and because of the above assumptions (Pinty et al., 2002). The temporal uncertainty in the composited MGVI value is given as the temporal deviation value, and included in the time composite product. The advantage of the FAPAR time composite algorithm is the unbiased selection of a representative value based on its favourable statistical properties which is an improvement on the widely used Maximum Value Composite (MVC) technique which assumes a negative bias of NDVI (Holben, 1986). Another advantage of the FAPAR time composite algorithm is the inclusion of statistics per pixel in the final product, which can be used for further statistical analysis of the time-composited values.

3.3 Methods and data for composite period selection

The selection of an appropriate time-composite interval for this study has been guided by the following two criteria:

1. Minimising the length of the composite period to be concurrent with the rate of spring greening in surface vegetation.

2. The inclusion of a sufficient number of days in the composite period so that each pixel will have at least one cloud-free day in the period and therefore a valid value

For the first criterion, *in-situ* observations of vegetation seasonality and for the second criterion, daily cloud amounts at a representative location on the island, were used to optimise the time composite period.

3.3.1 In-situ phenological data

The aim of the field campaign was to investigate how the composite period could be tuned to the temporal dynamics of spring greenup in mixed woodland vegetation. In particular, it was intended to investigate how frequently observations need to be made so that the rate of change of phenological stages from dormancy to budburst to leafout could be monitored across different tree species.

3.3.1.1 Description of Site

The location of the phenological field study, in an area of mixed woodland in Currabinny Wood, Cork Harbour, can be seen in figure 3.2. The forest is managed by Coillte, the national forestry management agency, who has recorded 1890 as the earliest planting year in Currabinny Wood and 1979 as the most recent. The Wood is 34.9 Hectares (1 ha = 10, 000 m^2) of mixed forest, which is 79 m above sea-level at its highest point (Coillte, 2003). There is an assemblage of deciduous tree species, such as Oak (*Quercus robur*), Ash *(Fraxinus excelsior*), Horse Chestnut (*Aesculus hippocastanum*), Sycamore (*Acer pseudoplatanus)*), Beech (*Fagus*

sylvatica) and Birch (*Betula pubescens*), varying in age from 100-year old mature trees to younger 30-year old trees. The woodland is fringed by Cork Harbour to the North, East and South and bordered by agricultural land to the West. The site was chosen due to the presence of a large number of tree species for sampling and its proximity to the CMRC (approx. 10 km. distance), practical for weekly visits to the site.

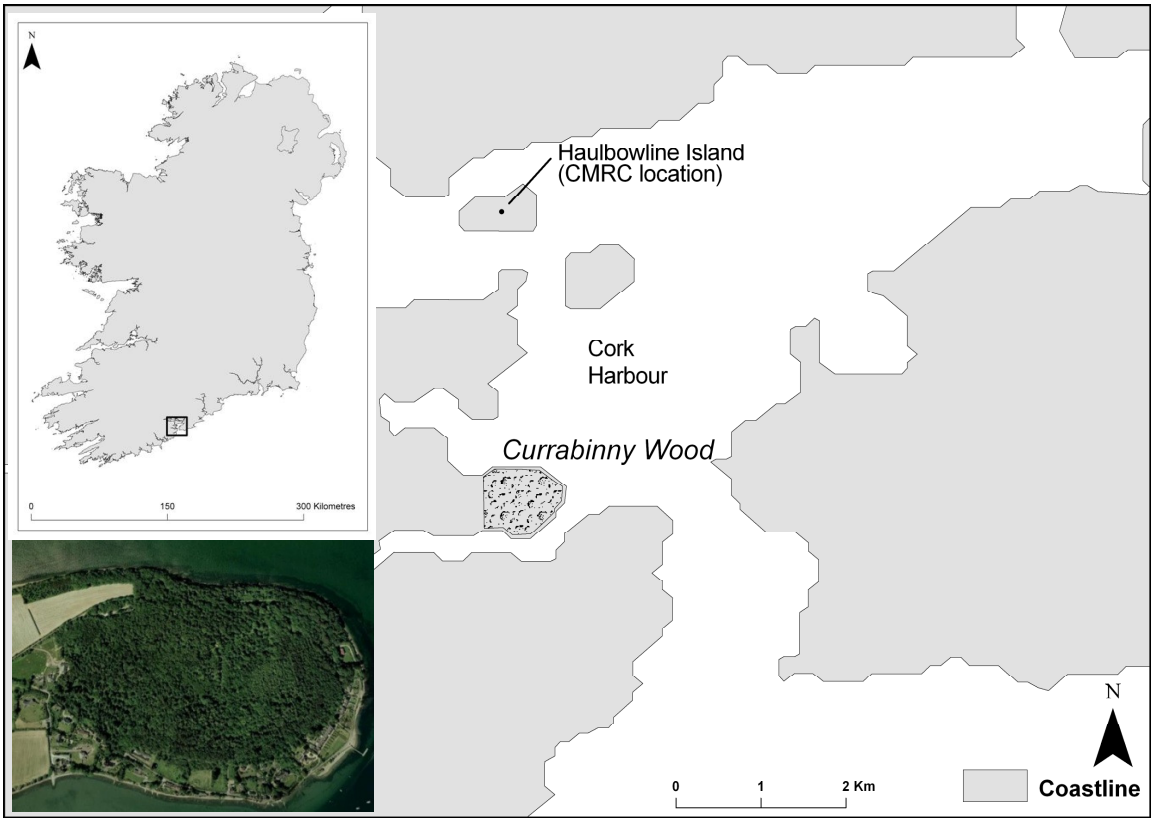

Figure 3.2: Location of in-situ field observations, Currabinny Wood, Co. Cork with an image of the area acquired on the 8th of June, 2008 from Google Earth

3.3.1.2 The recording of phenological data

A sample of eighteen trees from six different species, three trees per species, was selected and monitored on a weekly basis from March to May of 2008 and from late

February to May, 2009. The tree species sampled were Oak, Ash, Horse Chestnut, Sycamore, Beech and Birch. The deciduous species were chosen for monitoring as the budburst and leafout phenological stages are more readily observed than the equivalent phenological stages in coniferous species. Initially, the age, orientation, height, health and location of each tree was estimated by noting broad categories from young to middle-aged to old and approximate height. The Beginning of Leaf unfolding (BO) is one of the most commonly recorded phases at the Irish IPG sites and is recorded with the appearance of several leaves across the tree canopy (IPG, 2005). However, such a small amount of leaf unfolding was difficult to observe from the ground in the high tree canopy. Therefore, the date when 50% of the tree crown was estimated to have unfolded leaves was recorded, and deemed to be the beginning of the growing season (BGS). The date of site visit when 50% of the leaves had unfolded in each tree was noted, as well as the percentage of leaves unfolded in the canopy on every other site visit. Site visits continued until the canopies had reached maximum leaf cover. Other than phenological observations, a combination of a field journal, photographic documentation of the greening stages per tree and GPS-measured waypoints formed part of the field study. The observations recorded at each site visit and the field journal is shown in appendix A.

A field journal was initiated on the first site visit to record the location and species of each tree, the direction it faced (aspect) and the estimate of age and health. This was followed by observations on other site visits such as the weather conditions, a

general description of the tree canopy, the change observed since the previous observations, the appearance of other flowers, the dense understorey of ferns and other shrubs as well as hedgerows which would be expected to contribute to the overall greening signal as viewed by a satellite sensor.

Photographs of the greening stages of some of the observed trees were taken on every site visit to document the progression of spring greening in the canopy, and were used to support the estimates of the timing of budburst and leafout. These trees were marked so that the same tree was photographed on a weekly basis. Photographs were taken from the same position each week for further consistency.

A GPS was used to gather way points in geographic coordinates (latitude/longitude) at regular intervals along the perimeter of the woodland. These points were converted to a shapefile (.shp) using the ArcMap software. The shapefile was overlaid on a MERIS image to identify the pixels which corresponded to the site of fieldwork. As can be seen in figure 3.3, this was useful to relate pixel values to the phenological observations. However, Currabinny Wood crosses two pixels in which surrounding water and other vegetation types contribute to the reflectance measures used to derive FAPAR.

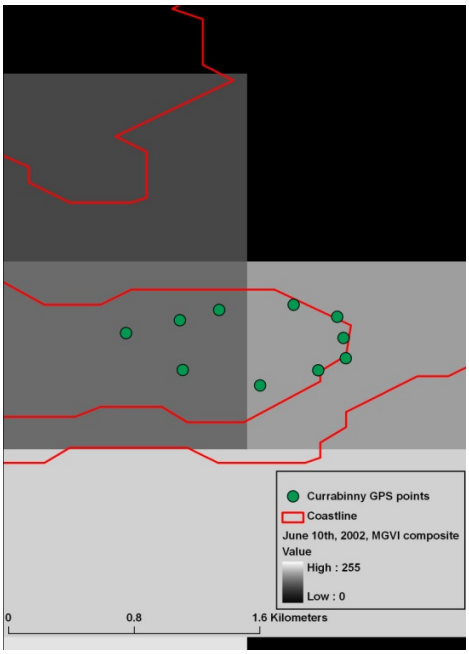

Figure 3.3: the Currabinny GPS points show the perimeter of the field site in relation to the coastline and the corresponding MGVI pixels. Currabinny Wood crosses two pixels in which surrounding water and other vegetation types contribute to the FAPAR response.

3.3.1.3 The rate of change in mixed woodland vegetation

Table 3.1 summarises the timing of the field BGS (timing of 50% unfolded leaves) in each tree species as observed at the field site in 2008 and 2009. Of the three trees per species, the tree with the earliest leaf unfolding and the latest leaf unfolding dates were selected in each year to show the annual range in leaf unfolding dates. The results show that for each species, the earliest and latest BGS events were between 3 and 17 days earlier in 2009 than in 2008. The dates for the Horse Chestnut tree were the same in both years; for all three sample trees.

Table 3.1: The earliest and latest BO of the sampled tree species in 2008 and 2009

	Year	Beech	Birch	Ash	Oak	Sycamore	Horse C.
	2008	07-May	09-Apr	14-May	09-Apr	09-Apr	09-Apr
Earliest BGS	**2009**	27-Apr	06-Apr	11-May	06-Apr	24-Mar	06-Apr
	2008	14-May	14-May	22-May	24-Apr	14-May	09-Apr
Latest BGS	**2009**	05-May	27-Apr	18-May	14-Apr	27-Apr	06-Apr

3.3.1.4 The inter-species variation in the timing of leafout

From table 3.1, it is evident that all tree species, except Horse Chestnut (Horse C.), produced leaves earlier in 2009 than in 2008 but the extent of the difference was not the same in all tree species. The rate of greening in the most common tree species in the woodland, Beech and Birch, is shown for both years in figure 3.4. The percentage of unfolded leaves observed on each site visit was averaged over the three trees per species. The cumulative percentage leaf cover is shown from the first observation until the tree canopy had 100% leaf cover, i.e. no further observable change in leaf cover on subsequent site visits.

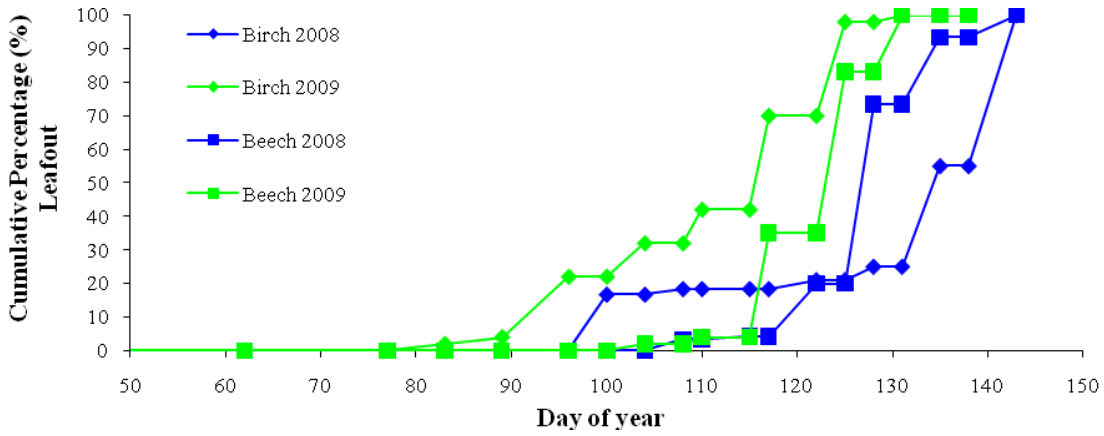

Figure 3.4: The average rate of leafout in the Beech and Birch trees in 2008 and 2009. The % leaf cover was estimated weekly and the values are plotted cumulatively until the canopies had 100% leaf cover (Day 50 represents the 20th February, 2008 and 2009 while day 150 represents May 30th in 2008 and May 29th in 2009).

The annual curves show that the rate of change is not consistent between years as the 2008 estimates (blue line) reveal a slow leafout initially followed by a quick rise from about day 125. The same effect is observed in 2009 (green line), but the surge of growth is less apparent and occurs earlier around day 115. The inter-species variation is evident by observing the difference in two curves from the same year. In 2008, the percentage of leaves accumulated in Birch trees (diamond symbol) is greater than in the Beech trees (rectangle symbol) up until day 115. The Beech percentage leaf cover then exceeds the Birch until both had maximum leaf cover towards the end of spring. In 2009, the leaf cover in both species was similar until about day 90 when the Birch increased in green canopy cover and maintained a thicker canopy than the Beech tree until the end of observations. These results show that in comparing both years, earlier growth was detected in 2009 than in 2008 for both Beech and Birch, but that within years, the Birch trees consistently greenup more rapidly than the Beech trees in this sample. Although these findings are based on two years of data and only three trees per species, they would be expected to represent the tree phenology in the area.

3.3.1.5 The photographic documentation of leaf unfolding in a tree canopy

The photographic data provided a visual record of the percentage of canopy cover of an individual tree, which supported estimates made in the field. A handheld digital camera was used to record the onset of growth in a Birch tree at Currabinny wood, in weekly intervals, from the first observation on 3/3/09 to the last observation on 11/5/09, can be seen in Figure 3.5 (A)-(H). The point from which the digital images

were taken was constant but the variation in daily illumination conditions can affect visual interpretation so that some stages appear more or less green than is suggested by the percentage estimates.

Figure 3.5: Various phases in onset of the beginning of leaf unfolding (BO) in Birch (*Betula pubescens*). (A) Birch in dormancy, (B) Budburst, (C) 20% BO, (D) 40% BO, (E) 50% BO, (F) 70% BO, (G) 90% BO, (H) 100% BO.

3.3.1.6 Fieldwork findings

A weekly revisit time was adequate to observe seasonality change, in terms of the percentage leafout. This suggested that a 7-day composite period would be optimal to monitor the BGS. However, it was necessary to verify whether combining daily MGVI data over a 7-day interval would produce enough cloud-free imagery for a national-scale study. Firstly, daily cloud observations at a representative location on the island were acquired to examine seasonal and annual cloud cover over 7-day intervals.

3.3.2 Armagh Observatory cloud data

Human observer networks are used to record a number of cloud variables, such as percentage cloud cover, to validate satellite observations of cloud cover, as well as a means to understanding daily cloud cycles (Chambers et al., 2004). Ground observations of cloud cover are provided at a number of weather stations throughout the country, but the data are provided on a request basis only and at cost from the Irish Meteorological service, Met Éireann. However, a readily available and free source of cloud observation data, dating back over 200 years, is available to the public from the Armagh Observatory Meteorological Station in Northern Ireland. The inland location of the Observatory (shown in figure 3.6) is also representative of the island in terms of its situation away from any coastal and upland influences in cloud formation. The observations are daily at 9 a.m. and are archived online where they are available to download for general use[2]. Cloud cover is estimated on a scale from zero to eight okta, where eight okta represents a fully-clouded sky. The current observer has been recording observations since 1998.

[2] http://climate.arm.ac.uk/main.html

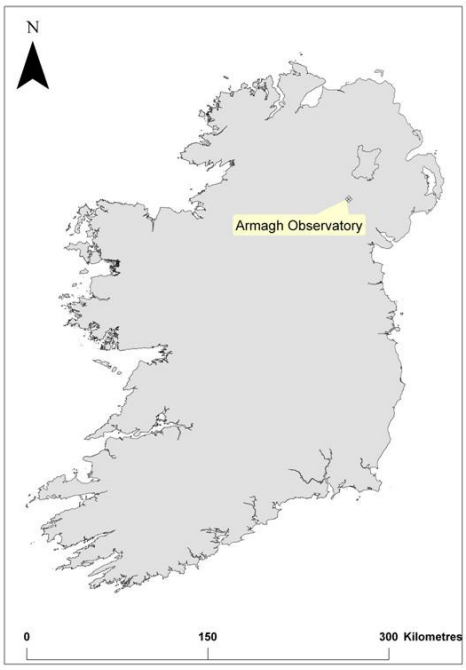

Figure 3.6: Location of Armagh Observatory, site of daily cloud estimates

3.3.2.1 Temporal patterns in cloud cover at Armagh Observatory

The first aim of using daily Armagh cloud observation was to investigate interannual trends in cloud cover during the growing season (February to October), and, secondly, to find out by how much cloud cover varied during the growing season. For this, the daily observations were averaged over seven days for three full growing seasons from 2005 to 2007. The temporal trends in cloud cover at Armagh, averaged over 7-day intervals are shown in figure 3.7.

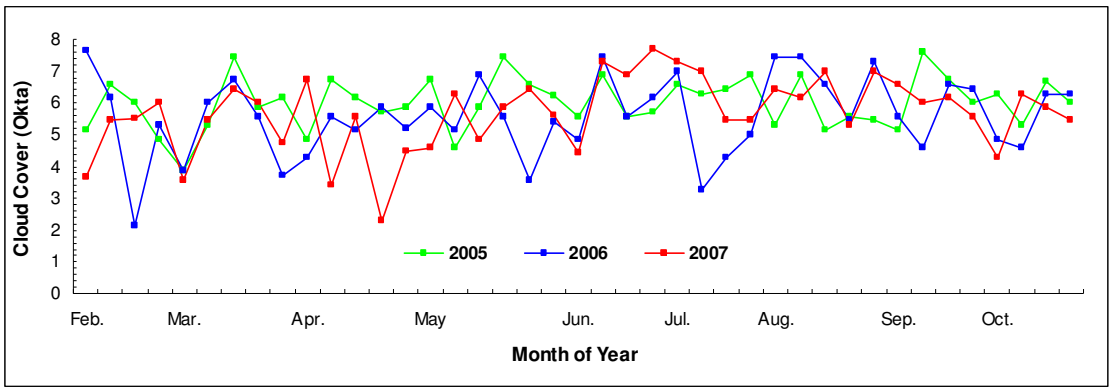

Figure 3.7: The 7-day average cloud cover amounts (Okta) observed at Armagh Observatory for the growing season of 2005 to 2007

From figure 3.7, it is difficult to discern seasonal trends in cloud cover because of the high variability in the 7-day averaged values. However, in 2006 and 2007 the period from March to June appears to have the lowest cloud cover followed by a shorter period in July and August, while there is no seasonal trend apparent in 2005.The 2006 and 2007 trends agree with averaged monthly satellite-derived cloud cover over Ireland, during the period 1983-1994, which show that April and May had the lowest average cloud cover (Pallé and Butler, 2001). Therefore, the 2005 cloud cover would appear to be anomalous. Owing to the high extent of cloudiness in the 7-day averaged values of the Armagh data, it would be unlikely to find a cloud-free day in every MERIS image pixel during 7-day intervals. Therefore, a longer interval of ten days was analysed further (figure 3.8).

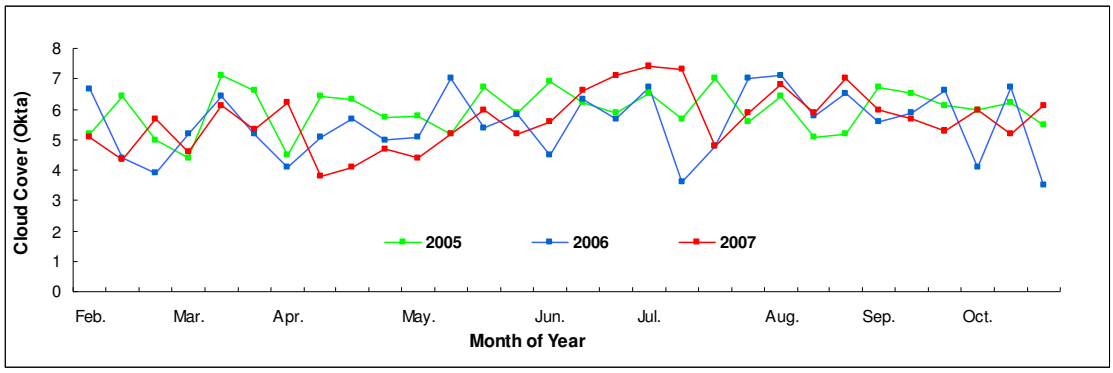

Figure 3.8: Same as in figure 3.7 but using a 10-day averaging period

The 10-day averaging period was applied to daily Armagh data, as shown in figure 3.8. A smoother temporal trend was produced from the 10-day averages, revealing the interannual and seasonal cloud cover variability. As suggested by figure 3.6 in 2007 (red line), the cloud cover was very low in April and May compared with the other two years. The inter-comparison of 10-day and 7-day averaged values of Armagh cloud observations showed that a longer averaging period produced a smoother cloud trend. However, in order to select the period which maximised the chance of finding a pixel with at least one cloud-free day in the period, it was necessary to analyse the number of cloud-cover periods per image pixel in a time series of 7-day and 10-day composite images.

In order to verify whether the Armagh cloud observations were a good indicator of island-wide cloud trends as detected in the MGVI composite images, and hence a suitable cloud dataset to inform the selection of a composite period, the Armagh Observatory observations were initially averaged over 10-day periods and compared with cloud amounts in MGVI 10-day image composites for the whole island over the

same time period: the beginning of February to the end of October, 2007. This period was chosen as monthly weather summaries showed that low cloud amounts were present across the country from the beginning of April to the beginning of June, 2007, owing to higher than normal sunshine hours (Andrade et al., 2011). Figure 3.9 illustrates the results of this comparison exercise.

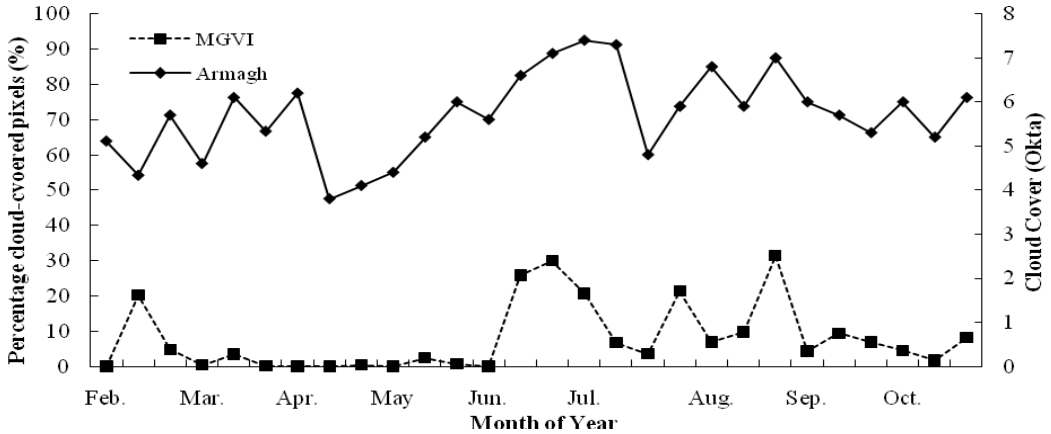

Figure 3.9: A comparison of cloud estimates at Armagh with the percentage of cloud-flagged pixels per MGVI 10-day composite for the growing season, beginning 1st of February and ending, 31st of October, 2007.

It is evident that cloud observations at Armagh are in reasonably good qualitative agreement with cloud amounts detected by MERIS over the whole island, except for the early spring period (March – April), where island-wide cloud trends, as detected in the MGVI, were extremely low (between 0 and 10 % for March, April and May) in contrast to reasonably large amounts of cloud cover observed at Armagh (between 4 and 7 Okta). Therefore, a representative year was chosen from the three years examined, on which to base the selection of a composite period for the MGVI data. Owing to the anomalously low cloud amounts in 2007 and the absence of seasonal variation in cloud cover in 2005, these were not considered appropriate years for

informing the selection of a composite period. Therefore, the period from March 1st to June 29th, 2006 was selected to compare cloud cover in 10-day and 7-day composite MGVI data and select an appropriate composite period.

3.3.2.2 Temporal analysis of cloud-flagged pixels in 10-day and 7-day MERIS image composites

Firstly, temporal analysis was conducted on the percentage of image pixels that were cloud-covered from March 1st to June 29th, 2006. Secondly, spatio-temporal analysis over the same period was used to reveal the spatial pattern in cloud-cover across the island. For the temporal analysis, the percentage of cloud-flagged land pixels in each composite image was calculated and plotted for each period in the time series, as can be seen in figure 3.10. Then, a threshold of 10% cloud-covered land pixels was selected as an acceptable minimum level of potential data loss. Less than 10% cloud cover was achieved on 77% of the 10-day composites, compared with 50% of the 7-day composites. This suggests that there will be fewer data gaps due to cloud in 10-day imagery than in 7-day imagery.

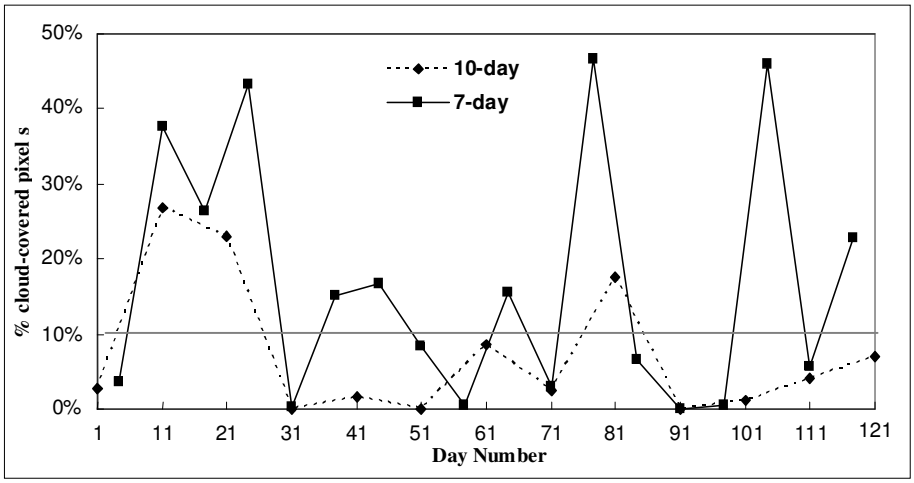

Figure 3.10: A comparison of the percentage of MERIS pixels over the island of Ireland that are cloud-covered per 7-day and 10-day composite period during spring 2006 (Day 1 represents March 1st and day 121, June 29th).

3.3.2.3 Spatio-temporal analysis of cloud-flagged pixels in 10-day and 7-day MERIS image composites

In the previous analysis, the temporal trend of cloud in different composite periods was examined. However, the spatial distribution of the cloud across the island was not shown. For this, binary images of the cloud and non-cloud pixels for each image composite were created using the cloud flag information. The number of cloud flags per pixel in a time-series of eighteen 7-day and thirteen 10-day composite images from March 1st to June 29th, 2006 was then calculated. This was carried out for both water and land pixels, as can be seen in figure 3.11 (a) and (b). Both images have a maximum of six cloud flags per pixel over the test period, i.e., there were no valid data for six composite periods. The surrounding ocean has relatively fewer cloud periods, but this is an artefact of MERIS processing rather than any meteorological

occurrence as cloud pixels over the ocean had already been removed from the scene before the MGVI cloud-detection algorithm was applied across the image (ESA, 2006b).

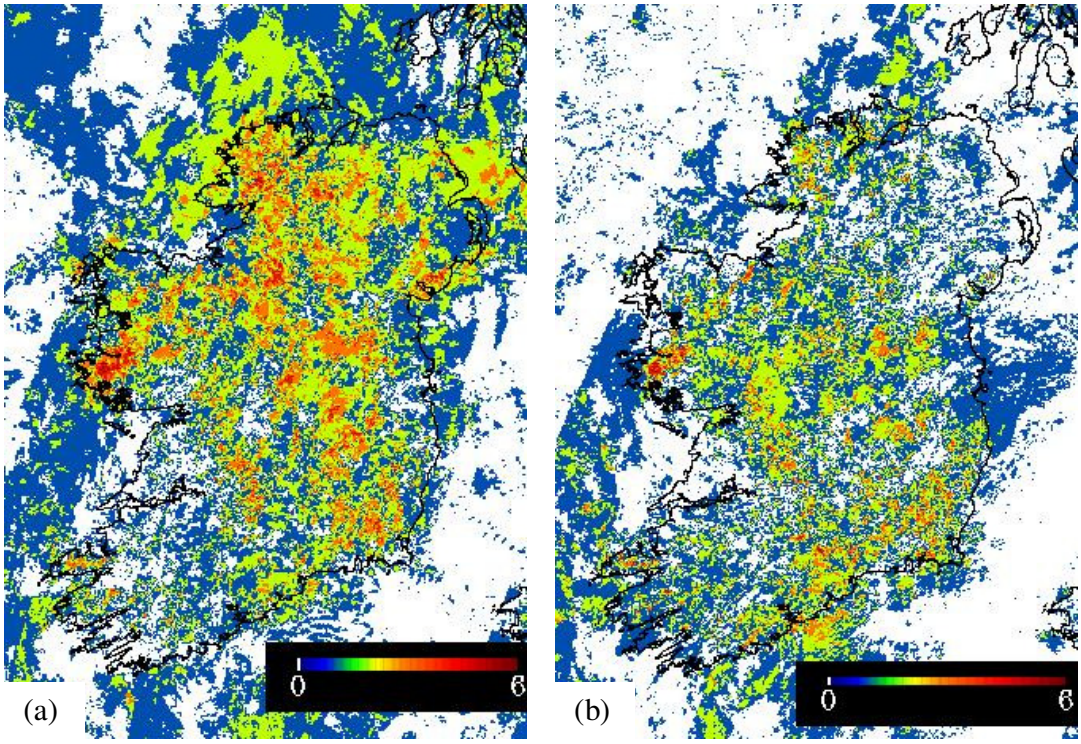

Figure 3.11: The number of cloud-covered composite periods per pixel over the island of Ireland in the period, March 1st to June 29th, 2006 (a) using 7-day composites and (b) using 10-day

From figure 3.11(a) and (b), the occurrence of cloud appears to follow a spatial trend across the island. The East coast appears to have the lowest amount of cloud relative to the rest of the island while the Northwest, West and Midlands tend to have more cloud than anywhere else. Small concentrations of cloud appear over the coastal peninsulas in the southwest, while some western coastal areas are almost totally cloud-free in both images. A frequency distribution of the number of cloud flags reported per pixel during the test period is presented in figure 3.12.

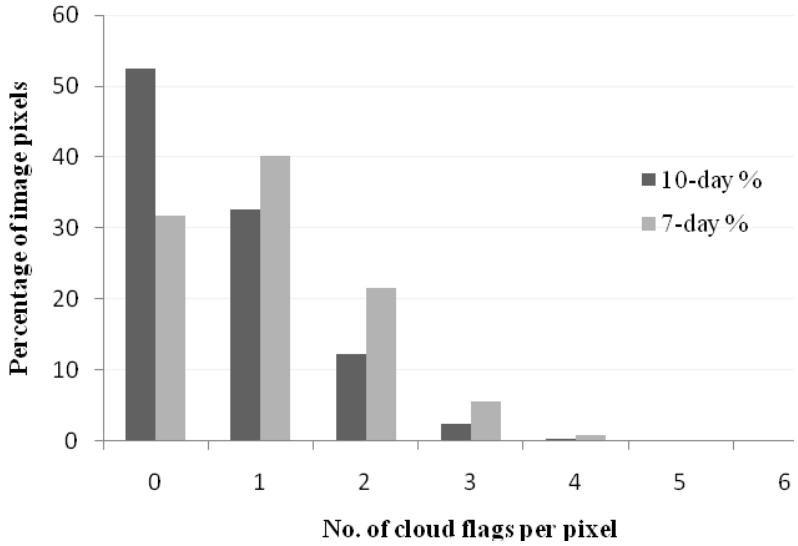

Figure 3.12: A frequency distribution of the number of cloud flags per pixel in a time series of eighteen 7-day and thirteen 10-day composite images in the period, March 1st to June 29th, 2006

Although both composite periods had a maximum of six cloud-covered periods in the March-June period, the percentage of image pixels per number of cloud-covered periods was quite different. For example, 52 % of the 10-day cloud composite image pixels had no cloud-covered periods, compared to 32% of the pixels in the 7-day image composite. However, 22% of the 7-day cloud composite pixels had two cloud-covered periods, compared to only 12% of the 10-day cloud composite pixels. Overall, there were a lower percentage of 10-day image pixels with one or more cloud-covered periods than 7-day image pixels. Therefore the 10-day period would be expected to offer better temporal coverage than the 7-day composite as it maximises the number of cloud-free days per pixel within the composite.

3.3.2.4 Generating annual cloud composite images from MERIS data

The spatial distribution of cloud discussed above is only indicative of cloud cover during four months of 2006. In order to investigate the spatial distribution of cloud detected by the MERIS cloud mask and the MGVI cloud detection algorithm across the island on an annual basis, the same method was applied, as described in the previous section, to annual time series of the 10-day image composites, i.e. thirty-six 10-day periods per year, which are shown in figure 3.13 (a)-(g).

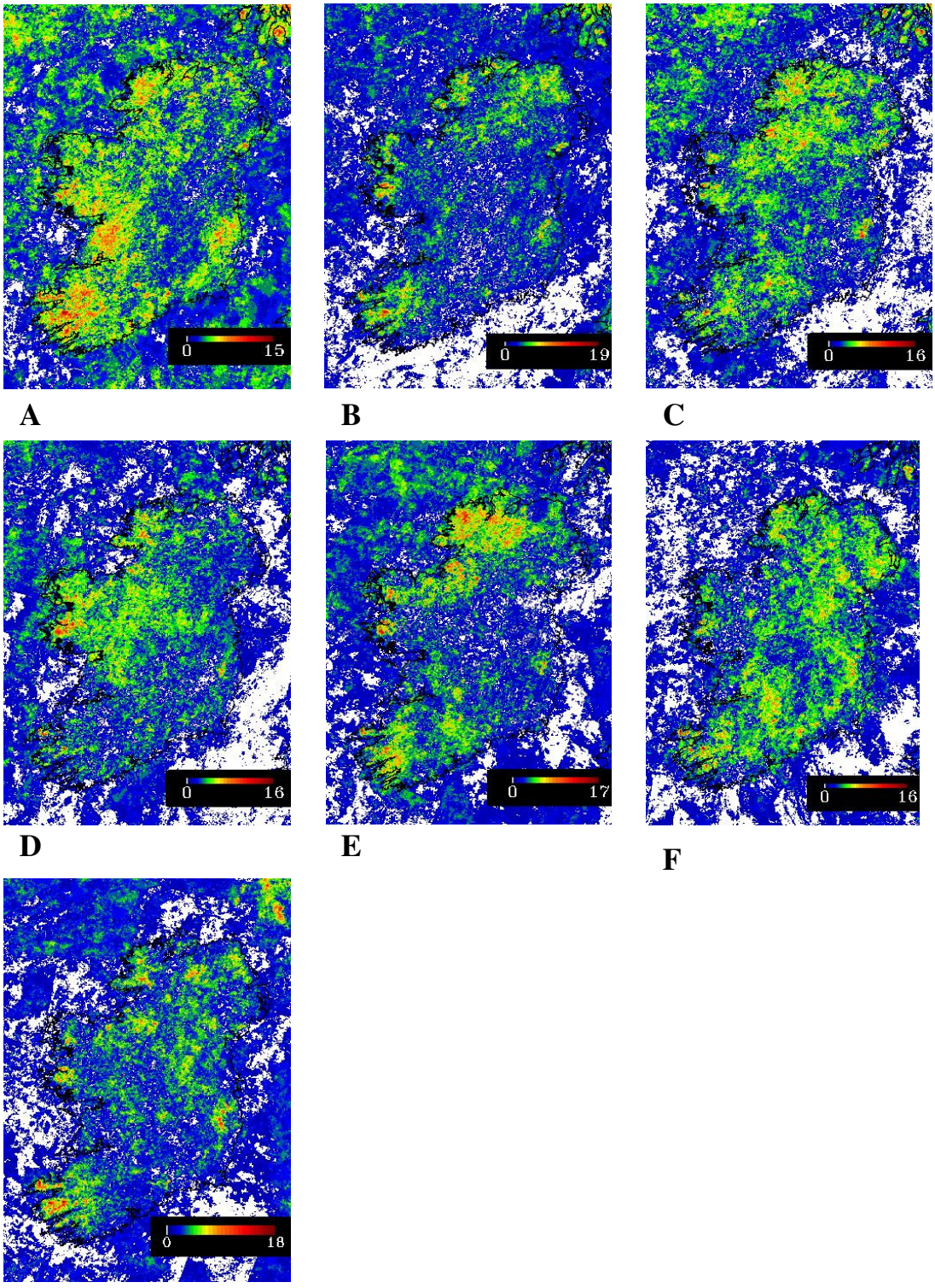

Figure 3.13: Annual 10-day cloud composites generated over the island of Ireland using both cloud flags derived from the MERIS cloud mask and the MGVI cloud-detection algorithm (A) 2003, (B) 2004, (C) 2005, (D) 2006 (E) 2007, (F) 2008, (G) 2009. The colour bar indicates the number of cloud-covered 10-day periods from a total of 36

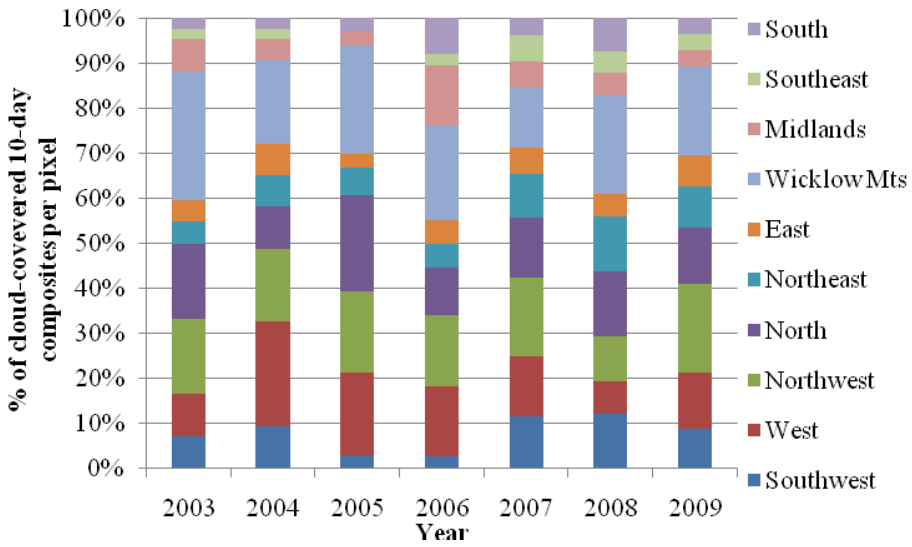

Figure 3.14: The percentage of cloud-covered 10-day periods per pixel from 2003 to 2009. The pixels were selected from each region of the country to show variability in cloud cover per year

In figure 3.13, there are consistent spatial patterns to the annual images. For example; the Northwest, West and Southwest are dominated by areas of high cloud concentrations. There are also high cloud amounts over the Wicklow Mountains. All these areas are upland and mountainous suggesting that orographic cloud (generated by moist air rising and cooling over mountains) is routinely detected in MGVI pixels. In figure 3.14, the percentage of cloud-covered periods per pixel, one selected for each region across the island, has been derived from the cloud composite imagery in figure 3.13. The spatial pattern in cloud cover is characterised by a high number of cloud-covered periods in the southwest, west and northwest and in the east over the Wicklow Mountains. The column chart in figure 3.14 demonstrates the higher frequency of cloud cover over mountains within each year as the highest proportions of cloud-covered periods occur in the Wicklow Mountains

followed by upland areas the northwest and west. In contrast, the south, southeast and east have a much smaller number of cloud-covered periods from the annual total. This relative difference in cloud-cover detected by MERIS cloud screening and MGVI cloud-detection has implications for the selection of local sites for satellite based phenological monitoring. The appropriate composite period at a regional scale would require further examination if phenological events are to be monitored without cloud preventing detection of changes in the VI time series. This is particularly the case in mountainous regions of the western seaboard, along the northern coast and over the Wicklow Mountains. However, areas with fewer cloud-covered periods, e.g. Midlands, will have comparatively fewer data lost due to cloud, and would therefore be more suited to satellite-derived phenological monitoring.

3.3.3 Summary of composite period selection

Cloud cover in the daily MGVI grids was the main justification for compositing the daily data, while ensuring the interval was also suited to tracking spatio-temporal variability in the vegetation BGS. However, there were considerable implications of shortening or extending the period. In extending the period, there are spatial gains in terms of coverage of cloud-free imagery. Yet, the period could not be extended indefinitely due to the reduced-sensitivity of the composite value to spatio-temporal variation in vegetation growth. Minimising the time period would have the opposite effect of maximising the sensitivity of the VI measure at the expense of cloud-free imagery. This was evident even in a 10-day period when data gaps still appeared in

the MGVI time series. Time-compositing inevitably adds uncertainty to studies of vegetation seasonality from remotely-sensed data, but is a necessary requirement for temperate mid-latitude regions given the reduced spatial and temporal coverage of valid MGVI data in the daily imagery.

3.4 Verification of MGVI clear sky values with the METEOSAT cloud mask

This section describes a validation of the effectiveness of the MGVI cloud screening strategy. The need for this validation exercise has been driven by the appearance of noise in the MGVI time series which may be caused by undetected cloud in MERIS pixels. Initial analysis of single pixel 10-day composite MGVI time series data showed that the transition between adjacent data points was not smooth but tended to be highly variable over short time periods. This resulted in frequent positive and negative spikes in the time series. An example of the instability in the MGVI time series is given in figure 3.15 (a). Although a smoothing function can be fit to the raw time series data (figure 3.15 b), noise in the underlying time series may still detract from the ability to accurately determine vegetation seasonality parameters (Eklundh and Jönsson, 2010).

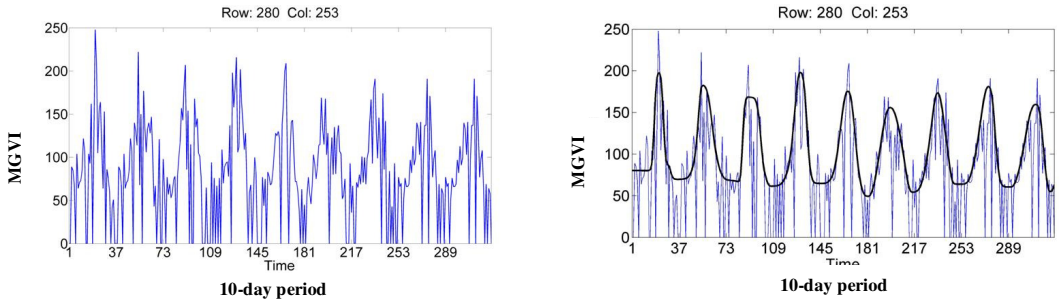

Figure 3.15: (a): The blue line represents the raw MGVI time series. (b) The thick black line shows the fitted smoothing function.

Previous concerns have been raised about the effectiveness of the MERIS cloud mask in that thin clouds are not consistently detected over land, while ice and snow are frequently mistaken for cloud (MERIS, 2006). These shortcomings have been recently documented in relation to land surface applications (Gomez-Chova et al., 2007). In order to ascertain the impact of these limitations on the quality of daily MGVI values within the 10-day composite, the METEOSAT Cloud Mask (CLM) was selected as a suitable independent cloud product for the comparison study. The daily valid MGVI values were compared to coincident CLM pixels, and the daily values of the allegedly cloud-free MGVI pixels were examined to investigate whether spikes of noise appeared where there was cloud in the CLM pixel.

3.4.1 Cloud detection in the MGVI product

Detection of cloud relies upon well known physical features in remotely sensed imagery, namely that they have a high albedo and low temperature (Gomez-Chova et al., 2007). Their presence in an image is detected by a set of thresholds in spectral bands, e.g. the thermal infrared because it is sensitive to cloud temperature, in order to discriminate them from other surfaces such as snow, ice and sand (Menghua and

Wei, 2006). Although the application of thresholds is a generally accepted method of cloud detection in the optical spectrum, the setting of specific threshold values is influenced by the sensor's spectral range. For example, the METEOSAT SEVIRI (Spinning Enhanced Visible Infra-Red Imager) sensor has been designed solely for meteorological applications, and therefore has the potential to detect types of cloud which the MERIS sensor cannot. The MERIS spectral range (0.4-0.9 µm) covers the visible to near infrared spectrum in narrow bandwidths while the SEVIRI instrument covers the same range, as well as the water vapour absorption region (5.7-7.1 µm), but in wider intervals. Furthermore, the SEVIRI cloud detection algorithm uses a combination of thirty-four threshold tests, combined with weather forecast data and radiative transfer model outputs (EUMETSAT, 2007). This is a more complex cloud-detection strategy than the simple threshold test on which the MGVI cloud-detection algorithm is based (Equation 9.3). The MGVI undergoes two distinct cloud screening stages, the application of the MERIS cloud mask to raw MERIS imagery followed by a scene analysis by the MGVI cloud-detection algorithm. Raw MERIS pixels represent TOA radiance values which are categorised into four surface types; ocean, land, bright surface over ocean and bright surface over land, based on their radiometric characteristics. Cloud is separated from other bright surfaces at this level using land surface and cloud top pressure tests in MERIS bands 10 (centered at 753.75 nm) and 11(centered at 760.63 nm) (Santer et al., 1997). Following the separation of cloud from land and ocean pixels, the land pixels are fed into the land branch of the processing chain. Here, atmospheric-corrections are applied and the

pixels are cloud-screened. A series of tests is done on the ratio of Rayleigh-corrected reflectance at different wavelengths, the results of which are used to index a decision tree identifying cloud pixels. The MERIS cloud mask is constructed on the basis of positively identified cloud pixels (ESA, 2006b). After further surface-specific atmospheric corrections, e.g. over areas of dense, dark vegetation, the FAPAR algorithm is applied to land pixels (ESA, 2006b). Internal MGVI spectral tests, one of which identifies pixels of clouds, snow and ice, provides the per-pixel flag information in the time-composited product (Pinty et al., 2002). The cloud spectral test relies on thresholds in three MERIS bands and is described below (Gobron et al., 2004).

Equation 3.3 the MGVI threshold test for cloud, snow and ice detection

$$\rho_{BLU} \geq 0.3$$
$$\text{or } \rho_{RED} \geq 0.5$$
$$\text{or } \rho_{NIR} \geq 0.7$$

Where ρ =BRF values and BLU= Blue band (442.5 nm), RED=Red band (681.25 nm) and NIR=near infrared band (865 nm)

3.4.2 The selection of the METEOSAT Cloud Mask (CLM)

EUMETSAT has been responsible for the operation of the METEOSAT satellite series since 1995, including the acquisition, processing, dissemination and archiving of the data, a task previously carried out by ESA (EUMETSAT, 2001). Due to the equatorial location of the geostationary orbit, the maximum latitude visible to the satellite is 81.27° N/S, and imagery of Ireland is acquired (EUMETSAT, 2001).

The data are acquired in thirty minute intervals as SEVIRI records a line of image data on every rotation. The sensor measures reflectance across three spectral wavebands; the visible (VIS) data are acquired at 2.5 km spatial resolution while the thermal infrared (IR) and the water vapour (WV) absorption bands acquire data at 5 km spatial resolution. The optimal spatial resolution of the sensor (3 km) is maintained at the sub-satellite point but degrades with distance (Pers comm, Richards, 3/11/2009). The METEOSAT-derived meteorological products were acquired from the Meteorological Archive and Retrieval Facility (MARF). Two cloud products were considered for this work, the Clear Sky Radiance (CSR) product which contains the percentage of clear sky in an image pixel and the Cloud Mask (CLM) product which only distinguishes cloud from clear sky areas (EUMETSAT, 2001). Although the CSR product gives more precise cloud information than the CLM, it is a coarser spatial resolution product. The CLM was selected for this work as it has a finer grid resolution and, since the launch of Meteosat-8 in 2006, data are acquired every fifteen minutes (Pers comm, Richards, 3/11/2009).

3.4.3The analysis of MGVI clear-sky values using the CLM

Daily valid MGVI data, i.e. non-cloud pixels, were compared to the CLM pixels for the same day and time defined as land, ocean and cloud. A sample of fifty daily METEOSAT CLM grids corresponding to five 10-day MGVI composite periods were selected for the comparison study. As the MERIS time-composite pixels were acquired on different days, over-pass times of the MERIS sensor had to be

confirmed so that coincident METEOSAT CLM data could be acquired. This information was obtained indirectly from an analysis of the solar zenith and azimuth angles provided per pixel in the MGVI composite product and corresponding time of day (UTC) calculated using the NOAA solar calculator (Cornwall et al., 2010). Although the acquisition time varied, even for pixels acquired on the same day within the composite image, the daily difference was not greater than the time interval between METEOSAT acquisitions. This can be seen from the calculated solar times in table 3.2 for five pixels in one composite image during the period, January 21st-30th. The difference in acquisition times between pixels on the far left and far right of the image is 38 seconds on the 29th January and 5 seconds on the 21st January. The full list of overpass times for MERIS and the corresponding METEOSAT acquisitions are given in Appendix B.

Table 3.2: The acquisition times of MERIS sensor per pixel during the composite period from 21st to the 30th January, 2006.

Pixel position	Day of month	Solar time (UTC)
Upper Left	29	11:41:02
Upper Right	29	11:40:40
Lower Left	21	10:53:47
Lower Right	21	10:53:52
Centre	26	11:36:32

3.4.3.1 The five comparison tests

The daily CLM grids were ordered in NetCDF format, using the online MARF tool, for the nearest time to the MERIS over-pass time, calculated from a pixel which was valid on that day. Next, the CLM cloud mask was remapped and resampled to a 1.2 km grid, equivalent in size to the MGVI grid over Ireland. For each day within the

MGVI composite period valid pixel values were extracted and compared to their CLM counterparts. The criteria for the five tests are summarised in table 3.3. The number of pixels corresponding to each test result was calculated as a percentage of the total number of daily valid pixels or the total number of daily invalid pixels, depending on the test. The 21st January 2006, was selected as a day to illustrate the remapping output and the results of the comparison tests as it was a relatively clear day across the island, with a high number of the time-composited values for this 10-day period (January 21st -30th) chosen on this day. The number of clear sky values extracted from the daily MGVI (dMGVI) can be seen in figure 3.16 (a) and the remapped CLM output with the dMGVI grid and computed test results in Figure 3.16 (b). A small number of MGVI pixels remain outside the extent of the CLM grid and therefore retain a value of 0.

Table 3.3: New pixel values assigned based on the comparison of coincident METEOSAT and MGVI pixels (note that an ocean mask prevents MGVI being calculated over open water) and the five test results from 21st January, 2006

Test	Description	Pixels (%)
1	Valid MGVI with CLM land	95
2	Invalid MGVI with CLM cloud	46
3	Valid MGVI with CLM cloud	4
4	Invalid MGVI with CLM land	31
5	Invalid MGVI with CLM ocean	23

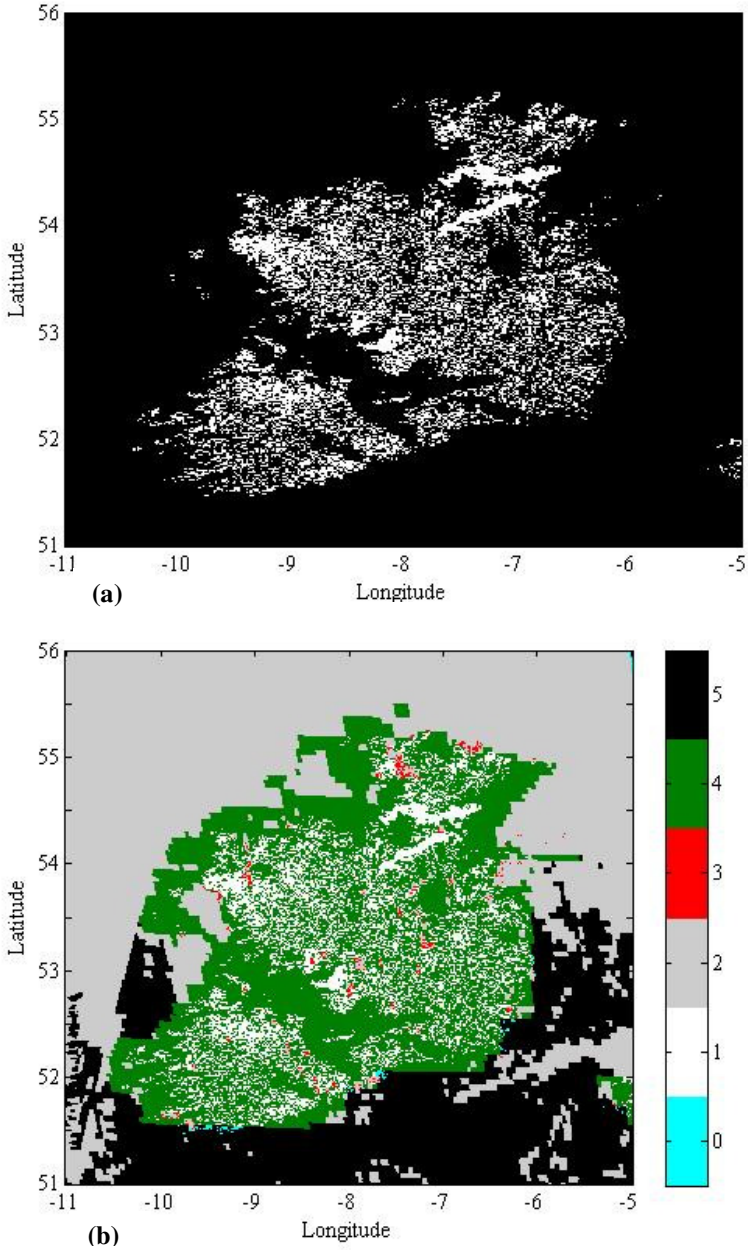

Figure 3.16: (a): The dMGVI grid on the 21st January, 2006. The representative MGVI pixels selected on that day to represent the composite period are shown in white, (b): The 21st January, 2006, result grid from the comparison of MGVI and METEOSAT CLM 11 a.m. grid: The grid pixel values correspond to the appropriate test number: 0 is un-compared value, 1 is valid MGVI and land, 2 is invalid MGVI and cloud, 3 is valid MGVI and cloud, 4 is invalid MGVI and land, 5 is invalid MGVI and ocean.

Given the relatively clear conditions on 21st January, 2006 , almost all the valid MGVI pixels corresponded to METEOSAT clear sky (95% in test 1), while only a very small proportion (4% in test 3) were defined as METEOSAT cloud, mostly under scattered cloud over land. Of the invalid MGVI pixels, a third of them (31% in test 4) occurred in areas identified as cloud-free land by METEOSAT, while a greater number were identified as cloud (46% in test 2). This indicates that factors other than cloud determine valid value selection. The remaining invalid MGVI values (23%) were in ocean pixels (table 3.3).

3.4.3.2 The verification of MGVI by the METEOSAT CLM for the total sample

This analysis was expanded to a 50-day sample, i.e. fifty daily CLM subsets and five 10-day MGVI composites, January 21st-30th, April 21st-30th, June 20th-29th, September 28th-October 7th and November 27th-December 6th, from 2006. These periods were selected to capture the annual variation in cloud cover across the island. There were no valid MGVI values available on twelve days of the fifty-day sample so only thirty-eight grid comparisons could be carried out. In table 3.4, the results of the validation tests for the daily valid MGVI are presented. The addition of

test results does not equal 100% in some cases due to the presence of MGVI pixels outside the extent of the CLM grid.

Table 3.4: The sample percentage values for test 1 and 3 were calculated from the number of pixels identified by each test as a percentage of valid MGVI values on that day. The mean test results per composite period are also included.

Date	Total MGVI daily valid pix	CLM cloud-covered but valid MGVI pix (test 3)	CLM land and valid MGVI pix (test 1)	Test 3 (%)	Test 1 (%)
20060121	16384	598	15637	4	95
20060123	1130	1130	0	100	0
20060124	1545	141	1404	9	91
20060126	2110	445	1599	21	76
20060127	1956	106	1798	5	92
20060129	33630	4515	28838	13	86
Comp. Mean				**25**	**73**
20060421	5	5	0	100	0
20060423	13048	7892	4937	60	38
20060425	7465	5821	1473	78	20
20060426	2551	2055	491	81	19
20060427	259	38	192	15	74
20060428	35841	1543	34032	4	95
20060429	2522	1035	1410	41	56
Comp. Mean				**54**	**43**
20060621	10573	8432	2132	80	20
20060622	6713	5726	923	85	14
20060623	3435	2483	949	72	28
20060624	2080	2018	48	97	2
20060625	21641	14893	6651	69	31
20060626	6723	5438	1230	81	18
20060627	1346	1160	138	86	10
20060628	5960	5911	37	99	1
20060629	1164	939	198	81	17
Comp. Mean				**83**	**16**
20060928	6360	6164	195	97	3
20060929	18523	15423	2853	83	15
20060930	45	35	10	78	22
20061001	9934	9311	566	94	6
20061002	10736	9311	978	91	9

20061003	1287	1047	226	81	18
20061004	9932	8971	949	90	10
20061005	222	222	0	100	0
20061006	1711	1507	204	88	12
20061007	1541	1536	5	100	0
Comp. Mean				**90**	**9**
20061127	6039	1003	5023	17	83
20061201	4225	2475	1731	59	41
20061202	22064	2353	19518	11	88
20061203	6	5	1	83	17
20061204	183	178	5	97	3
20061205	7193	2345	4785	33	67
Comp. Mean				**50**	**50**

Table 3.4: Continued

In table 3.4, it can be seen that there was a considerable range in the number of daily valid values on each day within the composite. For example, there were five valid pixels on 21st April and over thirty thousand on 29th January. This resulted in high variability in the percentage results from each of the tests applied. For example, on 23rd January all of the valid MGVI pixels were cloud-covered, according to the CLM, while on 27th January, there was only a small amount of misclassification (5%). Owing to the inconsistency in these results, there is no definitive conclusion as to whether cloud cover is routinely undetected in valid MGVI pixels, although it is suggested that most but not all cloud cover is detected in the MGVI product.

3.4.4. The influence of cloud-flagged values on MGVI time series data

In order to investigate whether the cloud-covered pixels produce anomalies in the MGVI time series, five MGVI values in the time series of ten randomly-selected MGVI pixels were inspected to investigate whether spiked values coincide with cloud-cover. Spikes in the time series were identified by comparing the mean of the

left and right neighbours of the inspected value to the value of interest. A positive (upward) spike was noted if the inspected value exceeded the mean by more than 20% of its value, and a negative (downward) spike noted when it was less than the mean by more than 20 %. There was no spike when the inspected value was within the mean ±20 % range. The process of spike identification is illustrated graphically in figure 3.17

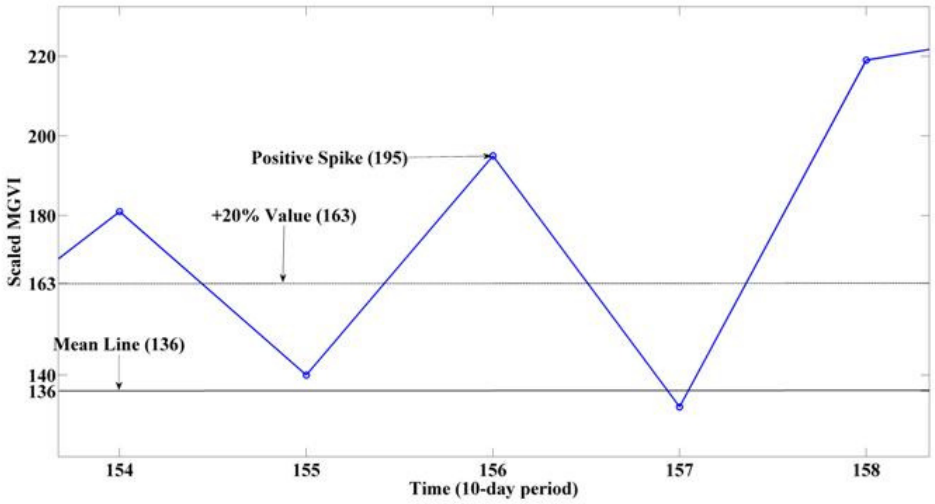

Figure 3.17: The composite value at period 156 is anomalous with respect to the left and right neighbour indicated by an upward spike. The mean line is calculated from the left and right neighbouring value and the +20% value is also shown.

The sample for the analysis consisted of fifty inspected MGVI values, i.e., ten pixels spread across the country within five composite periods. Their values were cross-checked with the corresponding CLM flags in order to investigate any link between undetected cloud and time series spiked values. Six tests were used to include all the possible combinations of clear and cloud-flagged pixels and the presence of positive

and negative spikes as well as normal values. The criteria for each test are presented in table 3.5.

Table 3.5: The criteria for the six tests used to cross-check spiked and non-spiked values with the corresponding cloud flags are shown.

Test	Criteria
1	Cloud,+ spike
2	Cloud,- spike
3	Cloud, no spike
4	No cloud, + spike
5	No cloud, - spike
6	No cloud, no spike

Of the fifty MGVI time series values, inspected for the presence of spikes, two were data drop-outs. This meant that the valid sample for the spike analysis contained 48 MGVI values of which 17 were cloud-covered and 31were cloud-free. Of the 17 cloud-contaminated values, 53% of them produced a spiked value while 47% did not. Of the 31 MGVI values that were validated as land by the CLM, 45% of them produced a spike while 55% produced no spike. The results are illustrated in the column chart in figure 3.18.

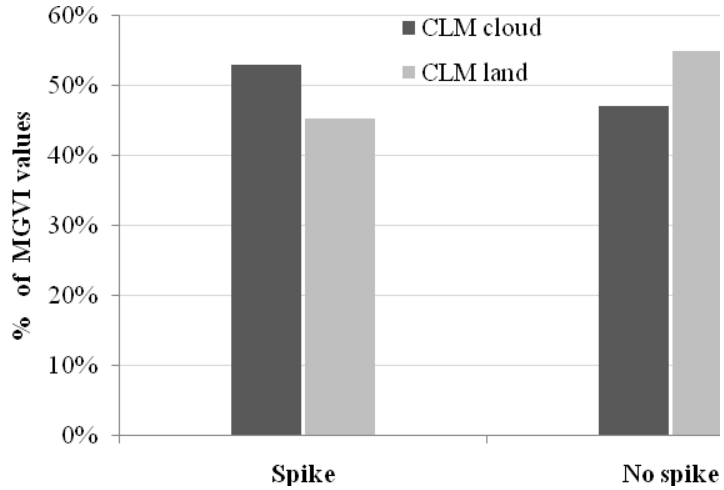

Figure 3.18: A column chart showing the percentage of cloud-covered and cloud-free MGVI values that produced spikes in the MGVI time series values

3.4.5 Summary of validation results

Comparing the MERIS data with coincident METEOSAT cloud mask data showed that valid FAPAR pixels were frequently cloud-covered, e.g. twenty-seven of the thirty-eight MGVI grids (71% of the sample) had 50% or more cloud-covered valid MGVI pixels across the image (calculated from test 3 values in table 3.6). This shows that apparently cloud-free values obtained by MERIS are in fact cloud-covered according to the METEOSAT CLM. The consequence of this is that there are fewer valid MGVI with land and cloud-free CLM than might be expected, i.e., only 39% of the sample had more than 50% of MGVI pixels per image that were cloud-free and valid. After inspecting the fifty time series values, anomalous spikes did not consistently occur where the values were cloud-covered as there were almost equal proportions of spikes present on occasions when the METEOSAT cloud

masks indicate clear and cloudy skies. This would suggest that anomalous variations in the MGVI time series could be potentially caused by cloud cover but it is not the sole cause of their occurrence.

3.4.6 Other contributing factors to MGVI time series noise

An examination of the literature suggested that factors other than cloud such as poor radiometric correction, uncorrected scattering by aerosols, or increased absorption by water vapour over Ireland resulting from its maritime climate might be likely causes in producing anomalous values in the MGVI time series. Others who have used the MGVI data have not reported such widespread noise when working at lower latitudes and in more continental climates (pers. comm.Gobron, 2010). Poor atmospheric corrections are a possible contributory factor to time series instability (Pinty et al., 2002). However, a rigorous analysis of the quality of atmospherically-corrected MERIS measurements was not within the scope of this study. The MGVI algorithm uses the 6S atmospheric model to simulate the absorption and scattering processes of the atmosphere and determine their effect on the MERIS reflectance data used in the construction of the index (Gobron et al., 1999). An example of atmospheric correction by the 6S atmospheric model is presented in figure 3.19 (Vermote et al., 1997). This example illustrates how atmospheric correction limits, but does not remove, the absorption processes of the atmosphere.

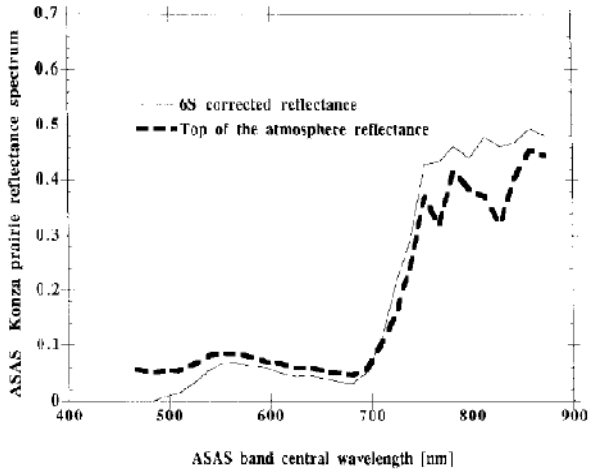

Figure 3.19: An example of atmospheric correction by the 6S model (Vermote et al., 1997). Note the absorption features at 760 nm and 865 nm in the top of atmosphere reflectance which are related to the presence of oxygen and water vapour. These are almost smoothed out in the corrected reflectance.

In figure 3.19, the top of atmosphere reflectance, derived from the small bandwidth sensor, ASAS, was corrected for absorption by oxygen and water vapour (Vermote et al., 1997). Although differing from the MERIS sensor in spectral range, the example serves to illustrate how the corrected vegetation profile is smoother than the input signal. For example, between 400 and 700 nm, the top of atmosphere reflectance is greater than the corrected version as the increased brightness from scattering of the signal in the atmosphere is removed by the model. However, while the absorption features at 760 nm (oxygen) and 865 nm (water vapour) are reduced, they are not totally removed from the corrected reflectance.

There is no evidence from the MGVI documentation that the 6S atmospheric model is geographically or temporally tuned for variability in atmosphere on a local scale. This is unlike the dynamic correction for Raleigh scattering using the MERIS blue band. In fact, only three possible parameter values for optical thickness are available in the 6S model for MGVI, accounting for only a limited set of atmospheric conditions (see Gobron et al., 2004). In contrast, the MERIS sensor would be expected to encounter a wide range of atmospheric conditions on a global scale. Like clouds, water vapour strongly absorbs radiation in the optical domain and is highly variable in vertical profiles of the atmosphere (Schroedter-Homscheidt et al., 2008). Over Ireland, water vapour levels tend to vary on a daily and seasonal basis (Rohan, 1986). Therefore, errors in the atmospheric correction of MERIS reflectance data would be expected without tuning the parameters of the atmospheric model for such variability.

3.4.6.1 MERIS top of atmosphere radiance

The intensity of reflected radiation is measured as brightness (watts) per wavelength interval (micrometre) per angular unit (steradian) and is known as radiance (W/m^2 sr µm) (Campbell, 2002). As input radiance from three MERIS bands is used in the MGVI calculation, it was intended to examine temporal variability in their values. Theoretical studies have shown that the impact of the top of atmosphere radiance uncertainties on the expected MERIS FAPAR products accuracy is about 5% to 10% (Gobron et al., 2008). The inter comparison of FAPAR products from the MERIS and SeaWiFS sensors showed differences in the range 5–10% when the bands of

each sensor have been inter-calibrated to lower than 4% uncertainty (Gobron et al., 2008). This accuracy estimate was within the stated accuracy of the MERIS FAPAR product. However, the average FAPAR uncertainty value can be larger than 10% if two bands have radiance uncertainty values of about 4–5%.Therefore, accurate radiometric calibration of the input MERIS radiance values is important so as to minimise uncertainty in the FAPAR product.

The MERIS Top Of atmosphere (TOA) daily radiance in the 15 MERIS bands was obtained from the JRC for one year, 2008, in order to inspect the temporal pattern in radiance values. The MERIS radiance values were acquired over a 15×15 pixel window centred on 51.836983°N and 8.154828°W. The study area consists of agricultural fields in southern Ireland which are classified as pastures in the CORINE landcover 2006 dataset. Four pixels were selected within the window to compare MGVI time series with their corresponding blue, red and near infrared radiance values. The coordinates of the MGVI and MERIS pixels are shown in Appendix C. There is a slight geometric offset between the grids which is approximately 0.5 pixels in the X and Y direction. As the compared pixels were composed of the same landcover class, the effect of any geometric offset would be expected to be minimal. Temporal consistency was ensured since the daily radiance values were averaged in 10-day periods coincident with the MGVI composite periods. The time series for the four pairs of pixels can be seen in figure 3.20 (a)-(h). The MGVI time series, on the left of figure 3.20, are plotted with error bars which

represent the temporal mean absolute deviation, calculated from the daily valid values, over the time compositing period.Therefore there are no error bars on composite values with only one valid day in the composite which are selected by the algorithm as they are the only available values, and may not necessarily be the most representative of the composite. Anomalous spikes occur on some of these values, particularly in the MGVI time series of figure 3.20 (e) and (g). The larger error bars do not seem to be on the anomalous data points however.

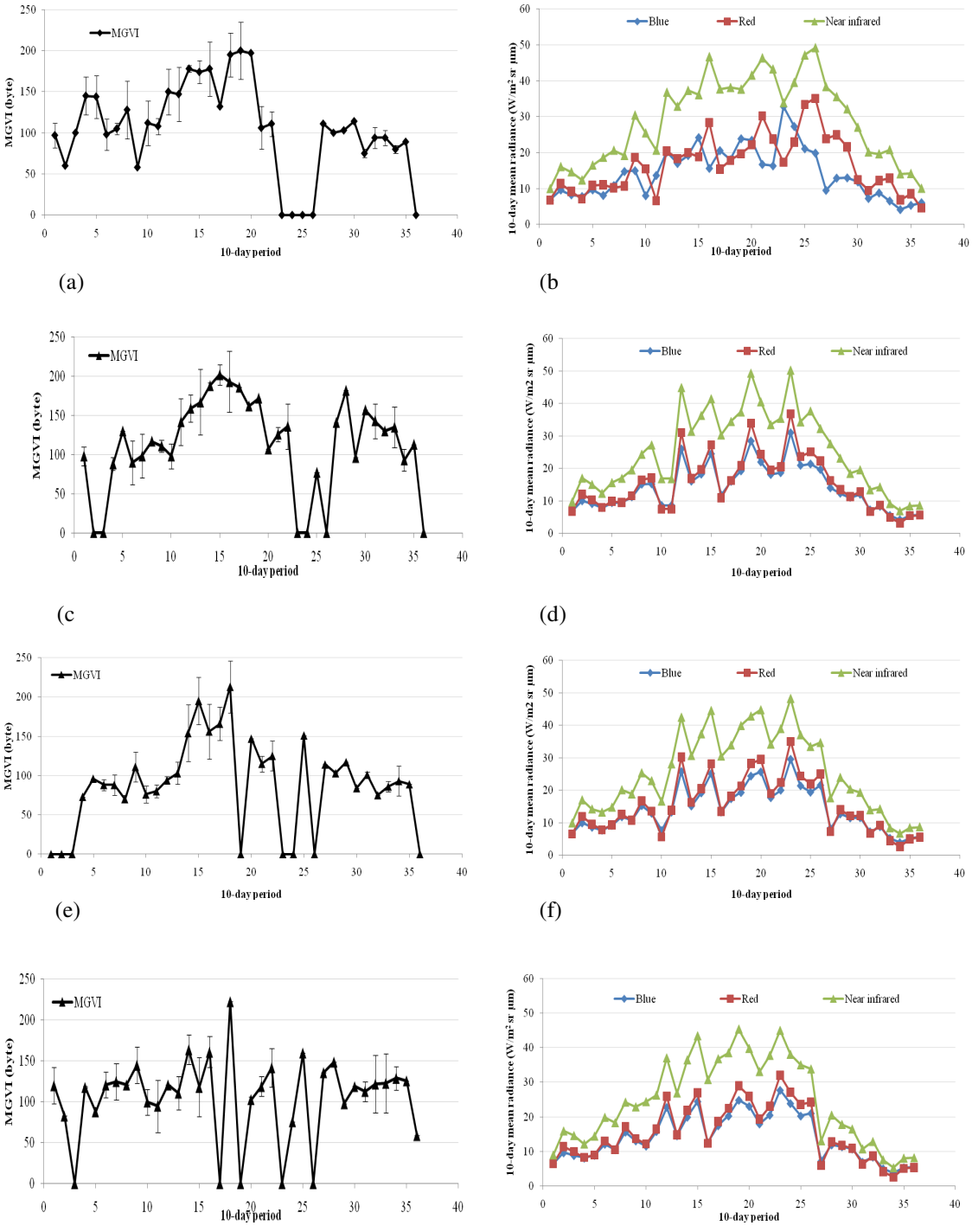

Figure 3.20: (a)-(h): The 2008 MGVI time series are displayed on the left (a,c,e,g), in black lines, with temporal deviation over the composite period represented as error bars. The 2008 MERIS radiance time series are located in their respective bands on the right (b,d,f,h), in multicoloured lines, with each pair corresponding to a single pixel and all four pixels identified as pastures

Data gaps in the MGVI time series occur where conditions prevent the acquisition of a daily value within the composite period. However, these conditions are not flagged in the MERIS radiance values but are detected using a spectral reflectance test at the next processing level. Therefore, the radiance time series is a continuum of values unperturbed by data gaps. Generally, the MGVI time series follows the seasonal profile of a vegetated land surface in a mid-latitude temperate climate like Ireland with one growing season. However, the MERIS radiance measurements represent both the brightness of the land surface and the atmosphere above it. Therefore, short-term variability in the radiance is probably due to the absorption and scattering processes of the atmosphere. As would be expected, the near infrared radiance is greater than that of the red and blue spectrum due to internal leaf properties. The red and blue band reflectance is known to be similar and the time series of red and blue radiance values demonstrate this (Govaerts et al., 1999). However, the blue band signal is more severely attenuated by Rayleigh scattering in the atmosphere (Campbell, 2002). The short-term variability in the seasonal profiles is characterised by both upward and downward spikes in the radiance and MGVI values and there is no apparent temporal pattern in their occurrence. However, the MGVI time series profile should be solely influenced by the photosynthetic activity of the vegetation surface. Yet uncertainty in the MGVI arises from the presence of this same short-term variation. Therefore, it is assumed that there is some variability in the MGVI profile which is not synchronised with the seasonal behaviour of the vegetation surface and the origin of this may be a combination of radiometric and atmospheric errors in the MERIS data.

3.5 Discussion

This chapter described an approach to derive an appropriate time-composite period for a national-scale study of vegetation spring greening. Composite satellite products are usually provided by space agencies at fixed temporal resolutions, e.g. 8-day, 10-day and 16-day. The advantage of the G-POD tool was the integration of the FAPAR time composite algorithm with grid computing resources which allowed the user to acquire daily MGVI data composited at any temporal resolution. Furthermore, the selection of the 10-day composite period was not arbitrary but based on carefully selected criteria which were guided by ground-based observations of temporal patterns in vegetation growth and cloud cover. However, even though a 10-day composite period was the optimal trade-off between data loss due to cloud cover and temporal resolution to track the SOS, MGVI data loss still occurred due to cloud. This demonstrates that due to the frequency of cloud cover over Ireland, even in a 10-day period, at least one cloud-free day could not be obtained for every image pixel. Extending the period indefinitely would undoubtedly satisfy this criteria but at the expense of sufficient temporal resolution to track the SOS effectively. The spatial patterns in data loss were seen over seasonal to annual time periods in the cloud composite images generated from the cloud flag data. This method is potentially useful for selecting local sites or regions of the country for monitoring local-scale vegetation phenology using higher spatial resolution products at the most appropriate temporal resolution. It was also observed that valid MGVI data were more frequently obtained over lowland than upland areas, suggesting that orographic cloud (generated by moist air rising and cooling over mountains) is routinely detected in MGVI pixels.

The study determined that a 10-day period is the minimum composite period length required, and implies that SOS monitoring cannot be done at finer temporal resolutions using the RR MGVI product at the national-scale in Ireland. Therefore, SOS dates will be estimated to a 10-day period or 'decad'. To estimate the day of year would suggest a level of accuracy which was not present in the input composite data. Nevertheless, a recent NASA white paper on LSP quoted daily precision and sub-weekly accuracy of ± 3 days, where possible, as requirements for a land surface phenology earth system data record (ESDR) (Friedl et al., 2010). However, as clouds limit the consistent use of daily optical satellite data; especially in mid to high latitude maritime areas, like Ireland, daily precision in a satellite-derived phenology measure would be rarely attainable. Ultimately, the adoption of an N-day or daily precision in LSP measures depends on the study aims. For instance, while general spatio-temporal patterns in SOS can be clearly detected using periods of days rather than daily precision, phenology trend estimation and comparison to ground-based observations require daily precision (Studer et al., 2007). The ground-based observations of spring greening were used in this study in different ways. Although the fieldwork was originally intended as a guide to select an optimal period to track the temporal development of tree phenology in spring, it proved useful to understand vegetation phenology from a ground-based perspective. For instance, it was seen that the rate of leafout in the forest canopy differed with the tree species and for individual trees of the same species depending on location, presumably in response to local scale factors of aspect, light availability, age of the tree and soil condition.The greening of the understorey vegetation preceded the greening of the forest canopy, and in some case leaves emerged at the top of the tree crown before

those at the base and vice versa. Such understory vegetation dynamics are strategic in responding to the limited availability of light when the overlying leaf canopy fills in. Although such subtle variations in spring phenology would not be detectable at the 1.2 km spatial resolution of a MERIS RR pixel, these observations have demonstrated that tree phenology can vary over very small areas (field site approx $1km^2$), even for the same tree species. Furthermore, the earlier greening of the understorey could potentially bias estimates of SOS in forested areas towards earlier dates.

The noise in MGVI time series was not restricted to pixels of particular landcover types, location or any particular year but was common to all pixels across the image. This raised concerns about the quality of the input MERIS data, which not only prompted an investigation of the MERIS radiance measurements used to construct the MGVI, but also a verification of cloud screening in the MGVI product. Results showed that over two-thirds of the sampled valid MGVI images had 50% of their pixels defined as METEOSAT cloud. Of those cloud-covered valid MGVI pixels, spikes occurred in the time series just as frequently as in cloud-free valid MGVI, suggesting that cloud-cover is not the sole cause of anomalous MGVI values. The use of a global MGVI atmospheric model with a limited number of parameter settings for atmospheric conditions is one potential cause of poor atmospheric corrections; hence noise in downstream MERIS products such as the MGVI. The time series noise was also present in the MERIS radiance time series, but these data represent radiance measurements uncorrected for atmospheric effects. Therefore, it is not possible to estimate the impact of atmosphere on MGVI using MERIS radiance

data. Over Ireland, where water vapour and cloud cover content are higher than those over continental areas, MERIS data quality issues require further attention, specifically more rigorous atmospheric corrections, tuning of the atmospheric model for a greater variety of atmospheric conditions, and more conservative cloud screening.

3.6 Conclusions

Cloud cover is largely an unknown quantity in global climate models, and remains notoriously difficult to predict in space and time (GCOS, 2010). Therefore, fixing a single composite period, selected on the basis of a test period in 2006, does not guarantee complete spatial-temporal coverage in the 10-day MGVI composites for the seven-year duration of the study. However, the 10-day period does represent an optimal trade-off between the two criteria established at the beginning of this chapter. The second criterion was for a composite period with at least one cloud-free day per pixel, which has been unachievable at certain times of the year. However, the first criterion was attainable as the 10-day interval was sufficient to track vegetation spring greening. The compromise between the criteria for composite period selection fulfilled the initial study objective of gathering sufficient cloud-free data for a national-scale study. Further research is required in deducing the cause of the anomalous spikes in the MGVI time series, but it would appear from this analysis to be a combination of undetected cloud cover, limited atmospheric corrections and, potentially, calibration issues with the radiance data used to construct the MGVI. Overall, this chapter has outlined an approach to composite period selection using information on cloud cover and vegetation phenology at point locations in the study

area. A validation of the quality of daily MGVI values, representative of a time-composite period, has shown that cloud may not be as rigorously detected in MERIS data as it is by meteorological satellites such as METEOSAT which has possible implications for the subsequent use of those data. Further work on validating the MGVI cloud-screening steps separately with METEOSAT and other reliable cloud mask data could be useful to assess their rigour.

Chapter 4. Optimising time series analysis software to estimate the Start of Season (SOS)

Time series of optically remotely-sensed land surface parameters such as the MGVI are frequently punctuated by data gaps due to errors in data acquisition (Colditz et al., 2008), and as shown in chapter 3. Additionally, when the quality of the VI time series is compromised due to sensor disturbances, the seasonality signal is not easily detected and the extracted seasonality information is uncertain (Jönsson and Eklundh, 2002). Therefore, time series data must be modelled if more robust seasonality information is to be determined from VI time series data (de Beurs and Henebry, 2008a). This chapter presents a methodological approach to the estimation of the vegetation Start of Season (SOS) from a seven year time series of the MGVI from 2003-2009. The spatio-temporal patterns in the extracted SOS metric across the island are discussed. Finally, the merits of the study methodology are evaluated in terms of reliability, accuracy and robustness, and recommendations on possible improvements to the method are made. Certain sections of this and chapter 5 have been written as a paper submitted to the International Society of Photogrammetry and Remote Sensing (ISPRS) Journal of Photogrammetry and Remote Sensing which is currently under review.

4.1 Time series analysis methods for land surface phenology monitoring

The MGVI time series was characterised by noise, manifested as locally high and low anomalous spikes (see section 3.4), which may be due to a combination of

factors as discussed in the previous chapter. In addition, data gaps were present in MGVI time series due to cloud, surface water, invalid Bidirectional Reflectance Function (BRF), missing reflectance data and the presence of non-vegetated surfaces (Aussedat et al., 2006). To fill in the data gaps created by missing daily MGVI data, and smooth the time series noise, a method was required to produce a model MGVI time series from which the SOS estimates could be derived with less uncertainty. Compositing techniques, e.g. Maximum Value Composites, as have been applied to NDVI (e.g., Holben, 1986), provide some certainty of obtaining valid values for continuous NDVI time series for the purpose of phenological monitoring. However, new composite methods have been developed to account for the temporal characteristics of more recently developed vegetation indices. Such techniques seek to reconstruct full time series without the data gaps, while allowing for methods of seasonality metric extraction. For example, a software tool for analysing MODIS time series data, TiSeG, interpolates between data gaps in MODIS land surface products based on gap length and the number of invalid pixels (Colditz et al., 2008). Similarly, the generic time series analysis software, TIMESAT, has incorporated two least-squares fitting methods based on asymmetric Gaussian and harmonic functions as well as a filtering method based on locally-fitted polynomials (Jönsson and Eklundh, 2004). These methods parameterise curves of vegetation seasonality in multi annual VI time series within software packages such as TiSeG or TIMESAT. Seasonality parameters are identified by curve thresholds, curve derivatives including points of inflection and maximum curvature, or filtering techniques such as the delayed moving average (Reed and Brown, 2005). Absolute curve thresholds are based on VI values which correspond to fixed conditions of

image acquisition, soil background contribution and vegetation type, but these do not perform well in heterogeneous vegetation cover (Reed et al., 1994; de Beurs and Henebry, 2005). However, they can at least be quantified given a sufficient density of ground-based measurements, e.g. a threshold set to 85% of the growing season mean MODIS 250m NDVI correlated best with 'onset of leafing of birch' in spring in Northern Fennoscandia (Karlsen et al., 2008). In contrast, the selection of relative thresholds is largely subjective relying on a fraction or percentage of the annual VI range in a pixel (Eklundh and Jönsson, 2010). A 10% curve threshold has been used in previous TIMESAT studies (Jönsson and Eklundh, 2002, 2004). This threshold has also been favoured by Hird and McDermid (2009), whilst a 20% threshold was selected after inspection of individual curve fits to pixels from various biomes in South Africa (Wessels et al., 2010). The same threshold was used by Heumann et al. (2007) to avoid error due to noise in dry season VI values in a study of Sahelian Africa based on NDVI. The season midpoint (50%) threshold based on NDVI was proposed by White et al. (1997) to capture the most rapid increase in greenness. This seasonal midpoint method was also adopted by Brown et al. (2010) in studying phenological change in Africa based on NDVI. A 50% threshold was not considered in this study as the aim of this research is to mark the beginning of measurable photosynthesis and not the season's midpoint. Most research on selecting thresholds to date has been conducted on the AVHRR NDVI. However, the relationships between thresholds in satellite-derived seasonality curves and specific phenological events are not universal, but depend on species specific traits. In deciduous vegetation and snow-free conditions, the NDVI is generally responsive to the development of leaf foliage, and the NDVI would start increasing after bud-burst

(L.Eklundh, pers comm., 2011). However, there is no indication of what constitutes start of growth when using MGVI as it has not been as widely used in vegetation phenology applications as NDVI. The variability in phenological metrics obtained from different vegetation indices complicates the task of relating interannual change in the metric to climatic and other factors which drive phenological change (Boyd et al., 2011). In a study of the length of the growing season in southern England, results varied depending on the VI dataset used: MODIS EVI, NDVI, MTCI or MGVI. The discrepancy in the length of the growing season between the different indices was between 38 days for 2006 and 18 days for 2007 (Boyd et al., 2011).

An alternative method to the detection of phenological events by thresholds is the use of curve derivatives or inflection points which correspond to a shift in the sequence of VI values from one seasonal event to the next (Moulin et al., 1997), similar to locating the maximum and minimum values in the rate of change of curvature (Zhang et al., 2003). Moving averages locate points of departure of the actual VI profile from an idealised curve (Reed et al., 1994). Fourier analysis relies on reconstructing the seasonal signal in VI time series into a series of sinusoidal waves of varying frequency (Dash et al., 2010). The seasonal component can then be separated from the long term phenological trend (Verbesselt et al., 2010). However, the technique cannot compensate for gaps created by clouds and the optimal number of Fourier components ultimately depends on data quality, the temporal resolution defined by the compositing interval, and the temporal variations of phenological features (Geerken, 2009). Generally, local time series changes cannot be captured with low order Fourier transforms, a task better suited to local model fits, which

when merged accurately follow the behaviour of the complete time series (Jönsson and Eklundh, 2002). Therefore, the TIMESAT software, based on a method which implements least-squares local model fits, was chosen for the analysis of phenological cycles in the MGVI time series . TIMESAT provides dual functionality: it can model the time series trend by curve fitting, and seasonality metric extraction is by relative or absolute VI thresholds. The advantage of using TIMESAT is that it is generic in its application to different satellite sensor products composited over different time intervals (Jönsson and Eklundh, 2002, 2004). In a model-based empirical study of six noise-reduction techniques, the TIMESAT double logistic and asymmetric Gaussian functions performed better than the alternative methods based on filters (Hird and McDermid, 2009). In comparing ten individual methods of SOS estimation from 1982-2006 across North America, the TIMESAT Savitzky-Golay filter corresponded most closely to the 1982-2006 ensemble of model SOS estimates (White et al., 2009). Although these authors did not suggest the TIMESAT method was superior, in their study it did produce the most consistent SOS estimates of all the compared methods. This consistency in the TIMESAT method is an important asset when comparing SOS between different sites and years (van Leeuwen, 2008). Therefore, TIMESAT was chosen as a flexible and versatile tool to explore methods for MGVI noise reduction, with various options for filtering noise and fitting model curves, while being freely available online (Eklundh, 2010).

4.2 Overview of the time series analysis software- TIMESAT

TIMESAT has been developed and modified over several years; the latest version of the program used in this study is TIMESAT 3.0 (Eklundh and Jönsson, 2010). The full range of the time-based and value-based seasonality metrics that can be estimated with TIMESAT is listed in table 4.1.

Table 4.1: A summary of the extracted seasonality metrics in TIMESAT 3.0

Category	Seasonality Metric	Abbreviation	Description	Units
Time-based Metrics	Time for the start of season	SOS	Time for which the left edge has increased to a user-defined level measured from the left minimum level	N-day period
	Time for the end of season	EOS	Time for which the right edge has decreased to a user-defined level measured from the right minimum level	
	Time for the mid-season	MOS	The mean value of the times for which the left edge has increased to the 80 % level and the right edge has decreased to the 80 % level respectively.	
	Length of the season	LOS	Time from the start to the end of the season	
Value-based Metrics	Base Level	Base	The average of the left and right minimum values	Digital Number range
	Largest data value for the fitted function during the season	Max	Maximum value of the fitted function	
	Seasonal amplitude	Difference between the maximum value and the base level		
	Rate of increase at the beginning of the season	The ratio of the difference between the left 20 % and 80 % levels and the corresponding time difference		
	Rate of decrease at the end of the season	The absolute value of the ratio of the difference between the right 20 % and 80 % levels and the corresponding time difference. The rate of decrease is thus given as a positive quantity		
	Large seasonal integral	Integral of the function describing the season from the season start to the season end		
	Small seasonal integral	Integral of the difference between the function describing the season and the base level from season start to season end.		

In figure 4.1, the seasonality measures used to parameterise the growing season from a TIMESAT-fitted curve are illustrated. The use of the fitted function rather than the underlying noisy times series produces more stable seasonality measures (Eklundh and Jönsson, 2010).

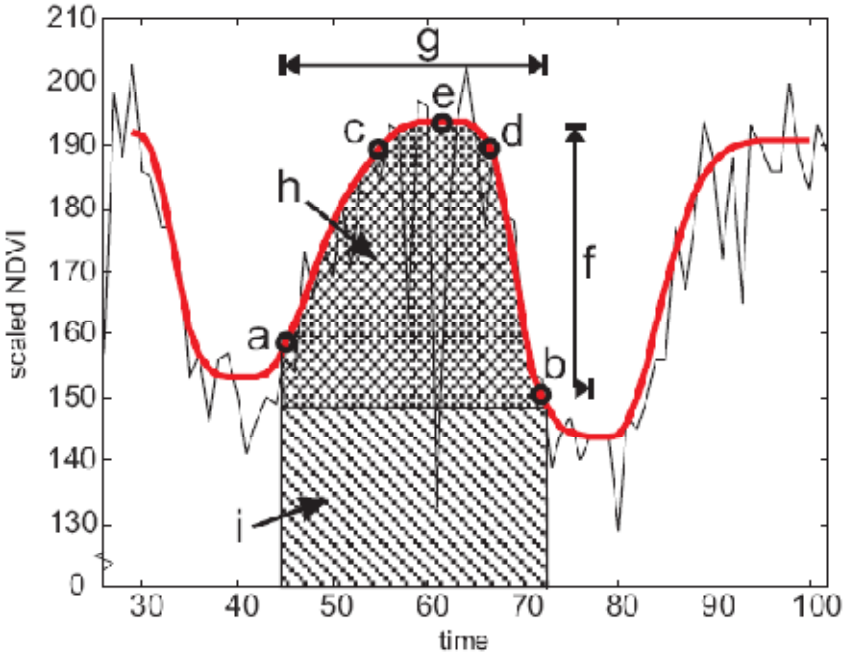

Figure 4.1: Key seasonality metrics extracted from TIMESAT: Points (a) and (b) correspond to the start and end of the season, (c) and (d) mark the mid-season levels , (e) is the season maximum, (f) is the seasonal amplitude, (g) is the season length, (h) is the small seasonal integral and (i), the large seasonal integral, both of which describe seasonal productivity (Eklundh and Jönsson, 2010).

4.3 TIMESAT processing of VI time series

TIMESAT firstly identifies the coarse number of seasons by approximating the seasonal component of the time series to a sine wave. The local model fits and moving filters then permit more accurate and realistic modelling of the individual seasons. Ancillary satellite data, such as quality flags can be used to weight the model and landcover data can be used to fine-tune the settings which parameterise the curve fits to pixels of known landcover type (Jönsson and Eklundh, 2002, 2004).

4.3.1 The Savitzky-Golay filter

The Savitzky-Golay (SG) method, based on a filtering window, applies a least-squares fit of the input data to a polynomial function. This ensures that the position, i.e. height and width, of seasonal peaks is maintained, which a simple moving average method does not preserve. The result is an upper-envelope adapted, smoothed curve fit. The width of the filter is specified by the user. Generally, a large window size results in greater suppression of noise and a smoother curve, however some natural variation in the time series can also be smoothed out. A narrow window often replicates time series noise. Therefore, the optimal window-length is a balance between the degree of smoothing and maintaining the original time series trend (Eklundh and Jönsson, 2010). As can be seen in figure 4.2 (a), the Savitzky-Golay method with a window size of 3 tends to follow the complexity of the raw data series very closely. The noise and drop outs (e.g. at time period 145) are not removed. In figure 4.2(b), however, the degree of smoothing has been increased by using a window size of 6. Therefore noisy data have been smoothed and drop outs removed.

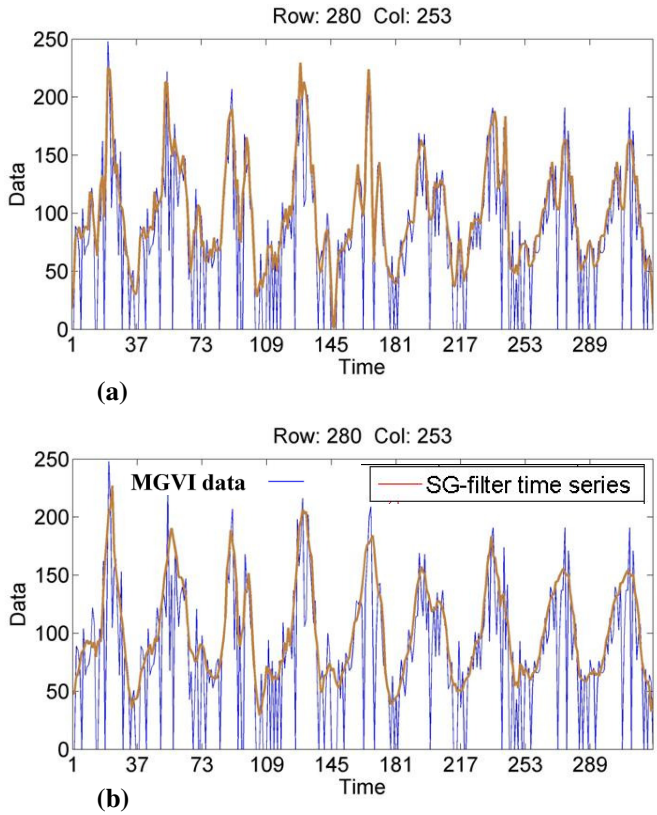

Figure 4.2: (a) The Savitsky-Golay (SG) filtering with a window size of 3 and (b) with a window size of 6.

4.3.2 Least-squares fit to a basis function

While all three curve fitting methods are least-squares fits to the upper time series envelope of the VI data, the Savitzky-Golay filter is constructed from locally-fitted polynomial functions in a moving window. The other two least-squares methods are based on local fits to logistic or asymmetric Gaussian basis functions in intervals around maxima and minima in the time series. The local model functions share the same general form shown in equation 4.1 (Jönsson and Eklundh, 2004).

Equation 4.10: General form of the local model functions

$$f(t) \equiv f(t;c,x) = c_1 + c_2 g(t;x)$$

The linear parameters $c = (c_1, c_2)$ define the base level and amplitude of the fitted model while non-linear parameters $x = (x_1, x_2, ..., x_p)$ determine the shape of the basis

function $g(t;x)$. In the case of a double logistic basis function, there are parameters to define both points of inflection on the left and right hand side of the curve and the corresponding rates of change of slope at these points (figure 4.3). In order to ensure a smooth curve, the range of possible parameter values is restricted.

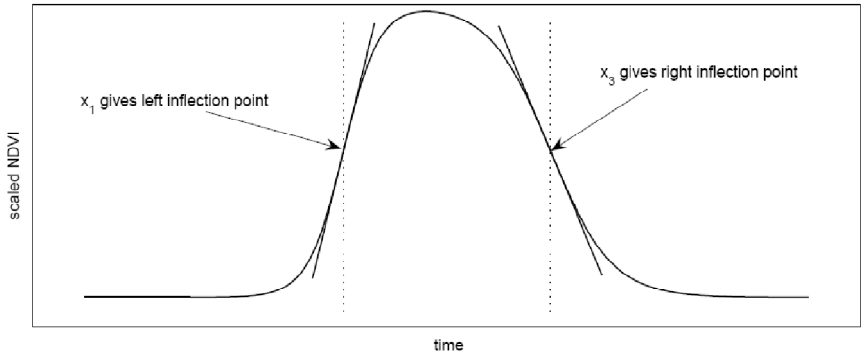

Figure 4.3: The double logistic basis function in which the parameters x_1 and x_3 determine the position of the left and right inflection points respectively (Eklundh and Jönsson, 2010)

In the case of a Gaussian basis function (figure 4.4), one parameter defines the position of the maximum or minimum point in the curve. A series of other parameters define the shape of the left and right hand side of the curve in terms of width and flatness. These shape parameters are also restricted in range so that the left and right hand side of the curve from two seasons are joined smoothly.

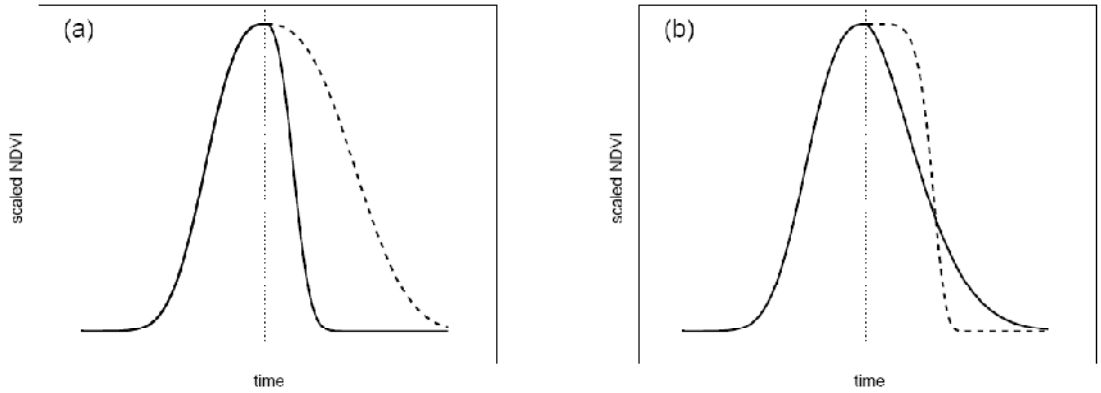

Figure 4.4: Asymmetric Gaussian local functions. In (a) the local parameter function which determines the width of the right function half has been decreased (solid line) and increased (dashed line) compared to the right function half. In (b) the parameter which determines the flatness of the right function half has been decreased (solid line) and increased (dashed line) compared to the value of the left half (Eklundh and Jönsson, 2010).

In order to model small-scale variation in the time series, the asymmetric Gaussian and double logistic function fits are constructed from smaller local model functions in intervals around the left minimum, central maximum and right minimum of one year of data. Although the local functions produce fits which are well adapted to local minima and maxima, the fits must be merged where they intersect to form the global model function to the full time series. This is obtained by merging the three local fits, using cut-off functions that ensure a smooth transition between overlapping elements of the left, central and the right portions of the local fits. In order to fit local functions across the entire time series, the season of the central year is modelled first. Fill years are inserted at the beginning and end of the time series to facilitate local model fitting to the first and last year of the valid time series. These are typically replicates of the first and last year of data.

4.3.3 Curve-fitting per pixel using the TIMESAT GUI

The TIMESAT package consists of numerical and graphical components coded in the Matlab and FORTRAN programming languages. The per pixel time-series analysis and curve-setting optimisation was done in the Matlab Graphical User Interface (GUI), (MATLAB licence 157192) as can be seen in figure 4.5, while an entire image was processed more efficiently in the FORTRAN-coded version.

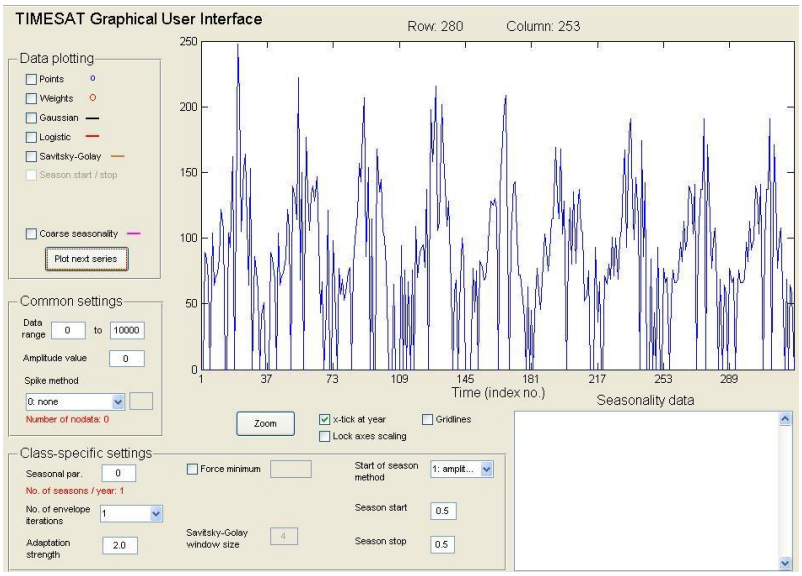

Figure 4.5: The TIMESAT Graphical User Interface (GUI) showing a time series of MERIS FAPAR data, 2003-2009, the first and last years are replicate years inserted to fit local model functions before they are merged for the global fit

The TIMESAT GUI allows the user to preview the changing of parameter settings and the resulting curve fits. The advantage of the GUI is that adjustments can be made to the settings on a per-pixel basis before processing entire images. The process of time series function-fitting for a single pixel in the TIMESAT GUI is illustrated in figure 4.6 a-d: (a) the per pixel time series is displayed in the GUI. The beginning and end of the time series was filled with a dummy year (Year X and Year Y) in order to facilitate the effective fitting of local model functions (as described in section 4.3.2). (b) A spike-removal setting is applied which removes outliers due to noise in the data: the severity of spike removal can be adjusted using this setting. (c) The approximate number of seasons is calculated based on the number of curve maxima and minima and their amplitude with respect to a baseline. (d) The local model fits, using either a double logistic or asymmetric Gaussian basis function, are merged into a global fit.

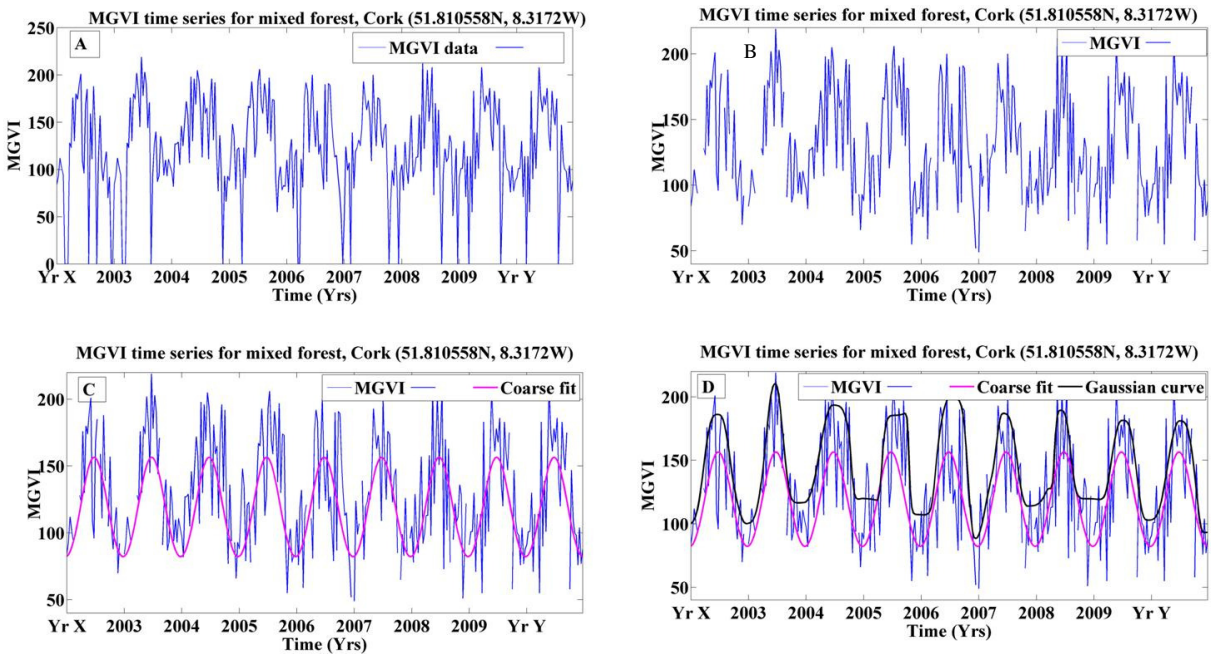

Figure 4.6: Four steps in applying TIMESAT curve fits to a pixel of mixed forest (51.810558N, 8.3172W). (A) Raw MGVI time series (B) Spike removal (C) Number of seasons calculated (D) Gaussian fit

4.4 Justification of a fitting method

The SG filter was not selected as a fitting method for this study given the variable extent of the noise in the MGVI time series and the difficulty in selecting an appropriate filter window size to process the entire dataset. It was found that no single optimum window size maintained the balance between the degree of smoothing and preserving the seasonal component of every SG-filtered time series at a national scale. However, as can be seen in a comparison of the SG-filtered time series with those fitted to asymmetric Gaussian (AG) functions in figure 4.7, using a wide filter size (14 values) produces model fits which closely resemble those produced from the Gaussian functions. The SG-filtered time series are noisy in some cases where AG fits are not, and the AG fits follow local variation more closely than the SG-filtered data, e.g. in detecting secondary peaks in the last two seasons of pixel (h).

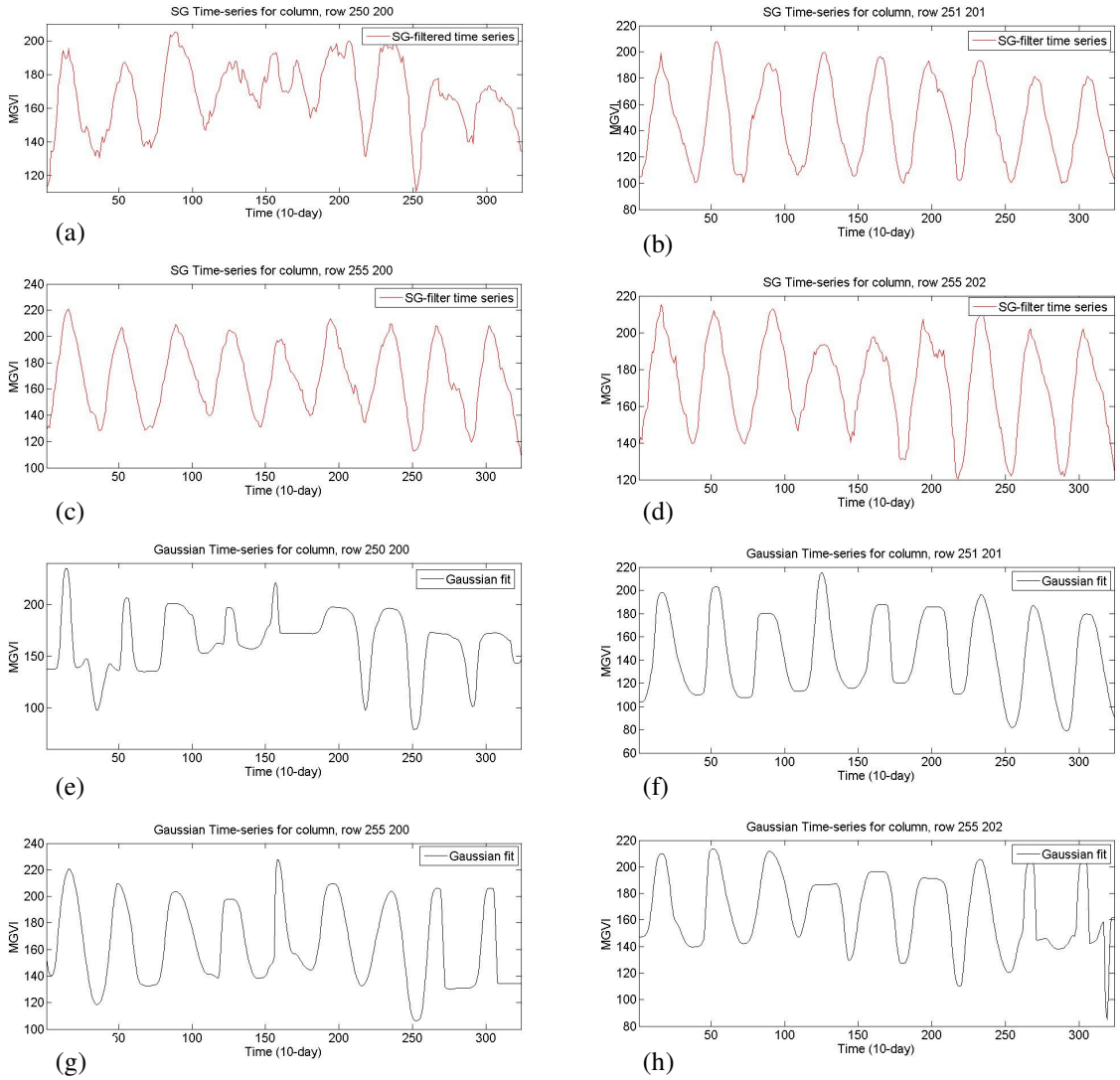

Figure 4.7: Inter-comparisons of four sample fits to pixels of pasture land with the Savitzky-Golay filter (a)-(d) and asymmetric Gaussian functions (e)-(h)

In order to illustrate the differences in SOS estimated by the AG and SG (filter window size of 14) methods, the full SOS image produced by each method in 2003 was compared. The minimum cut-off value, below which, values are forced to the specified minimum value, and explained in further detail in 4.5.5, was set at 50. The distribution of SOS estimates per image is shown by the accompanying histograms in figure 4.8. The spatial patterns in SOS estimates are consistent from both methods, although there is more spatial variation in the Gaussian estimates.

This is evident from the histograms, as the Gaussian-estimated dates have a much wider range of values and are less centralised than the SG- estimated dates which mostly occur between periods 4 and 8.

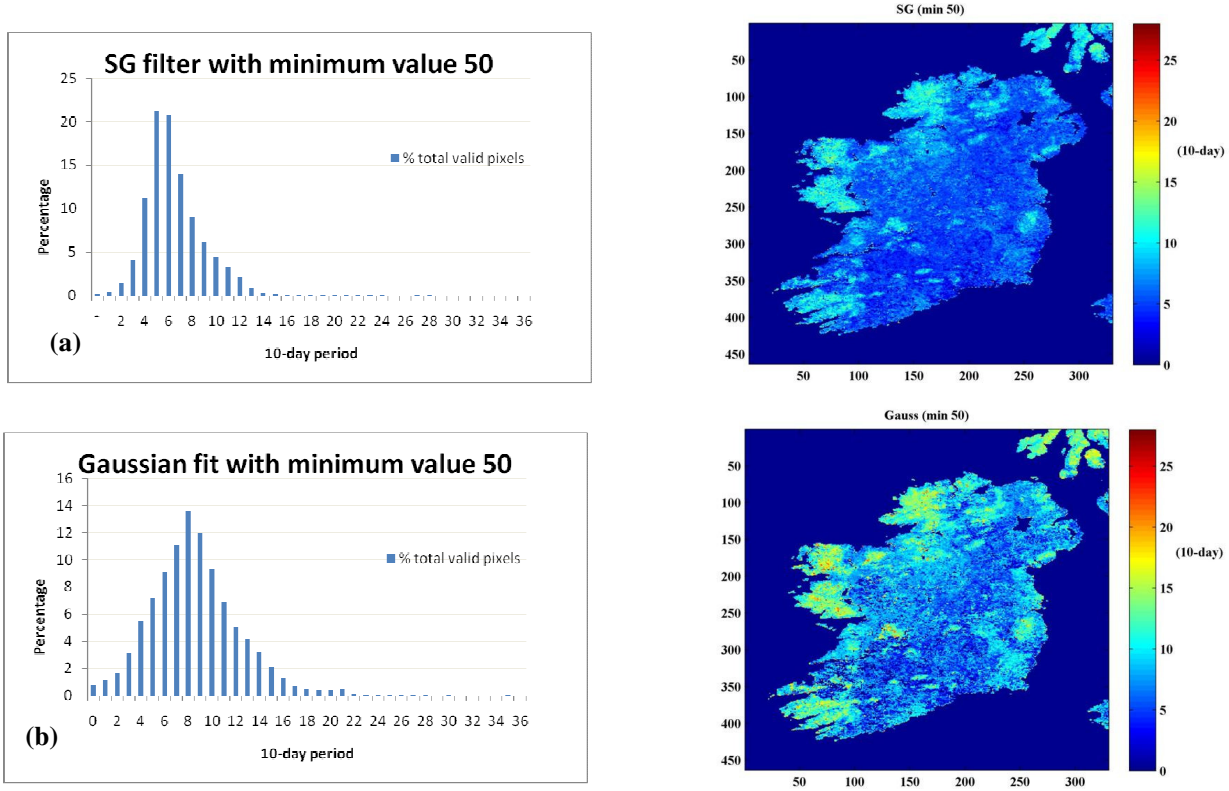

Figure 4.8: A comparison of the SOS image produced from the SG-filtered time series with a window size of 14 with that produced from fits to asymmetric Gaussian functions. The difference in range of SOS estimates produced by both methods can be seen in the histograms

The double logistic and asymmetric Gaussian fits give very similar results as demonstrated by Hird and McDermid (2009). An example of the similarity in fits produced is shown for a single pixel in figure 4.9. The only obvious slight differences in local model fits appear in season two, from period 37 to 73, potentially due to the differences in parameters used to define the shape of the left and right hand sides of the DL and AG local model fits, as described in section 4.3.2.

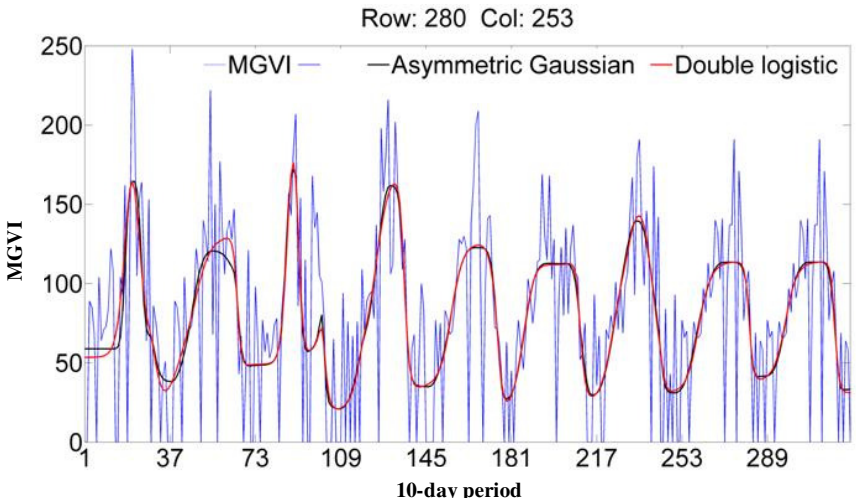

Figure 4.9: A single time series modelled with both asymmetric Gaussian and double logistic fits

Due to the similarity exhibited by both of these fitting models, Root Mean Square Error (RMSE) analysis was used as an overall indicator of model performance since it summarises the mean difference between observed and predicted values (Willmott, 1982). The objective of the RMSE analysis was to select the model which minimised the difference between the original time series and the modelled values. The observed values were the original MGVI time series values and the predicted values were generated from the fitting function, i.e. asymmetric Gaussian or double logistic. The model fits were applied to 288 data values across the time series within100 randomly-selected pixels in the MGVI grid, using equally-weighted fits with no upper envelope bias. The overall RMSE per model fit was averaged for the 100 pixel results. An analysis of the distribution of differences was also conducted between the observed MGVI values and predicted values from both double logistic and asymmetric Gaussian fits. Not surprisingly, the two averaged RMSE values were similar, being 44 for the double logistic fit and 43 for the Gaussian fit (measures in MGVI byte units). In figure 4.10 (a)-(b), an example of a scaled relative frequency histogram is shown of the difference between model-estimated and MGVI values for

100 pixels, fitted by each of the two model functions. The histogram is constructed in such a way that the summed area within the bars is 1, allowing the relative distribution of difference values from the two models to be compared. The frequency values have been divided by the sample size (n=288).

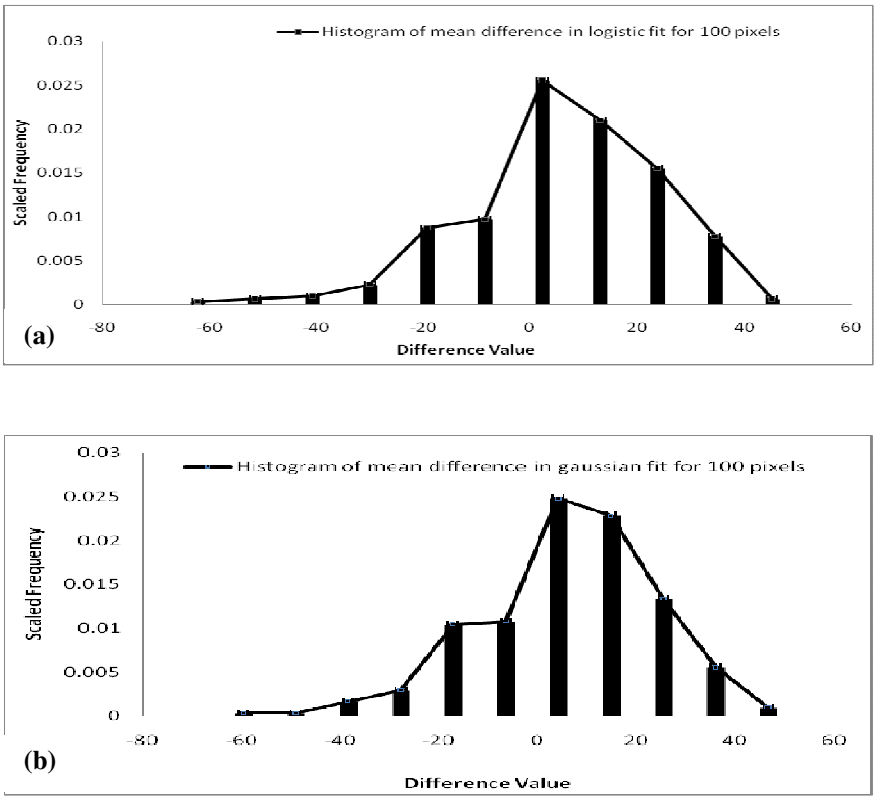

Figure 4.10: Scaled relative frequency histograms for comparing the distribution of differences from (a) Logistic and (b) Gaussian model fits averaged over 100 pixels

The shapes of the relative frequency distributions are broadly similar. They are both negatively skewed (to the right) and asymmetric in shape, meaning that the bulk of differences are positive, i.e. the models over-estimate MGVI. The distributions appear to be bimodal with a smaller peak of negative differences. The RMSE analysis, applied to modelled values of the general form, showed that the Gaussian fit had slightly less error, being 44 for the double logistic fit and 43 for the Gaussian

fit (measures in MGVI byte units). Therefore, the Gaussian fit was selected to model the entire dataset. A summary of the RSME analysis is presented in Figure 4.11.

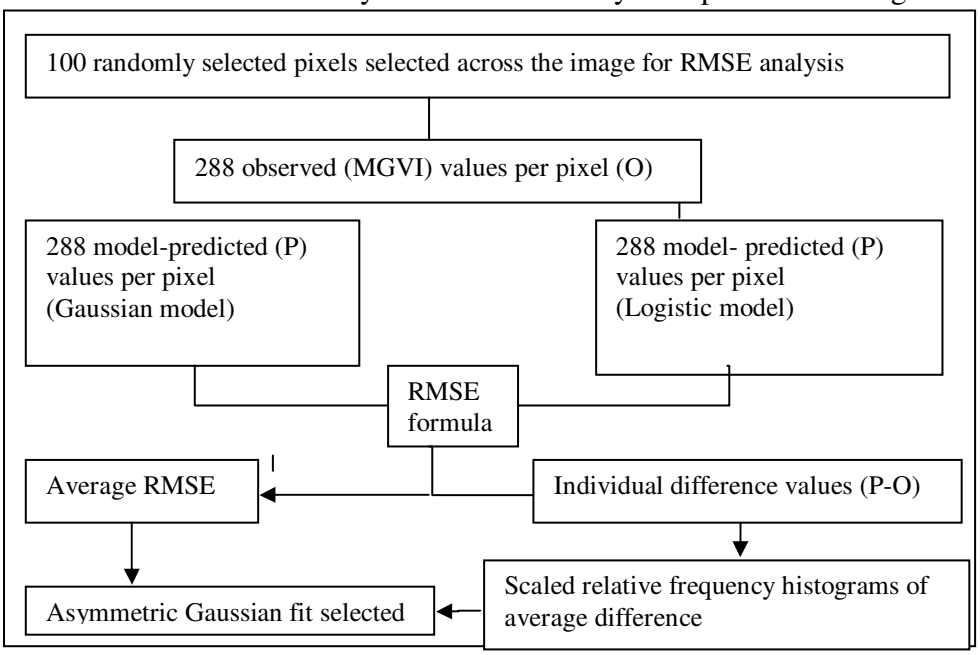

Figure 4.11: The approach to RMSE analysis from which the asymmetric Gaussian fitting function was selected

4.5 Setting sensitivity analysis

Once a model fit had been chosen to process the MGVI dataset, a set of parameter settings which control the model behaviour was selected. Visual analysis of curve fits to sample pixels from different landcover types in the TIMESAT GUI showed that there was not enough landcover-specific variation in the time series to warrant class-specific parameter settings. Therefore, a set of common parameter settings was tested on fifty randomly selected pixels by exploring the change in curve parameter values when each setting was modified. Some settings, e.g. data range, were already determined based on the characteristics of the dataset. The settings which were selected from the sensitivity analysis were used to process the entire dataset and are summarised in table 4.2, and subsequently explained in more detail.

Table 4.2: Summary of the chosen TIMESAT settings for processing the entire MGVI dataset

Common Settings	Value
Data Range	1-255
Spike Method	STL Replace
Seasonal parameter	1
No. of envelope iterations	2
Adaptation Strength	5
Force minimum	50
Start of Season	0.2

4.5.1 Data Range

The MGVI valid data range is 1 to 255 as they are stored in 8-bit unsigned integer format (Aussedat et al., 2006).Values of zero represent uncalculated MGVI values and were therefore excluded. The scaling factors used to convert MGVI to the FAPAR scale are described in Appendix D.

4.5.2 Spike method

There were two principal spike removal methods available in this version of TIMESAT 3.0; the running median method, best used with ancillary quality data, and a Seasonal-Trend decomposition procedure based on Loess[3] (STL). The STL method separates the seasonal from the overall time series trend and discards the remaining components, that do not fit either pattern, as noise (Cleveland et al., 1990). The running-median method identifies outliers based on their number of standard deviations difference from the running median value (Eklundh and Jönsson, 2010). The number of data values removed from the time series was counted for both the STL method and the running median method with a standard deviation value of 1 and 1.5. The number of removed spikes per pixel was averaged over fifty pixels.

There were 324 data points per pixel, as the remaining replicate year was added to the original 288 values, of which 45 points (13.8%) were removed using the STL method, 69 points (21.3%) using the running median with 1 standard deviation and 48 points (14.8%) using a running median with 1.5 standard deviations. The running median, set to remove spikes within 1 standard deviation of the median, removed over one fifth of the time series, which was deemed too much data lost for a valid fit. There were fewer data points removed by including values within 1.5 standard deviations and slightly fewer again using the STL method. To preserve data integrity and minimise loss of valid data points, the STL method was selected. Furthermore, STL proved to be more robust in that the number of spikes removed per pixel was similar in comparison to the high variability in spike removal per pixel with the running median method.

4.5.3 Seasonality parameter

The seasonality parameter is a ratio of the amplitudes of the first and second season detected within a year, ranging from 0 to 1. A value closer to one is suitable for single seasons, while a value closer to zero forces the curve fit to two seasons (Eklundh and Jönsson, 2010). The seasonality parameter was maintained at 1.0 to model a single season per year, as would be expected for the large majority of vegetation cover in Ireland, with the exception of some land use practices, e.g. silage cutting, which would induce a secondary growth season.

4.5.4 Upper envelope iterations and adaptation strength

Adaptation of the curve fit to the upper envelope is carried out because NDVI values tend to be negatively-biased due to atmospheric attenuation (Eklundh and Jönsson,

[3] STL method is based on the sequential application of the loess smoother

2010). Even though such an assumption does not hold for MGVI, without any upper envelope iterations the MGVI curve fits tended to model the central values within the time series without capturing the seasonal peaks. Upper-envelope adaptation consists of forcing the curve fit to the upper envelope of the time series in a multi-step procedure. The weights of low data values below the model function of the first fit are decreased, so that on the next fit the model adapts to the upper curve portion. This process of upper envelope adaptation is repeated twice, shown graphically in figure 4.12 (a)-(b). In figure 4.12 (a), no envelope adaptation is applied and the model fits to the central portion of the time series, while in Fig 4.12 (b), the adaptation is twice applied and the model adapts to the upper envelope.

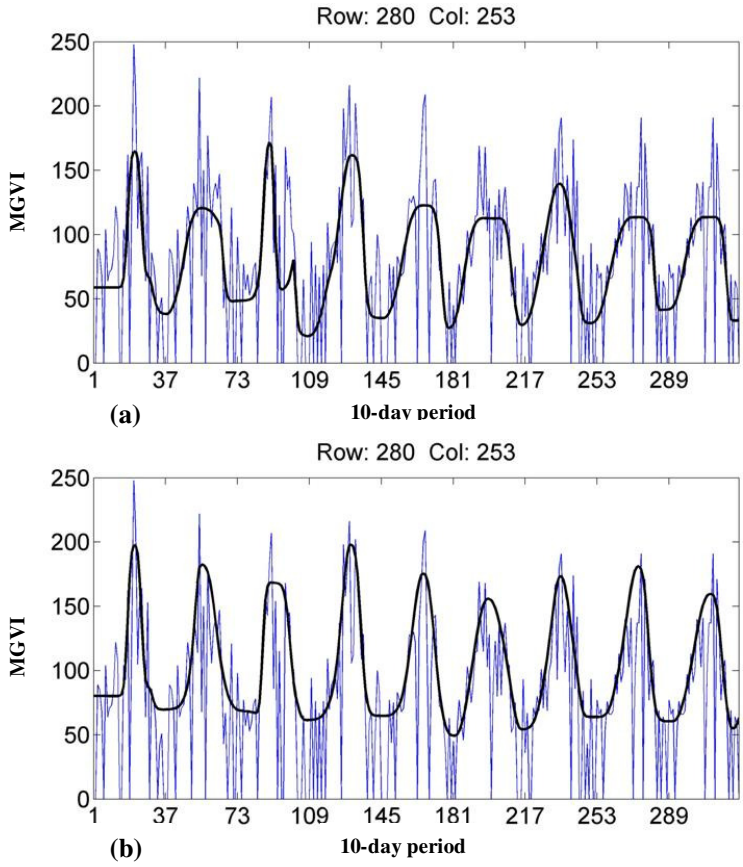

Figure 4.12: (a): The thin blue line represents raw MGVI time series. The thick black line shows the fitted Gaussian function from the first step without upper envelope setting applied, (b): Same as (a) except that the fitted Gaussian functions have been twice fitted to the upper envelope of the MGVI time series

The number of upper envelope iterations determines the extent of upper envelope weighting, i.e. the extent to which the curve fit is biased towards the time series maxima, or upper envelope. A value of 1 for the number of envelope fits instructs only one fit to data and no adaptation to the envelope. The values of 2 or 3 forces one or two additional fits (Eklundh and Jönsson, 2010). The strength of the envelope adaptation can be increased on a scale from 1 to 10 where 10 is the maximum fit strength. Strong adaptation, especially combined with 3 envelope iterations, was found to over-fit the data to single high peaks. However, no envelope adaptation, or weak adaptation strength, resulted in a model fit to the central portion of the time series only. Therefore, one additional fit (2 envelope iterations) combined with

medium adaptation strength (5) stabilised the model fit and was chosen to process the entire dataset.

4.5.5 Force to minimum value

This setting forced MGVI values lower than a minimum value to take the stated minimum value. This is an important parameter setting for estimating SOS since the position of the threshold is altered by forcing very low MGVI values, e.g. those in winter, to a minimum base value. The position of the base of the MGVI curve fit is illustrated in figure 4.13, but the actual minimum MGVI values are much lower than the base of the curve fit. No upper envelope iterations have been applied in this case.

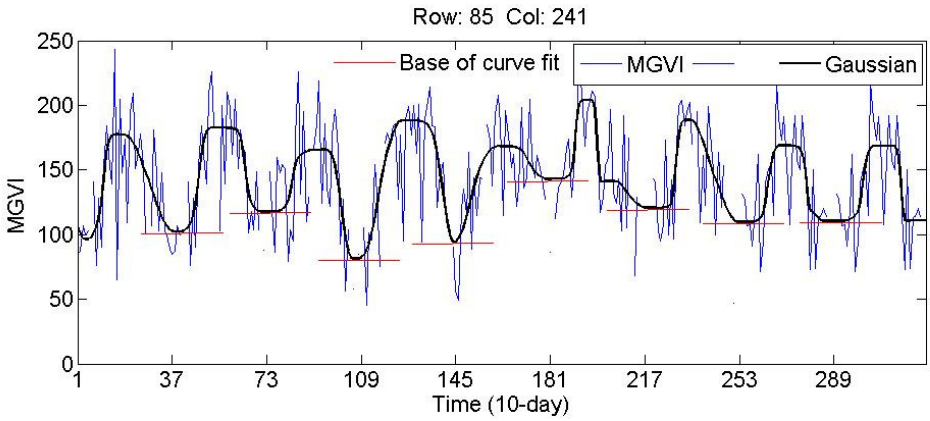

Figure 4.13: The Gaussian model was fit to the valid MGVI range (1-255) with spikes removed and no upper envelope iteration applied. The base of the curve fit is shown by a red line.

The effect of setting two minimum cut-off MGVI values of 50 and 100 was explored in the 2003 SOS image. These values are approximately 0.2 and 0.4 FAPAR which are the minimum and mid season values for deciduous and evergreen forest vegetation in Europe as described in chapter 2 (section 2.3.3.1). The 2003 image generated from a minimum cut-off value of 100 is shown in figure 4.14 while the 2003 image generated from a minimum cut-off value of 50 was previously shown in figure 4.8 (b). In figure 4.14, there are missing pixels in certain areas of the image as

no valid season could be calculated due to the number of MGVI values below the cut-off value; hence a missing data value is generated in the output. Interestingly, the 0.4 FAPAR cut-off value excludes pixels with late SOS (> period15 or day 151-160), which suggests that these areas have a small annual range of FAPAR and probably contain low productivity vegetation. In figure 4.8 (b), there were fewer data values below the cut-off value of 50, hence fewer missing SOS values in the image. As the aim of this study is national-scale covering all vegetation types, the lower minimum value of 50 was chosen to ensure as much SOS data could be generated as possible without compromising the accuracy of the SOS by the inclusion of anomalously low winter values.

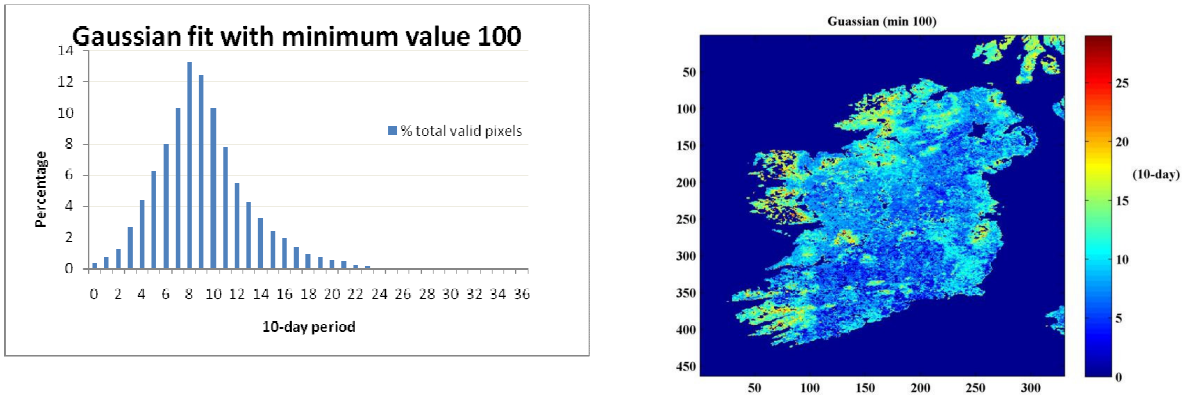

Figure 4.14: The 2003 SOS estimated from an asymmetric Gaussian fit with minimum values forced to 100 with data gaps appearing in areas of vegetation below the FAPAR cut-off value for that season

4.5.6 Threshold determination

There were two options for SOS determination in TIMESAT, the absolute value threshold and the relative measure of fractional amplitude. In the absence of empirical evidence for an appropriate MGVI value to mark season onset, and given the range of vegetation types across the island, an absolute threshold was not considered for this study. Instead, a relative measure of SOS was used as it allowed consistent comparison of SOS across landcover types and on an interannual basis. In

order to select an appropriate relative threshold, the threshold setting was tested from a fraction of 0.1 of the MGVI amplitude to 0.5 MGVI amplitude in intervals of 0.1, and the corresponding SOS date noted for fifty pixels. The number of 10-day period's difference in SOS dates using a threshold of 0.1 and 0.2 of the seasonal amplitude was considerably greater than any other 0.1 interval. This can be explained by the location of the 0.1 threshold at the base of the curve fit in the minimum winter period, when uncertainty due to cloud cover is highest in the time series. Placing the threshold measure beyond the 0.2 value captures the mid-season, and not the beginning of measurable photosynthesis as SOS has been defined in chapter 2 (section 2.4.2).Therefore, the selection of the 0.2 (20%), threshold rather than 0.1 (10%) or greater than 0.2, is a compromise between avoiding uncertainty around the winter minimum values and capturing the earliest photosynthetic activity in the growing season.

4.6 The SOS imagery estimated from the fitted functions

Once the entire dataset was processed with the optimal settings, grids of the SOS estimates were generated from each year of the time series. The 2003 to 2009 SOS grids are shown in figure 4.15, with the 7-year mean SOS also shown. The spatio-temporal pattern in the SOS is consistent on an annual basis, although there is local-scale variation in each year. Generally, the SOS begins first in the midlands, in the interior of North Munster, in Ulster around Lough Neagh and along some parts of the east coast, and follows later along the west coast where there is mostly upland terrain. However, there is also interannual variability in the SOS across the country

as the relative timing of the spatial patterns is variable from year to year. These results will be discussed in more detail in chapter 5.

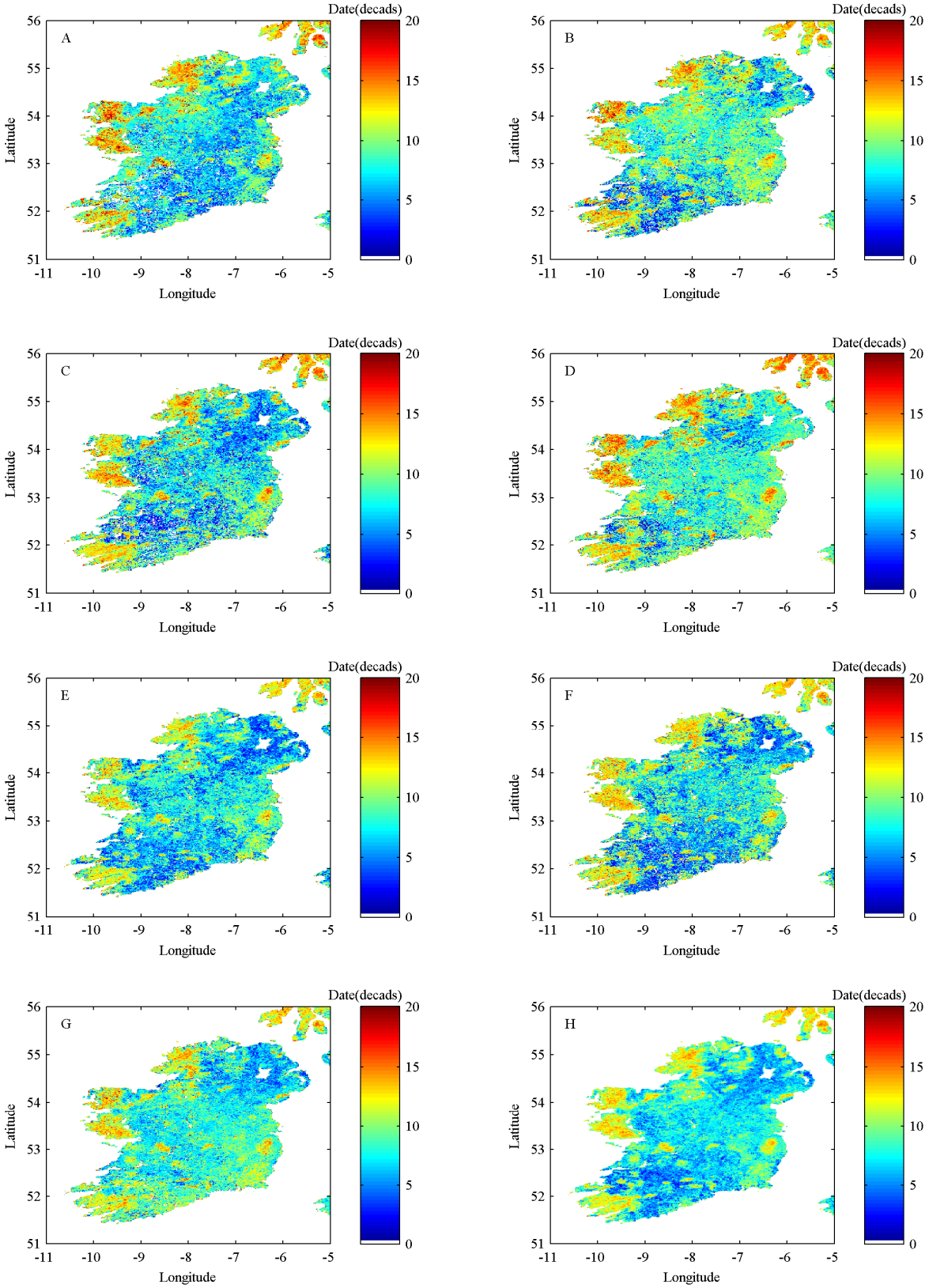

Figure 4.15 (a)-(h): Start of Season estimated from the asymmetric Gaussian fitted functions; (a) 2003, (b) 2004, (c) 2005, (d) 2006, (e) 2007, (f) 2008, (g) 2009, (h) 7-year mean. Time is in 10-day periods from 1 (Jan 1-10) to 20 (Jul 10-19) where 0 is no data.

4.7 Discussion

The benefits of the TIMESAT method include its versatility, flexibility and efficiency, with the only requirement being a consistent number of VI data points per year. The FORTRAN version of the programme processed the entire 7-year MGVI dataset over Ireland in approximately forty minutes and was not overly intensive on computer resources. The MATLAB GUI proved to be a useful tool to examine the effect of changing the parameter settings on the raw time series data before processing the full dataset. The FORTRAN and MATLAB executables of the TIMESAT programme were contained in the same software package, and it was therefore straightforward to run the programme from a Windows-based system. This interoperability of the GUI with the FORTRAN data processing capabilities allowed sensitivity analysis to be conducted on multiple pixels before deciding on the final parameter settings. Overall, the TIMESAT GUI permits the user to interact with the data, view the shape of the fitted curve, and allows the seasonality metrics computed per pixel to be seen on screen. In this way, the user retains control over the curve fitting process, unlike other methods, e.g. Fourier components, which are less transparent and more computationally intensive (Geerken, 2009). However, the full potential of the method was sometimes underutilised due to data constraints. For example, there was an option to enhance the curve fit by biasing the best quality pixel values using weights from ancillary cloud data. However, as the MGVI data are assumed to be cloud screened, and therefore all points of equal quality, the curve fits were unbiased and equally weighted to all time series values. Furthermore, insufficient landcover-specific variability in the data, and the indiscriminate nature of noise meant that landcover-specific characteristics were not obvious when

visually examined in the GUI. Therefore, a landcover file was not integrated with the TIMESAT tool, and the potential to identify the landcover type of each pixel and tune the parameter settings for landcover-specific variation not utilised.
Potential improvements in future versions of the programme should address the need for a statistical tool to quantify error in the fitted curves, a more quantifiable approach to estimating uncertainty in the parameter settings and the extracted seasonality metrics, as well as a method for detecting phenology trends from the time series. For example, the RMSE analysis necessitated exporting the fitted function values to other statistical software for analysis, while the original MGVI time series values were extracted independently of TIMESAT. A more efficient way for quantifying error, executable in TIMESAT, would permit the user to quickly select the best model fit for the dataset based on a representative sample of pixels. Although there was no in-built, systematic procedure for testing the sensitivity of the TIMESAT settings, an objective sensitivity analysis allowed the prime settings for the MGVI dataset to be chosen.

The TIMESAT method was specifically refined for the purpose of SOS metric extraction, but a range of other time-based and value-based metrics can be calculated as mentioned in section 4.1. The setting of a relative, rather than an absolute, threshold VI value meant that the SOS was a consistent threshold measure sufficient for relative comparisons of SOS timing across the country. There were many potential causes of the interannual variability evident in the SOS imagery; however there is currently no method for separating these short-term variations from any long term phenological time series trend in TIMESAT. One such method already in use,

but not integrated in a time series analysis tool, is Breaks For Additive Seasonal and Trend (BFAST) which de-trends the time series data into trend, seasonal and remainder components (Verbesselt et al., 2010). Integrating such a component into the TIMESAT tool would enhance the ability of the user to detect phenological change in the VI time series, even in the presence of noise.

A significant benefit of the TIMESAT technique is its versatility in processing different VI datasets acquired at varying temporal resolutions. In this study, TIMESAT has been used for the first time to analyse time series of MERIS FAPAR in 10-day periods. However, as the program was originally adapted for NDVI time series, the assumption of upper envelope adaptation for negatively-biased noise does not apply to other VI data which have been corrected for this effect, a point previously raised by Hird and McDermid (2009). Nevertheless, one upper-envelope iteration of the Gaussian model fit was found useful to adapt the curve fit to the seasonal MGVI peaks, and produce more realistic interpretation of the seasonality patterns. Increasing the adaptation strength also had the positive effect of bringing the base of the curve fit away from the more unstable winter minimum values. Therefore, future TIMESAT-based phenology studies might still need to consider the necessity to apply an upper-envelope adaptation, even if not using NDVI. The aim of the TIMESAT function fitting is to decrease uncertainty due to removal of the noise, but in some cases, like with the presence of large data gaps, uncertainty can increase. It is not possible to quantify this uncertainty however, since the shape of the "true" trajectory is not known (L. Eklundh, pers. comm.). Generally, however, it can be shown that the overall signal quality is improved (Hird and McDermid, 2009), and

several studies of a correlative nature have demonstrated that smoothed, rather than raw, data improve the results. Despite the uncertainty in SOS dates introduced by the temporal smoothing and time-compositing, the spatiotemporal coverage afforded by these techniques allowed the national-scale scope of the study to be achieved. The consistency in the spatial patterns, reproduced on an annual basis, was indicative of the robustness of the TIMESAT method. Furthermore, the method was sensitive enough to detect temporal variability in the patterns from one year to the next caused by variability in climate and land use. The most consistent feature of the spatial pattern was later SOS on higher ground and earlier SOS in lowlands, a trend particularly clear along the mountainous western peninsulas. These features of the SOS prove that processing the entire dataset with carefully selected common settings produces consistent results.

4.8 Conclusion

There are a variety of approaches to estimate land surface phenology events from time series of satellite data. However, at present there is no consensus regarding an optimal approach for producing a land surface phenology estimate (Friedl et al., 2010). The TIMESAT tool is however a popular method based on the prescription of thresholds in vegetation indices, and it is straightforward in its application. However, as with seasonality metrics derived from any method, it is difficult to interpret their meaning in terms of what is measured on the ground (White et al., 2009). In order to inter-compare SOS and equivalent ground-based measures of vegetation phenology, independent measures of vegetation seasonality are required whether from webcam observations (Richardson et al., 2011; PEN, 2011), *in-situ* monitoring of vegetation

parameters such as FAPAR (Jung et al., 2008) or from ground-based observations of tree species themselves (Studer et al., 2007, Soudani et al., 2008). Nevertheless, the requirement for a versatile and adaptable tool to derive an image-based SOS measure has been satisfied by the array of TIMESAT modelling options and parameter settings demonstrated in this chapter. Although the parameter settings were not optimised for landcover, as has been done in continental-scale datasets such as in Africa with extreme variation in vegetation type (Jönsson and Eklundh, 2002), the chosen settings are optimal for an island like Ireland dominated by grasslands but with mixed landcover and temperate climate. The initial results presented in this chapter are promising and show for the first time the national-scale patterns in the SOS derived from a remotely-sensed measure of FAPAR. External factors such as landcover, and physical features of the landscape such as mountains, appear to be consistent features in the SOS spatial patterns. Therefore, these factors and their impact on the SOS will be explored in greater detail in the next chapter. Notably there was also temporal variability in the spatial patterns from year to year. It is known that climatic factors such as air temperature determine the BGS as measured at the IPG gardens. Therefore the role of air temperature in causing interannual variability in the SOS will also be examined in chapter 6.

Chapter 5. The spatio-temporal patterns in SOS across the island of Ireland based on time series analysis

In this chapter, spatio-temporal patterns in the vegetation SOS have been described and the causes of these patterns explored at the national scale. The spatial patterns have first been explored using image analysis techniques to separate the spatial and temporal components of the SOS patterns per year. Additionally, SOS anomalies, presented as deviations from the 7-year mean SOS, were examined on a temporal and spatial basis to show the interannual variation in SOS over the 7-year period. Landcover and elevation have been used as explanatory factors to interpret the spatio-temporal patterns, while changes in regional air temperature have been used to examine the interannual variability in SOS.

The relationship between landcover and land surface phenology is well established as vegetation greenup dates differ according to species composition of the landscape (Studer et al., 2007), and patterns of temporal differences in phenology can be used to characterise landcover change (Lupo et al., 2007). The vegetation SOS is also known to exhibit a strong relationship with elevation, especially in mountainous environments (Hudson Dunn and de Beurs, 2011). Therefore landcover was used as a primary discriminator of inter-annual, as well as intra-annual; SOS variation, while elevation was examined as a secondary indicator of SOS since the topography of Ireland is not typically mountainous, being, for the most part, less than 1,000m in elevation. In the analyses concerning SOS variability within one year, 2006 was chosen as it was coincident with the most recent landcover information for the ROI.

In contrast, for general analyses of SOS, with elevation for example, the 7-year mean SOS values were used. A version of this chapter combined with sections of chapter 4 have been written as a paper submitted to the International Society of Photogrammetry and Remote Sensing (ISPRS) Journal of Photogrammetry and Remote Sensing which is currently under review.

5.1 Spatio-temporal variability in the SOS

The 7-year mean SOS values were calculated per pixel as an arithmetic average of the seven annual SOS values from 2003 to 2009. The mean SOS image is shown in figure 5.1. In order to examine the temporal pattern in mean SOS values, a histogram was constructed from this image. The histogram shows that 17% of the pixels in the mean SOS image had value of 7, which corresponds to a SOS from March 2nd-11th. In contrast, 15% of pixels had their SOS in period 6 (February 20th-March1st) and 14% in period 8 (March 12th-21st). Overall, 46% of the pixels had their SOS between period 6 and 8 (February 20th to March 21st), while 66% of the pixels had their SOS between period 5 and 9 (February 10th-March 31st). The full list of composite periods with the corresponding day of year and calendar dates is shown in Appendix E. The interpretation of spatial patterns in the SOS was aided by a line transect which was drawn across the mean image from west to east at approximately 53.5°N latitude indicated by the line A-B in figure 5.1.

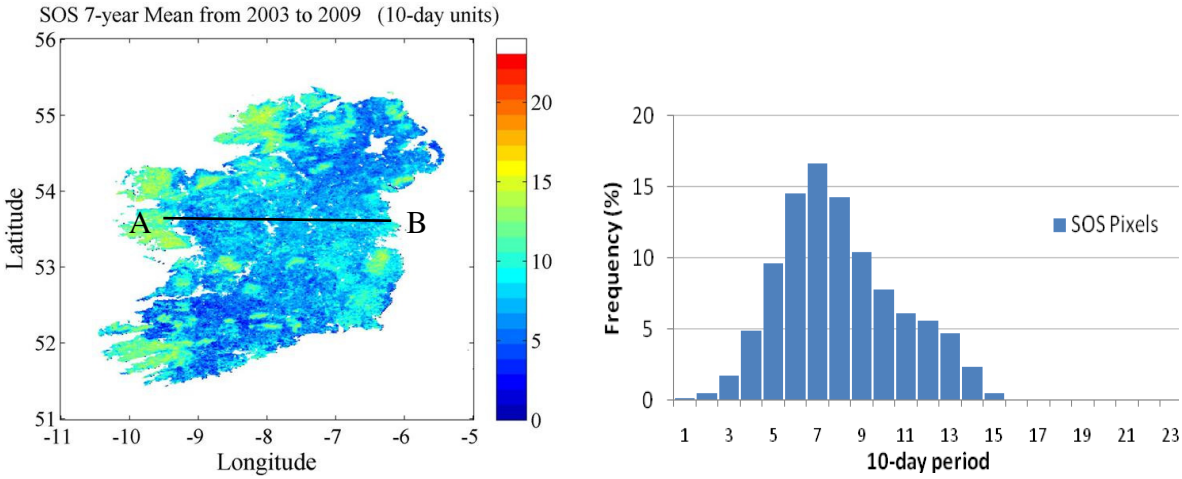

Figure 5. 1: The 2003-2009 mean SOS image calculated from an average of the annual input images from 2003 to 2009. A line transect has been drawn from West to East to show spatial variation in the SOS while the histogram, derived from the image, is indicative of the temporal trend in SOS.

Spatially, the SOS occurs first in the southern lowlands, coincident with an area in the interior of Ulster. The southern area includes the 'Golden Vale', covering parts of three counties: south Limerick, west Tipperary and north Cork. The SOS in the Midlands appears to be later than that further to the North and South. The timing of SOS is similar in parts of the Midlands and on the east coast of Ireland, while the SOS on the west coast is much later relative to the rest of the country. The location of these areas can be seen in the thematic map of Ireland presented in figure 5.2.

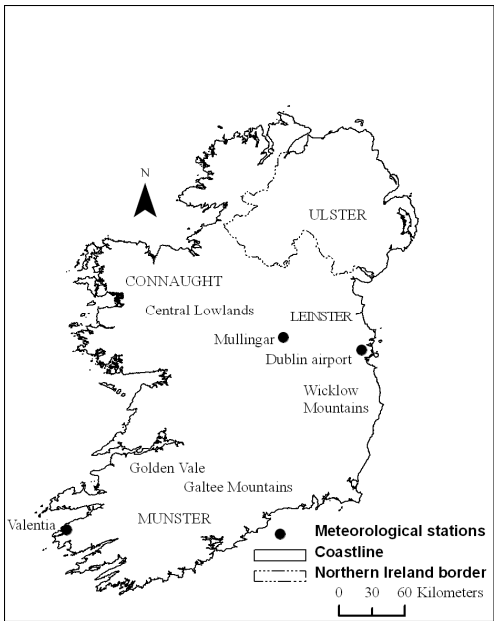

Figure 5.2: The location of place names referred to in the text, and meteorological stations in section 5.7

The mean SOS line transect by longitude for A-B, across the mean SOS image, is shown in figure 5.3, revealing a strong West to East gradient of earlier SOS as it occurs between period 10 and 15 on the west coast and between period 5 and 10 on the east coast.

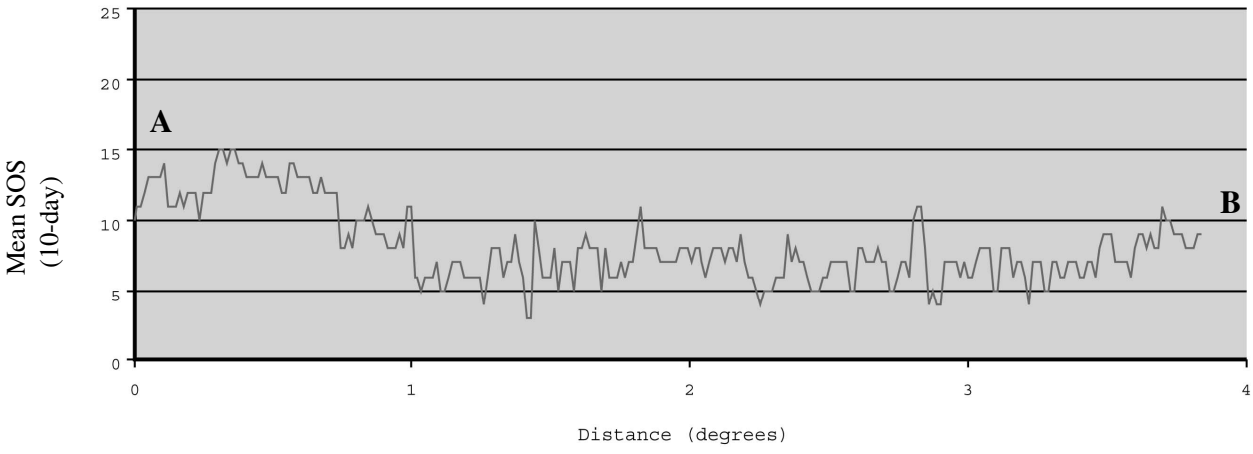

Figure 5.3: The variations in SOS dates over the marked transect (A-B) in figure 5.1.

A consistent feature of the spatial patterns in the SOS imagery was the occurrence of later start dates at higher elevation, e.g. upland areas of the northwest, west,

southwest, Wicklow Mountains and a number of other smaller ranges, e.g. the Galtee Mountains in the south. In the same way, low-lying flat areas such as the Golden Vale in North Munster and the interior of Ulster have earlier start dates relative to surrounding higher ground. The upland areas can be seen in the Digital Elevation Model (DEM) of Ireland (figure 5.4) which is a subset of the global GTOPO-30 DEM. This DEM has a horizontal grid spacing of 30 arc seconds (approximately 1 km spatial resolution) (Earth Resources Observation and Science (EROS) Centre, 2009).

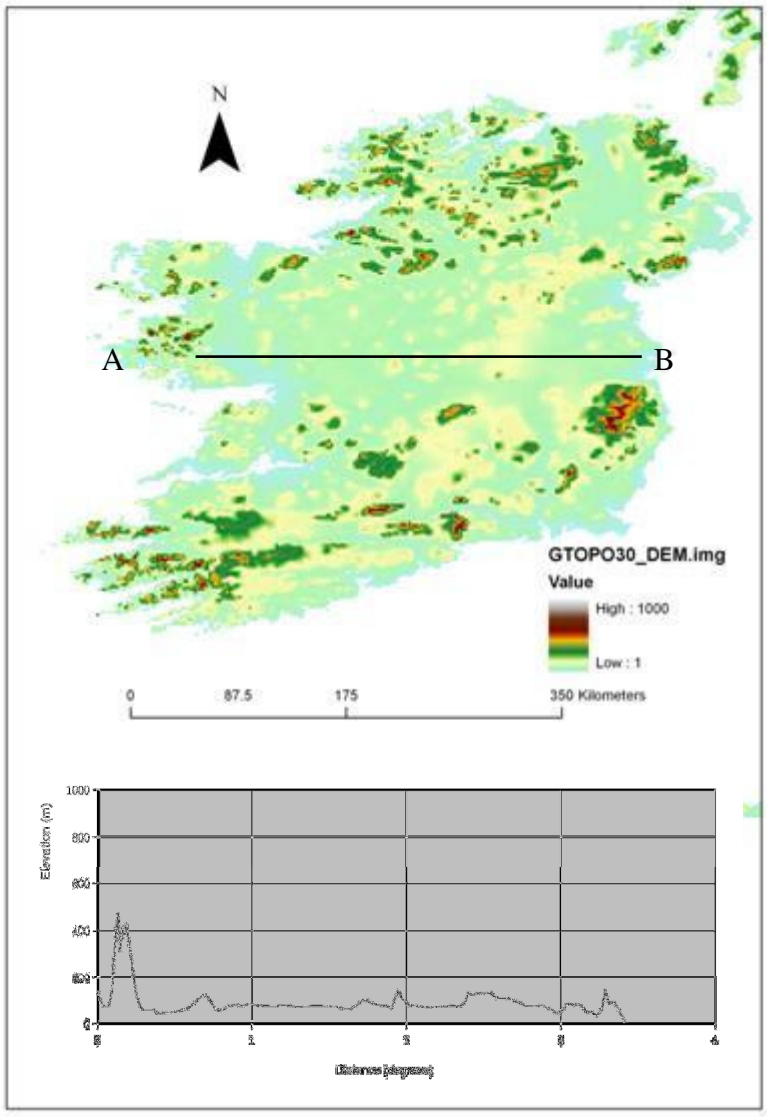

Figure 5.4: The GTOPO 30 Digital Elevation Model (DEM) of Ireland with an elevation profile derived from the GTOP30 DEM at the same latitude as the SOS profile in figure 5.1.

The elevation profile was extracted from a line transect across the GTOPO-30 DEM from the west to east coast at 53.5°N latitude and is shown in figure 5.4. The profile exhibits the spatial trend in elevation across the island at that latitude. Although there is more variability in the spatial profile of SOS extracted at the same latitude (figure 5.3), there is a broad agreement between the SOS and elevation trend as the mean SOS is later at higher elevation and earlier at low elevation.

5.2 Spatial analysis of SOS

In order to explore the SOS variation with latitude and longitude, the SOS pixels were counted in intervals of 10-day periods along rows for the latitudinal trend and along columns for the longitudinal trend. These quantities were divided by the number of land pixels in the respective image dimension to normalise the frequency measure. The numerical range was scaled to a maximum value of 1 so that the frequency of pixels in each 10-day period could be compared between years.

5.2.1 Latitudinal SOS analysis

In figure 5.5, the number of SOS pixels per10-day period is displayed with latitude. The north coast of Ireland is located at about 55.5°N. Between 55.5°N and 54.5°N, the 7-year mean SOS remains well distributed from period 5 (February 10th-19th) to 15 (May 21st-30th). This is probably due to a mixture of SOS dates from an area of homogenous pasture land in the interior of Ulster (early) with upland peat bog and scrub vegetation (late) in the mountains of Donegal.

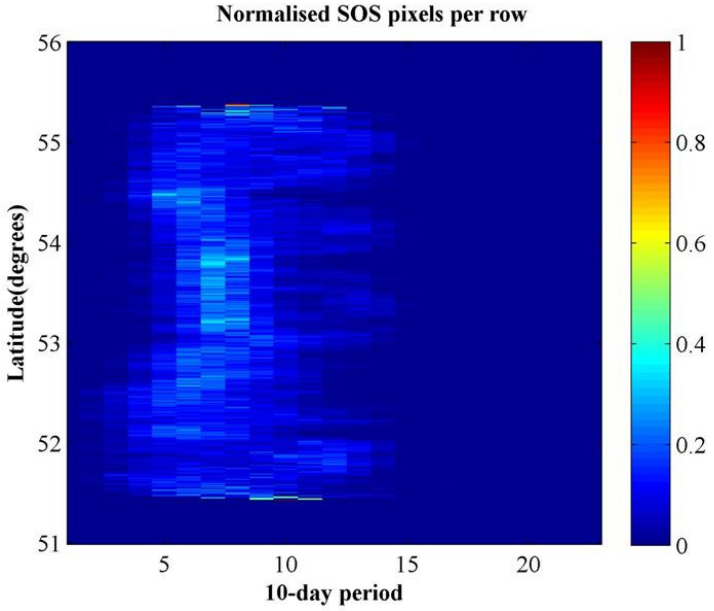

Figure 5.5: The 2003 to 2009 mean number of SOS pixels per row (latitude) counted per 10-day period and normalised by the number of land pixels per row.

At 53.5°N, SOS pixel density increases around period 7 where pastures, arable land and mixed agriculture is practiced. There are some pixels between periods 10 to 15 at this latitude due to the presence of Connemara highland vegetation. From 53 to 52°N of latitude, the pixel distribution begins to spread again due to the presence of a mix of vegetation types in the lower Midlands, but there is a shift towards SOS earlier than period 5 as the Golden Vale pastures influence the spatial pattern. From 52 to 51.5 °N, upland vegetation again influences the pattern as the SOS dates become later, e.g., there is a cluster of SOS pixels around period 11-12 (April 11th-30th) at the same latitude as Killarney National Park. In summary, variations in elevation, which creates differences in vegetation type, as well as land use practices, influence the spatial patterns in SOS when examined on a latitudinal gradient. In particular, extremes in the SOS dates feature strongly from the earliest SOS dates in pastures to the latest SOS dates in mountainous vegetation occurring along the same latitudinal range. This was most obvious in particular in the northern and southern parts of the island where upland areas and lowland plains occur at the same latitude. There is as much as 120 days difference in SOS from the earliest SOS (period 3) to the latest SOS (period 15) at some latitudes. The latitudinal analysis was applied to each SOS image from 2003 to 2009, shown in figure 5.6 along with the CORINE landcover classes analysed with the same method (codes for these classes are given in table 5.1). There is interannual variation in the latitudinal spatial pattern. For example, in 2003, there appears to be a south to north trend of later SOS. However, this is less apparent in 2004 where there is little spatial variation across the country. The SOS in 2005 occurs later in the south than in the north. In 2006, the range of SOS dates is narrower and occurs later compared to the other years. In contrast, the

2007 and 2008 range of SOS dates is wider than any of the other years, and an earlier SOS in the south is evident in both these years. The 2009 SOS dates are similar across the country except for a wider range of SOS dates in the North. As for the spatial pattern in landcover, class 8 (pastures) is the most frequently occurring class at all latitudes, and there is a very high density of pasture pixels between 52º and 53º. The influence of pastures on the SOS spatial patterns is also evident between 52º and 53º as the SOS is consistently earlier relative to the rest of the country. Class 5 (peat bogs) is the next most frequent class, occurring mostly south of 52º and north of 53º.

Table 5.1: CORINE Landcover classes and their codes used in spatial analysis of the SOS

Landcover class	**Code**
Broad Leaved forest	1
Mixed forest	2
Natural grassland	3
Moors and heaths	4
Peat bogs	5
Land principally occupied by agriculture with significant areas of natural vegetation	6
Green urban areas	7
Pastures	8
Complex cultivation patterns	9
Coniferous forest	10
Non-irrigated arable land	11
Transitional woodland scrub	12
Sparsely vegetated areas	13

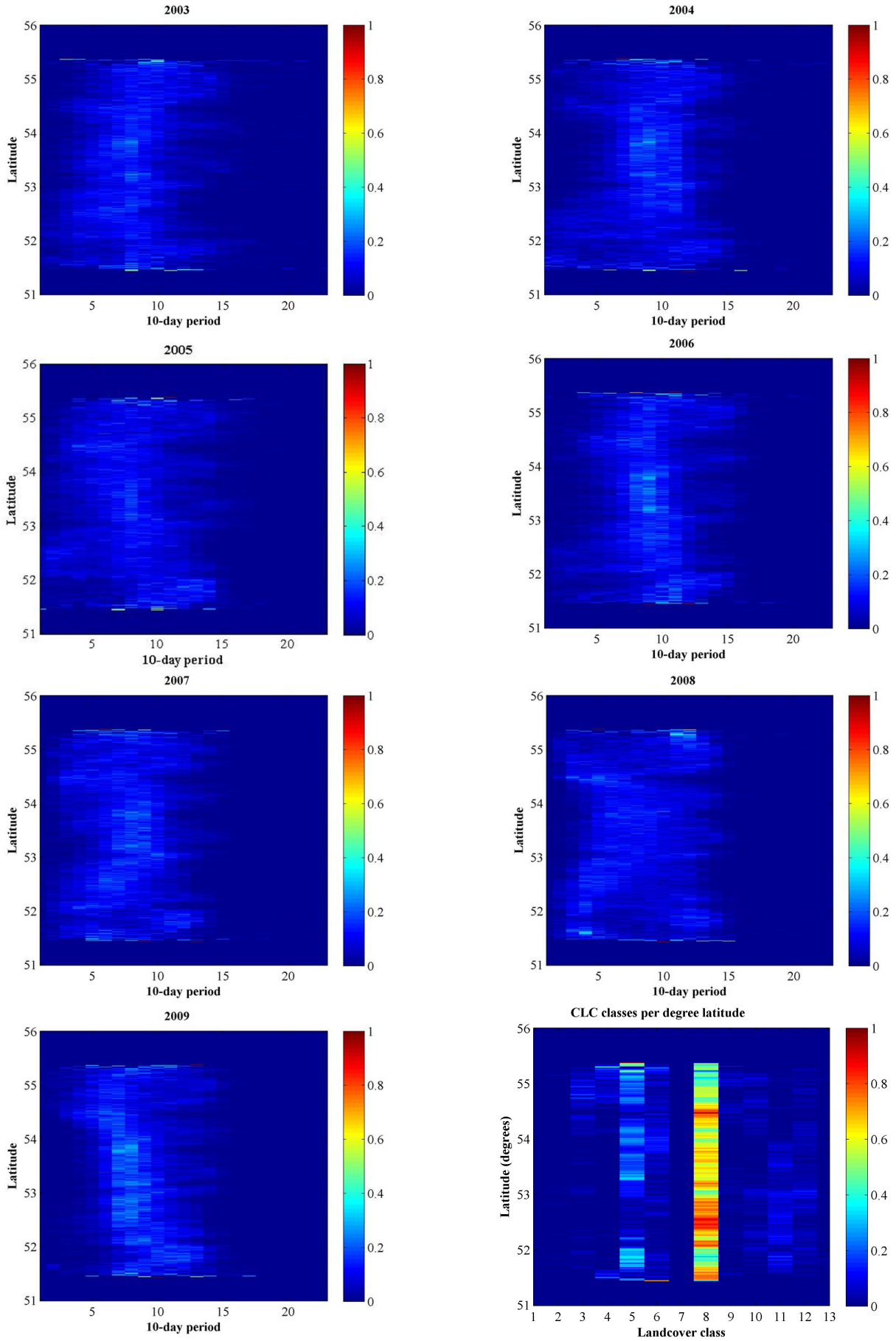

Figure 5.6: A relative density measure of SOS pixels per row (latitude) per 10-day period from 2003 to 2009. The number of SOS pixels has been normalised by the number of land pixels in each row. The scale shows the relative amount of SOS pixels per 10-day period. The same method was applied to CORINE landcover pixels to show the geographical distribution of landcover classes per degree latitude.

5.2.2 Longitudinal SOS analysis

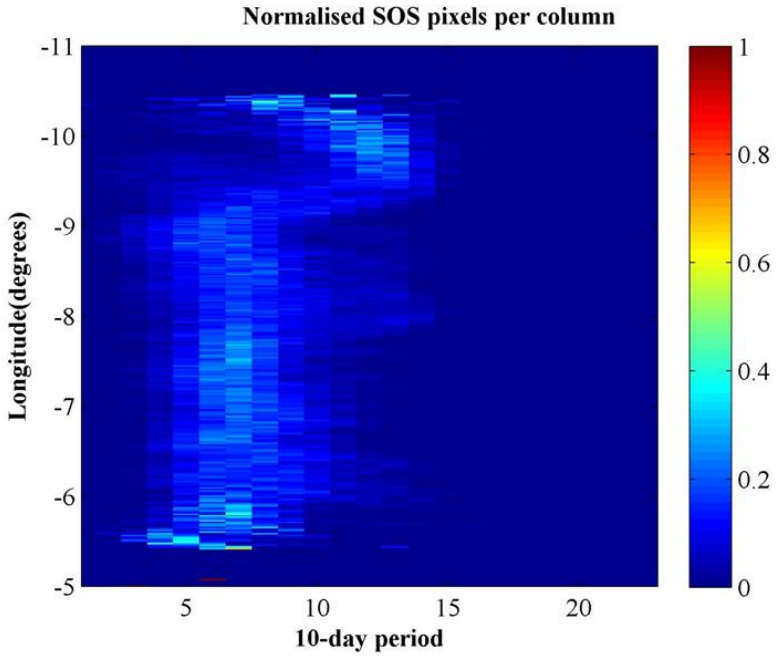

Figure 5.7: The 2003 to 2009 mean number of SOS pixels per column (longitude) counted per 10-day period and normalised by the number of land pixels per column.

In figure 5.7, the mean number of SOS estimates per10-day period are presented with longitude, using the same method described in section 5.2.1. However, the y-axis has been inverted to show the east coast of Ireland at the base (-5º) and the west coast at the top (-11 º). On the east coast of Ireland, located along 5.5ºW longitude, SOS estimates are well distributed between composite 3 (January 21st-30th) and 10 (April 1st-10th), although there is a higher count of SOS pixels around period 7 (March 2nd -11th). Between 6 and 9 ºW, the SOS is distributed between period 3 and 10, with a small cluster of pixels at period 7 between 7 ºW and 8 º W. This is possibly due to the practice of arable cropping in the east and southeast of the country. The presence of upland vegetation in the northwest, between 8 ºW and 9 ºW, has increased the temporal range of SOS dates to between period 3 and 15. At 9 ºW, the SOS is earlier however, as the SOS dates are between period 3 and 5 here. This is due to the path of 9 ºW longitude which passes through the agricultural

region of North Munster known as the Golden Vale. A distinctive feature of the longitudinal trend is a sudden shift in the SOS at 9.5 º W from period 5 to 10 to period 12 to 15. This abrupt change is due to the topographical change from central lowlands to upland mountainous areas along the western coastline and the subsequent change in vegetation type in which the SOS is delayed. Interestingly, the change in elevation on the east coast, due to the presence of the Wicklow Mountains, is not detected in the SOS trend. The presence of mostly arable cropping, at the same longitude, is a probable cause of this. The longitudinal analysis was also applied to each SOS image from 2003 to 2009 as well as landcover (figure 5.8). Much like the latitudinal pattern, the longitudinal spatial pattern in SOS dates is relatively stable from one year to the next, although the temporal pattern does vary on an interannual basis. This was evident especially in 2005, 2007 and 2008 when the SOS estimates varied considerably across the country. The years 2004, 2006 and 2009 have a much narrower range of dates in comparison. Once again the spatial pattern in landcover is dominated by pastures, except between 9ºW and 10ºW, where peat bogs are the most dominant landcover. The contrast in landcover between peat bogs and pastures is evident in the longitudinal pattern as there is an abrupt shift from earlier to later SOS dates at approximately 9.5 ºW.

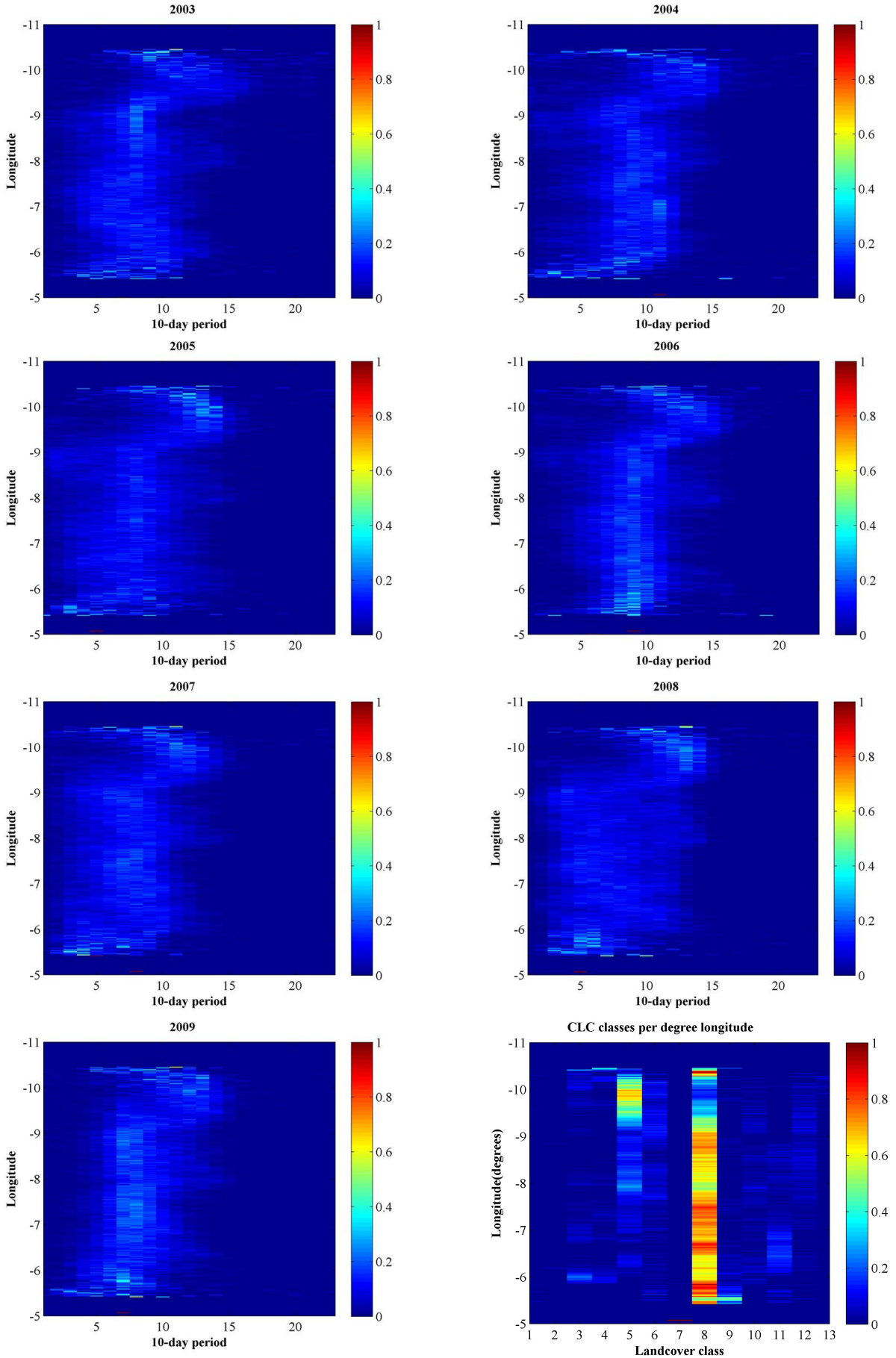

Figure 5.8: The number of SOS pixels per column (longitude) per 10-day period from 2003 to 2009. The number of SOS pixels has been normalised by the number of land pixels in each column. The scale shows the relative amount of SOS pixels per 10-day period. The same method was applied to CORINE landcover pixels to show the geographical distribution of landcover classes per degree longitude.

5.3 The SOS anomalies from 2003 to 2009

The annual SOS anomalies were calculated as 10-day deviations from the 7-year mean SOS. These images are shown in figure 5.9. Negative (positive) anomalies correspond to areas of earlier (later) than average growing seasons, and are shown from light to dark blue (yellow to red) colours. 94% of the anomaly values were found to be within ± 4 anomalies of the 7-year mean SOS. Therefore the image anomalies are scaled to this range, with any anomalies >+4 or <-4 put in the same bin. The adjoining histograms depict the full range of anomalies calculated in each year and are indicative of the temporal range in anomaly values within each year.

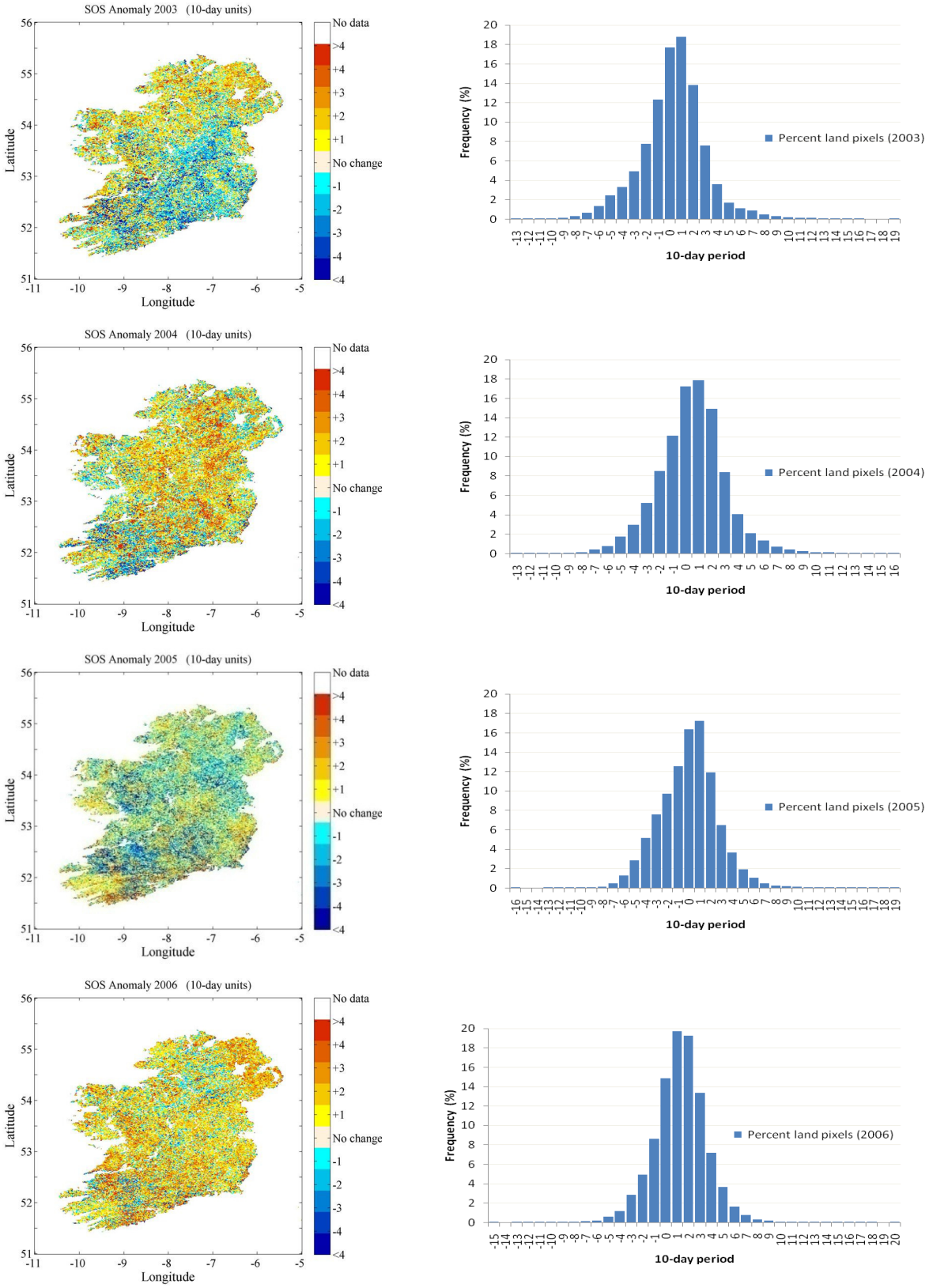

Figure 5.9: Annual SOS anomalies from the 7-year mean SOS in 10-day periods displayed as images (left) and histograms (right) showing the temporal patterns in anomaly values within each year

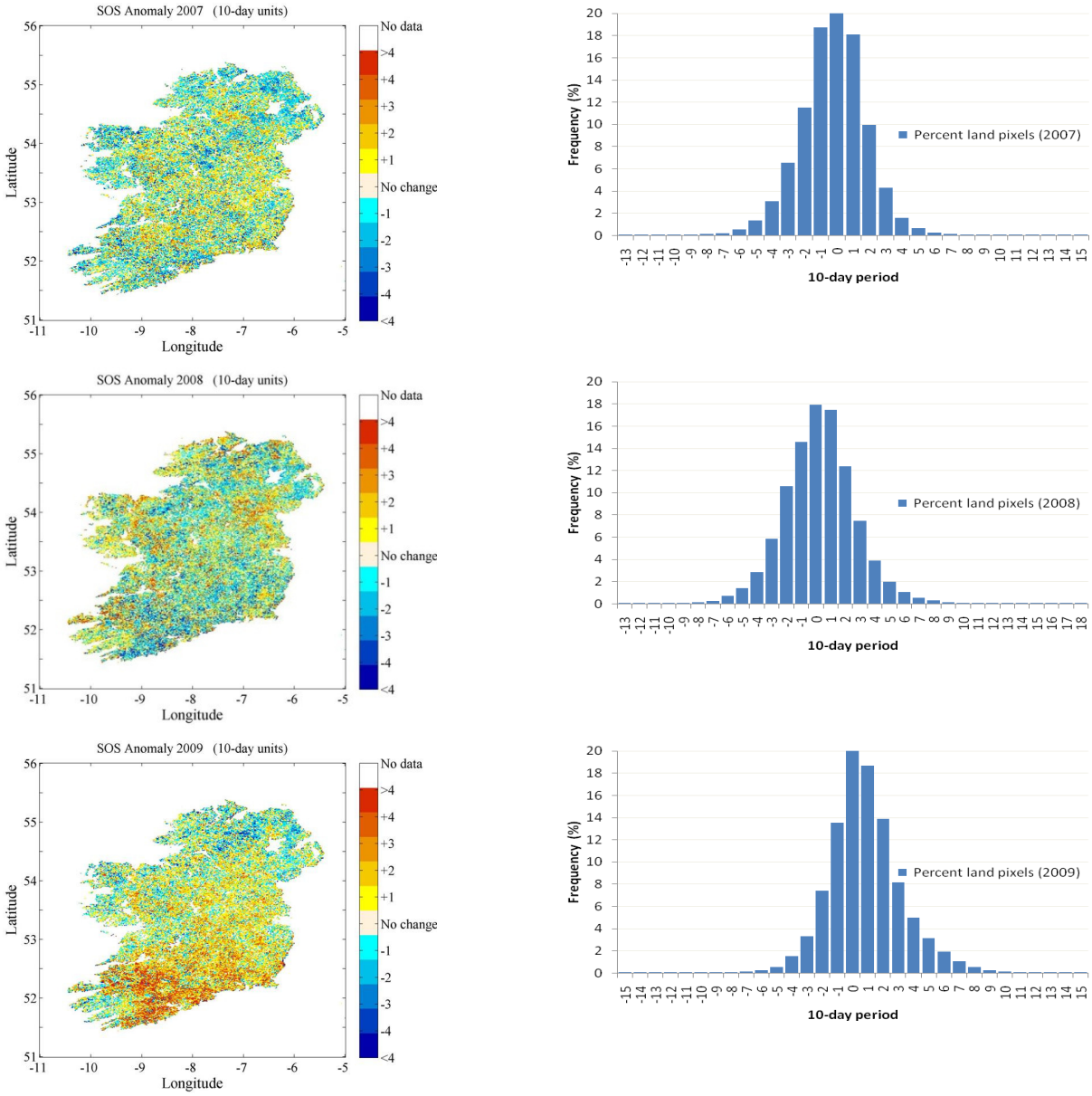

Figure 5.9: Continued

The anomalies in figure 5.9 demonstrate the extent of the spatio-temporal variability in SOS. For example, the 2003 SOS was earlier in the east, southeast, midlands and parts of the south coast as can be seen from the high number of negative anomalies in that area. In contrast, the anomalies were mostly positive in the rest of the country indicating later SOS. The 2004 SOS was later across most of the country, yet it was noticeably earlier in the south and southwest in the same year. Likewise, in 2009, there were a high number of positive anomalies, hence a later SOS, concentrated in

the south of the country while there were negative anomalies in the north. The SOS anomalies in other years show less of a localised response. For example, in the 2006 image the positive anomalies are well distributed across the country, while in 2007 and 2008, negative anomalies are present across most of the country, except for some variation in the midlands. A synthesis of the anomaly results is presented as a stacked column chart in figure 5.10. The number of pixels in each anomaly bin was calculated as a percentage of all the anomaly pixels in that year. The percentage anomaly values were stacked so that the interannual variation in the SOS could be compared across years. Both the magnitude and direction of temporal changes in SOS on a yearly basis can be viewed in this way without the spatial component. An anomaly of 0 indicates that the SOS was equal to the 7-year mean SOS and therefore showed no temporal variation.

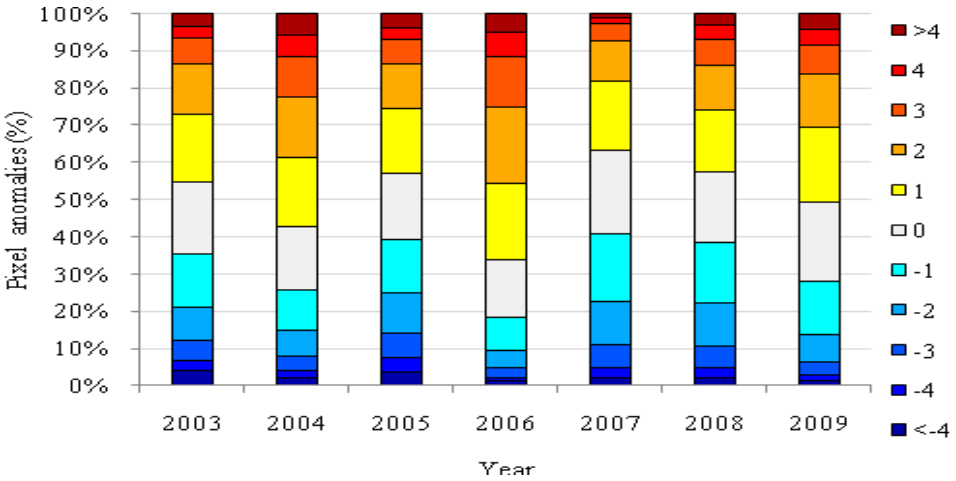

Figure 5.10: The annual percentage of pixels per anomaly bin. Changes in the magnitude and direction of the anomaly indicate shifts towards early or later SOS.

In 2006, the column is composed of more positive than negative anomalies as the bulk of the values are above zero, indicating the 2006 growing season was much later relative to the 7-year average. In contrast, the opposite effect was observed in 2007, when most of the anomalies were negative and the country experienced an

earlier than average SOS. The 2005 and 2008 SOS showed the least temporal deviation from the 7-year mean. The advantage of exploring the temporal pattern in SOS in this way is evident from the 2009 anomaly. While in the 2009 image (figure 5.9), there is a clear geographical gradient in the anomaly values, it is difficult to determine if the net SOS was later or earlier across the country. Yet in the 2009 column (figure 5.10), it can be seen that there were more positive than negative anomalies indicating that SOS was generally later that year.

5.4 The SOS and landcover

The spatial and temporal patterns in SOS have been explored on both a national and local scale across the island of Ireland, and geographical gradients have been detected in these patterns owing to the variation in vegetation type, landcover, elevation and proximity to the coast. The role of landcover type as a determinant of SOS will now be explored in further detail.

5.4.1 CORINE Land Cover (CLC)

Currently, the only national-scale landcover database for Ireland is available from the CORINE programme (Co-ORdination of INformation on the Environment). The European-wide CORINE land cover (CLC) map was created to produce a satellite-derived land cover database for EU member states with a minimum mapping unit of 25 ha (approx. 500 m^2) (ERA-Maptec Ltd., 2006). The CLC 2006 is the third, and most recent, dataset in a series, the previous datasets corresponding to base years of 1990 and 2000. The Environmental Protection Agency (EPA), Ireland, has overseen the production and release of CLC 2006, while the Centre for Ecology and Hydrology (CEH) in the U.K. is currently processing CLC 2006 for Northern Ireland

(NI) (Centre for Ecology and Hydrology, 2010). The CLC data have been previously used for observing landcover-specific phenological characteristics by calculating the fractional amount of landcover per satellite pixel. For example, CLC 1990 was used in Spain for optimising NDVI time series for the detection of crop cycles (Genovese et al., 2001), CLC 2000 in Germany for the detection of areas of broadleaf forest for phenology monitoring (Doktor et al., 2009), and CLC 2000 to select areas of deciduous broadleaf forest in southern France by only using pixels with 70% broadleaf forest content (Guyon et al., 2011). The CLC 2000 was validated across Europe with the LUCAS (European Land Use/Cover Area frame Statistical survey) data. However, no validation studies were carried out at the national scale. The overall accuracy of the CLC2000 is 87.0 ± 0.8 %. The percentage of total agreement found between CLC2000 and LUCAS is 74.8 ± 0.6 %, meaning that CLC2000 approximates LUCAS thematic data with a 74.8 % average accuracy (Büttner and Maucha, 2006). As the percentage of CLC changes between 2000 and 2006 was equivalent to only 1.25% of the surface of Europe, the overall accuracy of the CLC 2006 database was not calculated (Büttner et al., 2011). Instead, overall accuracy of the 2000-2006 change database was found to be 87.8%±3.3%. Some of the validation sites were located in the ROI and were found to be correct by the validation process (Büttner et al., 2011).

To produce an island-wide landcover database, the ROI CLC 2006 and NI CLC 2000 shapefiles were merged. The merged dataset was converted from vector to raster format, and resampled to 1.2 km using the maximum combined area algorithm in ArcMap. This was done so that the spatial resolution of the landcover and SOS data was equivalent while ensuring that their corner points and spatial extent were

aligned. The merged CORINE landcover dataset was then used to extract SOS statistics per landcover class. Landcover types which do not contain vegetation, and therefore do not exhibit seasonality, e.g. urban fabric, were excluded from this analysis. The remaining thirteen landcover classes represented both natural as well as managed vegetation cover types. The number of pixels in the merged CORINE image that were included and excluded, as well as their percentage coverage is shown in table 5.2. The spatial distribution of the thirteen CORINE vegetation classes can be seen in the merged CLC image in figure 5.11.

Table 5.2: The proportions of the CORINE dataset that were included and excluded for the analysis of SOS including the thirteen vegetation classes and their percentage coverage

Landcover type	**Percentage**	**Number of pixels**
Pastures	62.7	34685
Peat bogs	15.1	8378
Land principally occupied by agriculture with significant areas of natural vegetation	5.1	2834
Non-irrigated arable land	4.9	2703
Transitional woodland shrub	3.6	1997
Coniferous forest	2.7	1490
Natural grassland	2.3	1254
Complex cultivation patterns	1.6	883
Moors and heaths	1.4	777
Mixed forest	0.2	137
Sparsely vegetated areas	0.2	114
Broad Leaved forest	0.2	84
Green urban areas	0.0	14
Total included	95.6	55350
Total excluded (Water bodies, urban fabric)	4.4	2529
Total land pixels	100	57879

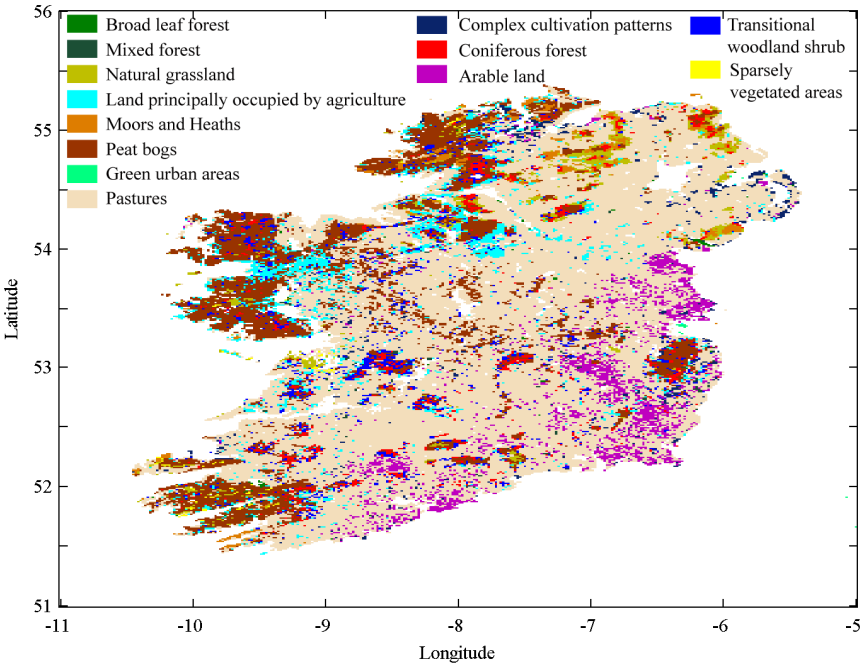

Figure 5.11: The merged CORINE 2000 (NI) and 2006 (ROI) landcover map with vegetation classes used in the analysis of SOS estimates

The landcover pattern shown in figure 5.11 is characterised by a number of spatially scattered minor landcover classes occurring over small areas, while the two most dominant classes, pastures and peat bogs, exhibit the only homogenous more contiguous distributions. There is a variety of vegetation types within each landcover class which share common spectral characteristics in remotely–sensed imagery. For example, pastures are inclusive of all managed grasslands while natural grassland is low productivity unmanaged grassland and non-irrigated arable land consists of cereals, legumes, fodder crops, root crops and fallow land. Land principally occupied by agriculture with significant areas of natural vegetation and complex cultivation patterns generally define heterogeneous agricultural areas interspersed with natural vegetation (EIONET: European Topic Centre on Land Use and Spatial Information, 2006). Of these last two classes, the first class comprises agriculture with natural or

semi-natural areas (including wetlands, water bodies and outcrops) while complex cultivation patterns represents a contrasting mix of small parcels of diverse annual crops, pasture and/or permanent crops. The transitional woodland shrub class is an intermediate class between forest and open ground consisting of newly planted forests (less than 5 years) as well as felled woodland and gorse vegetation (Green, 2010). Peat bogs generally occur in lowland areas as raised bog or as upland plateau blanket bogs. The spatial patterns in these landcover classes reflect the most favourable environmental conditions for optimal growth conditions. For example, the arable crops are confined to the south and southeast where there is little variation in topography, the soil is fertile and air temperatures generally warmer. In contrast, peat bog vegetation occurs where soils are wet and acidic and in upland areas where climatic conditions are more extreme.

5.4.2 Seperability analysis of the landcover classes by SOS dates in 2006

In order to define landcover groups to explore the temporal patterns in SOS, a statistical approach was adopted to group landcover types according to statistically significant differences in their SOS dates. The hypothesis that SOS was dependent on landcover type was examined using the Kruskal-Wallis (K-W) test (Ruxton and Beauchamp, 2008). The year 2006 was chosen for the statistical test as it was coincident with the CLC data. The non-parametric K-W test is well suited to ordinally scaled variables such as time-composited measures of SOS. Specifically, it was used to test for statistically significant differences in the distributions of SOS estimates between different landcover types in the same year. The null hypothesis tested was that there was no variance in the distributions of ranked SOS values between the different landcover classes. The alternative hypothesis was that there

were differences in the ranked SOS distributions per landcover type. 2006 was chosen as a reference year for the analysis since it was coincident with CLC 2006. A significance level of $p<0.05$ was used to determine whether there were significant differences in SOS between the entire set of thirteen landcover populations. As the SOS was treated as a non-parametric variable, the median SOS was calculated per landcover class and compared pair wise to examine if the median SOS values were significantly different ($p< 0.05$.) To account for the family-wise error rate, a Bonferroni adjustment was carried out to calculate a new significance level for the pair wise comparisons by dividing the p-value by the number of comparisons made (adjusted p-value = 0.0038). Landcover classes which were not significantly different were grouped together, denoted by a common letter. Those which had significantly different median SOS ($p<0.0038$) were assigned to separate groups. These groups were then used to explore inter-annual and intra-annual variation in the SOS per landcover type. Significant differences in the SOS were observed among the 13 landcover classes (Kruskal-Wallis test, H=14414.10, 12 df, $P<0.05$)[4]. The landcover types which had significantly different median SOS, i.e. below the adjusted threshold p-value, were grouped separately. The groups were denoted by letters a, b and c and are presented along with the median SOS per landcover type in table 5.3. For presentation purposes only, the A group was subdivided into two sub-groups, A_1 and A_2, whereby A_1 is composed of forested vegetation and A_2 is composed of agricultural landcover types. The landcover classes which share a common letter are not significantly different ($p>0.0038$).

[4] The K-W test statistic, H, is significant when greater than a critical value referenced from a look-up table determined by the number of degrees of freedom (df). The significance level of the differences between the land cover classes is described by the p-value.

Table 5.3: The landcover groups selected for SOS analysis by landcover type

Analysis Group		Landcover class	Median SOS	K-W group	Common letter(s)
A	A_1	Mixed forest	10	a	a
		Broad-leaf forest	10	a	
		Transitional shrub	11	a	
	A_2	Pastures	8	a	a
		Land principally occupied by agriculture	10	a	
		Complex cultivation	9	a	
		Arable land	10	a	
B		Natural grasslands	11	abc	ab
		Coniferous forest	12	abc	
		Green urban	9	ab	
C		Peat bogs	12	c	c
		Moors and heaths	12	bc	
		Sparse vegetation	12	bc	

5.4.3 The Cumulative Start of Season (SOS) in 2006

For the purpose of showing inter-class variation in SOS within one year, cumulative growth curves were derived from an interpolation of the percentages of pixels attaining certain SOS dates in 2006. The slope of the interpolated line is determined by the percentage differences per 10-day interval, i.e. larger differences between each interval create steeper slopes. Therefore, the rate at which the different landcover types attain their SOS can be compared by examining the slope and curvature of the interpolated line. The cumulative growth curves per landcover type are presented in figure 5.12 (a)-(d).

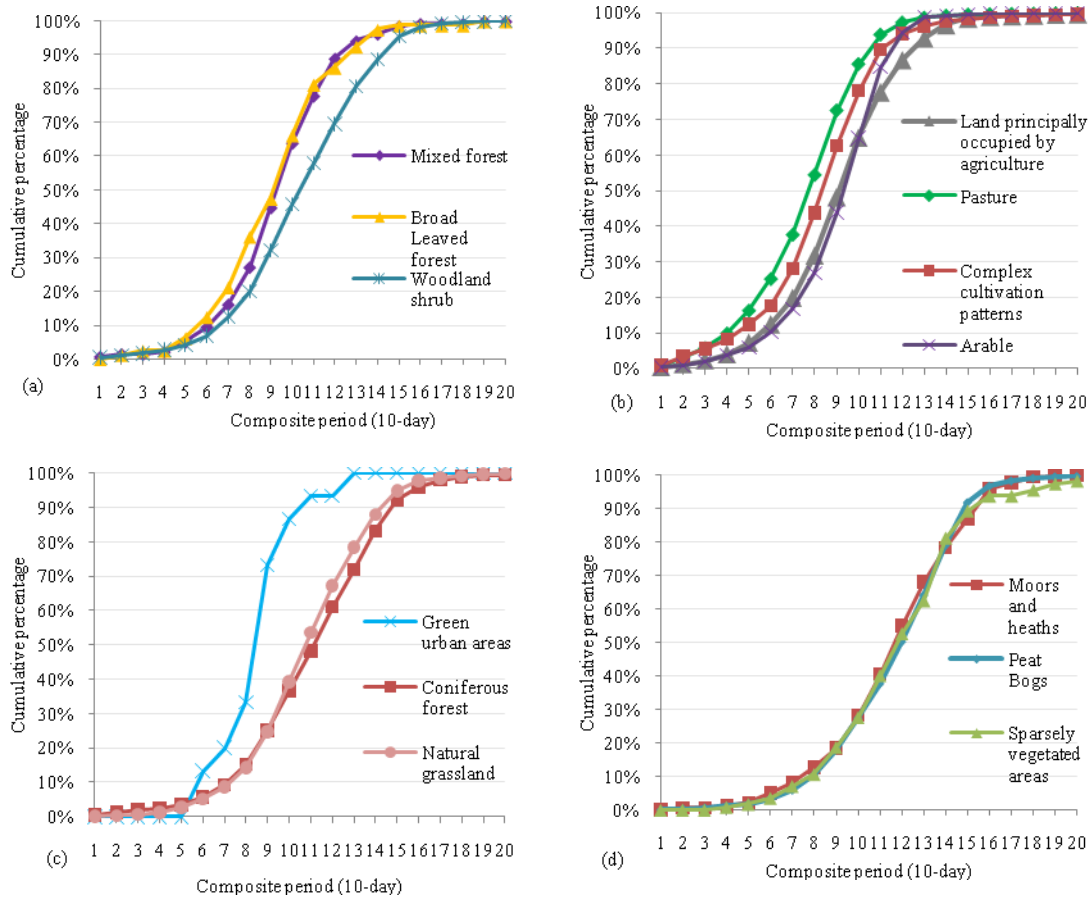

Figure 5.12 (a)-(d): Cumulative SOS in 2006 for three groups of landcover classes whose membership was derived from the K-W test. (a)Group A_1, (b) Group A_2 (c) Group B and (d) Group C

Comparison of SOS the percentage of SOS pixels between pastures and peat bogs, which are the most contrasting vegetation assemblages in Ireland, not only in terms of species composition, but also management regime, is interesting. For example, at period 7 (March 2nd-11th), the SOS had occurred in 38% of the pasture pixels compared to only 6% of peat bog pixels. This differential occurrence of SOS became even more apparent later in the year. For example, by period 12 (April 21st-30th), cumulative SOS was 97% for pastures and only 50% in peat bogs. The percentage difference in rate of accumulation of SOS over the fifty days, between period 7 and 12, is 59% for pastures and 44% for peat bogs. This would suggest that in 2006 the

SOS in peat bogs is slower to occur, and takes place over a longer time period, compared to pastures.

5.4.4 Interannual (2003-2009) variation in median SOS

The interannual variation in SOS was explored by calculating the median annual SOS from all the pixels within each landcover class from 2003 to 2009. The annual median SOS values are shown in 5.13-5.14 in the statistically different groups. The first and third quartiles of the SOS distribution have also been plotted as error bars. Within each group, the SOS varied by one 10-day period in most classes, although the median did vary by two 10-day periods between certain years, e.g. from 2005 to 2006 in broad-leaf forest and green urban areas. Temporal stability in the SOS is particularly evident in Group C in figure 5.14 (b) as the median SOS was 12 (April 21st-30th) in all but two years, 2007 and 2009, which were earlier. The similarity in the SOS between classes in group C is evident from a general overlap in their temporal patterns. No temporal trend emerged in the SOS in the short time series available.

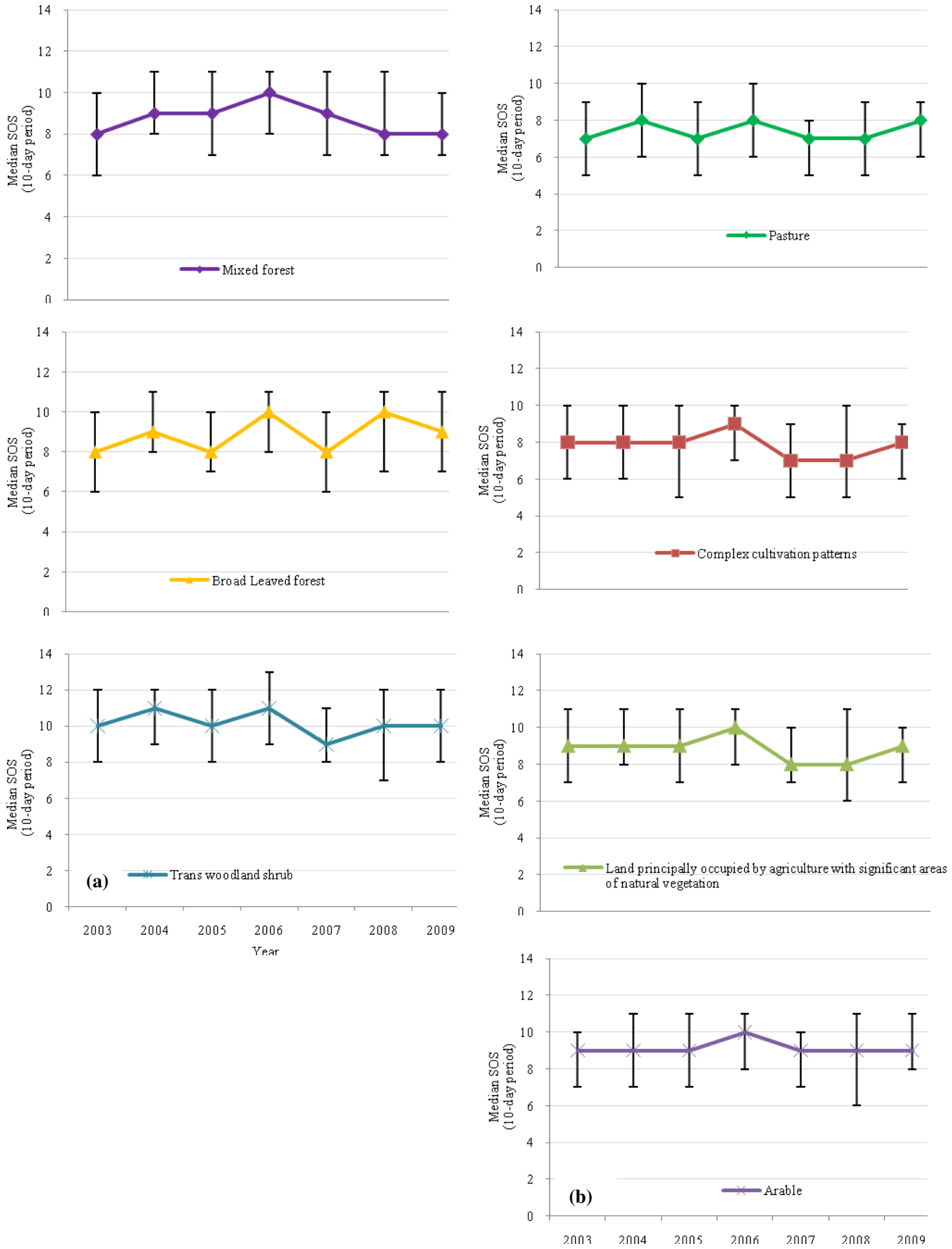

Figure 5.13: (a)-(d): Interannual variability in the median SOS for four groups of landcover classes whose membership was derived from the K-W test. (a)Group A_1 , (b) Group A_2, (c) Group B and (d) Group C . The first and third quartile values have been plotted as error bars.

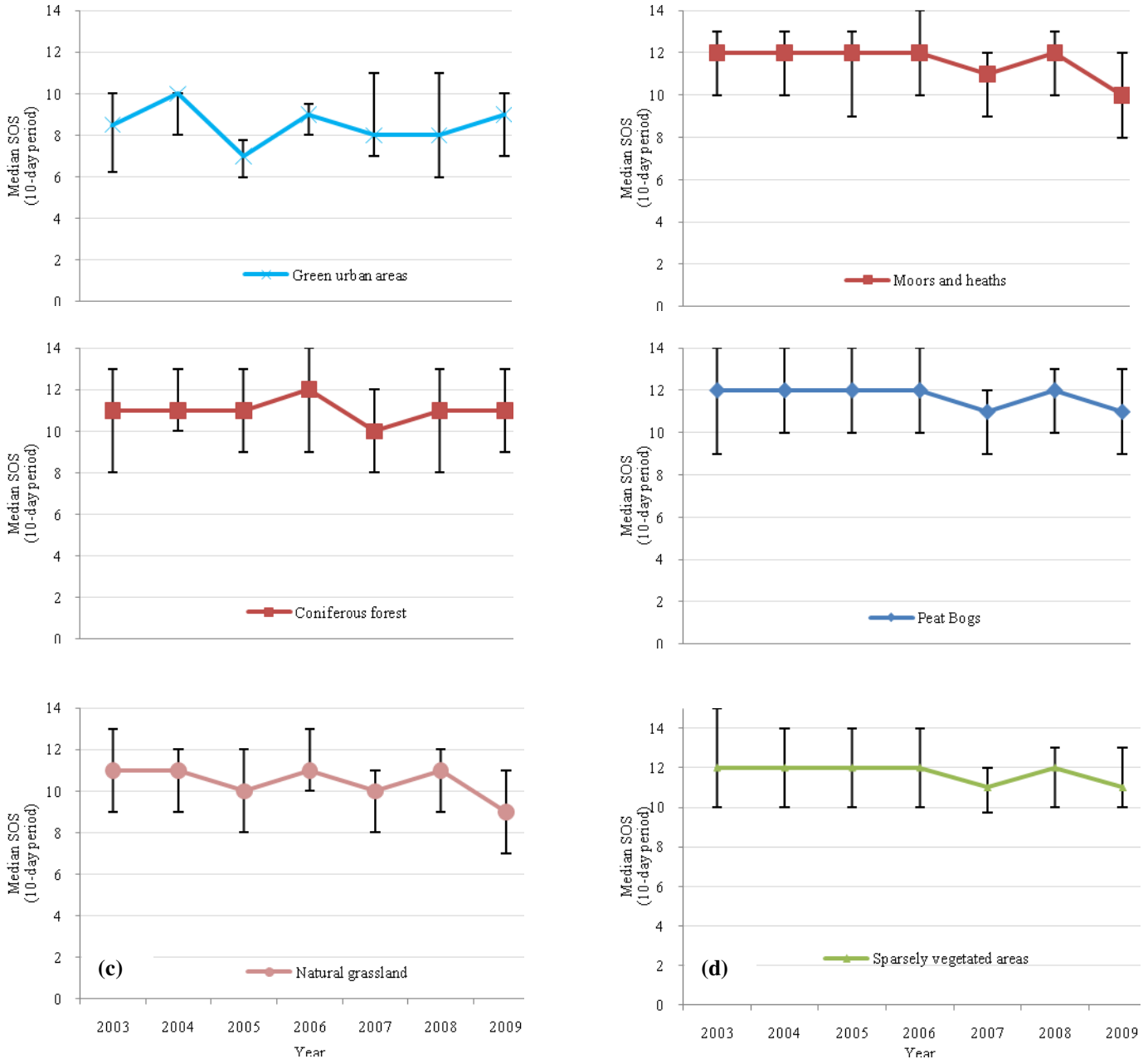

Figure 5.13: (c)-(d)

5.5 The SOS and Elevation

In mid-latitudes, the seasonal timing of spring events such as budding, leafing or flowering of plants is dependent on air temperature (Chmielewski and Rotzer, 2001). However, there is a known lapse rate in air temperature with altitude, i.e. there is a theoretical decrease in mean air temperature by 0.7ºC for every 100m rise in altitude

(Keane and Collins, 2004) which delays SOS at higher altitudes. Hopkins' bioclimatic law, which was originally developed for high altitude environments such as the North American Rockies, states that SOS is delayed 3.3 days for every 100 m increase in elevation (Hudson Dunn and de Beurs, 2011). Qualitative comparison of the 7-year mean SOS image and the GTOPO-30 DEM in section 5.1 showed that there were similarities in the spatial patterns in SOS and topography across the island. This was particularly evident where SOS occurred later in upland areas. To explore this further, a regression analysis was undertaken in order to determine a more quantifiable relationship between SOS and elevation.

Firstly, the DEM was resampled to 1.2 km using nearest neighbour resampling, and the distribution of the elevation values per 50 m elevation interval in the resampled DEM is shown in figure 5.14.

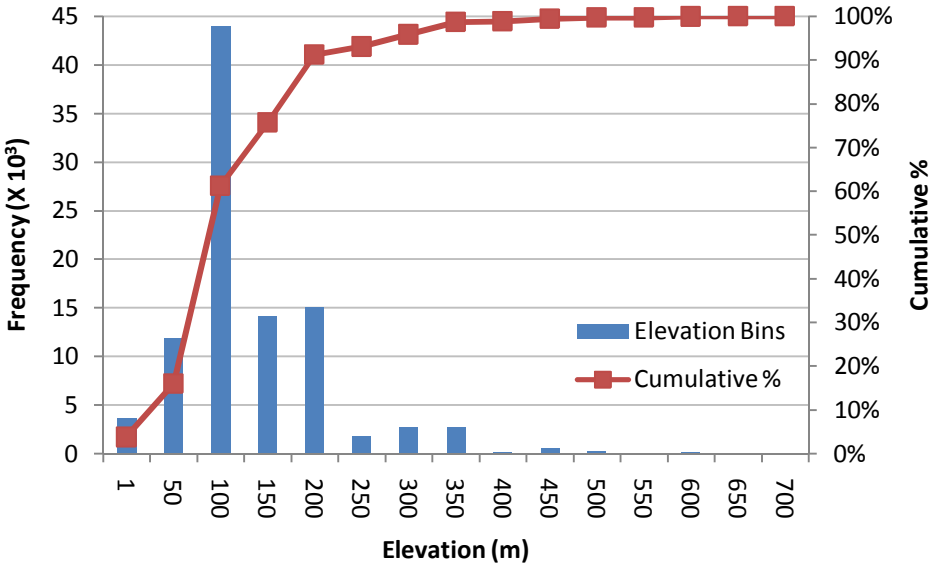

Figure 5.14: The frequency distribution of elevation values in the resampled DEM grid and the cumulative percentage of the values per 50m interval.

From figure 5.14, it is clear that the majority of the land area is between 50m and 150m elevation. In order to test the hypothesis that the SOS varies with elevation,

the Pearson correlation coefficient between the 7-year mean SOS values and the resampled DEM grid values was calculated, as well as the slope and intercept of the regression line. These results are presented in table 5.4.

Table 5.4: Coefficient of determination, slope and intercept of the linear regression of elevation and SOS

r^2	Slope	Intercept	n
0.11	9.50	32.27	97352

The linear regression analysis showed that, across the island, elevation had a weak positive correlation with SOS ($r^2 = 0.11$), i.e. 11% of variation in SOS is associated with elevation. The low level of correlation suggests that there are potentially multiple factors that determine the spatio-temporal pattern in the SOS values, of which elevation only plays a minor role.

5.6 The SOS and grassland management

Grass is Ireland's primary crop, occupying approximately 6.35 million hectares including managed grassland and rough grazing (Keane and Collins, 2004), and forms a stable animal feed for foraging animals such as cattle (Sweeney et al., 2008). The carbon storage potential of pastures across the whole island has been estimated at 0.9 t C ha^{-1}, which is comparatively low considering it is the majority Irish landcover (Cruickshank et al., 2000). Nevertheless, the start of the grass growing season is an important parameter for agricultural planning purposes. Here, the meteorologically-predicted start dates are compared to the 7-year mean SOS estimated for pastures. An agro-meteorological map (Connaughton, 1973), showing the median dates of beginning of grass growth was overlaid on the mean 7-year SOS estimates for pasture (figure 5.15). The median date for grass growth shown was estimated from a soil temperature threshold of 6ºC (100 mm depth), however, the

grass growing lines are valid at sea level only, without consideration of local-scale changes due to shelter, slope and aspect (Keane and Collins, 2004). The SOS values have been altered to fit the 8-week period of median start dates by fixing values greater than period 8 (March 12th-21st) and less than period 4 (January 31st-February 9th) to fit this range. The median grass dates show a southwest-northeast trend as grass growth occurs first in southwest Ireland due to the moderating influence of the sea on local temperatures. In contrast, grass growth is delayed until late March on the high ground of central Ulster (Collins and Cummins, 1996).

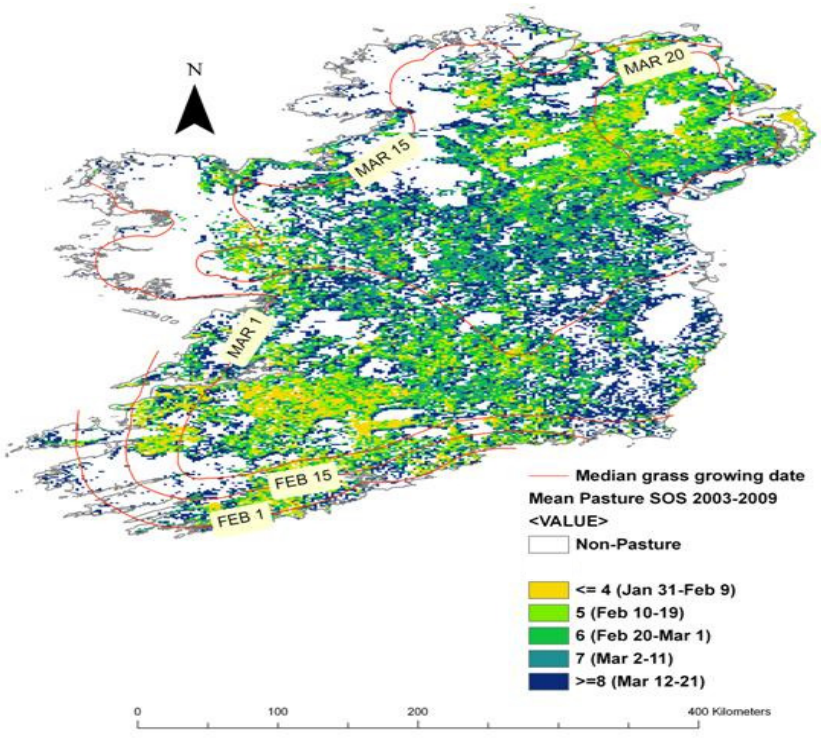

Figure 5.15: The median start dates for grass growth in Ireland derived from Connaughton (1973) are shown with the 7-year mean (2003-2009) SOS estimated for pastures

By contrast, the SOS is earlier in the southwest than in the midlands, and the SOS in the northeast is similar to that in the interior of Munster. For example, the predicted median start date for grass in the northeast of Ireland (March 20th) is considerably

later than the estimated SOS which is approximately from January 31st to February 9th. A possible explanation of the early start dates in northeast Ulster is the presence of Lough Neagh which has been known to moderate local temperature, and so bring about early grass growth (Collins and Cummins, 1996). Grass growth dates calculated using a 6ºC air temperature threshold from 1971 to 2000 appear to be a better estimate of SOS than the soil-derived dates. For example, air temperature-derived growth was estimated to occur from the start of January at Cork, Dublin and Shannon in certain years, while it was delayed as late as 11th April (Shannon), 22nd April (Dublin) and 3rd May (Cork) in some years

5.7 The SOS and air temperature

Regional air temperature variability and its impact on the SOS anomalies over the 7-year period was examined by calculating the monthly mean air temperature and the 1961-1990 mean air temperature from three meteorological stations across the island (Met Éireann, 2011b). The locations of the three stations, shown in figure 5.2, at Dublin airport, Valentia Observatory and Mullingar were considered to be representative of the climate across the island, sited in both coastal and inland locations, and they all had a continuous time series of temperature observations over the 2003-2009 period. The annual winter (November to January) and spring (February to April) mean air temperatures were calculated at each station, and compared to the 1961-1990 average to assess the variability in air temperature for each year. The winter mean and spring mean air temperatures for the three stations are presented in figure 5.16 (a)-(b), with 1 standard deviation error bars. Over the 2003 to 2009 period, the winter mean air temperature at Valentia Observatory was

higher than at Mullingar by 2.8°C, and Dublin airport by 2.3°C, similarly, in spring, the Valentia mean air temperature was higher by 1.9°C and 1.7°C respectively. The milder air temperatures at Valentia Observatory are due to the moderating effect of the North Atlantic drift along Ireland's west coast (Rohan, 1986). At all the stations, the 2003-2009 period had warmer winters and springs than the 1961-1990 average, except for the winter of 2005/2006 at Valentia Observatory which was cooler by 0.2°C, and the winter of 2008/2009 at Mullingar and Dublin airport which was cooler by 0.1°C and 0.8°C respectively. The spring air temperature of 2006 at Dublin airport was also lower than the 1961-1990 average by 0.1°C.

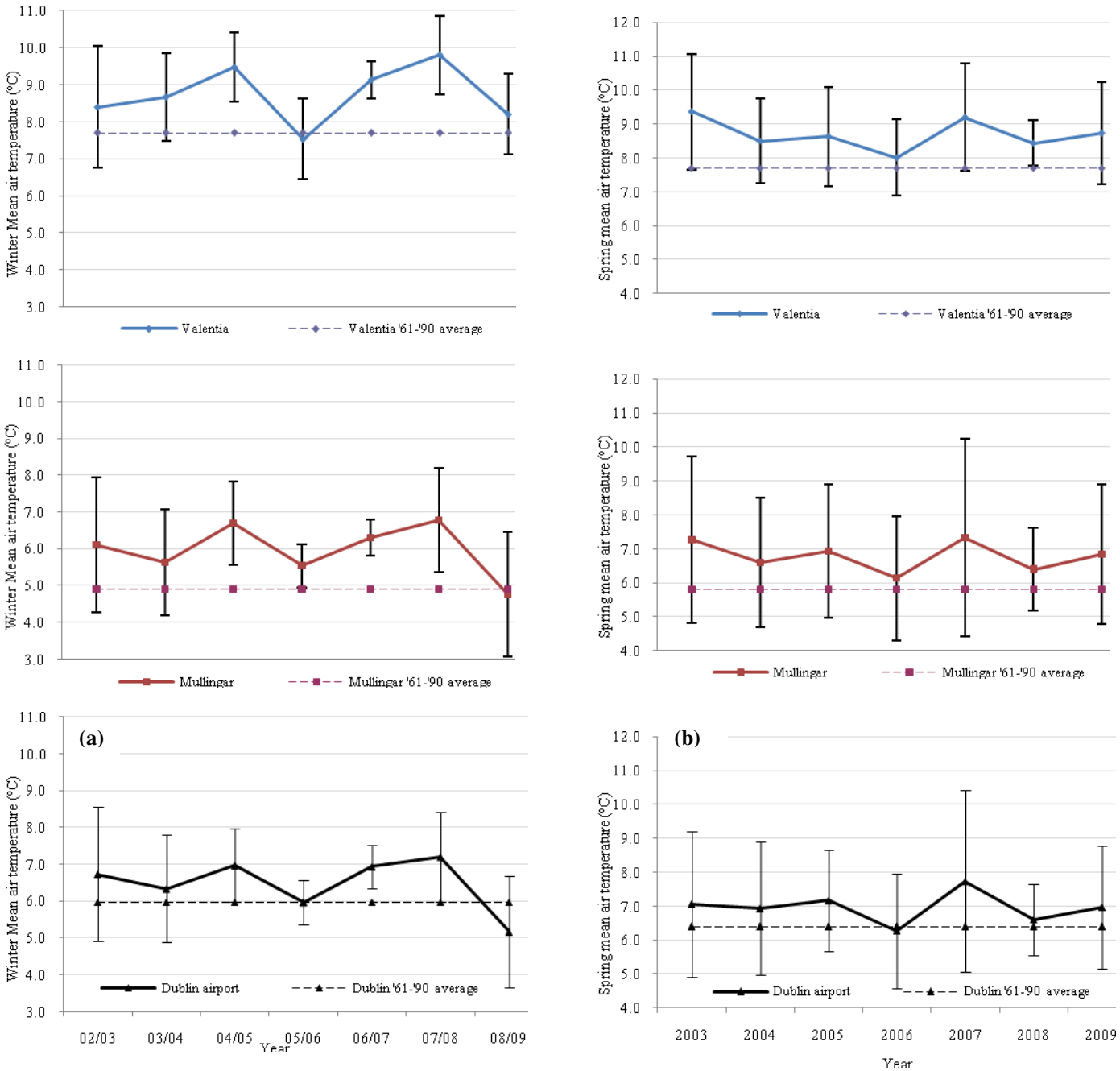

Figure 5.16: Winter (a) and spring (b) mean air temperature at Valentia Observatory, Mullingar and Dublin airport with errors bars of 1 standard deviation

Within the 2003 to 2009 period, the average of the mean winter and spring air temperatures was calculated for each meteorological station, as well as the annual deviations from the 7-year mean which are presented in table 5.5 (winter) and table 5.6 (spring) for each station.

Table 5.5: Mean and deviation from the 7-year mean winter temperatures (2003-2009) at the three meteorological stations used in the analysis of the SOS anomalies

Winter air temperature (°C)	7-year mean	Deviations from mean						
		'02/'03	'03/'04	'04/'05	'05/'06	'06/'07	'07/'08	'08/'09
Valentia	8.7	-0.3	-0.1	0.7	-1.2	0.4	1.1	-0.5
Mullingar	6.0	0.1	-0.3	0.7	-0.4	0.3	0.8	-1.2
Dublin airport	6.5	0.3	-0.1	0.5	-0.5	0.5	0.7	-1.3

Table 5.6: Mean and deviation from the 7-year mean spring temperatures (2003-2009) at the three meteorological stations used in the analysis of the SOS anomalies

Spring air temperature (°C)	7-year mean	Deviations from mean						
		2003	2004	2005	2006	2007	2008	2009
Valentia	8.7	0.7	-0.2	-0.1	-0.7	0.5	-0.3	0.0
Mullingar	6.8	0.5	-0.2	0.1	-0.7	0.5	-0.4	0.0
Dublin airport	7.0	0.1	0.0	0.2	-0.7	0.8	-0.4	0.0

The winter of 2005/2006 was colder than the 7-year average by 1.2°C at Valentia Observatory, by 0.4 °C at Mullingar and by 0.5 °C at Dublin airport (table 5.5). The winter of 2008/2009 was the coldest at Mullingar and Dublin airport by 1.2°C and 1.3°C respectively, while it was 0.5°C below average at Valentia. Interestingly, the spring of 2006 was the coldest at all three stations by 0.7°C, while the 2009 spring temperature did not deviate from the 7-year average at any of the three sites (table 5.6). The impact of the strongest winter and spring temperature anomalies in 2005/2006 and 2008/2009 is evident in the 2006 and 2009 SOS anomaly images in figure 5.8. For example, the combined effect of a colder than average winter and spring recorded at all three stations in 2006 appears to have delayed the SOS countrywide in 2006. However, there were differences in the interannual SOS per landcover type compared to the temperature anomalies, as can be seen in the temporal pattern in the 2006 median SOS values (figures 5.13-5.14). The 2006 SOS was delayed by at least one 10-day period relative to the previous years in groups A and B, but there was no change in the group C landcover types (peat bogs, moors and heaths and sparsely vegetated areas). However it is important to note that the Group C landcover types typically occur in areas away from the sites of the three

meteorological stations, so this may be an artefact of the data, and the temperature anomalies may not be indicative of air temperature in these landcover types. The combination of colder than average 2008/2009 winter temperatures with average 2009 spring temperatures at all three sites produced contrasting SOS anomalies in 2009. For example, the SOS was late, particularly in the south, east and midlands, potentially due to the strong negative deviation in winter temperatures, noted at Mullingar and Dublin. However, the SOS anomalies in the southwest, where the Valentia Observatory is located, were negative; suggesting that cooler temperatures there did not delay the SOS in the region but that the maritime influence may have moderated the impact of an anomalously cold winter. These results would suggest that a combination of a colder winter preceding the event and a cooler spring during the event delay the SOS. However, the extremes of both winter and spring temperatures may not be felt equally throughout the country depending on local conditions.

5.8 Discussion

The main focus of this chapter was on the analysis of spatial and temporal patterns of SOS at the national scale. The SOS occurred across a range of time periods within the first 6 months of the year, depending primarily on vegetation type. However, the extensive coverage of pastures has considerable influence on the national-scale trends in SOS as grass growth tends to occur from January to March. The 10-day composite period was appropriate to describe spatio-temporal patterns in the SOS at the national scale within any one year, to illustrate the spatio-temporal variation in SOS across the country, and to show the temporal patterns in SOS over the seven–

year period. This fulfilled the fourth study objective described in section 1.3 of chapter 1. Although the use of a composite period prevented daily estimates of SOS, the results are indicative of relative spatio-temporal variation in SOS across the country. Qualitatively, the spatial pattern in the SOS imagery appeared to be consistent with elevation. For example, a consistent feature of the SOS spatial pattern was the occurrence of later start dates at higher elevation, and the occurrence of earlier SOS in low-lying pastures. However, quantitative analysis showed only a weak relationship between the two parameters. A likely cause of this is that most of the Irish land area is below 150m, within which there is considerable variability in SOS due to the presence of pastures, arable agriculture as well as natural vegetation. Therefore, there would be considerable variability in SOS dates even at the same elevation weakening any potential elevation-SOS trend. In contrast, strong SOS-elevation relationships have been detected in North American mountain environments, with well distributed vegetation biomes defined by altitudinal range (Hudson Dunn and de Beurs, 2011). In Ireland, where the maximum peak is approximately 1000m and most of the land area below 150m, it is unlikely that there will be a strongly quantifiable relationship between SOS and elevation due to the absence of such distinct vegetation zones.

There was also a coherent spatial pattern between the 7-year mean SOS estimates and the distribution of the thirteen CLC classes across the country. However, these spatial patterns were dominated by the two most abundant landcover types, pastures and peat bogs, while the remaining classes tended to be spatially scattered. This potentially introduces a spatial dependency in the analysis of SOS by landcover type known as spatial autocorrelation. This effect was reflected in the group membership

as landcover types which were in close proximity to one another were sometimes grouped together. This spatial dependency appeared to be strongest in the Group C landcover types (peat bogs, moors and heaths and sparsely vegetated areas) which are generally upland, low-productivity vegetation assemblages. Advanced methods such as Moran's I index (de Beurs and Henebry, 2008b) could potentially be used to take such autocorrelation into account.

The presence of an international border between NI and ROI required that a merged landcover database be derived from an amalgamation of the CLC datasets. The creation of an all-island landcover database has not been done before in this way, and it highlights the need for a joint approach to address national -scale landcover needs apart from the current CORINE programme. Consequently, the amalgamation of two CLC datasets acquired six years apart, and the aggregation of finer spatial resolution CLC landcover classes to the 1.2km SOS spatial resolution, introduced temporal and spatial uncertainty in the landcover data. In particular, the resampling of the CLC data may have detracted from the ability to extract SOS estimates of pure landcover type. However, the resampling was also necessary to compare SOS and landcover at an equivalent spatial resolution. An alternative approach to the hard classification of landcover types, imposed by the maximum combined area algorithm used in this study, would be the use of class membership of SOS pixels. For example, the fractional amount of each landcover type in a 1.2 km pixel could be used as criteria for the categorisation of SOS pixels. This could strengthen the analysis of SOS per landcover type by only selecting SOS pixels with particular landcover content over a certain threshold.

The problem of exploring SOS at a coarse spatial resolution is an inability to resolve the natural variability that occurs at finer spatial scales. For example, at the 1.2 km spatial resolution of the SOS imagery, there is considerable variability in landcover, land use, air and soil temperature, and topography. A previous study of Landsat data of 30m spatial resolution has shown significant spatial heterogeneity of up to two weeks of variability over less than 500 m, even in contiguous deciduous stands (Fisher et al., 2006). Therefore, the timing of spring phenological development is strongly influenced by conditions at the micro scale. Coincident aerial photography, higher spatial resolution satellite imagery or field work investigations used in conjunction with coarse-spatial resolution VI data could potentially lessen this uncertainty in future studies, but it would be difficult to incorporate such detail into a national-scale study.

The SOS anomalies and geographical gradients were analysed independently of landcover, and therefore they provided a more objective view of spatio-temporal SOS variation across the country. However, abrupt changes in the SOS dates occurred where the landcover and elevation pattern changed. This was particularly evident where the dominant landcover changed from pastures to peat bogs, which usually coincided with a change in elevation. The spatial anomalies showed that there were anomalously early seasons in 2003 in the south, and across large parts of the country in 2005, 2007 and 2008. There were late seasons country-wide in 2004 and 2006, while in 2009 there was a strong geographical trend to the anomaly. The island-wide positive anomalies in 2006 appeared to be related to a colder than average preceding winter and spring which was recorded at the three meteorological

stations. Although temperature variations could explain most of the anomalous variation in SOS, some local variability could not be explained by air temperature alone. Other physical factors related to climate (soil temperature, precipitation, the number of frosty nights), topography (elevation, slope, aspect) and land use (management regime, cultivated or protected area) undoubtedly play a role in determining SOS on a local scale. Furthermore some areas, e.g. upland areas, were not represented by the synoptic station measurements, and therefore SOS anomalies in these areas could not be related to air temperature changes. The location of the three stations had advantages and disadvantages. They are representative of areas within a 100km radius of the station, and are sited in areas with minimal topographic variation (Keane and Collins, 2004). However, spatial heterogeneity at the meso to micro scale inevitably creates uncertainty in the interpretation of SOS anomalies by air temperature, e.g. cold air drainage and frost pockets may generate steep phenological gradients over very small scales (15 days over 500 m) . Such microclimates potentially bias the SOS dates at coarser spatial resolutions (Fisher et al., 2006).

The pair-wise comparisons yielded significant SOS differences between certain landcover types in 2006. The groupings indicated the influence of land management on the SOS as managed and non-managed vegetation types were grouped separately. However, the grouping of coniferous forest and natural grasslands in a single group with green urban areas was surprising. This may be due to the difficulty in monitoring coniferous forest as they have very little annual variability in photosynthetic activity and small annual changes in needle turnover (Jönsson et al.,

2010). Nevertheless, the groupings provided a convenient method for analysis of SOS by landcover type. Inter-comparison of the shapes and slopes of the cumulative curves revealed that the SOS occurred at different times in different landcover types. Generally, within any one year, the SOS occurred in managed systems before natural vegetation. The main feature of the interannual trend was the stability of the SOS measure over the seven-year period although the median SOS varied more in groups A and B than in Group C. A possible explanation of this could be the absence of human influence in the group C landcover types. Generally, the interannual variation in SOS rarely exceeded one 10-day period within any landcover type, however, it varied by a maximum of two 10-day periods in the most variable landcover types. No temporal trend emerged in the 7-year time series, a challenging task to detect even in longer satellite time series of 25 years (White et al., 2009). The very different temporal SOS patterns exhibited in the Group C landcover types highlighted the potential for non-climatic factors to influence the SOS trend. For example, environments such as peat bogs are subject to very different hydrological regimes and soil types, and such physical differences would be expected to delay SOS compared to other landcover types across the island. Therefore, in the absence of management, natural vegetation would be expected to be a more sensitive indicator of climate variability.

Two different meteorological measures of growing season start dates in grasslands were compared to the SOS for pastures, and showed quite different results. The first method based on median grass growing dates predicted from a soil temperature threshold of 6°C by Connaughton (1973) was quite different to the 7-year mean SOS

estimates. A time difference of approximately 30 years elapsed between the datasets during which time change in climate may have impacted grass growth dates. Aside from the time difference, inconsistencies between SOS and meteorologically-derived grass growth dates, could be due to other factors, e.g., the use of a soil temperature threshold calculated at mean sea level. Notably, the grass growth dates derived from the 6ºC air-temperature threshold proved more consistent with the interannual variability in SOS estimates for pastures at point locations.

5.9 Conclusion

The spatial patterns in the SOS metric varied with landcover and elevation as evidenced by abrupt change in SOS dates when the elevation and landcover pattern changed. Anomalies in the SOS were mainly due to air temperature differences but could potentially be influenced by other physical factors, especially as the regional air temperature measurements were based on three point locations in the ROI. On an interannual basis, the SOS metric rarely varied by more than one 10-day period, indicating that the TIMESAT method was robust, but there were statistically significant differences in SOS per landcover type. The relevance of this finding lies in the ability to arrange landcover types into statistically significant different groups to explore inter-annual and intra-annual variation in SOS. The first group consisted of agricultural land cover types, forests and a transitional woodland class, the second group consisted of peat bogs, moors and heaths and sparse vegetation while the third group consisted of a mix of both natural and semi-natural vegetation types. There was a strong geographical bias to the distribution of landcover classes as certain vegetation types, e.g. peat bogs, were mostly located in upland areas, while pastures

were generally found throughout the country. The consistently earlier SOS in managed landcover classes is probably due to a combination of intensive management and favourable climate conditions. Therefore, the SOS appears to be both an indicator of phenological change as well as land use practices. Although qualitatively, the SOS appeared to show a strong relationship with elevation, quantitative analysis proved that the relationship is quite weak due to landocver variability and a small elevation range across the island. However, the mostly upland Group C landcover types did show a later SOS relative to the other groups, which is most likely due to more limiting growth conditions at higher altitudes. The absence of any vegetation management only confounds the impact of these limiting growth conditions on upland vegetation, but does introduce temporal stability in the interannual pattern not seen in the other managed or semi-managed landcover types. Therefore, the different landcover groups could potentially be used to separate the climatic from the non-climatic influences on vegetation SOS in future studies. The SOS in some pastures is as early as January, suggesting that vegetation is actively photosynthesising all year round in such areas. This was confirmed by the median grass growing dates predicted from meteorological variables. Quantifiable methods of estimating uncertainty in the SOS dates are required in determining the accuracy of the metric. Factors such as landcover mixtures at the 1.2 km spatial resolution of the MGVI data, and the spatial autocorrelation in the analysis of SOS by landcover type should be accounted for, and their impact on SOS determination quantified in future studies. Due to the short time-series of MGVI data available no temporal trends emerged in the SOS dates. However, with the replacement of the MERIS sensor by the Sentinel mission in 2013, there is considerable potential for extension

of the MGVI time series from 2003, and therefore better determination of temporal trends.

Chapter 6. Air temperature as a determinant of SOS

6.1 Background

The Intergovernmental Panel on Climate Change (IPCC) has recognised with very high confidence that the earlier timing of spring events and the poleward and upward movement of the range of certain plant and animal species is due to recent climate warming (IPCC, 2007). Meanwhile, European annual mean air temperatures have increased by 0.3-0.6°C since 1900 (European Environment Agency, 2011). Predictions based on global climate models suggest a milder climate across Ireland if the warming trend persists, with temperature expected to rise by 2°C by 2100 (Met Éireann, 2010). The response of SOS to interannual variation in regional air temperature was demonstrated by the temperature and SOS anomalies in the previous chapter (sections 5.3 and 5.7). In this chapter a correlation study using air temperature as a climate variable was carried out to quantify the association between such air temperature changes and variation in the SOS across the Republic of Ireland from 2003 to 2009. Air temperature was chosen as a suitable variable as there is a proven link between it and phenological events such as leaf unfolding and flowering (Estrella et al., 2007). Furthermore, daily temperature readings from Met Éireann synoptic stations were available for the seven year study period. A measure of accumulated thermal time, known as growing degree days (GDD), was also derived from the temperature data to determine whether there was an optimum degree day accumulation for SOS in each landcover type. In order to address this research task, five smaller sub-objectives have been outlined. These are followed by a brief review of previous seasonality-climate correlation studies using both ground-based and

satellite–derived measures of vegetation phenology. The air- temperature correlation and calculation of GDDs per landcover type form two separate chapter sections. An overall chapter conclusion will consider the merits of using the raw temperature data for seasonality-climate correlation studies, and whether the derived measures of GDDs is an appropriate indicator of SOS. The objectives of the temperature correlation and GDD analysis are outlined below.

- To determine the most appropriate method of correlation to examine the strength of association between the SOS and air temperature
- To verify whether winter or spring mean air temperature is a stronger correlate of the SOS
- To describe the spatial patterns in the monthly maximum correlation values
- To select an appropriate base temperature for the calculation of growing degree days from the daily air temperature data
- To estimate the optimal number of degree days per landcover type for SOS to occur and examine the extent of interannual variation in the estimates

6.2 The SOS and air temperature

Numerous studies have indicated that there are strong correlations between the start of the growing season and air temperature in Europe (Chmielewski and Rotzer, 2001), the Northern Hemisphere (Schwartz et al., 2006) and Ireland (Sweeney et al., 2008). In Irish phenological gardens, negative correlation between spring air temperatures (average monthly temperature from February to April) and the

beginning of the growing season was shown at all sites with the strongest correlation for *Populus canescens* at Valentia Island (r= -0.72, $\rho < 0.05$) (Sweeney et al., 2008). It has been estimated that with an increase of 1°C in the spring temperature, the beginning of the growing season (averaged across the four sites) for White/Downy birch (*Betula pubescens)*, Common beech (*Fagus sylvatica* 'Har') and Small-leaved lime (*Tilia cordata)* is expected to be 5, 6 and 8 days earlier respectively (Sweeney et al., 2008). Furthermore, an increase in average annual air temperature has been responsible for a longer growing season at all sites except Johnstown Castle (strongest correlation of 0.51 for *Fagus sylvatica 'Tri'* at Valentia Island, $\rho \leq 0.01$). Donnelly *et al.* (2006) concluded that if spring temperatures increased on average by 1ºC, the beginning of growing season would occur 6 days earlier in Ireland. However, while these correlation studies did not examine the direct impact of winter air temperatures on the beginning of growing season in Ireland, experimental studies show that the duration of the winter chilling period, which commences when winter temperatures fall below a threshold temperature and buds enter the dormant stage, is an important determinant of the timing of budburst in spring (Sweeney et al., 2008). As the chilling requirements differ depending on the tree species, the rate of budburst after the spring temperature rise is highly species-specific (Sweeney et al., 2008). Furthermore, models show that the onset of spring events will advance by up to six days per 1 °C increase in winter air temperature (Menzel and Fabian, 1999). Therefore, in theory, a +1 °C temperature rise in winter and spring could hasten spring onset by as much as 12 days.

The temperatures of the 3 months leading up to the mean date of 78 agricultural and horticultural phenological events in Germany from 1951 to 2004 was found to be

particularly important evidenced by 72 % of the correlations being strongly negative (Estrella et al., 2007). The correlation between air temperatures and leaf colouring and leaf fall in autumn is generally weaker than in spring events (Chmielewski and Rotzer, 2001). Experimental studies suggest that factors other than temperature, such as photoperiod (day length in terms of sunshine hours), increasing atmospheric CO_2 concentration and other climatic factors such as wind (causing leaf fall), may have a stronger influence than temperature on the timing of events at the end of the growing season (Sweeney et al., 2008). From research to date (as discussed in section 1.1.3), it can be concluded that average spring temperatures and the beginning of growing season show the strongest correlations.

Temperature change related to latitude and longitude is not the only factor in determining the SOS as altitude is also a major factor, as was discussed in section 5.5. The lapse rate of air temperature with elevation has the effect of delaying the beginning of the growing season at higher altitudes.For example, average spring greening in Europe from 1961 to 1998 moved annually at a rate of 44 km/day from south to north, at 200 km/day from west to east and at 32 m/day with increasing altitude (Rotzer and Chmielewski, 2001). In elevated terrain and at high latitudes spring growth is temperature-limited, and because of the high soil moisture content, not reliant on precipitation (Stöckli and Vidale, 2004). However, air temperature at high altitude is also determined by slope aspect. For example, exposure to the Mediterranean climate on southern and eastern facing Alpine slopes hastens spring onset compared to cooler northerly facing slopes (Stöckli and Vidale, 2004).

In addition to these findings from ground-based phenological observations, satellite-derived phenological metrics, correlated with climatic variables such as air temperature and precipitation, have also shown climate-phenology trends. Globally, large areas that exhibited greening trends based on 1982-1998 AVHRR NDVI did not correlate with either temperature or precipitation but, for northern high latitudes and western Europe, there was a statistically significant correlation between temperature and the greening trend (Xiao and Moody, 2005). Precipitation showed weak or no correlation in all but a few regions where greening had occurred. Stöckli and Vidale (2004) calculated and classified, according to their F-test confidence values, phenological metrics for the Ireland and U.K. from 1982 to 2001 using the AVHRR Pathfinder NDVI dataset. Spring growth was earlier by 1.88 days per year ($p<0.10$), autumn occurred later by 0.51 days per year ($p<0.01$) and length of season extended by 2.38 days per year ($p<0.01$). Almost all trends were negative for spring dates and positive for autumn dates meaning a lengthening of the growing season for most of continental Europe. In the same study, spring growth was negatively correlated with winter temperatures while there was no significant correlation with precipitation and only a slight correlation with the North Atlantic Oscillation (NAO) index. Early springs occurred in 1989 and 1990 as well as 1994, 1995 and 2000. A positive winter NAO index led to warmer spring temperatures in 1989/1990 and in 1994/1995 across the continent and was a probable cause of earlier spring greening in those years. The NAO index shifted to negative in the period 1982-1987 which coincided with cooler winter and spring temperatures in Europe and delayed spring greening.

In the Rocky mountains of North America, the onset of spring growth is delayed between 3.6 (±0.2) and 3.9 (±0.3) days for every 100 m increase in elevation, depending on whether the NDVI or an alternative VI corrected for snowmelt is used respectively (Hudson Dunn and de Beurs, 2011). This trend agreed with Hopkins' bioclimatic law of a 3.3 day delay in SOS for every 100 m increase in elevation (Hopkins, 1918 cited in Hudson Dunn and de Beurs, 2011). In summary, ground-based and satellite-derived phenological measures indicate that the timing of phenological events such as leaf unfolding and flowering is most responsive to air temperature. However, this spring greening trend is also complicated by the requirement for a winter chilling period below a threshold temperature which is a highly species-specific phenomenon. Other variables such as duration of photoperiod also influence budburst timing in spring. In contrast, autumnal events such as leaf colouring and leaf fall have shown no or only a weak association with changes in air temperature.

6.3 Climate data

Currently there are 108 climatological stations across the Republic of Ireland, 20 of which are also synoptic stations (pers comm., Delaney, 2011). Hourly temperature and precipitation readings are taken at the synoptic stations while they are recorded once-daily at the climatological stations (09:00 UTC). However, of the current station network, the highest station is 259m at the North Kerry Landfill, Tralee, Co. Kerry, while the lowest is 7m at Wexford Wildfowl reserve. However, only three of the stations (3% of the network) are above 200m. As the land area below 200m elevation is approximately 92% (GTOPO-30 DEM), the network is largely

representative of the elevational range of the country. Spatially the network is quite dispersed as the maximum distance between the stations is 411km from Falcarragh, Lough Altan, Co. Donegal to Sherkin Island, Co. Cork and the closest stations are approximately 0.5kms apart and both located at Roche's Point in Co. Cork. The mean distance between stations is 155km. In light of this spatial distribution, it was decided to use a gridded climate product for the study as it would be more representative of climate across the island and in upland areas than point measures alone.

Precipitation and temperature grids have been produced by Met Eireann for the Republic of Ireland during the period 1941-2009 for rainfall and 1961-2009 for maximum and minimum temperature. The method used to interpolate between station precipitation measurements and temperature measurements differs. The precipitation grid is based on residual kriging of normalised rainfall but is not suitable for temperature data due to extremes in their values. Therefore an Inverse Distance Weighting (IDW) method is used to interpolate daily temperature maxima and minima anomalies calculated from the station 1961-90 averages. The mean temperature is the average of the daily maxima and minima (S.Walsh, 2010,Pers. comm). A correction for altitude was applied to the gridded temperature values, using a lapse rate of air temperature with elevation of 6.5º C per km, as follows:

1. The '61-'90 temperatures were initially calculated at mean sea level while linear regression was applied against combinations of easting, northing, coastal exposure and distance from the sea

2. The residuals (differences between the actual station value and the estimated station value) were interpolated onto the grid and added back to the trend terms in the regression
3. The grid points were adjusted by 0.65º C per km to give the final 61-90 grid
4. For daily temperature values, anomalies were calculated from the station 61-90 averages and, following regression, residuals of these anomalies were interpolated and then added to the 1961-1990 grids (already corrected for temperature variation with height).

The method assumes a standard variation of temperature with height which is not always the case however. Although the interpolations for both climate measures extended into Northern Ireland, predicted values there were considered unreliable as there was no input data available. The UK Meteorological Office (UKMO) provides daily and monthly temperature grids at 5km spatial resolution (only the 30-year averages are at 1km) and use the British National Grid projection as opposed to the Irish National Grid for the Met Éireann datasets. Moreover, these data were only freely available up until 2006 and a handling fee is payable for the more recent years. Owing to these limitations of the UK datasets, Northern Ireland was omitted from the climate correlation study. Thus, although daily minimum, maximum and mean temperature grids covering the 2003-2009 periods were provided by Met Éireann at 1 km spatial resolution for the whole island, only the ROI data were used. The daily data were aggregated into monthly files and provided by Met Éireann in text format (ASCII).

6.4 Statistical techniques

The null hypothesis tested was that variability in the SOS is independent of air temperature. The alternative hypothesis was that variability in the SOS is associated with changes in air temperature. Correlation and regression are standard tests of the validity of the null hypothesis of which there are many variations depending on the type of data being examined. Correlation tests indicate the strength of the relationship between two variables with a single value but do not indicate the effect of changes in one variable on the response of the other. For this, regression is a more appropriate modelling tool to describe the direction and proportionality of a relationship between two variables. The relationship described by such a model can then be used to predict the response in one (dependent) variable from changes in another (independent) variable.

6.4.1 Correlation methods

The correlation technique is a test of the measure of association between two variables. The magnitude of the test statistic produced by a correlation test is indicative of the degree to which an independent variable determines variation in the response variable. However, it cannot be assumed to be a cause of the response variable, i.e. correlation is not a measure of causal relationships. Evidence of causation must be obtained independently of the statistical test (Helsel and Hirsch, 2002).

6.4.1.1 Pearson product-moment correlation

The standard Pearson correlation r value can range from -1 (perfect negative correlation) to 0 (no correlation) to 1 (perfect positive correlation). However there are limitations to the use of this parametric coefficient since it assumes that both

variables are measured on a continuous scale and both are normally distributed (Dytham, 2003). Neither condition can be assumed in this study since the SOS is measured on an ordinal scale in 10-day intervals and the variables are not normally distributed.

6.4.1.2 Spearman rank-order correlation

This is the non-parametric equivalent to the Pearson coefficient. The test statistic, rho (ρ), is measured on the same scale as that of the Pearson test except that it is applied to ranked observations before calculating the test statistic. Ranking of the data automatically produces a normally distributed dataset. It can also be used with non-continuously distributed data. The Spearman method is also a more conservative measure of association than the Pearson coefficient (Dytham, 2003) and is less sensitive to outliers (Helsel and Hirsch, 2002). However, a weakness of the test lies in the lack of clear interpretation of Spearman's rho (Dalgaard, 2008).

6.4.1.3 Statistical significance of correlation

The probability of the null hypothesis being true is measured by the significance level (p-value). Low p-values allow the null hypothesis to be rejected and the alternative hypothesis to be accepted. In biology, a p-value of 0.05 is accepted as the critical level of rejection of the null hypothesis (Dytham, 2003). However, a critical p-value for the rejection of the null hypothesis has not been established for studies using remotely-sensed measures such as SOS. Generally, large sample sizes are used when working with remotely sensed imagery, e.g. n>30,000 which can lead to a large number of false positive findings (Brown et al., 2010). This can lead to error as the null hypothesis is falsely rejected, e.g. if the p-value is equal to 0.01, the null hypothesis will be true for every 1 in every 100 correlations. False positive errors

accumulate in large sample sizes and become known as the family-wise error rate. Although techniques such as the Bonferroni adjustment correct for the family-wise error rate in multiple tests, they are considered too stringent in very large sample sizes as the alternative hypothesis would only be accepted if the p-value < 0.05/n (Brown et al., 2010). For example, if n=10,000 or more as is commonly the case in remotely-sensed imagery, the null hypothesis could only be rejected for a pixel if p<.000005. As there is no consensus on an appropriate significance level or a method for controlling the family-wise error rate, no corrections have been applied in the multiple correlation tests carried out here.

6.4.2 Regression models

Regression is a test for the prediction of one variable from another. The output is a p-value and r^2 value that is very similar to that produced by the Pearson correlation test. The p-value from a standard linear regression indicates the probability that the best-fit slope of the relationship between the two variables is zero, i.e. that the null hypothesis is true and that there is no measurable relationship between them. However, there is another way to test the null hypothesis in regression analysis if the value of y is zero when x is zero which is measured by the intercept. The value of the intercept is where the best-fit line passes through the origin. Linear regression analysis has an advantage over the Pearson test in that both variables are not required to be normally distributed. However, the following assumptions need to be satisfied for a legitimate regression.

Regression assumes that:

- The ‘x’ (independent) variables are measured without error
- The variation in ‘y’ (dependent) is the same for any values of ‘x’

- ‘y’ values should be normally distributed at any value of ‘x’
- For linear regression, the relationship between x and y can be described by a straight line between all values
- One strong significant relationship exists between ‘x’ and ‘y’

A preliminary review of the above conditions would suggest the SOS-air temperature relationship is unlikely to be described by a linear fit due to the complexity of soil- vegetation- atmosphere interactions (Stöckli and Vidale, 2004). Theoretical studies have also shown that the response of vegetation to changes in climate is non-linear (Bonan, 2002 cited in Brown et al., 2010). The first condition for regression cannot be satisfied since there is error produced by the interpolation of temperature measurements which is summarised across all stations for each year in table 6.1. The method used for estimating error across the interpolated temperature grids is known as leave one out cross validation (loocv) (pers comm, Walsh, 2011). The method consists of omitting each station one by one and calculating its value from the remaining stations, then comparing it to the actual station value and calculating the resulting error. The error statistics in table 6.1 were calculated on a daily basis for T_{max} and T_{min} and are averaged over the year. The IDW interpolation method used in the daily grids does not give any estimation of errors per grid cell. For the second and third conditions, the standard tests of normality would need to be applied to the temperature values to ensure that the distribution is constant with each 10-day interval of SOS.

Table 6. 1: Error statistics for T_{max} and T_{min}, calculated on a daily basis and averaged over the year

Year	T_{max} RMSE (°C)	T_{min} RMSE (°C)
2002	0.79	1.04
2003	0.8	1.08
2004	0.8	1.04
2005	0.78	1
2006	0.79	1.04
2007	0.79	1.06
2008	0.78	1.02
2009	0.81	1.03
Mean	0.79	1.04

Although simple linear regression methods do not capture the SOS-air temperature relationship for the reasons described, a subset of Generalised Linear Models (GLM) known as ordinal regression models potentially offer a better approach for semi-quantative data (Guisan and Harrell, 2000). An ordinal scale is considered to be an ordering of measurements, with only relative, instead of quantitative differences between values (Guisan and Harrell, 2000). Therefore, SOS can be defined by an ordinal scale from earliest to latest in 10-day intervals Ordinal regression permits orders of the dependent variable (SOS), to be predicted from values of the independent variable (temperature), once the 'best-fit' line has been created (Torra et al., 2006). It has been suggested that remotely-sensed measures, e.g. NDVI time series, are inappropriate for any regression analysis as they have been found to typically violate assumptions underpinning regression. Specifically, ordinate values, i.e. time composites of NDVI mapped on the y axis, are not mutually independent because there is usually high positive autocorrelation between consecutive observations (de Beurs and Henebry, 2005). Therefore, alternatives to trend analysis by regression, such as the seasonal Mann-Kendall trend test have been proposed (de Beurs and Henebry, 2010, 2005). The Mann-Kendall trend is a non-parametric test based on ranks- therefore, resistant to the most common problems affecting standard

trend tests such as non-normality, missing observations, seasonality and temporal autocorrelation (Hirsch and Slack, 1984 cited in de Beurs and Henebry, 2005). It was used to test for differences and trends between the average normalized difference vegetation index (NDVI) and average growing degree-days (GDD) of 1985–1988 and 1995–1999 in high latitude ecoregions (de Beurs and Henebry, 2005) and in detecting greening trends in a 8-year NDVI time series of the northern polar regions (de Beurs and Henebry, 2010). Since trend analysis did not form part of the objectives of this preliminary climate study, neither the Mann-Kendall test nor a regression model were considered for further use.

6.4.3 Preparation and use of the climate data

The monthly temperature text files were imported to MATLAB and the daily temperature values extracted which were then gridded and resampled to the 1.2 km spatial resolution of the MGVI grid using nearest neighbour (NN) resampling since it does not change any of the values of the original grid cells but duplicates values from the nearest cells instead (Wade and Sommer, 2006). The daily mean temperature grids were stacked and the mean monthly and seasonal values calculated per grid cell. The spring mean temperature was derived from the average monthly temperature from February to April inclusive as has been done in previous ground-based Irish studies (Donnelly et al., 2004). Therefore, the winter temperatures were taken as the average of the previous three months (November-January inclusive). The mean temperature and SOS grids were both masked with a land mask of NI provided by Met Éireann.

6.4.4 Initial correlation results

The correlation study aimed to test the null hypothesis (H_0) that there is no correlation between the SOS metric and mean air temperature and the alternative hypothesis (H_1) that the SOS metric and air temperature are correlated. The correlation was initially done spatially, i.e. across the grid of valid values for any monthly or seasonal time period. In the case of SOS, the number of land pixels for which a valid season was calculated varied per year as seasons were not modelled where there were too many missing data points due to cloud cover. Therefore, the valid sample size (n) varied from 45089 to 47141grid cell values. The SOS and the associated monthly temperature grids were imported to IDL. The valid SOS values were extracted first, i.e. zero values removed. The corresponding grid cells in the temperature grids were then located and their values extracted to ensure that for every valid SOS value, there was a valid temperature value. Spearman's rho (rank order correlation coefficient) and the p-value were then calculated treating temperature as *X* (the independent variable) and SOS as *Y* (the dependent variable). This process was repeated for each month (November-April) and season (winter and spring) within each year for the seven years. In table 6.2 the Spearman's rho is presented for each of the SOS –temperature correlations.

Table 6.2: Spearman's rho (ρ) for the SOS and monthly and seasonal mean air temperature correlations, all correlations in bold are significant (p<0.05)

Year	November	December	January	Winter	February	March	April	Spring
2002	**0.019**	**-0.020**						
2003	**0.025**	-0.005	**0.016**	**0.05**	**-0.024**	**-0.039**	**0.029**	**-0.014**
2004	**0.107**	**0.127**	**0.039**	**0.039**	**0.029**	**-0.011**	-0.004	0.006
2005	**0.133**	**0.146**	**0.084**	**0.108**	**0.119**	**0.022**	**0.060**	**0.074**
2006	**0.088**	**0.040**	**0.134**	**0.139**	**0.126**	**0.046**	**-0.012**	**0.063**
2007	**0.131**	**0.048**	**0.051**	**0.061**	**0.037**	**0.058**	**-0.088**	**0.015**
2008	**0.158**	**0.170**	**0.017**	**0.066**	**0.072**	**0.043**	**0.027**	**0.049**
2009			**0.139**	**0.158**	**0.084**	**0.067**	-0.008	**0.053**

When there is no correlation between two variables, $\rho = 0$, when Y tends to increase when X increases, $\rho > 0$, but when Y tends to decrease when X increases, $\rho < 0$. Overall, the low rho values in table 6.1 show that when the values across the grid are taken together, the correlation between the mean air temperature in any given month or season and SOS is very weak. However, nearly all the correlations are significant ($p<0.05$) due to the very large sample size. Therefore, in addition to the very low amount of variance in the SOS explained by air temperature, the likelihood of false positive findings is high, i.e. the false rejection of the null hypothesis. This creates uncertainty in the interpretation of the correlation results. Nevertheless, the monthly maximum correlation value is 0.17 in December 2008, while the maximum seasonal correlation is 0.074 in spring 2005 and 0.158 in winter 2008/2009. In figure 6.1, the scatter plot of the December 2008 monthly mean temperature values with SOS 2009 is shown since these values showed the strongest correlation. The plot demonstrates the scattered pattern produced from a mixture of ordinal (SOS) and continuous (temperature) data and also the distribution of their values with histograms. The temperature values do not appear to be normally distributed being heavily skewed however the SOS values are normally distributed.

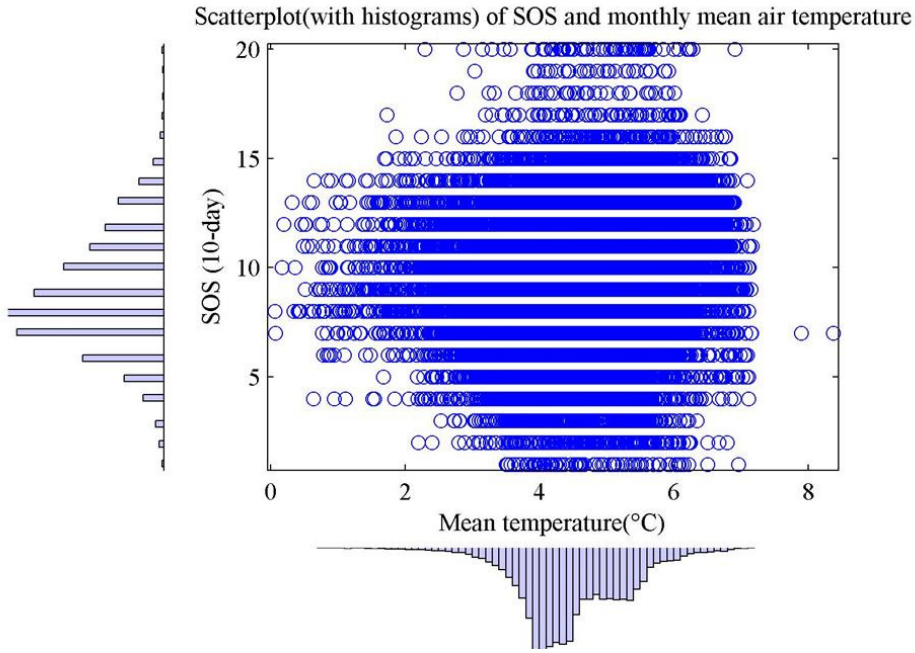

Figure 6.1: The scatter plot of SOS in 2009 and mean December temperature (2008). The marginal histograms show the distribution of values in the sample. The mixture of ordinal and continuous data creates a striped pattern in the scatter plot.

The fact that the strongest SOS-temperature correlations are from the winter of 2008/2009 is probably related to the strongly negative temperature anomalies in winter of that year, indicated by the temperature values at the three meteorological stations in chapter 5, section 5.7. Generally, the correlation values tend to be slightly stronger for winter than spring and in the individual winter months than in the spring months (table 6.1). Most of the correlations are positive. This shows that as air temperature increases, SOS occurs later. For winter months, this implies that warmer winter temperatures correspond to a delay in SOS, possibly due to a failure to satisfy the winter chilling requirements. For spring months, the interpretation of a positive relationship is less clear as warmer spring temperatures would be expected to hasten spring onset. The few negative correlations that exist are generally in the spring months, especially in April. Overall these results suggest that the complexity of vegetation-atmosphere interaction cannot be explained by air temperature alone.

Furthermore, it is likely that the combination of all landcover types and variation due to elevation in the gridded data compete to weaken the SOS-air temperature trend. There is also a certain degree of spatial dependency in the X and Y variables inherited from the treatment of the data, i.e. transformed from grids to single column variables and correlated against each other. As the SOS variable is a measure of time and the grid cells dependent on location, the correlation results may contain both a temporal and spatial component.

6.4.5 Temporal trend correlation

The main objective of this section of the correlation study was to separate the spatial from the temporal components of the SOS-air temperature relationship by correlating seven pairs of temperature and SOS values in each grid cell independently. Therefore, Spearman's correlation was applied per grid cell over the seven year study period, i.e. n=7 compared to n≈45,000 in the previous analysis. As the SOS is a measure of time, this can be considered as a test for a temporal trend (Helsel and Hirsch, 2002), in contrast to the previous analysis in which there was a spatial dependency. The analysis included November to April and seasonal mean temperature values over seven years. In order to reduce the possibility of missing value affecting the correlation results, only valid pairs of values, i.e. those without missing values, were used in the correlation. In order to summarise the correlation results, the maximum rank correlations between SOS and monthly air temperature were mapped per pixel across the ROI in figure 6.2. (a). The monthly and seasonal timing and the significance level of the maximum correlations are shown in figure 6.2 (b)-(d).

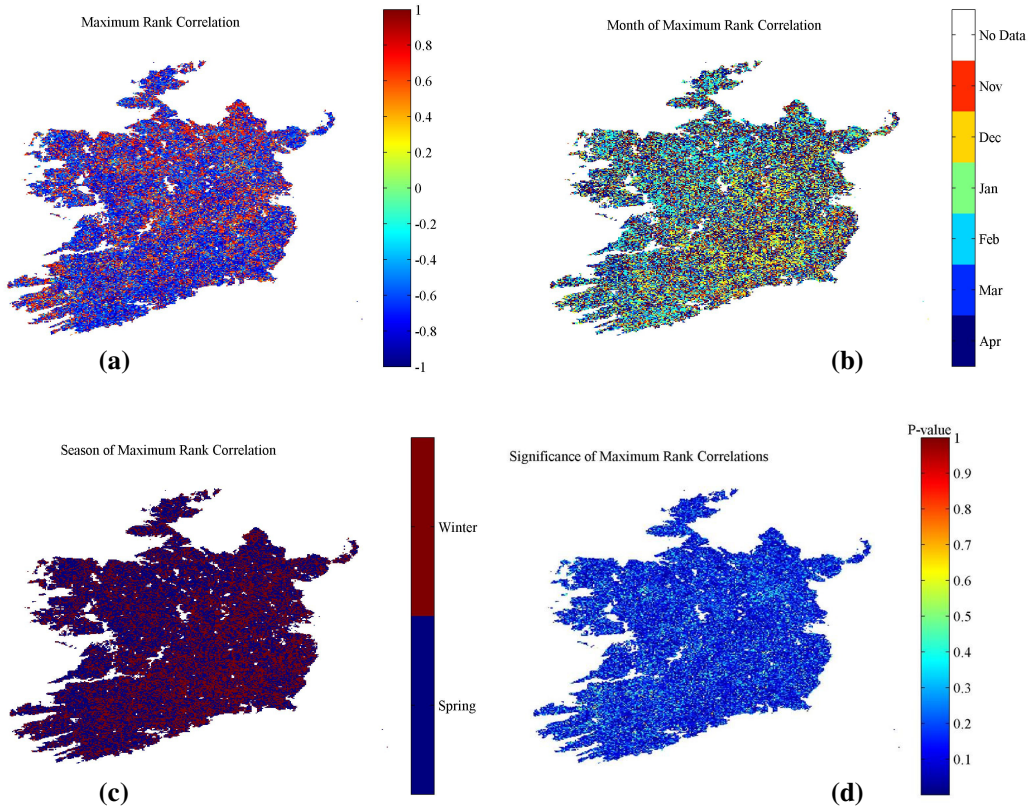

Figure 6.2: (a) Maximum rank correlation between SOS and mean monthly air temperature. (b) Timing of the maximum rank correlation (month), (c) Timing of the maximum rank correlation (season), (d) *p*-value of the maximum rank correlation

There are contrasting patterns in the maximum rank correlations in figure 6.2(a) as there are negative correlations in the south, southeast and parts of the west and northwest and positive correlations in the southwest, midlands and along the Northern Ireland border. The correlation timing per month (fig 6.2 (b)) shows that the November, December and January correlates are strongest in the south, east and southeast, while the February, March and April correlates are strongest in the northwest, west and southwest. The seasonal timing of these correlations (fig 6.2 (c)) was derived from an aggregation of the monthly correlates in figure 6.2 (b). However, from figure 6.2(d) less than half the correlations are significant ($p<0.1$). For example, only 4.1 % are extremely significant ($p<0.01$), 21.95% are highly significant ($p<0.05$), 41.34% are significant ($p<0.1$) and 58.66% are not significant

(p≥0.1), i.e. the null hypothesis is true for over half the correlations. The spatial distribution of the significant and insignificant correlations is shown in figure 6.3 (a)-(d).

Figure 6.3 (a)-(d): The spatial distribution of the (a) extremely significant (b) highly significant (c) significant and (d) non-significant maximum rank correlations

The spatial patterns illustrated in figure 6.3 (a)-(d) would suggest that there is no geographical trend in the significance of the maximum rank correlation values and no relation to landcover type. In order to exclude the non-significant correlations from further analysis, only the significant correlates (p<0.1) were used. Of the significant maximum rank correlations, 54.5% correlated best with spring temperature while 45.5% correlated with winter temperatures. The significant winter and spring correlates were extracted from the maximum correlation grid and are shown in figure 6.4 (a)-(b). Of the winter correlates in fig 6.4 (a), 27% of them are positive while 73% are negative. Similarly, of the spring correlates, 36.3% of them

are positive while 63.7% are negative. These results suggest that for approximately two thirds of the pixels, as winter and spring mean air temperature increases, SOS becomes earlier. In the remaining one third, however, an increase in mean air temperature results in a delay in SOS. There is also a very clear geographical trend to the correlates as most of the negative winter correlates are in the southeast half of the country and the negative spring correlates in the northwest half including small areas of the southwest and south.

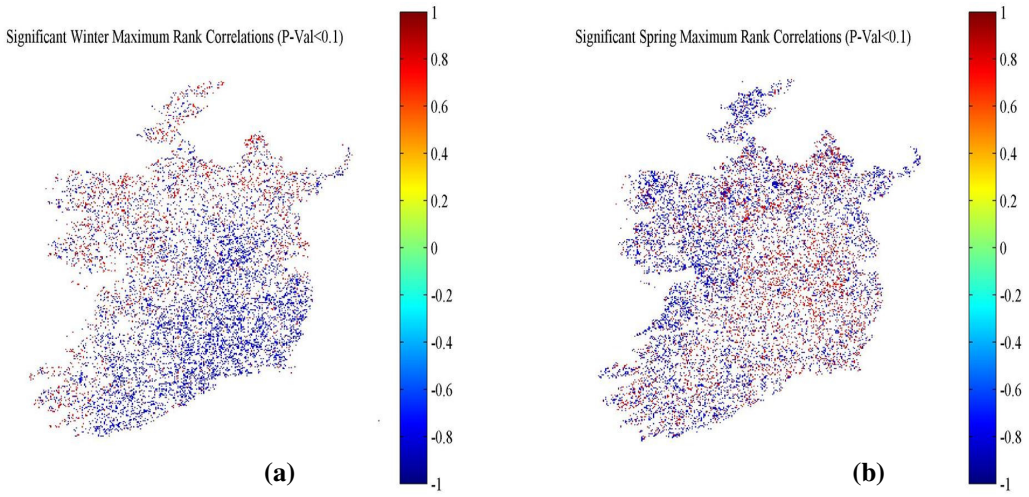

Figure 6.4 (a) The significant winter maximum rank correlates (b) significant spring maximum rank correlates

The inverse is true for the positive correlates, i.e. while the SOS in south eastern areas correlate negatively with winter air temperature, it is positively correlated with spring temperature and vice versa for the Northwest. Therefore in the southeast, characterised by a more continental climate, , a rise in winter temperature was associated with an earlier SOS date while a rise in spring temperature will delay the SOS date. In contrast, in the Northwest and some parts of the south and southwest, where the climate is more maritime Atlantic, increasing winter temperature will delay the SOS while increasing spring temperature will advance the SOS. These

tendencies would appear be a factor of general climate patterns in Ireland but also due to differences in land use between these regions. For example, the eastern and south eastern areas are largely used for arable cropping while the = vegetation in the west and northwest is generally unmanaged peat bogs and sparsely vegetated areas with some mixed agriculture.

6.5 The North Atlantic Oscillation (NAO) Index

The NAO index measures the differences in atmospheric pressure between the North Atlantic regions under the influence of the sub-polar Greenland low pressure system and the sub-tropical Azores High. These pressure gradients determine the path of mid-latitude weather systems hence general weather patterns over Northern Europe (Julien and Sobrino, 2009). Strong positive phases of the NAO tend to be associated with above-normal temperatures across Northern Europe (Menzel, 2003) but also below-normal temperatures across Southern England (Stöckli and Vidale, 2004). Therefore a negative index indicates the opposite patterns of temperature anomalies. Spring phenology across Europe has been shown to correlate particularly well with anomalies in winter temperature and the winter North Atlantic Oscillation (NAO) index (December, January, February and March) from 1981 to 2001 (Stöckli and Vidale, 2004).

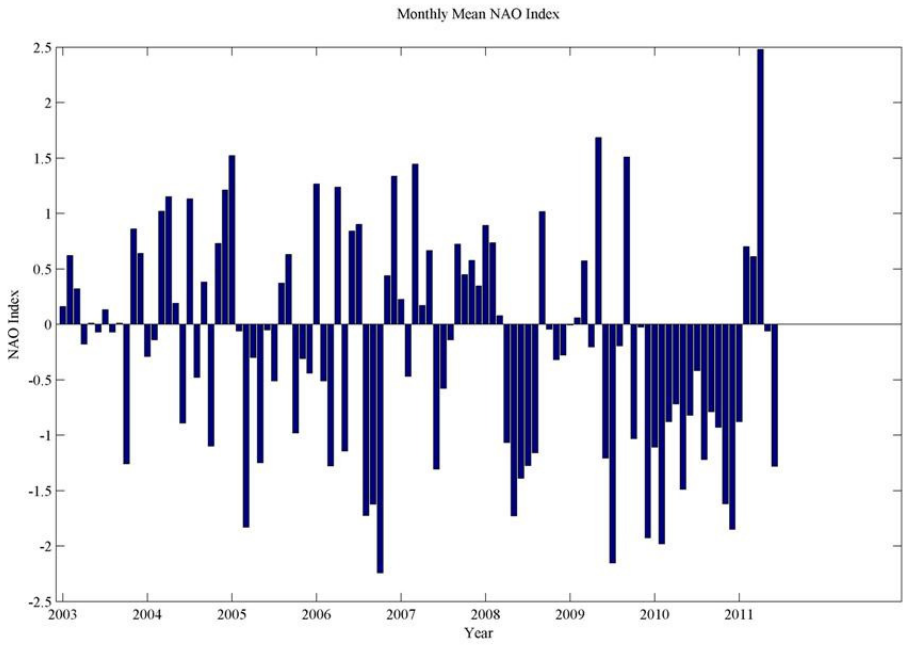

Figure 6.5: Monthly mean NAO index from 2003 to 2011

The monthly mean NAO index, from 2003 to 2011, obtained from the U.S. National Weather Service Climate Prediction Centre (Climate Prediction Center Internet Team, 2011), is shown in figure 6.5. The NAO anomalies can be used to interpret the interannual variability in SOS as shown by the SOS anomalies in section 5.3. There were positive NAO anomalies in 2003, 2004, and 2007 while the 2008 and 2009 anomalies are mostly negative. Since 2009, a persistent and strong negative NAO index has resulted in severely cold winters across Northern Europe and very wet winters in southern Europe (Andrade et al., 2011). In terms of SOS, the positive NAO anomalies in the winter of 2006/2007 appear to have caused an early SOS country wide in 2007. Conversely; a negative NAO in the winter of 2005/2006 caused an island-wide delay of SOS in 2006. However, there was more local scale variability in the SOS anomalies in other years, which cannot be explained by the NAO anomalies alone. For example, in the winter of 2003/2004, the index switched from weakly negative to strongly positive but the SOS was later across most of the country except in the southwest where it was earlier. The competing effects of local

scale variability due to landcover, elevation and weather patterns and large scale climate systems such as the NAO undoubtedly influence the SOS anomalies.

6.6 The SOS and Accumulated Growing Degree Days (AGDD)

Temperature control on vegetation growth is additive so that the rate of vegetation canopy development can be related to accumulated temperature (Keane and Collins, 2004). Accumulated temperature is usually measured in degree days above a threshold temperature by calculating the number of Accumulated Growing Degree Days (AGDD), i.e. the number of degree days above a base temperature from a point in time. The number of AGDDs normally exhibits a linear relationship between the number of emerged leaves and accumulated air temperature, e.g. between winter wheat and AGDD over 0 ºC (Keane and Collins, 2004). A critical number of AGDDs can also be used as a meteorological measure of vegetation SOS. For example, in temperature-limited polar phenoregions, 100 ºC AGDD appears to be a consistent indicator for the onset of the growing season (de Beurs and Henebry, 2010). These authors used a base temperature of 0°C as it is an accepted threshold for high latitude crop growth.

Growing degree days are used to measure the amount of heat units accumulated by plants in a given season and have been used as a predictor of phenological stages (Masin et al., 2005). The heating requirements for the initiation of vegetative development in spring are species-specific therefore different base temperatures must be used when working with multiple vegetation types. However, base temperatures of 5 ºC or 6 ºC are frequently used for agro-meteorological purposes in

Ireland (Keane and Collins, 2004) , e.g. 6 ºC was used as a base temperature to determine the feasibility of growing tillage crops in Co. Westmeath (Finch, 1977). Further afield, the potential of different grass species as fodder plants in Pakistan was examined by calculating their growth development using a base temperature of 6 ºC (Akmal et al., 2011). Base temperature is also an important consideration for phenology modelling studies. In simulating budburst in several tree species in southern Germany, base temperatures of 0ºC and 5 ºC were used (Rotzer et al., 2004) but these base temperatures may not be appropriate for other regions or other tree species.

For meteorological purposes, base temperatures of 15.0, 15.5, 17.0, 18.0 and 18.5 ° C are used (Met Éireann, 2011a) which is related to the calculation of heating degree days for home heating purposes, typically a base temperature of 15.5° C is used (Day, 2006). The geographical variation for degree-day thresholds of 0 ºC, 5 ºC and 6 ºC has been mapped across Ireland for a time period from 1961 to 1990 in order to understand the likely impact of climate change on the distribution of arable cropping areas. The methodology allowed degree days to be accurately predicted for unmeasured locations using location parameters to account for distance from the nearest meteorological station (Fealy and Fealy, 2008). While the thresholds used were not specific to any plant species they were indicative of the likely spatial variation in degree days due to location and elevation (Keane and Collins, 2004).

In Ireland, a soil temperature threshold of 6 ºC has been established for grass growth which is equivalent to an air temperature threshold of 5.6 ºC because of a tendency

for soil temperature to be slightly higher than air temperature at the beginning of the growing season (Keane and Collins, 2004). However, grass growth models do not use the degree day concept but rather a threshold (5 continuous days over 5 ºC) to determine the start of the growing season (pers comm, Green, 2011).

6.6.1 Calculating growing degree days

For this study, a base air temperature of 6 ºC was used as it is appropriate for grass growth which is the predominant landcover type in Ireland. The method for calculating Degree Days has been taken from the Meteorological Office standard also known as the 'McVicker' or the 'British Gas' formulae as they have been used to calculate home heating requirements as well as heat units for crop growth (Day, 2006). There are four scenarios considered to calculate daily degree days (DD) which require daily minimum and maximum air temperatures (Met Éireann, 2011a):

Case 1

If the minimum air temperature (Tmin) is above the base temperature (Tbase).

$$DD = mT - T_{base} \text{ where } mT = \frac{(T_{\max} + T_{\min})}{2}$$

Case 2

If the maximum air temperature (Tmax) is below the base temperature.

$$DD = \frac{(T_{\max} - T_{base})}{2} - \frac{(T_{base} - T_{\min})}{4}$$

Case 3

If the maximum air temperature is above and the daily minimum air temperature is below the base temperature but the mean temperature (mT) is greater than the base temperature.

$$DD = \frac{(T_{\max} - T_{base})}{4}$$

Case 4

If the maximum air temperature is above and the minimum air temperature is below the base temperature but the mean temperature (mT) is less than the base temperature.

$DD = 0$

The accumulated Growing Degree Days were calculated by simple summation of the daily DDs above 6°C commencing each 1 January until the estimated SOS date had occurred for each of the seven years. Negative GDDs, i.e. case 4, were treated as if there were zero daily degree days. Once the AGDDs were calculated across the ROI grid for each year of the time series, the CORINE landcover mask was used to extract summary AGDD statistics on the five landcover classes with the highest area coverage, i.e. pastures, peat bogs, arable land, agriculture with significant areas of natural vegetation and transitional woodland shrub. The AGDD grids from 2003 to 2009 are shown in figure 6.6 where the spatial patterns in GDDs are repeated in each year of the seven year period. The highest number of AGDDs is in the West and Southwest and Midlands with fewer degree days accumulated in the Midlands and East. The number of accumulated degree days is the lowest over mountainous areas regardless of location. These are also generally areas of peat bogs and sparse vegetation.

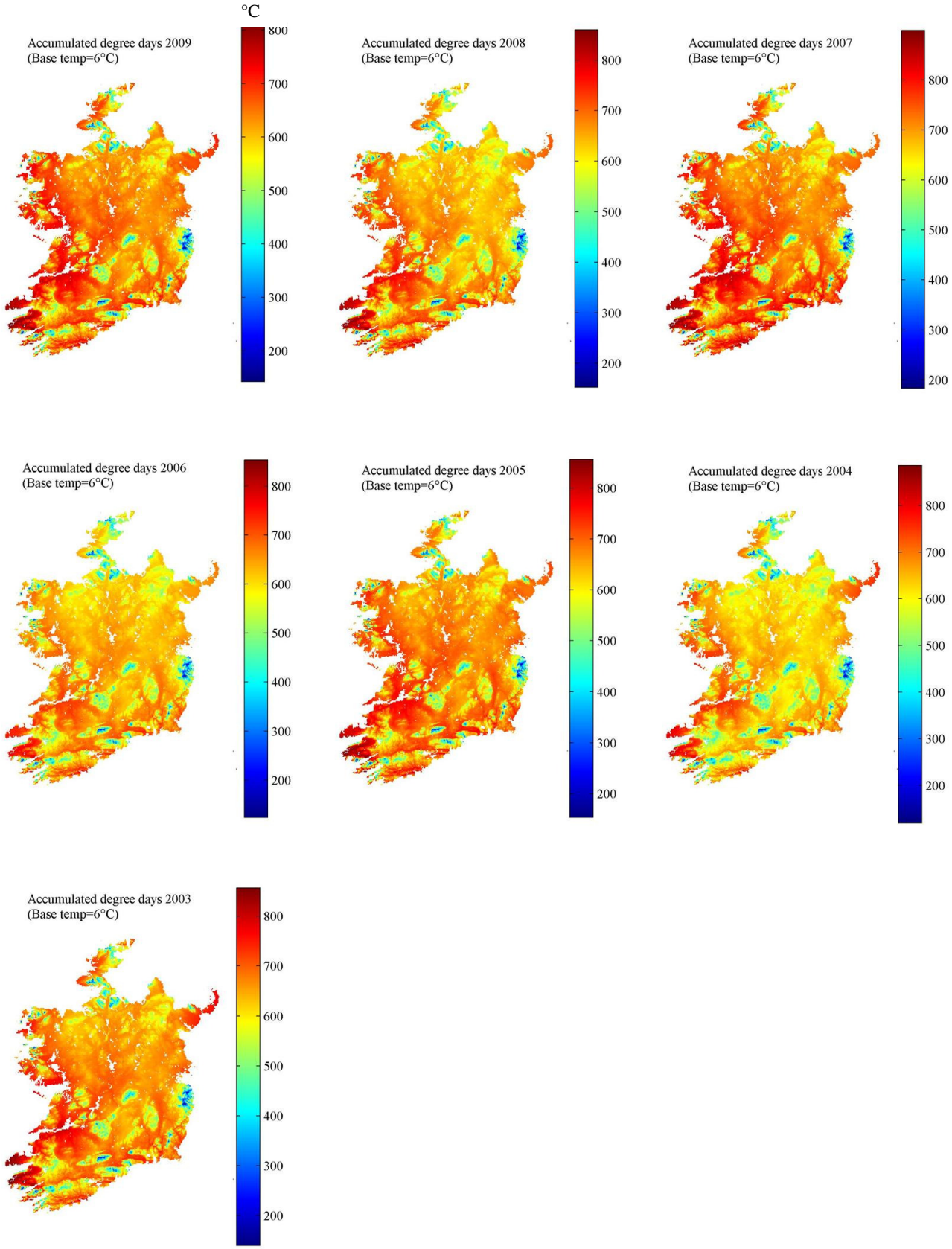

Figure 6.6: The 2003-2009 annual grids of accumulated degree days from January 1st until day of year prior to SOS, calculated from daily minimum and maximum temperature data

6.6.2 Statistical treatment of growing degree days per landcover type

In order to determine the appropriate statistical treatment of the data, i.e. parametric or non-parametric methods, the frequency distributions of AGDDs per landcover class were examined. The frequency distributions and summary statistics; median, skewness and kurtosis, for the five most abundant landcover classes are shown for 2009 in figure 6.7. Skewness is a measure of the distribution symmetry while kurtosis is measure of whether the data are peaked or flat relative to a normal distribution (NIST/SEMATECH, 2011). For example, the kurtosis for a standard normal distribution is three but distributions that are more outlier-prone than the normal distribution have kurtosis greater than 3 while distributions that are less outlier-prone have kurtosis less than 3 (Mathworks, 2009). Similarly, the skewness for a normal distribution is zero. Negative values for the skewness show that data are skewed left and positive values indicate that data are skewed right (NIST/SEMATECH, 2011). The median has been used as a measure of centrality since the GDD distributions cannot be assumed to be normal. In figure 6.7, the kurtosis is greater than 3 indicating outlier-prone distributions with distinct peaks. They are all negatively skewed. Therefore, they do not exhibit the characteristics of normally distributed data and will be treated with non-parametric statistics.

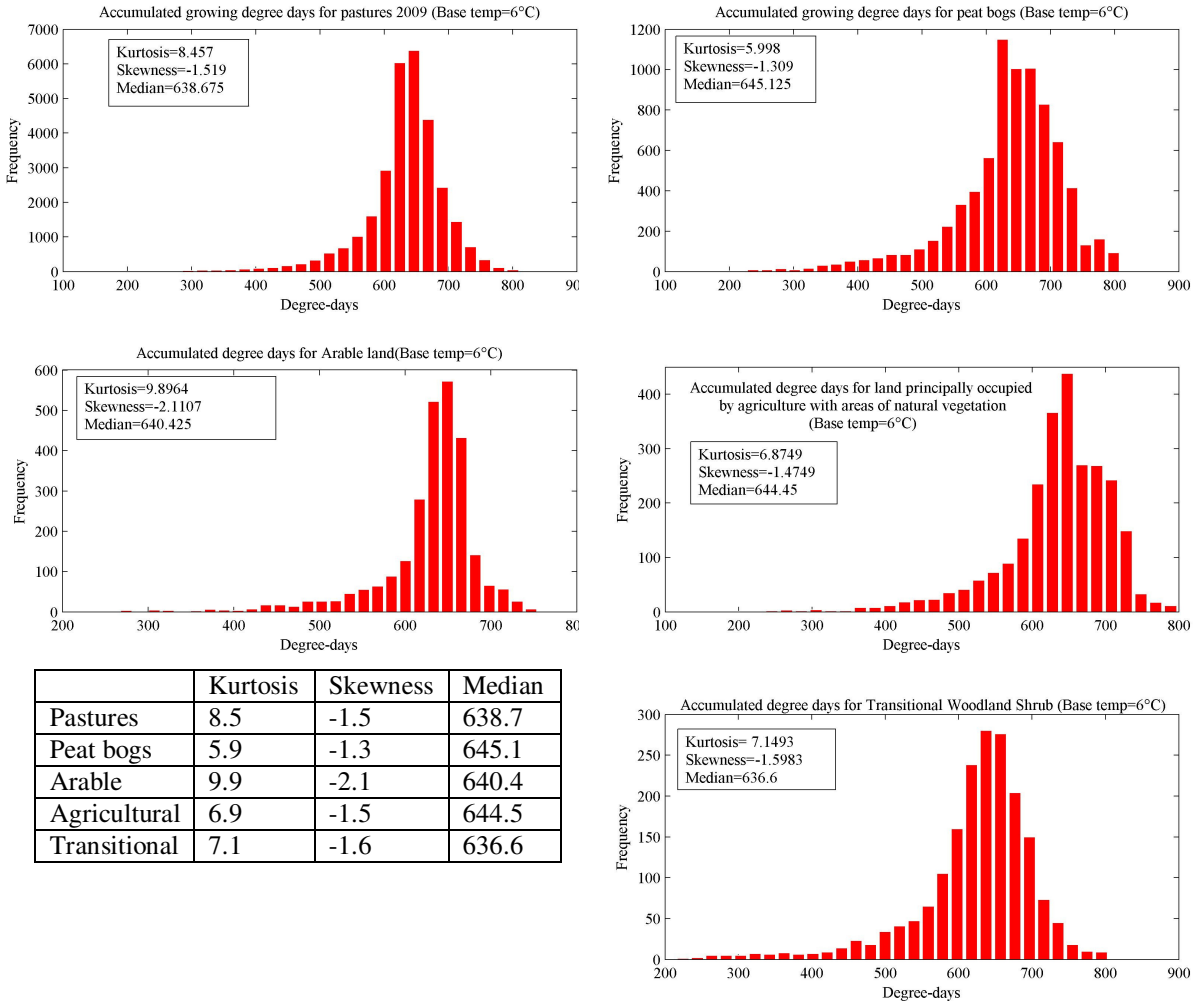

	Kurtosis	Skewness	Median
Pastures	8.5	-1.5	638.7
Peat bogs	5.9	-1.3	645.1
Arable	9.9	-2.1	640.4
Agricultural	6.9	-1.5	644.5
Transitional	7.1	-1.6	636.6

Figure 6.7: Frequency distributions and summary statistics for AGGDs in 2009 for the five most abundant landcover classes

6.6.3 Variation in growing degree days per landcover type

The median number of AGDDs for all seven years per landcover type is shown in table 6.3. The 7 year median AGDD values are also shown as well as the inter quartile range (IQR) per landcover class as an indicator of the spread of the annual values around the 7-year median.

Table 6.3: The median AGDD per landcover type from 2003 to 2009, the 7-year median is included as a summary measure and the inter quartile range (IQR) is included to indicate the extent of variance within the seven year record

AGDD (°C)	Pastures	Peat Bogs	Arable	Ag Land[5]	Trans[6]
2003	662.55	662.45	668.45	660.08	656.60
2004	633.40	635.18	643.05	633.33	627.83
2005	672.70	670.13	679.03	670.95	666.20
2006	631.05	624.28	640.45	624.83	622.93
2007	719.73	723.03	725.90	720.75	717.45
2008	648.93	655.88	653.00	652.45	646.38
2009	638.68	645.13	640.43	644.45	636.60
7 yr median	648.93	655.88	653.00	652.45	646.38
IQR	35.44	30.54	35.28	32.13	33.78

The 7 year median AGDD values show that peat bogs have the highest GDD requirement of all the landcover types and that transitional woodland shrub has the lowest. The IQR is the lowest in peat bogs (30.54°C) and highest in pastures (35.44°C) but these values are greater than the difference between the median values per landcover class. This indicates that it is difficult to distinguish the landcover types based on annual AGDD values. The size of the IQR per landcover class would also indicate that there is considerable variability in the number of AGDDs from year to year. Therefore an exact estimate of GDDs for SOS per landcover type is not possible without some uncertainty. In order to explore the interannual variation in these rankings, the landcover classes have been ranked in terms of the number of AGDDs from highest (1) to lowest (5) in table 6.4.

[5] Land principally occupied by agriculture with significant areas of natural vegetation

[6] Transitional Woodland Shrub

Table 6.4: The ranked landcover classes in terms of the number of AGDDs per year

Rank	2003	2004	2005	2006	2007	2008	2009
1	Arable	Arable	Arable	Arable	Arable	Peat Bogs	Peat Bogs
2	Pastures	Peat Bogs	Pastures	Pastures	Peat Bogs	Arable	Ag Land
3	Peat Bogs	Pastures	Ag Land	Ag Land	Ag Land	Ag Land	Arable
4	Ag Land	Ag Land	Peat Bogs	Peat Bogs	Pastures	Pastures	Pastures
5	Trans	Trans	Trans	Trans	Trans	Trans	Trans

Certain landcover types are more consistent than others in terms of the relative ranking of AGDDs per year. For example, the transitional woodland shrub class accumulates the least number of degree days before SOS for all seven years while arable land accumulated the highest number from 2003 to 2007 while in 2008 and 2009 it was peat bogs. These results demonstrate that of the five landcover types examined, arable land had the highest GDD requirements in five of the seven years studied while transitional woodland shrub had the least in all seven years. This is a slightly different result to that shown by the ranking of the 7-yr median values (table 6.3). This is to be expected, however, since the difference between the median values is far smaller than the inter quartile range over the seven year period and therefore the interannual variation likely to be high. In order to graphically illustrate the interannual variation in AGDDs per landcover type, box plots were constructed which can be seen in figure 6.8. Box plots provide an indication of the location and dispersion of the data and are useful to identify outliers (Dytham, 2003). Furthermore, by compiling the annual box plots on the same axes in each figure, the following measures can be compared between years: locations of the distribution, minimum and maximum values, dispersions and shapes of the distributions

(O'Sullivan, 2009). These plots are useful to graphically illustrate variability in the number of AGGDs from year to year within each landcover type. The box plot is characterised by a central line where the median of the distribution lies, while the upper and lower bounds of the box are defined by the first and third quartile of the data. The length of the box is determined by the spread of the data. Lines extend from the box to the values within 1.5 times the inter quartile range. The lower adjacent value is less than the first quartile-1.5IQR while the upper adjacent value is greater than the third quartile+1.5IQR. Outliers are classed as values beyond the upper and lower adjacent values and are indicated by a cross symbol.

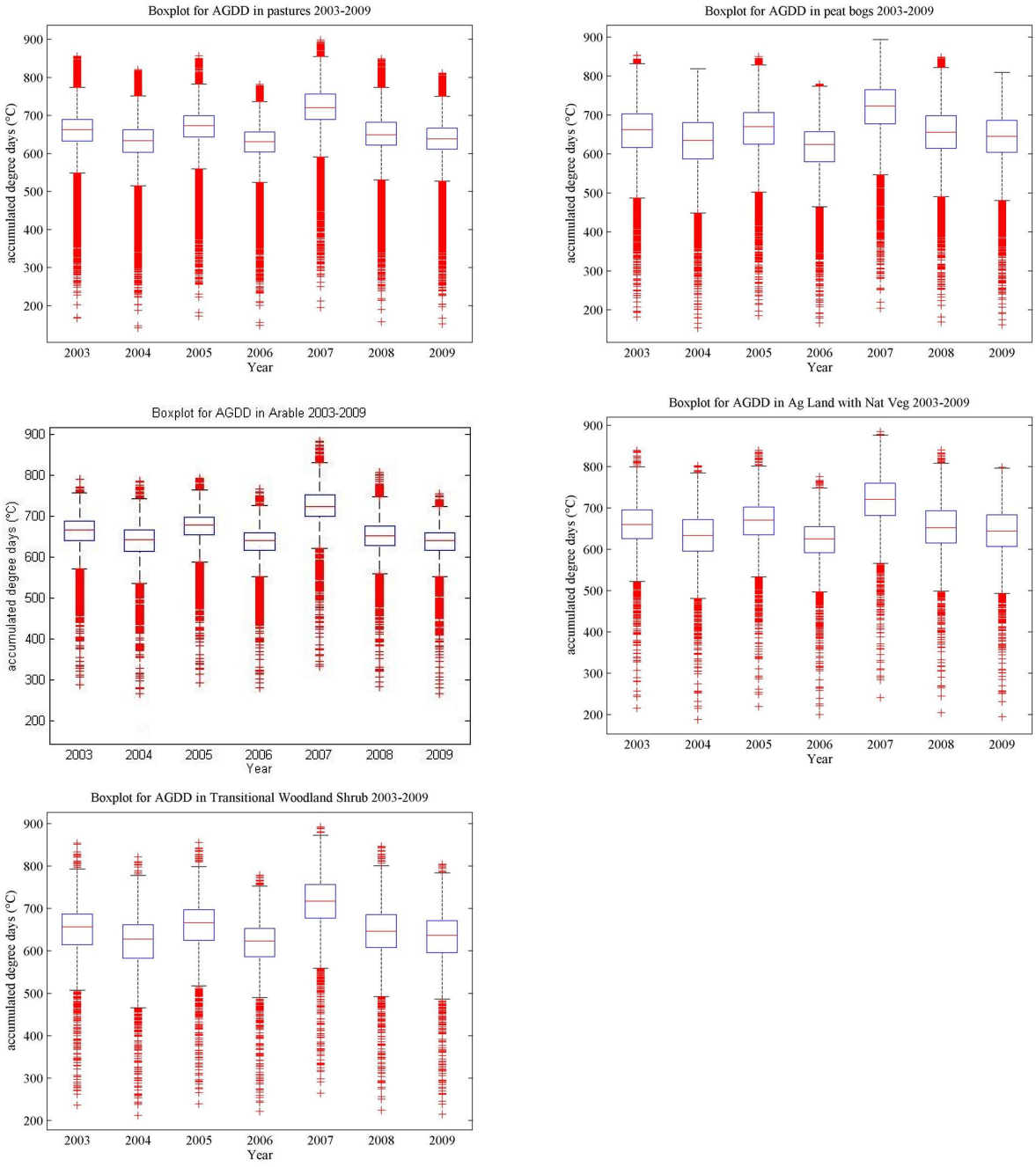

Figure 6.8: Box plots for the five landcover types illustrating the dispersion of the AGDDs on an interannual basis and the extent of outliers

In figure 6.8, the position of the median line does vary from year to year indicating a certain amount of interannual variation in the AGDD values. However, the pattern of interannual variation appears to be consistent in each landcover type with fewer GDDs accumulated in 2006, 2008 and 2009 and the most accumulated in 2007. This temporal pattern is related to the interannual SOS patterns shown in figure 5.13 -5.14 in chapter 5 since the degree days were accumulated until the time when SOS had

occurred. However, the exact relationship between these two variables has not been determined. As the number of AGDDs for SOS varies from year to year it must be assumed that other factors could determine the SOS date, e.g. soil temperature or the occurrence of weather extremes such as frost. There are a considerable number of outliers per year in all the landcover classes typically lower in value than the lower adjacent value. The outliers are very rarely higher than the upper adjacent value especially in peat bogs where there are no outliers greater than this value in some years. These outliers are responsible for the negative skew observed in the landcover class distributions in figure 6.7. The bias towards low AGDD values is possibly due to the presence of areas at higher elevation in each landcover class. There appears to be a consistent elevation bias in each landcover type and within each year. The interannual variation in AGDDs is replicated in all the landcover classes which suggest some island-wide climate influence in degree day accumulations. However, this finding does not support the idea of a fixed number of degree days for spring growth in different vegetation species. Nevertheless, it can be concluded from the 7-year median values of the five landcover types examined that SOS occurs between 646.4±33.78°C and 655.9 ±30.54°C over a base temperature of 6ºC.

6.6.4 Varying the base temperature for pastures

In order to test the sensitivity of the accumulated degree day's values to base temperature, the base temperature was lowered to 0°C for the same five landcover types in 2006. The resulting box plots per landcover class are shown in figure 6.9. Despite changing the threshold temperature, the same systematic bias of outliers below the lower adjacent value can be seen. This shows that changing the base

temperature does not change the distribution of the AGDD values although more degree days are accumulated as would be expected with a lower base temperature.

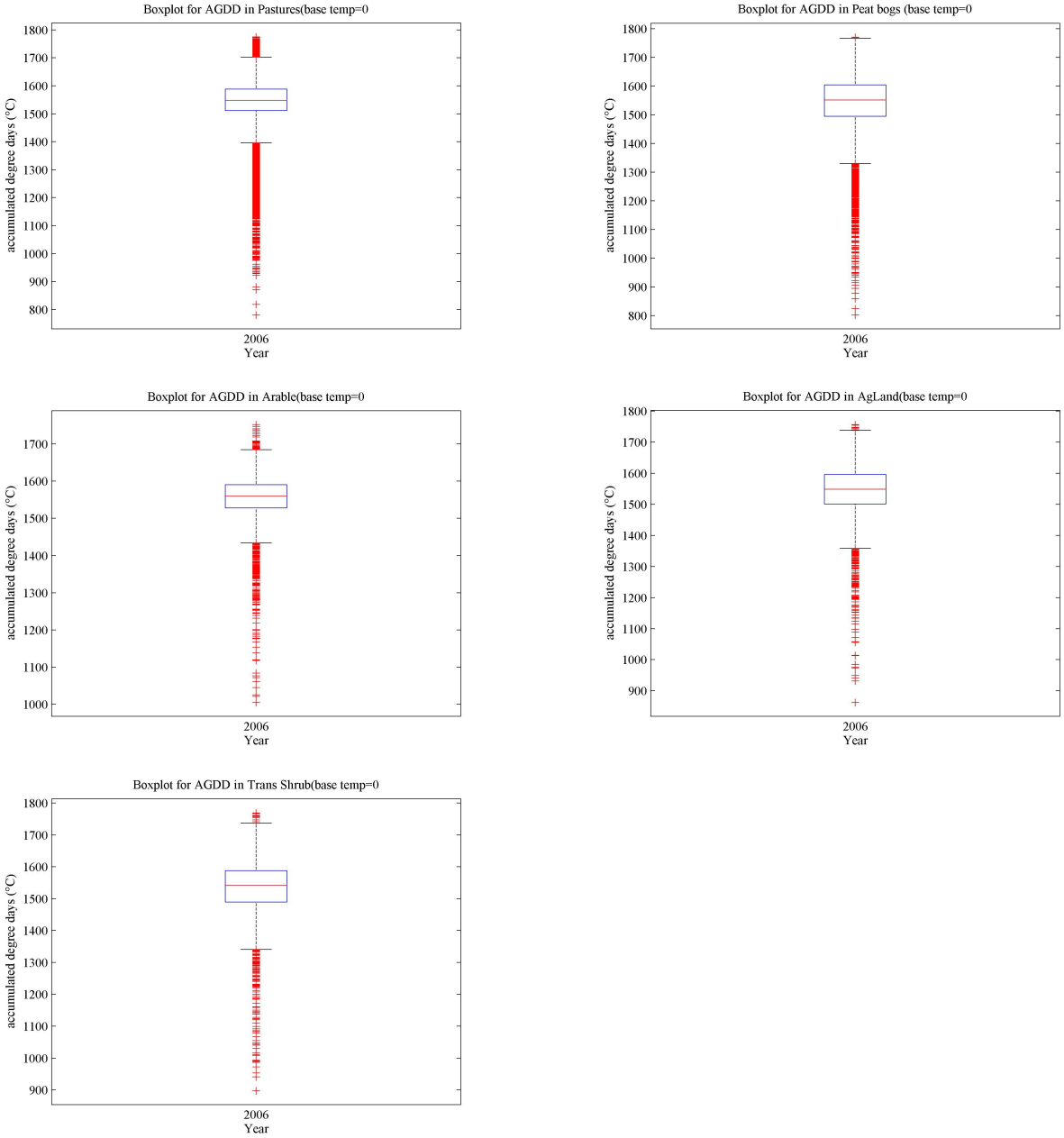

Figure 6.9: AGDDs for the five landcover types using a base temperature of 0°C

6.7 Discussion

The statistical techniques used to explore the air temperature-SOS relationship have been selected to account for the use of continuous temperature and ordinal SOS data which required particular statistical treatment. In addition the spatial component in gridded datasets added further complexity to the correlation studies. Large sample sizes resulted from analysing data at the national scale which introduces the possibility of false positive findings, i.e. rejecting the null hypothesis when it is in fact true. Although the Bonferroni correction is the most commonly used method, less stringent corrections have been proposed in the remote sensing literature. For example, the false discovery rate is an alternative method to controlling the family-wise error rate by indicating the expected minimum number of false positive findings before a feature is considered significant. The q-value gives this minimum false discovery rate when calling a specific feature significant (Benjamini and Hochberg, 1995, cited in Brown et al.,2010). However, there is no consensus on the best statistical approach to correlating remotely-sensed variables with other gridded measurements while controlling the family-wise error rate.

The correlation method used non-spatial statistics to describe a spatial trend, i.e. when examining SOS-temp correlations across the grid for one time period. However, non-spatial statistics, i.e. straightforward correlations, cannot take account of spatial configuration and do not have the tools to adequately describe or summarise spatial distributions (Cook, 2009). This was evident from the weak correlation coefficients which did not adequately represent a very complex spatio-temporal relationship. Undoubtedly other environmental variables such as soil

temperature, the number of frosty nights, precipitation, elevation and landcover type influence the timing of the SOS (White et al., 2009, White et al., 2005, Hudson Dunn and de Beurs, 2011). Elevation in particular is an important determinant of air temperature differences hence SOS variation. In contrast to more mountainous environments, Ireland's elevational range is quite small with the highest peak at approximately 1000m and 92% of the land surface below 200m (according to the GTOPO-30 DEM). In such minor elevation variation, temperature remains relatively constant, resulting in negligible impact on SOS (Hudson Dunn and de Beurs, 2011). The influence of these multiple factors on SOS would be more suitable modelled using multiple regression analysis in future studies. Nevertheless a positive aspect of the Spearman rank correlation measure is that it does not assume the frequency distribution of the variables to be normal, an important consideration for this study (de Beurs and Henebry, 2010). Future studies should consider spatial configuration as an important part of statistical exploration of these datasets e.g. by the use of geostatistics.

The Met Éireann gridded temperature products were valuable in estimating temperature parameters across the country at an equivalent spatial scale to the SOS data. However, the weakness of the gridded temperature product is that it is generated by interpolation, i.e. from samples of points which are spatially unevenly distributed and therefore may be more accurate in some areas than others. However, this uncertainty could not be estimated at any single grid point but overall error estimates given per year instead. Correlation at the pixel level yielded more promising results as a temporal trend was measured over coincident areas rather than

across the entire grid for one time period. When the maximum rank correlates were gridded, spatial patterns emerged in the timing of the correlations. There was not a characteristic landcover pattern to the correlations as was seen in the SOS data for example but a general geographical trend which was probably related to general climate across the country and to a certain extent vegetation management. For example, there was a west/east divide in the timing of the significant correlations ($p<0.1$) with the southeast correlating negatively with winter temperatures and the northwest correlating negatively with spring temperatures. This implies that as winter temperature rises, SOS in the southeast will become earlier while if spring temperature rises, SOS in the northwest will be earlier. The contrasting patterns in maximum correlation timing illustrates the complexity of SOS-climate interactions at the national scale in comparison to the straightforward spring greening trend observed at the IPG sites. Indeed the results suggest that SOS in certain parts of the country correlates with temperature as early as November and as late as April. This would suggest that SOS responds to temperature changes over a time period of 6 months. This important finding was also shown by Estrella *et al.* (2007) who found strong negative correlations between phenological events and air temperature of the three months prior to the event. One potential contributory factor to the observed complexity in the SOS-air temperature relationship is the dependency of certain vegetation types on soil temperatures for leaf canopy development while others rely on air temperature and this may vary depending on the growth stage of the plant species. For example, in grass species at the beginning of the growing season when the growing leaf is close to the ground, soil temperature is a determinant of growth timing while in crops and larger plants air temperature is a more important

determinant of vegetative development while these relationships vary depending on growth stage of the plant (Keane and Collins, 2004).

A carefully-selected regression model would be required for a modelling study of air temperature as a determinant of SOS. Ordinal regression is a potential method as the SOS data are ordinal. However, linear methods would not adequately capture the multiple factors involved in SOS determination. Future studies must clarify these uncertainties if the impact of predicted air temperature changes in Ireland on the observed spatio-temporal patterns in SOS is to be accurately predicted. This is particularly important given that the mean ensemble of downscaled global climate model predictions for Ireland, suggest that by the 2020s, average seasonal temperatures will increase by between 0.75 and 1.0°C (Fealy and Sweeney, 2008). By the 2050s, it is expected that Irish temperatures will increase by 1.4–1.8°C, with the greatest warming occurring during the autumn. The frequency of climate extremes, such as the prolonged summer heat of 2006 which resulted in soil moisture deficits across Ireland, is also expected to increase. This will mean fewer frost nights per decade and an increase in heat wave durations, according to modelling studies (Fealy and Sweeney, 2008). While such a changing climate will undoubtedly offers benefits such as the growth of new crop types, an enhanced 'continental' effect will be become more pronounced during all seasons and, according to the mean ensemble estimate, the mean temperature in all seasons is projected to increase by 2°C or more (Fealy and Sweeney, 2008). Such climate change will potentially alter the temporal dynamics of land surface phenology and the spatial distribution of landcover types.

The growing degree day analyses have yielded useful insights into the different heating requirements for vegetation SOS between the landcover classes examined although there was insufficient landcover-specific variation in the GDD values to detect a landcover trend. Furthermore, altering the base temperature did not change the distribution of values nor did readily identifiable differences between the landcover types emerge. Although soil temperature has been used in modelling of grass growth (Keane and Collins, 2004, Connaughton, 1973), Met Éireann do not produce gridded soil temperature products. Therefore, gridded air temperature data were used given the proven relationship between air temperature and vegetation development. Although the estimated SOS provided the closing date for GDD calculation, the GDDs were accumulated from a fixed start date, i. e. January 1st. Other studies however, have used a start date that correlates best with the SOS. For example, accumulated degree days of individual plant species from a date which correlated with the daily mean air temperature to the beginning of flowering (Wielgolaski, 1999). Estimates of AGDDs have been reported for specific plant species at specific locations, e.g. 566±23.8°C for the beginning of flowering in hawthorn in north-eastern Italy (Masin et al., 2005). However, the mix of vegetation species in each of the CORINE landcover classes and the geographical distribution in their coverage introduces some uncertainty to the interpretation of the AGDD estimates per landcover type in this study. Nevertheless the differences in the 7-year median values per landcover type and the variation in the annual rankings within each year suggest that there is some link between landcover, AGDDs and SOS. For example, when ranked in order of magnitude within each year, there appears to be a hierarchy in the five landcover types. Arable land had the highest requirements in

terms of AGDDs while transitional woodland shrub had the least. This is somewhat intuitive since arable crops would be expected to have high thermal requirements for leaf development and storage in fruits and tubers for subsequent growing seasons (Keane and Collins, 2004). In contrast the GDD requirement of the transitional woodland class, which largely consists of newly-forested plantations as well as felled woodland and gorse vegetation, is less easily defined. It is likely that such vegetation types are in the early stages of development and perhaps demand lower air temperatures for SOS. Another notable feature of the AGDD trend is the similarity in median values between arable and land principally occupied by agriculture with natural vegetation. The latter class is a mixed agricultural class and is likely to include vegetable crops (EIONET: European Topic Centre on Land Use and Spatial Information, 2006). The ranking of peat bogs and pastures shows the most variation in rank from year to year although it would appear from the 7-year median values that peat bogs have slightly higher heating GDD requirements than pastures overall. It is likely that peat bog vegetation species are subject to more climate extremes and therefore require more heat accumulation than grazed grasslands. This is the first time in Ireland that GDDs have been accumulated from a fixed date until an estimated SOS date rather than annual totals and on the basis of landcover type rather than species level. However, the variability from year to year in the number of degree days per land cover type and the lack of difference between landcover types within any one year indicates that landcover may be too spatially-coarse as a unit to explore to AGDD across the country. Habitat maps at the species level may provide the species-specific information required to accurately determine a growth start data from the temperature data. However, higher spatial resolution

satellite data may be preferable for analysis at this scale. From this analysis, using a 6ºC base temperature, an approximate range of AGDDs for SOS to occur has been shown for the most common vegetation types, which is indicative of temperature requirements for land surface vegetation at the national scale.

6.8 Conclusions

Information extracted from gridded air temperature data has offered considerable insight into the spatial and temporal variability of the SOS with air temperature over the seven year study period. Non-parametric statistics have been used to account for the non-normally distributed temperature data and as a more conservative measure of association between the variables.

Initially, the spatial variability of SOS with mean monthly air temperature was examined by correlation at the grid level. Although the correlation coefficients were weak, suggesting very little association of SOS with air temperature across the country within any one month, the weakness of non-spatial statistics to address explicitly spatial issues was shown. Issues such as spatial autocorrelation and controlling the family-wise error rate in large sample sizes emerged as challenging topics which were not expected when the study was undertaken. Furthermore, the weakness of the relationship suggested that the presence of other factors such as landcover, elevation, soil temperature and agricultural practice also determine the SOS spatial variability. Consequently, future studies should consider a multivariate approach with the use of geostatistics.

The exploration of the temporal variability of SOS with air temperature over the 7-year period showed more promising results however. The spatial patterns in the timing, strength and significance of the maximum monthly correlations indicated that agricultural practice is an important determinant of the SOS-air temperature relationship. For example, the sowing of winter cereals in the south, southeast and east are most likely the cause of a negative correlation with winter temperatures and a positive correlation with spring temperatures. In contrast, the mixture of agricultural practices in the west, combined with the predominant landcover made up of areas of pastures and natural vegetation are associated with a negative correlation with spring temperature and positive correlation with winter temperature. The underlying causes of these temporal patterns require further examination but their clear spatial pattern indicate that agricultural practices have a significant influence on the air temperature-SOS correlates.

As well as the analysis of raw air temperature data, a derived agro-meteorological measure, the growing degree day, was calculated and used to explore any landcover-specific growth differences. A base temperature of 6°C was first selected based on an examination of the literature. However, the similarities in growing degree days accumulated per landcover type indicated that to discern any landcover-specific differences in heating requirements, based on the SOS, would be difficult. Nevertheless, for the first time, this study has accumulated degree days to estimate growth per landcover type until the SOS had occurred rather than annual accumulations. Although the differences between landcover types were marginal, an approximate range of AGDDs has been estimated for SOS to occur in the vegetation

types with highest percentage coverage. An area requiring further investigation is the appropriate date from which to accumulate degree days as the use of a fixed start date may not adequately represent the temporal development of vegetation in response to air temperature variation.

Given the predicted air temperature changes in Ireland in the coming decades, there may be changes in Irish landcover and land use, with adaptation to new agricultural practices, and changes to the state of natural systems. This initial climate study has highlighted some of the methodological issues associated with exploring statistical relationships between gridded datasets. Furthermore, some interesting air temperature-SOS trends have been shown which require more in depth analysis in future studies. However, such studies need to refine the methodology used for a more comprehensive statistical analysis.

Chapter 7. Conclusions and Perspectives

7.1 Conclusions

The overall objective of this study was to determine whether vegetation seasonality metrics such as the Start of Season (SOS) could be reliably estimated from a multiannual time series of medium to low spatial resolution satellite data, from 2003 to 2009 across the island of Ireland. In order to achieve this objective, more specific aims were identified: namely, to select an appropriate time-composite period for the daily MGVI data; to explore time series analysis as a tool to extract the SOS metric; to characterise the spatio-temporal patterns in SOS across the island using explanatory variables such as landcover, and finally, to assess the relationship of certain climate parameters with the SOS over the seven year period.

Visual analysis suggested that the patterns in the SOS grids were aligned with the spatial distribution of different landcover types. At the same time, the metric was sufficiently sensitive to demonstrate the temporal variability in these spatial patterns from year to year. Further quantative spatial analysis confirmed the role of landcover as a determinant of SOS, while also suggesting that factors of location, proximity to the sea and elevation compete to determine when SOS occurs. Climate variability over the seven year period, as revealed in the air temperature record, was shown to drive interannual variability in the SOS. Anomalous temperature variation, from the seven year mean, also caused anomalies in the SOS, as was demonstrated by the delayed SOS countrywide in 2006 as a result of the cooler than average winter of 2005/2006 and spring of 2006.

Evidence has shown that climate variability influences the timing of phenophases over time at point locations. However, this study concluded that landcover and land use has more influence on the SOS when examined at a synoptic scale over large spatial extents at low spatial resolution. In fact, landcover has proven to be a major determinant of the SOS spatial variability. The grouping of landcover types based on significant differences in the SOS showed that SOS in managed vegetation types can be from two to four 10-day periods earlier than in similar but unmanaged vegetation, e.g. between improved pastures and natural grassland. It can be concluded from this result that the land surface phenology of managed vegetation is a combination of land use practices and climatic factors, resulting in maximum growth efficiency. In the absence of soil treatment, artificial fertilisation, grazing and other land management activities, non-managed vegetation SOS is more finely-tuned to ecosystem drivers, i.e. the biosphere, lithosphere and atmosphere. However, a multi - decadal rather than a multi- annual time series would be required to separate the climatic from the human impact on land surface phenology, and to discern which factors are the most influential on each landcover type.

The initial exploration of air temperature as a correlate of the SOS, across the whole island, suggested a very weak relationship with mean monthly and seasonal air temperature. However, the timing, strength and direction of the maximum correlations, when calculated on a per pixel basis over the seven year period, demonstrated a much stronger association between the two variables. Nevertheless, the strength and timing of correlation was highly dependent on location. Overall, two thirds of the significant seasonal correlates were negative, i.e. as winter and spring temperature increases, the SOS advances, consistent with the spring greening trend

observed at the IPG gardens. However, the remaining one third of correlates shows the opposite trend and the cause of this requires further investigation, e.g. into other driving factors by the use of a multivariate correlation.

The interaction of landcover, elevation and climate at the national scale presented a more complex picture of land surface phenology than the linear air temperature/BGS trend, observed at the IPG sites. Although the SOS had occurred across most of the country (66%) by March 12th-21st according to the seven year average, the estimated SOS spanned a considerable period of time from January in the lowest lying pastures to July in the most upland peat bogs. Ireland's temperate climate is characterised by a moderate range in annual air temperature, yet there is enough variability in weather patterns and other non-climatic factors to produce a mosaic of SOS dates, occurring, for the most part, within the first 6 months of the year. This finding contrasts with vegetation phenology in less temperate climates, e.g. in arid biomes, where the SOS is more constrained by climatic factors, such as precipitation, and therefore occurs within a much narrower time range. While the semi-quantative analysis of landcover, contrasted with the quantative analysis of air temperature, justified their treatment as separate variables in the analysis of SOS, they could be modelled together using advanced spatial statistics and multiple regression models. Indeed, the statistical treatment of large gridded datasets, as was used in this study, proved particularly challenging due to issues such as spatial autocorrelation and controlling the family-wise error rate. Furthermore, the approaches to managing these issues in the literature vary and are often adapted from other disciplines which may not necessarily be appropriate for geographical studies with thousands of data points,

e.g. the stringency of the Bonferroni adjustment for multiple pair wise comparisons. It has become clear from this study that the SOS is an integrated indicator of land surface phenology and represents an ensemble of different variables and not just climate alone. Therefore, there is an urgent requirement to refine the statistical and quantitative approaches used in correlating remotely-sensed data with several other spatially-dependent datasets. For example, this might involve the use of non-linear correlation methods such as Gradient Pattern Analysis (GPA), to parameterise the satellite and climate or other explanatory datasets in terms of their gradient moments (Gradient Asymmetry, Gradient Diversity and Gradient Entropy) (Ramos et al., 2000). A multivariate rather than a univariate approach should be considered in future studies but only if appropriate statistical tests and correlation methods are used.

The limitations of using a global vegetation index for local to regional scale applications have also been highlighted in this study. For example, the MGVI time series was characterised by noise and data drop outs which appeared to be a factor of Ireland's frequent cloud cover and high atmospheric water vapour content which are not adequately parameterised in global atmospheric models. Therefore, atmospheric correction methods in global datasets need to be refined for local scale variability in atmospheric conditions for a more robust dataset.

7.2 Perspectives

A major outcome of this work is the ability to discriminate landcover differences based on their characteristic seasonality signal. This information can be used to enhance current methods of characterising landcover and land use across the country

and, when applied to mapping agricultural land uses, can potentially be used for carbon accounting. Indeed, as a result of this work, a call for projects using this approach to land use mapping in Ireland, has been issued by the EPA in 2011. Land surface characterisation using seasonality characteristics of vegetation, is only one of the potential future applications of LSP monitoring in Ireland. The ESA is developing five new missions called Sentinels, exclusively for the operational demands of the Global Monitoring for Environment and Security (GMES) programme. A key requirement of the United Nations Framework Convention on Climate Change (UNFCCC), established in 1992, was a commitment to the systematic observation of, and archiving of data on, the Earth's climate system (Plummer, 2009). The Global Climate Observing System (GCOS), set up under the UNFCCC, provides the framework to achieve this aim, by the systematic observation of Essential Climate Variables (ECV). The FAPAR, for example, is a terrestrial ECV and ESA is monitoring it as part of the GCOS initiative. Within the framework of the ESA Climate Change Initiative (CCI), there are eight individual sensors dedicated to monitoring FAPAR including MERIS, MODIS, SeaWiFS and the AVHRR (Doherty, 2010). Sentinel 3 is seen as a replacement for the MERIS mission, with 21 spectral bands, acquiring data at 300m spatial resolution, while Sentinel 2 is a Landsat-like high spatial resolution, land monitoring sensor. There is considerable potential in the application of the data from these upcoming sensors, not only to enhance the continuity of SOS and FAPAR monitoring, but to experiment with alternative metrics and biogeophysical products at such high spatial resolutions.

There was a remarkable consistency in the interannual SOS pattern observed in peat bog vegetation in this study, in comparison to the interannual variability exhibited by most other landcover types. This could be due to the fragile equilibrium between peat bog vegetation, hydrological regime, climate and soil type which results in a very narrow time window in which SOS can occur. However, the presence of rocky ground, surface water and other non-vegetated surfaces within peat bog vegetation might also cause this steady temporal pattern. The health and status of certain peat bog vegetation species is recognised as an important indicator of climate change while the rich organic soil stores significant amounts of carbon. Therefore, peat bog habitats are an appropriate starting point to assess the feasibility of ESA Sentinel 2/3 satellite data to track phenological variability, at medium to high spatial resolution. Considering the vulnerability of these ecosystems to climate change and their relative abundance in Ireland, this presents an interesting and worthwhile avenue for further research. Nevertheless, it appears that the MERIS sensor will continue to yield data until 2013 when it will be replaced with Sentinel-3.The time series can also be extended further back in time by the use of other sensor FAPAR products.

The potential of higher spatial resolution data, to track phenological variability at finer spatial scales, is worthy of further attention, especially with the availability of 300m MERIS FAPAR products from the GEOLAND 2 [7]initiative and 1km MODIS FAPAR/LAI from the Boston University Climate Change and Vegetation Group[8]. The GEOLAND 2 project, established under the GMES programme, seeks to

[7] http://www.gmes-geoland.info/

[8] http://cliveg.bu.edu/

establish a long-term sustainable service for satellite-derived products of the land surface, at regional, European and global scales, which are provided to end users freely and online (geoland2, 2011). The validation of the GEOLAND 2 products is guided by the standards of the CEOS LPV subgroup, demonstrating the increased cooperation among international organisations in providing accurate and consistent satellite data products. As part of its global land monitoring programme, GEOLAND 2 provides biophysical parameters such as the fraction of vegetation cover, FAPAR, and derived phenology parameters in near real time. The FAPAR data are derived from the MERIS and SPOT VGT sensors, and are provided in 10-day composites, at 300m and 1 km spatial resolution, and are fully documented with metadata. However, as GEOLAND 2 runs from 2008-2012, the full resolution MERIS data products became available too late for use in this study. Nevertheless, there is the possibility of a comparative study between the full and reduced spatial resolution MERIS FAPAR in the future.

There is an increased need to achieve coherency between the various algorithms used to derive seasonality metrics such as the SOS so that they represent the same phenomena in terms of physical plant development. The scarcity of ground-based observations and the subjective nature of human observer measurements is a challenge to this task however. Alternative methods of *in-situ* monitoring, e.g. digital cameras or *in-situ* PAR sensors, mounted on towers, might enhance efforts to validate seasonality metrics. Indeed, automated observations of vegetation canopy reflectance by fixed position digital cameras, is potentially more suited to validating satellite-derived measures, than human-observed phenophases as there are limitations to the comparison of subjective observations to satellite-based trends due

to the nature of the measurement. While a satellite measures a radiometric signal, human observations are visually-based stages in plant development. Other factors which make them different include the temporal precision (daily vs. 10-day) and the spatial resolution (individual plant vs. area). While ground-based observations are point finite measures, satellites are synoptic sensors whose measures are generalised over large areas and incorporate a multitude of factors including artefacts of the satellite sensor itself. These factors combined constitute an Earth System Data Record (ESDR) of land surface phenology, as described by Friedl et al. (2010), in contrast to a database of species-specific phenological stages collated by phenology garden and citizen observer networks. The challenge posed to studying climate change from an ESDR is the difficulty in separating the influence of climate from other factors. From discussions within the CEOS LPV subgroup, there are a variety of opinions on what constitutes a satellite-derived phenology product, but, as yet, no consensus has been achieved between remote sensing and plant scientists. The two distinct interpretations of phenology, as that of variation in phenology across the land surface, or an observed stage in the life cycle of a plant or tree, highlights the need to find common ground between the two disciplines and further interdisciplinary dialogue.

The spatial and temporal resolutions of the MGVI were key determinants of the sensitivity of the SOS to phenological variability across the island. For this study, relative spatio-temporal variation in the SOS was observed, however no absolute estimates (day of year) of SOS were made, given the use of composite data. Daily precision with ideal accuracy of ± 3 days has been proposed as a key scientific requirement for a land surface phenology ESDR(Friedl et al., 2010). However, there

is still no consensus on whether this precision is achievable or not, while the temporal precision of LSP metrics in published studies continues to vary. Although the use of composite data is a necessity for remote sensing in the optical domain when carrying out national and regional studies, it is impossible to observe changes of a fraction of a day per year with a time resolution of 10 days, especially in cloudy climates which do not guarantee regular daily measurements. As a result, satellite – derived trends in phenology generally differ from trends in ground-based observations. For example, when translating the SOS anomalies into days change per year, the numbers exceed the ground-based observed changes over Europe of 2.5 days per decade (Menzel et al., 2006). To address this, the temporal resolution of the input data could be refined, e.g. by the use of daily, instead of composite data. Although this would enhance the ability to detect phenological variability in time series data, the intermittency of valid, cloud-free data could be an issue for generating realistic curve fits.

7.3 The future of land surface phenology studies

It is clear that with an ever increasing number of satellite sensors, free access to a range of biogeophysical parameters through initiatives such as GEOLAND 2, experimentation with microwave remote sensing for retrieving phenological parameters and a commitment to establish ground validation sites worldwide that the study of land surface phenology is set to evolve. A large number of earth observation satellites already provide a global LSP monitoring network which is gradually being enhanced by emerging technologies. For example, *in-situ* sensors, mounted on towers above the vegetation canopy, can measure FAPAR and LAI as well as reflectance in the same spectral range as satellite sensors. As mentioned, digital

cameras, mounted in fixed positions, can acquire daily imagery of vegetation canopies and monitor the progression of the seasons in the visible to near infrared wavelengths. Vegetation indices can also be derived from digital camera reflectance data, and the imagery can be disseminated via websites. Such webcam technology has the power to bring the science of phenological observation into the school, home and everyday life. Furthermore, *in-situ* sensors and digital cameras do not suffer the atmospheric interference inherent in satellite-measured reflectance data, although their location is fixed and spatial range limited to the level of the vegetation canopy of mostly homogenous vegetation cover. Unmanned airborne vehicles (UAVs) are also emerging technologies which provide the capacity for mobile, local-scale monitoring with more user interaction and sensor experimentation. Such a nested approach to phenological monitoring, at different spatial scales, from satellite and airborne sensors to UAVs, digital cameras and *in-situ* sensors, complemented by ground-based observers of phenophases, undoubtedly represents the future of phenological monitoring.

Ireland has a role to play in these emerging methods. The network of phenological gardens has already expanded, during the course of this study, from the original four IPG gardens to an additional 12 IPG gardens and 11 native gardens. This work has been led by the EPA-funded CCIP project at Trinity College, Dublin, established in 2007, to oversee the development of a sustainable phenology network in Ireland. The expanded network now comprises 27 locations, across the island. The launch of Nature Watch on the National Biodiversity Data Centre website, as a focal point for citizen observers to record their observations, presents an additional source of data and, given time, has the potential to complement the historical record provided by

trained observers. However, it is now timely to consider the use of *in-situ* sensors, or digital cameras, in Ireland, to enhance this human observer network.

The status of phenology as a research discipline in Ireland has been strengthened by the media attention, and outreach work, of the CCIP project. Furthermore, the international and interdisciplinary Phenology 2010 conference organised by the project attracted researchers from the discipline worldwide. The momentum gathered after the Phenology 2010 conference will now be carried forward to the Phenology 2012 conference at Milwaukee, Wisconsin, U.S.A. The Phenology 2010 conference also provided the location for the first meeting of the CEOS LPV subgroup, at which international researchers across a variety of disciplines, agreed to collaborate and combine efforts for a global protocol to validate LSP products. A consensus was achieved on a synthesis of methods, from flux towers to digital cameras, to validate satellite-derived products at 10-20 carefully selected validation sites. The current activities of the subgroup are now focused on gathering 100km by 100km satellite phenology product subsets for the validation sites as well as comparable in-situ observations within 100km of the site centre.

Despite the considerable progress that has been made, LSP is still maturing as a science, as are the algorithms and techniques used to derive LSP products. Some areas of the discipline are still in need of precise definition, for example, in what constitutes an LSP metric in terms of physical plant development. There is more consensus-building required among its practitioners on the goals to be achieved and the appropriate strategy to achieve these goals in the coming decades. However, continued effort on behalf of the members, combined with the ongoing renaissance

in the science of phenology, is ensuring a bright future for the field as a topic of major scientific importance. This research has contributed to the discipline by adapting existing time series analysis methods to an optimised VI index at a new location, previously unstudied in terms of its land surface phenology characteristics.

References

ACKERMAN, S. & WHITTAKER, T. 2011. *Incoming and Outgoing Radiation* [Online]. Tools of the Atmospheric Scientist. Available: http://www.ux1.eiu.edu/~cxtdm/met/sirs.html [Accessed 8th August,, 2008].

AKMAL, M., FARID, U., ASIM, M. & FARHATULLAH, M. 2011. Growth Comparison of Exotic Species for Green Forage. *Pakistan Journal of Botany.* **43** (3) 1557-1561.

AMANO, T., SMITHERS, R. J., SPARKS, T. H. & SUTHERLAND, W. J. 2010. A 250-year index of first flowering dates and its response to temperature changes. *Proceedings of the Royal Society B-Biological Sciences.* **277** (1693) 2451-2457.

ANDRADE, C., SANTOS, J. A., PINTO, J. G. & CORTE-REAL, J. 2011. Large-scale atmospheric dynamics of the wet winter 2009-2010 and its impact on hydrology in Portugal. *Climate Research.* **46** (1) 29-41.

ARNDT, D. S., BARINGER, M. O. & JOHNSON, M. R. 2010. State of the Climate in 2009. *Bulletin of the American Meteorological Society.* **91** (7) s1-s222.

AUSSEDAT, O., GOBRON, N., PINTY, B. & TABERNER, M. 2006. MERIS Level 3 Land Surface Time Composite, Product File Description. Global Environment Monitoring Unit, European Commission Joint Research Center.

BEAUBIEN, E. G. & FREELAND, H. J. 2000. Spring phenology trends in Alberta, Canada: links to ocean temperature. *International Journal of Biometeorology.* **44** (2) 53-59.

BELOTELOV, N. V., BOGATYREV, B. G., KIRILENKO, A. P. & VENEVSKY, S. V. 1996. Modelling of time-dependent biome shifts under global climate changes. *Ecological Modelling.* **87** (1-3) 29-40.

BENJAMINI, Y. & HOCHBERG, Y. 1995. CONTROLLING THE FALSE DISCOVERY RATE - A PRACTICAL AND POWERFUL APPROACH TO MULTIPLE TESTING. *Journal of the Royal Statistical Society Series B-Methodological.* **57** (1) 289-300.

BONAN, G. 2002. *Ecological climatology,* London, Cambridge University Press

BOYD, D., ALMOND, S., DASH, J. & CURRAN, P. J. 2011. Phenology of Vegetation in Southern England from Envisat MERIS Terrestrial Chlorophyll Index (MTCI) data. *International Journal of Remote Sensing.***32** (23) 8421-8447.

BROWN, M. E., DE BEURS, K. & VRIELING, A. 2010. The response of African land surface phenology to large scale climate oscillations. *Remote Sensing of Environment.* **114** (10) 2286-2296.

BUTTERFIELD, H. S. & MALMSTROM, C. M. 2009. The effects of phenology on indirect measures of aboveground biomass in annual grasses. *International Journal of Remote Sensing.* **30** (12) 3133-3146.

BÜTTNER, G. & MAUCHA, G. 2006. The thematic accuracy of Corine land cover 2000: Assessment using LUCAS (land use/cover area frame statistical survey). *In:* EUROPEAN ENVIRONMENT AGENCY (ed.). Copenhagen.

BÜTTNER, G., MAUCHA, G. & KOSZTRA, B. 2011. European Validation of Land Cover Changes in CLC2006 Project. *In:* EARSeL.Prague.HALOUNOVA, L., ed. 2011.

CAMPBELL, J. B. 2002. *Introduction to Remote Sensing,* London & New York, Taylor & Francis

CENTRE FOR ECOLOGY AND HYDROLOGY. 2010. *CEH data holdings* [Online]. Available: http://www.ceh.ac.uk/data/index.html [Accessed 28th July, 2010].

CHAMBERS, L. H., COSTULIS, P. K., YOUNG, D. F. & ROGERSON, T. M. 2004. Students as Ground Observers for Satellite Cloud Retrieval Validation. *In:* 13th Conference on Satellite Meteorology and Oceanography Norfolk, VA 20th-23rd September, 2004. American Meteorological Society.

CHEN, X., HU, B. & YU, R. 2005. Spatial and temporal variation of phenological growing season and climate change impacts in temperate eastern China *Global Change Biology.* **11** (7) 1118-1130.

CHMIELEWSKI, F.-M., MÜLLER, A. & BRUNS, E. 2004. Climate changes and trends in phenology of fruit trees and field crops in Germany, 1961–2000. *Agricultural and Forest Meteorology.* **121** 69–78.

CHMIELEWSKI, F.-M. & ROTZER, T. 2001. Response of tree phenology to climate change across Europe. *Agricultural and Forest Meteorology.* **108** 101–112.

CIHLAR, J., MANAK, D. & D'IORIO, M. 1994. Evaluation of compositing algorithms for AVHRR data over land. *Geoscience and Remote Sensing, IEEE Transactions on.* **32** (2) 427-437.

CLELAND, E. E., CHUINE, I., MENZEL, A., MOONEY, H. A. & SCHWARTZ, M. D. 2007. Shifting plant phenology in response to global change. *Trends in Ecology & Evolution.* **22** (7) 357-365.

CLEVELAND, R. B., CLEVELAND, W. S., MCRAE, J. E. & TERPENNING, I. 1990. STL: A Seasonal-Trend Decomposition Procedure Based on Loess. *Journal of Official Statistics.* **6** (1) 3-73.

CLIMATE PREDICTION CENTER INTERNET TEAM. 2011. *North Atlantic Oscillation* [Online]. NOAA/ National Weather Service. Available: http://www.cpc.ncep.noaa.gov/products/precip/CWlink/pna/nao.shtml [Accessed August 4th, 2011].

COILLTE 2003. Curraghbinny Wood Inventory Listing Report. Coillte Southern Region.

COLDITZ, R. R., CONRAD, C., WEHRMANN, T., SCHMIDT, M. & DECH, S. 2008. TiSeG: A Flexible Software Tool for Time-Series Generation of MODIS Data Utilizing the Quality Assessment Science Data Set. *Geoscience and Remote Sensing, IEEE Transactions on.* **46** (10) 3296-3308.

COLLINS, J. F. & CUMMINS, T. (eds.) 1996. *Agroclimatic Atlas of Ireland,* Dublin: Joint Working Group on Applied Agricultural Meteorology.

CONNAUGHTON, M. J. 1973. *The Grass Growing Season in Ireland*. Dublin: Agroclimatic Atlas of Ireland.

COOK, S. 2009. Exploratory Spatial Data Analysis (ESDA) and Spatial Statistics.Lecture (21st May). University of Ulster.

CORNWALL, C., HORIUCHI, A. & LEHMAN, C. 2010. *NOAA ESRL Solar Position Calculator* [Online]. Available: http://www.srrb.noaa.gov/highlights/sunrise/azel.html [Accessed 18th March, 2010].

CRISP. 2001. *Principles of Remote Sensing* [Online]. Available: http://www.crisp.nus.edu.sg/~research/tutorial/intro.htm [Accessed 12th May, 2011].

CRUICKSHANK, M. M., TOMLINSON, R. W. & TREW, S. 2000. Application of CORINE land-cover mapping to estimate carbon stored in the vegetation of Ireland. *Journal of Environmental Management.* **58** (4) 269-287.

DALGAARD, P. 2008. *Introductory Statistics with R*, Springer.Statistics and Computing,

DANSON, F. M. & CURRAN, P. J. 1993. Factors Affecting the Remotely Sensed Response of Coniferous Forest Plantations. *Remote Sensing of Environment.* **43** (1) 55-65.

DANSON, F. M. & PLUMMER, S. E. 1995. Red-Edge Response to Forest Leaf-Area Iindex. *International Journal of Remote Sensing.* **16** (1) 183-188.

DASH, J., JEGANATHAN, C. & ATKINSON, P. M. 2010. The use of MERIS Terrestrial Chlorophyll Index to study spatio-temporal variation in vegetation phenology over India. *Remote Sensing of Environment.* **114** (7) 1388-1402.

DAY, T. 2006. Degree-days:theory and application. The Chartered Institution of Building Services Engineers,.

DE BEURS, K. M. & HENEBRY, G. M. 2004. Land surface phenology, climatic variation, and institutional change: Analyzing agricultural land cover change in Kazakhstan. *Remote Sensing of Environment.* **89** (4) 497–509.

DE BEURS, K. M. & HENEBRY, G. M. 2005. Land surface phenology and temperature variation in the International Geosphere-Biosphere Program high-latitude transects. *Global Change Biology.* **11** (5) 779-790.

DE BEURS, K. M. & HENEBRY, G. M. 2008a. Introduction to Land Surface Phenology. *In:* A Workshop on Land Surface Phenology Madison, U.S.A., 8th April. USA National Phenology Network

DE BEURS, K. M. & HENEBRY, G. M. 2008b. Northern annular mode effects on the land surface phenologies of northern Eurasia. *Journal of Climate.* **21** (17) 4257-4279.

DE BEURS, K. M. & HENEBRY, G. M. 2010. A land surface phenology assessment of the northern polar regions using MODIS reflectance time series. *Canadian Journal of Remote Sensing.* **36** S87-S110.

DELANEY, B. 4th August 2011. *RE: Met Eireann climate and synoptic stations*Type to O' CONNOR, B.

DIGITALGLOBE. 2011. *DigitalGlobe* [Online]. Available: http://www.digitalglobe.com/ [Accessed May 8th, 2011].

DOHERTY, M. 2010. ESA Climate Change Initiative overview. *In:* ESA Living Planet Symposium.Bergen, Norway 2010.

DOKTOR, D., BONDEAU, A., KOSLOWSKI, D. & BADECK, F.-W. 2009. Influence of heterogeneous landscapes on computed green-up dates based on daily AVHRR NDVI observations. *Remote Sensing of Environment.* **113** (12) 2618-2632.

DONNELLY, A., JONES, M. B. & SWEENEY, J. 2004. A review of indicators of climate change for use in Ireland. *International Journal of Biometeorology.* **49** (1) 1-12.

DONNELLY, A., SALAMIN, N. & JONES, M. B. 2006. Changes in tree phenology: An Indicator of spring warming in Ireland? *Biology and Environment: Proceedings of the Royal Irish Academy.* **106B** (1) 49-56.

DYTHAM, C. 2003. *Choosing and Using Statistics, A Biologist's Guide*, Blackwell Publishing

EARTH RESOURCES OBSERVATION AND SCIENCE (EROS) CENTRE. 2009. *GTOPO30* [Online]. U.S. Geological Survey Available: http://eros.usgs.gov/#/Find_Data/Products_and_Data_Available/gtopo30_info [Accessed 8th September, 2010].

EIONET: EUROPEAN TOPIC CENTRE ON LAND USE AND SPATIAL INFORMATION. 2006. *CORINE Land Cover (CLC) classes* [Online]. European Environment Agency. Available: http://etc-lusi.eionet.europa.eu/CLC2000/classes/Pictures?CLCcategory=2/2.1/2.1.1&CLCtitle=Non-irrigated%20arable%20land [Accessed 16th November, 2010].

EKLUNDH, L. 2010. *TIMESAT, a software package for analysing time-series of satellite sensor data* [Online]. Lund and Malmo Universities

Available: http://www.nateko.lu.se/TIMESAT/timesat.asp [Accessed 1st October, 2010].

EKLUNDH, L. & JÖNSSON, P. 2010. TIMESAT 3.0 Software Manual. Department of Earth and Ecosystem Sciences, Lund University, S-223 62 Lund,Sweden and Center for Technology Studies, Malmö University, S-205 06 Malmö, Sweden.

ERA-MAPTEC LTD. 2006. CORINE Land Cover – IRELAND: Land Cover Update for 2006 Final Report. *CLC 2006/GMES FTSP land monitoring final report-Ireland.* Environmental Protection Agency, Ireland.

EROS. 2011. *Glossary* [Online]. United States Geological Survey (USGS). Available: http://eros.usgs.gov/#/Guides/glossary/e_g [Accessed 13th May, 2011].

ESA. 2005. *MERIS, Frequently Asked Questions* [Online]. Available: http://earth.esa.int/pub/ESA_DOC/ENVISAT/MERIS/VT-P017-DOC-005-E-01-00_meris.faq.1_0.pdf [Accessed 12th May, 2011].

ESA. 2006a. *Envisat Home Page* [Online]. Available: http://envisat.esa.int/category/index.cfm?fcategoryid=61 [Accessed May12th, 2011].

ESA 2006b. MERIS Product Handbook. European Space Agency.

ESA G-POD TEAM 2008. Earth Observation Grid Processing-On-Demand Portal User Manual. 3 ed.

ESTRELLA, N., SPARKS, T. H. & MENZEL, A. 2007. Trends and temperature response in the phenology of crops in Germany. *Global Change Biology.* **13** (8) 1737-1747.

EUMETSAT 2001. The Meteosat Archive User Handbook. EUM TD 06 ed.: EUMETSAT, Am Kavalleriesand 31, D-64295 Darmstadt, Germany.

EUMETSAT 2007. Cloud Detection for MSG - Algorithm Theoretical Basis Document. EUM/MET/REP/07/0132 ed.: EUMETSAT, Am Kavalleriesand 31, D-64295 Darmstadt, Germany.

EUROPEAN ENVIRONMENT AGENCY. 2011. *Europe's Environment: The second assessment* [Online]. Copenhagen. Available: http://www.eea.europa.eu/publications/92-9167-087-1/page014.html [Accessed January 31st, 2011].

FEALY, R. & FEALY, R. M. 2008. The spatial variation in degree days derived from locational attributes for the 1961 to 1990 period. *Irish Journal of Agricultural and Food Research.* **47** (1) 1-11.

FEALY, R. & SWEENEY, J. 2008. Climate Scenarios for Ireland. *CLIMATE CHANGE –Refining the Impacts for Ireland.* Environmental Protection Agency, Ireland.

FELDMAN, G. C. 2011. *SeaWiFS Project Information* [Online]. Available: http://oceancolor.gsfc.nasa.gov/SeaWiFS/BACKGROUND/ [Accessed 12th May, 2011].

FENSHOLT, R., RASMUSSEN, K., NIELSEN, T. T. & MBOW, C. 2009. Evaluation of earth observation based long term vegetation trends - Intercomparing NDVI time series trend analysis consistency of Sahel from AVHRR GIMMS, Terra MODIS and SPOT VGT data. *Remote Sensing of Environment.* **113** (9) 1886-1898.

FINCH, T. F. 1977. *Soils of Co. Westmeath*, Teagasc.National Soil Survey of Ireland,Soil Survey Bulletin No. 33.

FISHER, J. I., MUSTARD, J. F. & VADEBONCOEUR, M. A. 2006. Green leaf phenology at Landsat resolution: Scaling from the field to the satellite. *Remote Sensing of Environment.* **100** (2) 265-279.

FITTER, A. H. & FITTER, R. S. R. 2002. Rapid Changes in Flowering Time in British Plants. *Science.* **296** (5573) 1689-1691.

FRIEDL, M. A., HENEBRY, G. M., REED, B., HUETE, A., WHITE, M., MORISETTE, J., NEMANI, R., ZHANG, X. & MYNENI, R. 2010. NASA White Paper on Land Surface Phenology. NASA

GCOS 2010. Implementation Plan for the Global Observing System for Climate in Support of the UNFCCC (2010 Update). DRAFT v1.0 ed.: World Meteorological Organisation, Intergovernmental Oceanographic Commmission, United Nations Environment Programme,International Council for Science.

GEERKEN, R. A. 2009. An algorithm to classify and monitor seasonal variations in vegetation phenologies and their inter-annual change. *Isprs Journal of Photogrammetry and Remote Sensing.* **64** (4) 422-431.

GENOVESE, G., VIGNOLLES, C., NEGRE, T. & PASSERA, G. 2001. A methodology for a combined use of normalised difference vegetation index and CORINE land cover data for crop yield monitoring and forecasting. A case study on Spain. *Agronomie.* **21** (1) 91-111.

GEOEYE. 2011. *GeoEye* [Online]. Available: http:www.geoeye.com [Accessed 8th May 2011].

GEOLAND2. 2011. *geoland2 - Supporting the Monitoring, Protection and Sustainable Management of our Environment* [Online]. European Union. Available: http://www.gmes-geoland.info/ [Accessed 22nd August, 2011].

GOBRON, N. 12th February 2009. *RE: Query on FAPAR time series for Ireland.*pers. comm. Type to CONNOR, B. O.Institute for Environment and Sustainability, Joint Research Centre

GOBRON, N. 18th June 2010. *RE: Noise in MGVI time series over Ireland.*Personal communication Type to O' CONNOR, B.

GOBRON, N. 25th May 2011. *RE: FAPAR time series for Ireland*Type to O' CONNOR, B.

GOBRON, N., AUSSEDAT, O., PINTY, B., TABERNER, M. & VERSTRAETE, M. 2004. An optimized FAPAR algorithm, Theoretical Basis Document. 3 ed.: Institute for Environment and Sustainability, European Commission Joint Research Centre

GOBRON, N., BELWARD, A., PINTY, B. & KNORR, W. 2010. Monitoring biosphere vegetation,2009. *Geophys. Res. Lett.* **37** (15) L15402.

GOBRON, N., MÉLIN, F., PINTY, B., TABERNER, M. & VERSTRAETE, M. M. 2003. MERIS Global Vegetation Index: Evaluation and Performance. *In:* MERIS User Workshop.Frascati, Italy 10 – 13 November 2003. ESA.

GOBRON, N., PINTY, B., AUSSEDAT, O., CHEN, J. M., COHEN, W. B., FENSHOLT, R., GOND, V., HUEMMRICH, K. F., LAVERGNE, T., MELIN, F., PRIVETTE, J. L., SANDHOLT, I., TABERNER, M., TURNER, D. P., VERSTRAETE, M. M. & WIDLOWSKI, J. L. 2006a. Evaluation of fraction of absorbed photosynthetically active radiation products for different canopy radiation transfer regimes: Methodology and results using Joint Research Center products derived from SeaWiFS against ground-based estimations. *Journal of Geophysical Research-Atmospheres.* **111** (D13) -.

GOBRON, N., PINTY, B., AUSSEDAT, O., TABERNER, M., FABER, O., MELIN, F., LAVERGNE, T., ROBUSTELLI, M. & SNOEIJ, P. 2008. Uncertainty estimates for the FAPAR operational products derived from MERIS - Impact of top-of-atmosphere radiance uncertainties and validation with field data. *Remote Sensing of Environment.* **112** (4) 1871-1883.

GOBRON, N., PINTY, B., MELIN, F., TABERNER, M., VERSTRAETE, M. M., BELWARD, A., LAVERGNE, T. & WIDLOWSKI, J. L. 2005. The state of vegetation in Europe following the 2003 drought. *International Journal of Remote Sensing.* **26** (9) 2013-2020.

GOBRON, N., PINTY, B., MÉLIN, F., TABERNER, M., VERSTRAETE, M. M., ROBUSTELLI, M. & WIDLOWSKI, J.-L. 2007. Evaluation of the MERIS/ENVISAT FAPAR product. *Advances in Space Research.* **39** (1) 105-115.

GOBRON, N., PINTY, B., TABERNER, M., MÉLIN, F., VERSTRAETE, M. M. & WIDLOWSKI, J. L. 2006b. Monitoring the photosynthetic activity of vegetation from remote sensing data. *Advances in Space Research.* **38** (10) 2196-2202.

GOBRON, N., PINTY, B., VERSTRAETE, M. & GOVAERTS, Y. 1999. The MERIS Global Vegetation Index (MGVI): description and preliminary application. *International Journal of Remote Sensing.* **20** (9) 1917-1927.

GOBRON, N. & VERSTRAETE, M. 2008 ECV T10: Fraction of Absorbed Photosynthetically Active Radiation (FAPAR). Essential Climate Variables. . Rome: Global Terrestrial Observing System
GOMEZ-CHOVA, L., CAMPS-VALLS, G., CALPE-MARAVILLA, J., GUANTER, L. & MORENO, J. 2007. Cloud-Screening Algorithm for ENVISAT/MERIS Multispectral Images. *Geoscience and Remote Sensing, IEEE Transactions on.* **45** (12) 4105-4118.
GOVAERTS, Y. M., VERSTRAETE, M. M., PINTY, B. & GOBRON, N. 1999. Designing optimal spectral indices: a feasibility and proof of concept study. *International Journal of Remote Sensing.* **20** (9) 1853-1873.
GREEN, S. 27th May 2010. *RE: CORINE classes* Type to O' CONNOR, B.Teagasc,Kinsealy, Co. Dublin
GREEN, S. 25th July 2011. *RE: Growing degree days*Type to O' CONNOR, B.
GUISAN, A. & HARRELL, F. E. 2000. Ordinal Response Regression Models in Ecology. *Journal of Vegetation Science.* **11** (5) 617-626.
GUYON, D., GUILLOT, M., VITASSE, Y., CARDOT, H., HAGOLLE, O., DELZON, S. & WIGNERON, J.-P. 2011. Monitoring elevation variations in leaf phenology of deciduous broadleaf forests from SPOT/VEGETATION time-series. *Remote Sensing of Environment.* **115** (2) 615-627.
HELSEL, D. R. & HIRSCH, R. M. 2002. Correlation. *Statistical Methods in Water Resources Techniques of Water Resources Investigations.* U.S. Geological Survey
HEUMANN, B. W., SEAQUIST, J. W., EKLUNDH, L. & JONSSON, P. 2007. AVHRR derived phenological change in the Sahel and Soudan, Africa, 1982-2005. *Remote Sensing of Environment.* **108** (4) 385-392.
HIRD, J. N. & MCDERMID, G. J. 2009. Noise reduction of NDVI time series: An empirical comparison of selected techniques. *Remote Sensing of Environment.* **113** (1) 248-258.
HIRSCH, R. M. & SLACK, J. R. 1984. A Nonparametric Trend Test for Seasonal Data with Serial Dependence. *Water Resources Research.* **20** (6) 727-732.
HOLBEN, B. N. 1986. Characteristics of maximum-value composite images from temporal AVHRR data. *Int. J. Remote Sensing.* **7** (11) 1417-1434.
HOOKER, S. B., ESAIS, W., FELDMAN, G., GREGG, W. & MCCLAIN, C. 1992. An overview of SeaWiFS and ocean colour. *NASA Technical Memo.* 104566
HOPKINS, A. D. 1918. The bioclimatic law. *Monthly Weather Review.*
HUDSON DUNN, A. & DE BEURS, K. M. 2011. Land surface phenology of North American mountain environments using moderate resolution imaging spectroradiometer data. *Remote Sensing of Environment.* **115** (5) 1220-1233.
HUETE, A., DIDAN, K., MIURA, T., RODRIGUEZ, E. P., GAO, X. & FERREIRA, L. G. 2002. Overview of the radiometric and biophysical performance of the MODIS vegetation indices. *Remote Sensing of Environment.* **83** (1-2) 195-213.
HUETE, A. R. 1988. A Soil-Adjusted Vegetation Index (Savi). *Remote Sensing of Environment.* **25** (3) 295-309.
IPCC 2007. Climate Change 2007:Synthesis Report *Summary for Policymakers.*
IPG 2005. Phenological Observation Guide of the International Phenological Gardens. Revised version of the observation guide of 1960 ed.

JACKSON, J., KENT, C. & BORG, A. 2011. MERIS 99th Cyclic Report. 1st Edition ed.
JOHN HOPKINS UNIVERSITY 2011. Spectrum. *In:* SPECTRUM.GIF (ed.). Baltimore, Maryland.
JOINT RESEARCH CENTRE (JRC). 2011. *FAPAR Website* [Online]. Available: http://fapar.jrc.ec.europa.eu/WWW/Data/Pages/FAPAR_Algorithms/FAPAR_Algorithms_Fapar.php [Accessed 23rd June, 2011].
JÖNSSON, A. M., EKLUNDH, L., HELLSTRÖM, M., BÄRRING, L. & JÖNSSON, P. 2010. Annual changes in MODIS vegetation indices of Swedish coniferous forests in relation to snow dynamics and tree phenology. *Remote Sensing of Environment.* **114** (11) 2719-2730.
JÖNSSON, P. & EKLUNDH, L. 2002. Seasonality Extraction by Function Fitting to Time-Series of Satellite Sensor Data. *IEEE Transactions on Geoscience and Remote Sensing.* **40** (8) 1824-1832.
JÖNSSON, P. & EKLUNDH, L. 2004. TIMESAT—a program for analyzing time-series of satellite sensor data. *Computers & Geosciences.* **30** 833–845.
JULIEN, Y. & SOBRINO, J. A. 2009. Global land surface phenology trends from GIMMS database. *International Journal of Remote Sensing.* **30** (13) 3495–3513.
JUNG, M., VERSTRAETE, M., GOBRON, N., REICHSTEIN, M., PAPALE, D., BONDEAU, A., ROBUSTELLI, M. & PINTY, B. 2008. Diagnostic assessment of European gross primary production. *Global Change Biology.* **14** (10) 2349-2364.
JUSTICE, C. O., TOWNSHEND, J. R. G., HOLBEN, B. N. & TUCKER, C. J. 1985. Analysis of the phenology of global vegetation using meteorological satellite data. *International Journal of Remote Sensing.* **6** (8) 1271-1318.
KARLSEN, S. R., TOLVANEN, A., KUBIN, E., POIKOLAINEN, J., HØGDA, K. A., JOHANSEN, B., DANKS, F. S., ASPHOLM, P., WIELGOLASKI, F. E. & MAKAROVA, O. 2008. MODIS-NDVI-based mapping of the length of the growing season in northern Fennoscandia. *International Journal of Applied Earth Observation and Geoinformation.* **10** (3) 253-266.
KAUTH, R.J. & THOMAS, G.S. 1976. The tasseled Cap -- A Graphic Description of the Spectral-Temporal Development of Agricultural Crops as Seen by LANDSAT. *Proceedings of the Symposium on Machine Processing of Remotely Sensed Data*, Purdue University of West Lafayette, Indiana, pp. 4B-41 to 4B-51
KAWAMURA, K., AKIYAMA, T., YOKOTA, H.-O., TSUTSUMI, M. WATANABE, O. & WANG, S. 2004. Estimation model for NOAA/NDVI changes of meadow steppe in Inner Mongolia using meteorological data. *Grassland Science.* **49** (6) 547-554.
KAWAMURA, K., AKIYAMA, T., YOKOTA, H., TSUTSUMI, M., YASUDA, T., WATANABE, O. & WANG, S. 2005. Comparing MODIS vegetation indices with AVHRR NDVI for monitoring the forage quantity and quality in Inner Mongolia grassland, China. *Japanese Society of Grassland Science.* **51** 33–40
KEANE, T. & COLLINS, J. F. 2004. *Climate, Weather and Irish Agriculture,* Dublin, AGMET

KEELING, C. D., CHIN, J. F. S. & WHORF, T. P. 1996. Increased activity of northern vegetation inferred from atmospheric CO2 measurements. *Nature.* **382** (6587) 146-149.

LEITH, H. 1974. *Phenology and Seasonality Modeling*, Chapman and Hall, London, and Springer-Verlag, Berlin, Heidelberg, New York

LUPO, F., LINDERMAN, M., VANACKER, V., BARTHOLOMÉ, E. & LAMBIN, E. F. 2007. Categorization of land-cover change processes based on phenological indicators extracted from time series of vegetation index data. *International Journal of Remote Sensing.* **28** (11) 2469-2483.

MACCHERONE, B. 2011. *MODIS Home Page* [Online]. NASA. Available: http://modis.gsfc.nasa.gov/about/ [Accessed August 2nd, 2011].

MAIGNAN, F., BREON, F. M., BACOUR, C., DEMARTY, J. & POIRSON, A. 2008. Interannual vegetation phenology estimates from global AVHRR measurements: Comparison with in situ data and applications. *Remote Sensing of Environment.* **112** (2) 496-505.

MASIN, R., ZUIN, M. C. & ZANIN, G. 2005. Phenological observations on shrubs to predict weed emergence in turf. *International Journal of Biometeorology.* **50** (1) 23-32.

MATHER, P. M. 1999. *Computer processing of remotely-sensed images, an introduction*, John Wiley & Sons.

MATHWORKS 2009. MATLAB Help Manual. R2009a ed. Licence Number 161051.

MCCALLUM, I., WAGNER, W., SCHMULLIUS, C., SHVIDENKO, A., OBERSTEINER, M., FRITZ, S. & NILSSON, S. 2010. Comparison of four global FAPAR datasets over Northern Eurasia for the year 2000. *Remote Sensing of Environment.* **114** (5) 941-949.

MENGHUA, W. & WEI, S. 2006. Cloud Masking for Ocean Color Data Processing in the Coastal Regions. *Geoscience and Remote Sensing, IEEE Transactions on.* **44** (11) 3196-3105.

MENZEL, A. 2003. Plant phenological anomalies in Germany and their relation to air temperature and NAO. *Climatic Change.* **57** (3) 243-263.

MENZEL, A. & FABIAN, P. 1999. Growing season extended in Europe. *Nature.* **397** (6721) 659-659.

MENZEL, A., SPARKS, T. H., ESTRELLA, N., KOCH, E., AASA, A., AHAS, R., ALM-KUBLER, K., BISSOLLI, P., BRASLAVSKA, O., BRIEDE, A., CHMIELEWSKI, F. M., CREPINSEK, Z., CURNEL, Y., DAHL, A., DEFILA, C., DONNELLY, A., FILELLA, Y., JATCZA, K., MAGE, F., MESTRE, A., NORDLI, O., PENUELAS, J., PIRINEN, P., REMISOVA, V., SCHEIFINGER, H., STRIZ, M., SUSNIK, A., VAN VLIET, A. J. H., WIELGOLASKI, F. E., ZACH, S. & ZUST, A. 2006. European phenological response to climate change matches the warming pattern. *Global Change Biology.* **12** (10) 1969-1976.

MERIS 2006. MERIS Products Quality Status Report (MEGS7.4 and IPF 5). Paris, France: The MERIS Quality Working Group.

MET ÉIREANN. 2011a. *Degree Days* [Online]. Glasnevin Hill, Dublin 9, Ireland Available: http://www.met.ie/climate/degree-day.asp [Accessed 8th July 2011].

MET ÉIREANN. 2011b. *Met Éireann Monthly Weather Bulletin* [Online]. Met Éireann,Glasnevin Hill, Dublin 9, Ireland. Available: http://www.met.ie/climate/monthly-weather-bulletin.asp [Accessed 9th March, 2011].
MET ÉIREANN. 2010 AAgricultural Meteorology Unit, UNIT*Climate Change in Ireland. How do we predict the future climate?* [Online]. Met Éireann,. Available: www.met.ie [Accessed 28th January, 2011].
MONITORING AGRICULTURE WITH REMOTE SENSING (MARS). 2011. *MARS Bulletins for Europe* [Online]. Available: http://mars.jrc.ec.europa.eu/mars/About-us/AGRI4CAST/MARS-Bulletins-for-Europe [Accessed 24th June 2011].
MOULIN, S., KERGOAT, L., VIOVY, N. & DEDIEU, G. 1997. Global-Scale Assessment of Vegetation Phenology Using NOAA/AVHRR Satellite Measurements. *Journal of Climate.* **10** (6) 1154-1170.
NATIONAL BIODIVERSITY DATA CENTRE. 2009. *Irish Phenology Network* [Online]. National Biodiversity Data Centre. Available: http://phenology.biodiversityireland.ie/introduction/why-monitor-phenology/ [Accessed 2nd August 2011].
NICKESON, J. 2011. *Land Product Validation Subgroup* [Online]. NASA. Available: http://lpvs.gsfc.nasa.gov/ [Accessed 24th June 2011].
NIST/SEMATECH. 2011. *e-Handbook of Statistical Methods:Measures of Skewness and Kurtosis* [Online]. Available: http://www.itl.nist.gov/div898/handbook/ [Accessed 13th July, 2011].
O'CONNOR, B., DWYER, N. & CAWKWELL, F. 2008. Satellite remote sensing as a tool for monitoring vegetation seasonality. *In:* SPIE Europe Remote Sensing.Cardiff, Wales, United Kingdom.NEALE, C. M. U., OWE, M. & D'URSO, G., eds. 16th September, 2008.
O'SULLIVAN, K. 2009. *RE: Statistics and data analysis for postgraduate research students.*Course notes.Statistical Consultancy Unit, Dept. of Statistics,University College Cork
PALLÉ, E. & BUTLER, C. J. 2001. Sunshine records from Ireland: cloud factors and possible links to solar activity and cosmic rays. *International Journal of Climatology.* **21** (6) 709-729.
PARMESAN, C. 2007. Influences of species, latitudes and methodologies on estimates of phenological response to global warming. *Global Change Biology.* **13** (9) 1860-1872.
PEN. 2011. *Phenological Eyes Network (PEN)* [Online]. Available: http://pen.agbi.tsukuba.ac.jp/index_e.html [Accessed 14th February 2011].
PINTY, B., GOBRON, N., MÉLIN, F. & VERSTRAETE, M. 2002. A Time Composite Algorithm for FAPAR products, Theoretical Basis Document. EUR Report No. 20150 EN ed.: Institute for Environment and Sustainability, Joint Research Centre, Ispra, Italy.
PINTY, B. & VERSTRAETE, M. M. 1992. GEMI: a non-linear index to monitor global vegetation from satellites *Journal of Plant Ecology.* **101** (1).
PINTY, B. & VERSTRAETE, M. M. 1998. Modeling the scattering of light by homogeneous vegetation in optical remote sensing. *Journal of the Atmospheric Sciences.* **55** (2) 137-150.

PLUMMER, S. 2009. The ESA Climate Change Initiative: Description. 1st ed.: ESA/ESRIN.
PROCTOR, H. & DONNELLY, A. 2009. EPA report - Phenological Gardens in Ireland 2009 a review of the national network. Environmental Protection Agency (EPA) Ireland.
RAMOS, F. M., ROSA, R. R., NETO, C. R. & ZANANDREA, A. 2000. Generalized complex entropic form for gradient pattern analysis of spatio-temporal dynamics. *Physica A: Statistical Mechanics and its Applications.* **283** (1-2) 171-174.
RAST, M. & BEZY, J. L. 1999. The ESA Medium Resolution Imaging Spectrometer MERIS a review of the instrument and its mission. *International Journal of Remote Sensing.* **20** (9) 1681-1702.
REED, B. & BROWN, J. F. 2005. Trend Analysis of Time-series Phenology Derived from Satellite Data. *Ieee Transactions on Geoscience and Remote Sensing.* 166-168.
REED, B., BROWN, J. F., VANDERZEE, D., T.R., L., MERCHANT, J. W. & OHLEN, D. O. 1994. Measuring Phenological Variability from Satellite Imagery. *Journal of Vegetation Science.* **5** (5) 703-714.
RICHARDS, D. 3/11/2009. *RE: Cloud Mask Product Query*Type to O' CONNOR, B.User Service Helpdesk, EUMETSAT User Service,
RICHARDSON, A. D., BRASWELL, B. H., FRIEDL, M. A., HOLLINGER, D. Y., OLLINGER, S. V. & JENKINS, J. P. 2011. *Phenocam: Improving our understanding of vegetation phenology with a canopy camera network* [Online]. Available: http://klima.sr.unh.edu/ [Accessed 14th February, 2011].
ROHAN, P. K. 1986. *The Climate of Ireland*, Meteorological Service, Dublin
ROTZER, T. & CHMIELEWSKI, F. M. 2001. Phenological maps of Europe. *Climate Research.* **18** (3) 249-257.
ROTZER, T., GROTE, R. & PRETZSCH, H. 2004. The timing of bud burst and its effect on tree growth. *International Journal of Biometeorology.* **48** (3) 109-118.
RUXTON, G. D. & BEAUCHAMP, G. 2008. Some suggestions about appropriate use of the Kruskal-Wallis test. *Animal Behaviour.* **76** (3) 1083-1087.
SAKAMOTO, T., YOKOZAWA, M., TORITANI, H., SHIBAYAMA, M., ISHITSUKA, N. & OHNO, H. 2005. A crop phenology detection method using time-series MODIS data. *Remote Sensing of Environment.* **96** (3-4) 366-374.
SANTER, R., CARRÈRE, V., DESSAILLY, D., DUBUISSON, P. & ROGER, J. C. 1997. Pixel Identification, Algorithm Theoretical Basis Document: . Laboratoire de Physique Appliquée aux Milieux Océaniques et Côtiers (PAMOC), Université du Littoral-Côte d'Opale, Wimereux, France.
SCHROEDTER-HOMSCHEIDT, M., DREWS, A. & HEISE, S. 2008. Total water vapor column retrieval from MSG-SEVIRI split window measurements exploiting the daily cycle of land surface temperatures. *Remote Sensing of Environment.* **112** (1) 249-258.
SCHWARTZ, M. D., AHAS, R. & AASA, A. 2006. Onset of spring starting earlier across the Northern Hemisphere. *Global Change Biology.* **12** (2) 343-351.

SCHWARTZ, M. D. & REITER, B. E. 2000. Changes in North American spring. *International Journal of Climatology.* **20** (8) 929-932.
SEDAC. 2011. *Remote Sensing tutorial* [Online]. U.S. National Aeronautics and Space Administration. Available: http://sedac.ciesin.org/tg/guide_glue.jsp?rd=rs&ds=3 [Accessed 12th May 2011].
SEIXAS, J., CARVALHAIS, N., NUNES, C. & BENALI, A. 2009. Comparative analysis of MODIS-FAPAR and MERIS-MGVI datasets: Potential impacts on ecosystem modeling. *Remote Sensing of Environment.* **113** (12) 2547-2559.
SOUDANI, K., LE MAIRE, G., DUFRENE, E., FRANCOIS, C., DELPIERRE, N., ULRICH, E. & CECCHINI, S. 2008. Evaluation of the onset of green-up in temperate deciduous broadleaf forests derived from Moderate Resolution Imaging Spectroradiometer (MODIS) data. *Remote Sensing of Environment.* **112** (5) 2643-2655.
SPARKS, T. H., JEFFREE, E. P. & JEFFREE, C. E. 2000. An examination of the relationship between flowering times and temperature at the national scale using long-term phenological records from the UK. *International Journal of Biometeorology.* **44** (2) 82-87.
STÖCKLI, R. & VIDALE, P. L. 2004. European plant phenology and climate as seen in a 20-year AVHRR land-surface parameter dataset. *International Journal of Remote Sensing.* **25** (17) 3303 - 3330.
STUDER, S., STÖCKLI, R., APPENZELLER, C. & VIDALE, P. 2007. A comparative study of satellite and ground-based phenology. *International Journal of Biometeorology.* **51** (5) 405-414.
SWEENEY, J., ALBANITO, F., BRERETON, A., CAFFARRA, A., CHARLTON, R., DONNELLY, A., FEALY, R., FITZGERALD, J., HOLDEN, N., JONES, M. & MURPHY, C. 2008. Climate Change –Refining the Impacts for Ireland. *STRIVE Report.* Environmental Protection Agency, Ireland.
SWEENEY, J., DONNELLY, A., MCELWAIN, A. & JONES, M. 2002. Climate Change: Indicators for Ireland (Final Report). *In:* ENVIRONMENTAL PROTECTION AGENCY (ed.) *Environmental RTDI Programme 2000–2006.*
THACKERAY, S. J., SPARKS, T. H., FREDERIKSEN, M., BURTHE, S., BACON, P. J., BELL, J. R., BOTHAM, M. S., BRERETON, T. M., BRIGHT, P. W., CARVALHO, L., CLUTTON-BROCK, T., DAWSON, A., EDWARDS, M., ELLIOTT, J. M., HARRINGTON, R., JOHNS, D., JONES, I. D., JONES, J. T., LEECH, D. I., ROY, D. B., SCOTT, W. A., SMITH, M., SMITHERS, R. J., WINFIELD, I. J. & WANLESS, S. 2010. Trophic level asynchrony in rates of phenological change for marine, freshwater and terrestrial environments. *Global Change Biology.* **16** (12) 3304-3313
THAYN, J. B. & PRICE, K. P. 2008. Julian dates and introduced temporal error in remote sensing vegetation phenology studies. *International Journal of Remote Sensing.* **29** (20) 6045-6049.
TORRA, V., DOMINGO-FERRER, J., MATEO-SANZ, J. M. & NG, M. 2006. Regression for ordinal variables without underlying continuous variables. *Information Sciences.* **176** (4) 465-474.

TOWNSHEND, J. R. G., GOFF, T. E. & TUCKER, C. J. 1985. Multitemporal Dimensionality of Images of Normalized Difference Vegetation Index at Continental Scales. *Ieee Transactions on Geoscience and Remote Sensing.* **23** (6) 888-895.

USA NPN. 2011. *Development of the USA National Phenology Network* [Online]. USA National Phenology Network, National Coordinating Office,1955 E. Sixth St., Tucson, AZ 85721. Available: http://www.usanpn.org/archive/history [Accessed 26th May, 2011].

VAN LEEUWEN, W. 2008. Monitoring the Effects of Forest Restoration Treatments on Post-Fire Vegetation Recovery with MODIS Multitemporal Data. *Sensors.* **8** (3) 2017-2042.

VAN LEEUWEN, W. J. D., HUETE, A. R. & LAING, T. W. 1999. MODIS Vegetation Index Compositing Approach: A Prototype with AVHRR Data. *Remote Sensing of Environment.* **69** (3) 264-280.

VAN VLIET, A. J. H., OVEREEM, A., et al. 2002. The influence of temperature and climate change on the timing of pollen release in the Netherlands. *International Journal of Climatology* **22** (14) 1757-1767.

VEGETATION INDEX AND PHENOLOGY (VIP) RESEARCH GROUP. 2011. *Remote sensing based phenology and nuances* [Online]. Tucson, Arizona: University of Arizona. Available: http://vip.arizona.edu/VIP_LSP_Semantics.php [Accessed 24th January].

VERBESSELT, J., HYNDMAN, R., ZEILEIS, A. & CULVENOR, D. 2010. Phenological change detection while accounting for abrupt and gradual trends in satellite image time series. *Remote Sensing of Environment.* **114** (12) 2970-2980.

VERMOTE, E. F., TANRE, D., DEUZE, J. L., HERMAN, M. & MORCRETTE, J. J. 1997. Second Simulation of the Satellite Signal in the Solar Spectrum, 6S: An overview. *Ieee Transactions on Geoscience and Remote Sensing.* **35** (3) 675-686.

VERSTRAETE, M. M., GOBRON, N., AUSSEDAT, O., ROBUSTELLI, M., PINTY, B., WIDLOWSKI, J.-L. & TABERNER, M. 2008. An automatic procedure to identify key vegetation phenology events using the JRC-FAPAR products. *Advances in Space Research.* **41** (11) 1773-1783.

VERSTRAETE, M. M. & PINTY, B. 1996. Designing optimal spectral indexes for remote sensing applications. *Ieee Transactions on Geoscience and Remote Sensing.* **34** (5) 1254-1265.

WADE, T. & SOMMER, S. (eds.) 2006. *A to Z GIS,* Redlands, California: ESRI Press.

WALSH, S. 22nd June 2010. *RE: UCC/Met Éireann seasonality-climate correlation study*Type to O' CONNOR, B.

WALSH, S. 2nd August 2011. *RE: Error in interpolated temperature grids*Type to O' CONNOR, B.

WARDLOW, B. D., EGBERT, S. L. & KASTENS, J. H. 2007. Analysis of time-series MODIS 250 m vegetation index data for crop classification in the US Central Great Plains. *Remote Sensing of Environment.* **108** (3) 290-310.

WESSELS, K., STEENKAMP, K., VON MALTITZ, G. & ARCHIBALD, S. 2010. Remotely sensed vegetation phenology for describing and predicting the biomes of South Africa. *Applied Vegetation Science.* 1-19.

WHITE, M. A., DE BEURS, K. M., DIDAN, K., INOUYE, D. W., RICHARDSON, A. D., JENSEN, O. P., O'KEEFE, J., ZHANG, G., NEMANI, R. R., VAN LEEUWEN, W. J. D., BROWN, J. F., DE WIT, A., SCHAEPMAN, M., LIN, X. M., DETTINGER, M., BAILEY, A. S., KIMBALL, J., SCHWARTZ, M. D., BALDOCCHI, D. D., LEE, J. T. & LAUENROTH, W. K. 2009. Intercomparison, interpretation, and assessment of spring phenology in North America estimated from remote sensing for 1982-2006. *Global Change Biology.* **15** (10) 2335-2359.

WHITE, M. A., HOFFMAN, F., HARGROVE, W. W. & NEMANI, R. R. 2005. A global framework for monitoring phenological responses to climate change. *Geophysical Research Letters.* **32** (4) -.

WHITE, M. A., THORNTON, P. E. & RUNNING, S. W. 1997. A continental phenology model for monitoring vegetation responses to interannual climatic variability. *Global Biogeochemical Cycles.* **11** (2) 217-234.

WIELGOLASKI, F. E. 1999. Starting dates and basic temperatures in phenological observations of plants. *International Journal of Biometeorology.* **42** (3) 158-168.

WILLMOTT, C. 1982. Some Comments on the Evaluation of Model Performance. *Bulletin American Meteorological Society.* **63** (11).

XIAO, J. & MOODY, A. 2005. Geographical distribution of global greening trends and their climatic correlates: 1982-1998. *International Journal of Remote Sensing.* **26** (11) 2371-2390.

YANG, W., SHABANOV, N. V., HUANG, D., WANG, W., DICKINSON, R. E., NEMANI, R. R., KNYAZIKHIN, Y. & MYNENI, R. B. 2006. Analysis of leaf area index products from combination of MODIS Terra and Aqua data. *Remote Sensing of Environment.* **104** (3) 297-312.

ZHANG, X., FRIEDL, M. A., SCHAAF, C. B., STRAHLER, A. H., HODGES, J. C. F., GAO, F., REED, B. C. & HUETE, A. 2003. Monitoring vegetation phenology using MODIS. *Remote Sensing of Environment.* **84** (3) 471-475.

ZHANG, X. Y., FRIEDL, M. A., SCHAAF, C. B. & STRAHLER, A. H. 2004a. Climate controls on vegetation phenological patterns in northern mid- and high latitudes inferred from MODIS data. *Global Change Biology.* **10** (7) 1133-1145.

ZHANG, X. Y., FRIEDL, M. A., SCHAAF, C. B., STRAHLER, A. H. & SCHNEIDER, A. 2004b. The footprint of urban climates on vegetation phenology. *Geophysical Research Letters.* **31** (12) -.

ZURITA-MILLA, R., CLEVERS, J. G. P. W., SCHAEPMAN, M. E. & KNEUBUEHLER, M. 2007. Effects of MERIS L1b radiometric calibration on regional land cover mapping and land products. *International Journal of Remote Sensing.* **28** (3) 653-673.

ZURITA-MILLA, R., KAISER, G., CLEVERS, J. G. P. W., SCHNEIDER, W. & SCHAEPMAN, M. E. 2009. Downscaling time series of MERIS full resolution data to monitor vegetation seasonal dynamics. *Remote Sensing of Environment.* **113** (9) 1874-1885.

Appendix A: Fieldwork observations and field journal

33 trees (17/4/08)	**Beech**						**Birch**						**Oak**						
Name	Be1	be2	be3	be4	be5	be6	bi1	bi2	bi3	bi4	bi5	bi6	Oak1	Oak 2	Oak3	Oak4	Oak5	Oak 6	Oak 7
Age	M	m	o	o	o	m	o	o	o	o	Y	Y	O	O	M	Y	~	Y	o
Orientation	N	n	ne	ne	ne	se	n	?	w	n	N	ne	N	N	Ne	W	~	W	n
Height (ft.)	50	50+	40	40	40	50	20	30	15	30	25	20	40	30	40	15	30	30	40
Loc	Ent	Pth	Pth left	Pth left	Pth left	Pth left	Cp	Pth right	Pth right	Cp	Cp	Pth right on bank	Pth left	Pth left	Pth left	Pth left	Pth left	Pth right	Pth left

Sycamore						**Ash**			**HC**		**Other**		
Syc 1	Syc 2	Syc3	Syc 4	Syc 5	Syc6	Ash1	Ash 2	Ash 3	Hc1	Hc2	Un1	Un2	Un 3
Y	M	M	O	Y	y	O	O	Y	Y	O	o	y	Y
Sw	Sw	~	Sw	w	w	Ne	Ne	S	Sw	Sw	N	Ne	N
20	~	40	30	25	20	35	40	25	20	35	45	30	30
~	Pth right	Pth right	Pth right	Pth left	Pth right	Pth left	Pth left	Pth right	Pth right	Pth left	Ent right	Pth right	Road right

m:mature, o:old, y:young, n:north, ne:northeast, se:southeast, ent:entrance to path, pth: pathway, cp:carpark, Un: Unidentified

2008

9/4/08	Be1	Be2	Be3	Be4	Be5	Be6	Bi1	Bi2	Bi3	Bi4	Bi5	Bi6	oak1	oak2	oak3	oak4	oak5	oak6	Oak7	Syc1	Syc2	Syc3	Syc4	Syc5	Syc6	Ash1	Ash2	Ash3	Ash4	Ash5	Ash6	Hc1	Hc2	Hc3	Hc4	Hc5	Hc6	Un1	Un2	Un3
%leafout	0	0	0	0	0	0	30		0	60	0	10	50	60	10	20	30	40	40	50	0	10	5	5		0	0	0				70	60					0	0	0
%budburst	d	d	40	d	30	d	90		20	90	10	70	90	90	90	90	90	90	90	90	90	90	90	90		D	D	D				90	90					50	d	D

d: dormant

17/4/08	Be1	Be2	Be3	Be4	Be5	Be6	Bi1	Bi2	Bi3	Bi4	Bi5	Bi6	oak1	oak2	oak3	oak4	oak5	oak6	Oak7	Syc1	Syc2	Syc3	Syc4	Syc5	Syc6	Syc7	Ash1	Ash2	Ash3	Ash4	Ash5	Ash6	Hc1	Hc2	Hc3	Hc4	Hc5	Hc6	Un1	Un2	Un3	Un4	Un5
%leafout	0	0	10	0	10	0	30	80			0		50	60	20	50	60	80		50	0	50	0	50	30	50	0	0	0				90	90					0	10	0	20	0
%budburst	D	90	90	90	90	50	90	90			50		90	90	90	90	90	90		90	90	90	70	90	90	90	50	50	50				90	90					90	90	d	90	80

d: dormant

24/4/08	Be1	Be2	Be3	Be4	Be5	Be6	Bi1	Bi2	Bi3	Bi4	Bi5	Bi6	oak1	oak2	oak3	oak4	oak5	oak6	oak7	Syc1	Syc2	Syc3	Syc4	Syc5	Syc6	Syc7	Ash1	Ash2	Ash3	Ash4	Ash5	Ash6	Hc1	Hc2	Hc3	Hc4	Hc5	Hc6	Un1	Un2	Un3	Un4	Un5
%leafout	10	5	0	0	10	0	40	60			10		60	70	60	20	50	50	60	40	0	40	10	30	30	20	0	0	0				90	90					0	0	0	30	
%budburst	90	90	90	90	90	90	90	90			90		90	90	90	90	90	90	90	90	90	90	90	90	90	90	d	50	D				90	90					90	90	90	90	

1/5/08	Be1	Be2	Be3	Be4	Be5	Be6	Bi1	Bi2	Bi3	Bi4	Bi5	Bi6	oak1	oak2	oak3	oak4	oak5	oak6	oak7	Syc1	Syc2	Syc3	Syc4	Syc5	Syc6	Syc7	Ash1	Ash2	Ash3	Ash4	Ash5	Ash6	Hc1	Hc2	Hc3	Hc4	Hc5	Hc6	Un1	Un2	Un3	Un4	Un5
%leafout	30	20	40	0	0	30	40				20		60	70	40	70	80	90		80	10	80	30	80	80	70	0						100	100					10	0	10	70	0
%budburst	90	90	90	60	70	90	90				90		90	90	90	90	90	90		90	90	90	90	90	90	90	D						100	100					90	90	70	90	60

Un.2=sycamore, Un4=beech, Un5=beech

7/5/08	Be1	Be2	Be3	Be4	Be5	Be6	Bi1	Bi2	Bi3	Bi4	Bi5	Bi6	oak1	oak2	oak3	oak4	oak5	oak6	oak7	Syc1	Syc2	Syc3	Syc4	Syc5	Syc6	Syc7	Ash1	Ash2	Ash3	Ash4	Ash5	Ash6	Hc1	Hc2	Hc3	Hc4	Hc5	Hc6	Un1	Un2	Un3	Un4	Un5
%leafout	90	90	90	30	60	80	90				60		80	100	90	60	80	90	100	100	30	90	90	90	80		10						100	100					70	30	10		30
%budburst	90	90	90	90	90	90	90				90		90			90	90	90	100		90	90	90				90						100	100					90	90	90		80

14/5/08	Be1	Be2	Be3	Be4	Be5	Be6	Bi1	Bi2	Bi3	Bi4	Bi5	Bi6	oak1	oak2	oak3	oak4	oak5	oak6	oak7	Syc1	Syc2	Syc3	Syc4	Syc5	Syc6	Syc7	Ash1	Ash2	Ash3	Ash4	Ash5	Ash6	Hc1	Hc2	Hc3	Hc4	Hc5	Hc6	Un1	Un2	Un3	Un4	Un5
%leafout	100	90	90	90	90	100	90		80		80	80	80	80		80	90	100		100	70	100	90	90	100				50										90	70	50		
%budburst	100	100	100	100	100	100	90		90		90	90	90	90		90	100	100		100	90	100	100	100	100				90										90	90	90		

Be7: 80% leafout Un 3: El

22/5/08	Be1	Be2	Be3	Be4	Be5	Be6	Be7	Bi1	Bi2	Bi3	Bi4	Bi5	oak1	oak2	oak3	oak4	oak5	oak6	oak7	Syc1	Syc2	Syc3	Syc4	Syc5	Syc6	Syc7	Ash1	Ash2	Ash3	Ash4	Ash5	Ash6	Hc1	Hc2	Hc3	Hc4	Hc5	Hc6	Un1	Un2	Un3
%leafout	100	100	100	100	100	100	100	100				100	100	100	100	100	100	100		100	100	100	100	100	100	100	90						100	100					100	90	80
%budburst	100	100	100	100	100	100	100	100				100	100	100	100	100	100	100		100	100	100	100	100	100	100	100						100	100					100	100	100

Be7=bi6

30/5/08	Be1	Be2	Be3	Be4	Be5	Be6	Bi1	Bi2	Bi3	Bi4	Bi5	oak1	oak2	oak3	oak4	oak5	oak6	oak7	Syc1	Syc2	Syc3	Syc4	Syc5	Syc6	Ash1	Ash2	Ash3	Ash4	Ash5	Ash6	Hc1	Hc2	Hc3	Hc4	Hc5	Hc6	Un1	Un2	Un3
%leafout	100	100	100	100	100	100	100	100	100	100	100	100	100	100	100	100	100	100	100	100	100	100	100		100						100	100					100	100	100
%budburst	100	100	100	100	100	100	100	100	100	100	100	100	100	100	100	100	100	100	100	100	100	100	100		100						100	100					100	100	100

Be7=bi6

2009

18/2/09	Be1	Be2	Be3	Be4	Be5	Bi1	Bi2	Bi3	Bi4	Bi5	oak1	oak2	oak3	oak4	oak5	Syc1	Syc2	Syc3	Syc4	Syc5	Ash1	Ash2	Ash3	Ash4	Ash5	Hc1	Hc2
%Budburst	d	d	d	d	d	d	d	d	d	d	d	d	d	d	d	50	50	d	50	d	d	d	d	d	d	30	30

d: dormant

3/3/09	Be1	Be2	Be3	Be4	Be5	Bi1	Bi2	Bi3	Bi4	Bi5	oak1	oak2	oak3	oak4	oak5	Syc1	Syc2	Syc3	Syc4	Syc5	Ash1	Ash2	Ash3	Ash4	Ash5	Hc1	Hc2
%Budburst	d	d	d	d	d	d	d	d	d	d	d	d	d	d	d	100	100	100	100	100	d	d	d	d	d	100	100
% Leafout																20				20							

d: dormant

18/3/09	Be1	Be2	Be3	Be4	Be5	Bi1	Bi2	Bi3	Bi4	Bi5	oak1	oak2	oak3	Syc1	Syc2	Syc3	Syc4	Syc5	Ash1	Ash2	Ash3	Ash4	Ash5	Hc1	Hc2
%Budburst	d	d	d	d	d	d	d	d	d	d	d	50	d	100	100	100	100	100	d	d	d	d	d	100	100
% Leafout												0		40	20	0	0	20						30	20

d: dormant, European Larch: 30% leaflets emerged

24/3/09	Be1	Be2	Be3	Be4	Be5	Bi1	Bi2	Bi3	Bi4	Bi5	oak 1	oak 2	oak 3	Syc 1	Syc 2	Syc 3	Syc 4	Syc 5	Ash 1	Ash 2	Ash 3	Ash 4	Ash 5	Hc 1	Hc 2
%Budburst	d	d	d	d	d	50	50	70	90	100	50	100	100	100	100	100	100	100	d	d	d	d	d	100	100
% Leafout	0	0	0	0	0	0	0	0	0	10	0	10	10	50	30	0	10	30	0	0	0	0	0	50	30

d: dormant

European Larch: 50% leaflets emerged

30/3/09	Be1	Be2	Be3	Be4	Be5	Bi1	Bi2	Bi3	Bi4	Bi5	oak 1	oak 2	oak 3	Syc 1	Syc 2	Syc 3	Syc 4	Syc 5	Ash 1	Ash 2	Ash 3	Ash 4	Ash 5	Hc 1	Hc 2
%Budburst	10	10	10	10	n/a	70	70	100	100	100	100	100	100	100	100	100	100	100	d	d	d	d	d	100	100
% Leafout	0	0	0	0	0	0	0	0	0	20	0	30	20	60	40	00	20	40	0	0	0	0	0	60	40

d: dormant

06/4/09	Be1	Be2	Be3	Be4	Be5	Bi1	Bi2	Bi3	Bi4	Bi5	oak 1	oak 2	oak 3	Syc 1	Syc 2	Syc 3	Syc 4	Syc 5	Ash 1	Ash 2	Ash 3	Ash 4	Ash 5	Hc 1	Hc 2
%Budburst	20	20	20	20	n/a	100	90	100	100	100	100	100	100	100	100	100	100	100	d	d	d	d	d	100	100
% Leafout	0	0	0	0	0	20	10	10	10	60	20	50	60	80	40	10	50	60	0	0	0	0	0	80	60

d: dormant

14/4/09	Be1	Be2	Be3	Be4 south	Be5	Bi1	Bi2	Bi3	Bi4	Bi5	oak 1	oak 2	oak 3	Syc 1	Syc 2	Syc 3	Syc 4	Syc 5	Ash 1	Ash 2	Ash 3	Ash 4	Ash 5	Hc 1	Hc 2
%Budburst	50	30	20	40	n/a	100	100	100	n/a	100	100	100	100	100	100	n/a	100	100	30 *	30	30	n/a	n/a	100	100
% Leafout	10	0	0	0	0	40	30	10		80	40	60	80	90	60		60	70	0	0	0	0	0	90	70

20/4/09	Be1	Be2	Be3	Be4 south	Be5	Bi1	Bi2	Bi3	Bi4	Bi5	oak 1	oak 2	oak 3	Syc 1	Syc 2	Syc 3	Syc 4	Syc 5	Ash 1	Ash 2	Ash 3	Ash 4	Ash 5	Hc 1	Hc 2
%Budburst	60	30	20	40(not found)	n/a	100	100	100	n/a	100	100	100	100	100	100	100	100	100	30 *	30	30	n/a	n/a	100	100
% Leafout	20	0	0	0	0	50	40	30		90	60	80	90	90	80	30	80	90	0	0	0	0	0	100	90

d: dormant * Ash flowering

27/4/09	Be1	Be2	Be3	Be4 (original)	Be5	Bi1	Bi2	Bi3	Bi4	Bi5	oak1	oak2	oak3	Syc1	Syc2	Syc3	Syc4	Syc5	Ash1	Ash2	Ash3	Ash4	Ash5	Hc1	Hc2
%Budburst	100	50	50	100	n/a	100	100	100	n/a	100	100	100	100	100	100	100	100	100	50*	50	50	n/a	n/a	100*	100
% Leafout	50	10	30	50	0	70	60	50		100	80	90	100	100	90	50	90	100	20	20	0	0	0	100	100

- 1st swallow
- Ash flowering, HC flowering
- d: dormant

5/5/09	Be1	Be2	Be3	Be4 (original)	Be5	Bi1	Bi2	Bi3	Bi4	Bi5	oak 1	oak 2	oak 3	Syc 1	Syc 2	Syc 3	Syc 4	Syc 5	Ash 1	Ash 2	Ash 3	Ash 4	Ash 5	Hc1	Hc2
%Budburst	100	90	100	100	n/a	100	100	100	n/a	100	100	100	100	100	100	100	100	100	60*	100	100	n/a	n/a	100*	100
% Leafout	100	50	80	100	0	90	100	100		100	90	100	100	100	100	80	100	100	20	30	30	0	0	100	100

11/5/09	Be1	Be2	Be3	Be4 (original)	Be5	Bi1	Bi2	Bi3	Bi4	Bi5	oak 1	oak 2	oak 3	Syc 1	Syc 2	Syc 3	Syc 4	Syc 5	Ash 1	Ash 2	Ash 3	Ash 4	Ash 5	Hc 1	Hc2
%Budburst	100	100	100	100	n/a	100	100	100	n/a	100	100	100	100	100	100	100	100	100	100 *	100	100	n/a	n/a	100 *	100
% Leafout	100	100	100	100	0	100	100	100		100	100	100	100	100	100	90	100	100	30	50	50	0	0	100	10 0

26/5/09	Be1	Be2	Be3	Be4	Bi1	Bi2	Bi3	Bi4	Bi5	oak1	oak2	oak3	Syc1	Syc2	Syc3	Syc4	Syc5	Ash1	Ash2	Ash3	Hc1	Hc2
%Budburst	100	100	100	100	100	100	100	n/a	100	100	100	100	100	100	100	100	100	100*	100	100	100*	100
% Leafout	100	100	100	100	100	100	100		100	100	100	100	100	100	100	100	100	70	90	90	100	100

*Facing Crosshaven

- Bb=budburst (Ash buds surrounded by feather-like flowers)
- n/=not checked

2010

4/3/10	Be1	Be2	Be3	Be4	Be5	Bi1	Bi2	Bi3	Bi4	Bi5	oak 1	oak 2	oak 3	oak 4	oak 5	Syc 1	Syc 2	Syc 3	Syc 4	Syc 5	Ash 1	Ash 2	Ash 3	Ash 4	Ash 5	Hc 1	Hc 2
%Budburst	d	d	d	d	d	d	d	d	d	d	d	d	d	d	d	100	100	100	100	100	d	d	d	d	d	d	d
% Leafout																											

d: dormant

- Bi beginning to show some elongation of buds but no greening
- Be showing same effect but only at top of canopy
- Syc has green tips on all the buds
- HC shows thick buds but no greening
- Ash and Oak are dormant

25/3/10	Be1	Be2	Be3	Be4	Be5	Bi1	Bi2	Bi3	Bi4	Bi5	oak 1	oak 2	oak 3	oak 4	oak 5	Syc 1	Syc 2	Syc 3	Syc 4	Syc 5	Ash 1	Ash 2	Ash 3	Ash 4	Ash 5	Hc 1	Hc 2
%Budburst	d	d	d	d	d	d	d	100	100	100	d	d	d	d	d	100	100	100	100	100	d	d	d	d	d	d	d
% Leafout																20				10						30	10

d: dormant

- Honeysuckle leafing since last week
- Cherry blossom emerged in last few days
- These are part of understorey greening
- Syc is all green buds with a few inches of bud extended but only a few have leaves unfolded
- Bi buds have green tips but no elongation or signs of leaf unfolding
- Be tips are getting thicker

- Oak buds thickening
- HC buds very thick and leaves unfolded in several buds

8/4/10	Be1	Be2	Be3	Be4	Be5	Bi1	Bi2	Bi3	Bi4	Bi5	oak 1	oak 2	oak 3	oak 4	oak 5	Syc 1	Syc 2	Syc 3	Syc 4	Syc 5	Ash 1	Ash 2	Ash 3	Ash 4	Ash 5	Hc 1	Hc 2
%Budburst	d	d	d	d	d	d	50	100	100	100	d	d	d	d	d	100	100	100	100	100	d	d	d	d	d	d	d
% Leafout									10							30	40		10	20						40	20

d: dormant

- Cherry blossom in full bloom
- Syc is all green buds with a few inches of bud extended and many leaves unfolded
- Bi buds have green tips on smaller trees
- Signs of leaf unfolding on mature trees and some still dormant
- HC buds burst and leaves unfolded

22/4/10	Be1	Be2	Be3	Be4	Be5	Bi1	Bi2	Bi3	Bi4	Bi5	oak 1	oak 2	oak 3	oak 4	oak 5	Syc 1	Syc 2	Syc 3	Syc 4	Syc 5	Ash 1	Ash 2	Ash 3	Ash 4	Ash 5	Hc 1	Hc2
%Budburst			d	d			100	100	100	100				d	d	100	100	100	100	100	bb	bb	bb	n/	n/	d	d
% Leafout	10	10			50*	20	30	50	20		20	30	20	n/	n/	50	50	30	20	60						60	50

d: dormant

29/4/10	Be1	Be2	Be3	Be4	Be5	Bi1	Bi2	Bi3	Bi4	Bi5	oak 1	oak 2	oak 3	oak 4	oak 5	Syc 1	Syc 2	Syc 3	Syc 4	Syc 5	Ash 1	Ash 2	Ash 3	Ash4	Ash5	Hc1	Hc2
%Budburst			d	d			100	100	100	100				d	d	100	100	100	100	100	bb	bb	bb	n	n/	d	d
% Leafout	40	20	20	20	70*	30	50	70	50	n/a	40	40	50	n/	n/	70	70	50	n/a	80		10	10			80	70

d: dormant

7/5/10	Be1	Be2	Be3	Be4	Be5	Bi1	Bi2	Bi3	Bi4	Bi5	oak 1	oak 2	oak 3	oak 4	oak 5	Syc 1	Syc 2	Syc 3	Syc 4	Syc 5	Ash 1	Ash 2	Ash 3	Ash 4	Ash 5	Hc 1	Hc 2
%Budburst			d	d			100	100	100	100				d	d	100	100	100	100	100	bb	bb	bb	n/	n/	d	d
% Leafout	60	50	50	50	80*	50	60	80	70	n/a	50	60	70	n/	n/	90	90	70	n/a	100	10	20	30			90	80

d: dormant

14/5/10	Be1	Be2	Be3	Be4	Be5	Bi1	Bi2	Bi3	Bi4	Bi5	oak 1	oak 2	oak 3	oak 4	oak 5	Syc 1	Syc 2	Syc 3	Syc 4	Syc 5	Ash 1	Ash 2	Ash 3	Ash 4	Ash 5	Hc 1	Hc 2
%Budburst							100	100	100	100						100	100	100	100	100				n/	n/		
% Leafout	80	100	100	100	100 *	70	80	90	90	n/a	80	70	90	n/	n/	100	100	90	n/a	100	20	30	40			100	90

*Facing Crosshaven

- n/=not checked

3/6/10	Be1	Be2	Be3	Be4	Be5	Bi1	Bi2	Bi3	Bi4	Bi5	oak 1	oak 2	oak 3	oak 4	oak 5	Syc 1	Syc 2	Syc 3	Syc 4	Syc 5	Ash 1	Ash 2	Ash 3	Ash 4	Ash 5	Hc 1	Hc 2
%Budburst							100	100	100	100						100	100	100	100	100				n/	n/		
% Leafout	80	100	100	100	100 *	70	80	90	90	n/a	80	70	90	n/	n/	100	100	90	n/a	100	20	30	40			100	90

Field Work Journal:

13/3/08

Oak, no budburst. Beech and birch, no budburst observed. Ash no budburst. European larch identified as first deciduous conifer.

20/3/08:(accompanied by ND)

Undergrowth has grown along path margins. Coniferous high forest is continually green. Birch is budding and leafing out, the level of development varies according to the part of the forest and the age of the tree, it can be difficult to identify when catkins are absent. Beech showing no sign of budburst yet. Horse Chestnut has leafed out to full extent in some trees and budburst has occurred in all trees. Oak is budding/leafing. Sycamore is budding; leaves are beginning to emerge. European Larch always green. No Ash specimens taken. The forest in overall state of transition. A few unidentified twigs remain from those collected.

27/3/08:(accompanied by ND, PW)

Sunny, blue sky. Cold.

Wood has undergone more greening since last week, birch has undergone budburst in all observed trees and some have undergone leafout. Oak, horse chestnut, thorny shrubs (black/white thorn) have leafed out. Beech is still dormant. Sycamore buds are bursting and would expect to see leaves emerging in coming days. Rowan has been observed this week and last week but it has yet to undergo budburst. Conifers remain unidentifiable except for European larch which is fully green except for some unhealthy trees, Scots Pine observed for the first time. The undergrowth (scrub) has begun to green up significantly in the

continuing absence of a canopy cover and would expect to see this mature in coming weeks. Ivy, Holly and other unidentified creepers (e.g. Scotsman's Beard) are abundant. For some species, Sycamore, Birch etc., juvenile trees appear to bud before mature trees. Budburst and leafout occur according to the forcing of both water and light, both factors affect the rate of bud development. For example, buds nearer the ground respond to the availability of water in close proximity and emerge first, whereas buds higher up are more responsive to light. This, as well as the tree's orientation, creates a differential response in buds on the same tree to the competing effects of water and light, buds of the same tree emerge at different times.

To Do:

- Tag representative trees from each species (½ dozen or so)

  Birch, Beech, Oak, Sycamore, Horse Chestnut, Ash, Rowan, Thorny shrub, European Larch.
- Tag individual branches on tree and count number of buds emerged and leaves out.

Observations to note:

- Orientation of tree (north facing etc.)
- Age of tree
- Health of tree
- % of buds emerged
- % of leaves fully out
- Canopy appearance on approach to Woods (% greening)

Calculations:

% of conifers/deciduous in land cover of Wood.

2/4/08

Sunny, intermittent clouds, mild, slight breeze.

Progressively greener, birch has shown the most greening as has some of the thornier shrubs and unidentified scrub. Horse Chestnut almost 100% green. Oak has also greened up significantly, between 30% and 50 % for most trees. Ash showing no signs of budburst. Beech trees showing differential development, where the lower branches contain dormant buds but the upper branches are greening and thicker in size. Sycamore trees also display an uneven development, the lower branches generally are leafing out and in some places leaves have fully extended, before the upper branches where buds are green and thick. Proximity to the ground and other trees seems to be encouraging leaves to emerge earlier in the lower storey. Could there be a potential link with the emergence of leaves in nearby trees, encouraging leaves on other trees to emerge?

Evergreen trees remain largely unknown and have not attempted to identify them.

Activities:

Successfully marked 30 trees with white paint.

Birch (4)

Unknown (3)

Beech (6)

Oak (6)

Ash (3)

Sycamore (6)

Horse Chestnut (2)

Trees vary in age and position in the forest (all are either on path, road or in the car park area) but they were chosen for easy access and trees overgrown by Ivy/holly or looked anyway unhealthy were not chosen. Though individual trees were marked, marking branches proved more challenging as some remained above head height and out of access, therefore a qualitative estimate of greening will have to be made rather than counting individual buds and/or leaves on the tree. It is intended to observe these trees for the remainder of the growing season, once weekly;

Take photo

Observe qualitative estimate of leaves and/or buds emerged

Note the scrub, undergrowth around the tree that might be greening

Comparing observations between trees of the same species type could reveal variation in the timing of phenological events within one species. Contrasting the phenology of different species types will reveal the overall greenup pattern of the forest.

<u>9/4/08</u>

Cool morning, slight breeze, clear with some cloudy spells.

Intended to note the % budburst and % leaf emergence of trees tagged last week and tag more trees if necessary. The forest did not show large scale change since last week as there was a cold spell over the weekend. Leaflets beginning to emerge on the oak and sycamore trees with Horse Chestnut already well leafed

out. Ash buds are still dormant but on some Ash trees, growth of a frond or some structure was evident adjacent to the buds. The birch tree is beginning to green up with definite budburst and some leaf emergence on certain trees. Those birch trees in open light (car park) are greening up quicker than those in the forest canopy. The beech tree has largely dormant buds in the lower canopy but the upper buds are greening now. There is more evidence of other life in the forest such as bird activity and butterflies.

Activities:

More photographic evidence of phenology

Three more trees tagged

Noted qualitative estimate of phenology

17/4/08

Blustery easterly winds. Dull with some sunny spells.

Generally observed forest to be greening up significantly, approximately 60% green at this stage. Ash trees are largely dormant although the buds appear thicker and ready to emerge. The Beech tree is also dormant but some leaves have emerged by chance on the upper branches. The birch tree is in varying stages of leaf emergence with almost all trees exhibiting budburst (some unknown species though to be birch are still dormant).The oak tree is becoming steadily greener although individual trees are showing differing stages of development throughout the forest. This is also true for the Sycamore tree which is at varying stages of development depending on the location of the tree in the forest and the height of the branches on the tree. The Horse Chestnut trees have become almost completely green; the leaves are fully emerged at this stage. The

under storey of grass and other shrubs is very green. Lower trees and shrubs (hedgerows too) are greening up. Note: Poplar trees aligning the road between Carrigaline and roundabout and on the way to Shanbally are greening significantly, approx. 80% green, non-native species but very distinct colour.

24/4/08

Showery morning, fresh breeze, some sunshine

Continuing on from last week, wood appears greener, especially grasses and shrubs along path edge and some of the canopy. Beech tree buds have finally come out of dormancy; they appear green and have emerged from bud. The buds on the upper canopy appear to be budding first before those closer to the ground. Some beech trees have leaves showing. The birch trees are greener in general, their leaves are small and resemble those of beech but birch is smaller and is more pointed at the end than those of the beech tree. The Oak and Sycamore trees are greening up at a steady rate. Although the leaves on the oak tree seem to emerge all at the same time, those on the sycamore are staggered, with the leaves closest to the ground emerging first and upper canopy leaves emerging last. The Horse Chestnut tree would appear fully leafed-out, however maybe the leaves have more leaf area yet to extend. The Ash tree is the slowest to show signs of greening; however some buds on the upper canopy appeared to be greening, other buds still dormant. The agricultural site in Crosshaven appears greener, it could be grass, would need to verify this. First appearance of snowdrop recorded.

26/4/08

First swallow sighting-Baltimore

1/5/08

Warm day, southerly breeze, some clouds.

The Wood canopy is starting to fill in and undergrowth appears to be at its maximum stage. The Wood is moving towards maximum greenup with most of the trees in leaf. Bluebells and snowdrops are abundant on path and in the undergrowth. The Beech tree has shown the most change since last week with leaf emergence on most trees. The Birch trees are steadily greening up. The Horse Chestnut seems to be at maximum leaf area. The Oak and Sycamore trees are nearing maximum leaf emergence, the oak trees is leafing out evenly while the Sycamore shows more of a differential development depending on the height of the branches. The Ash tree is largely dormant except for a few saplings which are green. The agricultural site is green as are hedgerows.

7/5/08

Warm day, mild breeze, hazy sunshine

Temperatures have risen considerably during the week which has caused a marked increase in the appearance of vegetation, the difference since the last field outing has been the most significant yet. Both the Wood canopy and the undergrowth are becoming dense. The canopy may need more time to fill in before it is at its maximum growth. Some saplings such as Beech and Ash showed no leafout yet, these may be exceptions. Snowdrops/bluebells/ other grasses are starting to appear in abundance. All the trees have shown considerable growth since last week, especially the Beech tree. The Ash tree has finally come out of dormancy and buds are greening with leaf emergence evident in some trees. The agricultural site is green, probably grass. The hedgerows appear to be bushy.

14/5/08

Very warm, cloudless, slight easterly breeze

Temperatures consistently warm since last week which has corresponded to an overall greening of vegetation over all land cover types. The Wood seems to be in transition again from the greenup phase to the mature phase. I would estimate the Wood to be mature in 2-3 weeks. This week Ash is showing abundant leafout, in most cases tree leaves look to be about 50% emergent. Horse Chestnut and Sycamore would appear to be at maximum leafout. Beech is approaching its maximum and birch is still midway between greenup and maximum. Oak is also approaching the maximum. The forest under storey is thick and dense with shrubs (rhododendron evident and in flower). There are bluebells, snowdrops and other flowers and tall grasses on the path edges and forest floor.

Note: Problem with monitoring method. The tagging of trees has not worked for two reasons; one is the filling in of leaves and moss over the paint which obscures them and the removal of these tags by people. This has created confusion in recording the phenology of the same tree each week. In the data tables, the same tree is not always recorded on a weekly basis. There is also human error in remembering the site of each tagged tree and consistently recording the same tree on a weekly basis. Either taking a GPS point at each tree or labelling the tree in some other way would be potential solutions.

22/5/08

Warm, humid, cloudy with showers

Initial observations would show the Wood to be in summer. The paths are filled in by a dense canopy and grasses along the edge are very green and bushy. The hedgerows are equally green.

Snowdrops, buttercups, bluebells, rhododendron, flowers and ferns comprise the growth on the canopy floor. Horse chestnut trees have become heavy with leaves and are in flower. Sycamore trees, oak and beech trees appear to be fully green. The birch trees have a less dense covering of leaves but seem to be fully green. The ash trees are green; the younger saplings most noticeably while the older trees are slower to green up. 28 trees recorded.

30/5/08

Overcast, mist/drizzle with a light easterly breeze

Forest canopy has thickened and parts of Wood are dark where leaves have blocked out incoming light. There has been little change since last week in leaf cover except for Ash trees whose leaves are fully extended now and some younger sycamore trees which were slow to leaf out. Some Horse chestnut and Sycamore trees appear laden with a full leaf canopy. The undergrowth is dense, includes daisies and dandelions. Hedgerows have shown a lateral growth, encroaching on the road in places.29 trees recorded, missing some Ash trees and Sycamore in places.

16/10/08

BOC, D de V, KK (school student)

The opposite end of the growing cycle to spring greenup in autumn is known as brown-down where vegetation experiences decolouration and leaf fall. This phase begins in early autumn (e.g. September) and the effects were noticeable

across most tree species at the time of this visit. While all tree species exhibited signs of leaf decolouration, not all trees experienced leaf fall and some continued to maintain a green canopy with less than 5% of leaves decoloured. For example, the Beech trees were largely green and there were few signs of any leaves being shed. Birch trees exhibited a similar trend. In contrast, the Oak tree appeared to maintain a full canopy; however the leaves appeared dead and were largely yellow or brown in colour. The Ash tree had black/brown and yellow leaves and the percent cover was reduced. The Sycamore tree exhibited the largest decrease in leaf cover, many were brown, and the cover had decreased to 10 or 20%. The evergreen tree species such as Scots Pine, Noble Fir, European Larch and shrubs such as Laurel, Rhododendron, Ivy and Holly dominate the undergrowth. They will continue to maintain a base- level green reflectance throughout the autumn and winter months.

18/2/09

BOC and work experience student

- Sycamore buds had emerged on approx. 50% of tree canopy
- Horse Chestnut buds were large but not all appeared green, approx. 30% of canopy
- Identified Elm tree
- Identified Rowan tree
- European Larch shed needles (deciduous coniferous tree)
- Blossoming tree with white flowers noticed

Appendix B: METEOSAT/MERIS overpass times

Date of comparison (YYYYMMDD)	MERIS overpass time (UTC)	METEOSAT CLM time (UTC)	Difference (mm:ss)
20060121	10:53:50	11:00	06:10
20060122	n/a		
20060123	11:30:34	11:30	00:34
20060124	10:58:35	11:00	01:25
20060125	n/a		
20060126	11:36:10	11:30	06:10
20060127	10:56:46	11:00	03:14
20060128	n/a		
20060129	11:41:55	11:45	03:05
20060130	n/a		
20060421	12:04:07	12:00	04:07
20060422	n/a		
20060423	11:02:02	11:00	02:02
20060424	n/a		
20060425	11:39:13	11:45	05:47
20060426	11:07:58	11:15	07:02
20060427	10:37:06	10:30	07:06
20060428	11:44:55	11:45	00:05
20060429	11:13:55	11:15	01:05
20060430	n/a		
20060620	n/a		
20060621	11:47:00	11:45	02:00
20060622	11:16	11:15	01:00
20060623	10:43	10:45	02:00
20060624	11:52	11:45	07:00
20060625	11:14	11:15	01:00
20060626	10:51	10:45	06:00
20060627	11:59	12:00	01:00
20060628	11:28	11:30	02:00
20060629	11:00	11:00	00:00
20060928	11:36	11:30	06:00
20060929	11:05	11:00	05:00
20060930	10:33	10:30	03:00
20061001	11:41	11:45	04:00
20061002	11:10	11:15	05:00
20061003	10:38	10:45	07:00
20061004	11:48	11:45	03:00
20061005	11:14	11:15	01:00

20061006	10:45	10:45	00:00
20061007	11:52	11:45	07:00
20061127	11:50	11:45	05:00
20061128	n/a		
20061129	n/a		
20061130	n/a		
20061201	11:47	11:45	02:00
20061202	10:53	11:00	07:00
20061203	12:02	12:00	02:00
20061204	11:30	11:30	00:00
20061205	11:00	11:00	00:00
20061206	n/a		

Appendix C: The coordinates and offset of the MERIS Level 1 (L1) radiance and MGVI pixels

Pixel		Row	Column	lat	lon	Y-diff	X-diff	Y sampling	X sampling	Y offset	X offset
	L1	8	8	51.836983	-8.154828	0.005397	0.00878	0.010802	0.017484	0.49963	0.502173
1	MGVI	387	157	51.831586	-8.163608			0.010799	0.018182	0.499768	0.482895
	L1	7	7	51.847786	-8.172311	-0.0054	-0.008703			-0.49972	-0.49777
2	MGVI	385	157	51.853184	-8.163608					-0.49986	-0.47866
	L1	6	6	51.858589	-8.189797	-0.00539	-0.008007			-0.49935	-0.45796
3	MGVI	384	156	51.863983	-8.18179					-0.49949	-0.44038
	L1	5	5	51.869389	-8.207281	-0.00539	-0.007309			-0.49926	-0.41804
4	MGVI	383	155	51.874782	-8.199972					-0.4994	-0.40199
	L1	4	4	51.880192	-8.224764	-0.00539	-0.00661			-0.49889	-0.37806
5	MGVI	382	154	51.885581	-8.218154					-0.49889	-0.37806
	L1	12	12	51.793775	-8.084889	0.005385	0.005991			0.498519	0.342656
6	MGVI	391	161	51.78839	-8.09088					0.498657	0.329502
	L1	9	9	51.826183	-8.137344	0.005396	0.008082			0.499537	0.462251
7	MGVI	388	158	51.820787	-8.145426					0.499676	0.444506
									AVERAGE error	-0.16652	-0.14947

Appendix D: MERIS Level 3 data format (hdf 4.2)

Applying the scaling factor

The MERIS Global Vegetation Index (MGVI) is in 8-bit integer format, the valid MGVI range is from 1 to 255 with 0 representing invalid values. A scaling factor, using a simple linear transformation, provided in the hdf metadata, converts the MGVI (byte) data to the FAPAR scale (float) from 0 to 1. The scaling factor follows the linear equation:

$$Y = mX + c$$

Table 1: A description of the quantities used in MGVI/FAPAR conversion

Symbol	Term	Value
Y	Numerical values of FAPAR	Between zero and one, double floating point
m	Slope	0.003937008
X	8-bit MGVI	Range from 1 to 255
C	Intercept	-0.00393701

Appendix E: Composite period, day of year and calendar dates

Composite	Interval (days)	Calendar date (non-leap year)	Calendar date (leap year)
1	1-10	Jan 1-10	January 1-10
2	11-20	Jan11-21	January 11-21
3	21-30	Jan 21-30	January 21-30
4	31-40	Jan 31- Feb 9	January 31- February 9
5	41-50	Feb10-19	February 10-19
6	51-60	Feb 20-Mar 01	February 20-29
7	61-70	Mar 2-11	March 1-10
8	71-80	Mar 12-21	March 11-20
9	81-90	Mar 22-31	March 21-30
10	91-100	April 1-10	March 31-April 9
11	101-110	April 11-20	April 10-19
12	111-120	April 21-30	April 20-29
13	121-130	May 1-10	April 30-May 9
14	131-140	May 11-20	May 10-19
15	141-150	May 21-30	May 20-29
16	151-160	May 31-June 9	May 30-June 8
17	161-170	June 10-19	June 9-18
18	171-180	June 20-29	June 19-28
19	181-190	June 30-July 9	June 29-July 8
20	191-200	July 10-19	July 9-18
21	201-210	July 20-29	July 19-28
22	211-220	July 30-Aug 8	July 29-Aug 7
23	221-230	Aug 9-18	Aug 8-17
24	231-240	Aug 19-28	Aug 18-27
25	241-250	Aug 29-Sep 7	Aug 28-Sep 6
26	251-260	Sep 8-17	Sep 7-16
27	261-270	Sep 18-27	Sep 17-26
28	271-280	Sep 28-Oct 7	Sep 27-Oct 6
29	281-290	Oct 8-17	Oct 7-16
30	291-300	Oct 18-27	Oct 17-26
31	301-310	Oct 28-Nov 6	Oct 27-Nov 5
32	311-320	Nov 7-16	Nov 6-15
33	321-330	Nov 17-26	Nov 16-25
34	331-340	Nov 27-Dec 6	Nov 26-Dec 5
35	341-350	Dec 7-16	Dec 6-15
36	351-360	Dec 17-26	Dec 16-25